Electrolyte interactions in dye-sensitised solar cells: Catalysis, corrosion and corrosion inhibition.

Wragg, David Alexander

Swansea University
Prifysgol Abertawe

Electrolyte Interactions in Dye-Sensitised Solar Cells: Catalysis, Corrosion and Corrosion Inhibition

David Alexander Wragg

Thesis submitted to Swansea University in fulfilment of the requirements for the Degree of Doctor of Philosophy
Materials Research Centre, College of Engineering

2015

Declaration

This work has not previously been accepted in substance for any degree and is not being concurrently submitted in candidature for any degree.

Signed .. .. (candidate)

Date ..27/02/15.....

STATEMENT 1

This thesis is the result of my own investigations, except where otherwise stated. Other sources are acknowledged by footnotes giving explicit references. A bibliography is appended.

Signed .. .. (candidate)

Date ..27/02/15.....

STATEMENT 2

I hereby give consent for my thesis, if accepted, to be available for photocopying and for inter-library loan, and for the title and summary to be made available to outside organisations.

Signed .. .. (candidate)

Date ..27/02/15.....

NB: *Candidates on whose behalf a bar on access has been approved by the University (see Note 7), should use the following version of Statement 2:*

Summary

The focus of this thesis is the development of fast low temperature platinisation for dye solar cell (DSC) counter electrodes substrates. Initial studies indicated that direct deposition results in poor catalytic material due to unrestrained growth, characterised through the limiting current obtained through cyclic voltammetry. These counter electrodes were further characterised through I-V measurements of DSCs, SEM and EIS measurements. As a result of this study an indirect route for platinisation was developed using galvanic replacement. A lead deposit formed a templating material, followed swiftly by electroless replacement with platinum metal. Analysis showed viable Pt deposits on the FTO surface, which proved to be catalytic towards triiodide. DSC devices produced using this catalyst resulted in 3.2% efficiency, compared to thermal Pt devices (3.9%) and chemically platinised devices (3.5%).

This research also developed an innovative observation and analysis technique for use in the quality assessment and control of mass produced metal substrate DSCs. RGB colour data was collected for 1000 hours. The progression of cell degradation through the reduction of triiodide was recorded and the vulnerability of critical industrial substrates assessed. Nitrogen containing heterocyclics (NHC's) electrolyte additives that have a unique corrosion inhibition effect were identified during this analysis. Electrolytes containing several NHC's were compared, showing that a critical concentration of 0.5M or 1M could retard corrosion in several vulnerable substrates such as activated Al and Ni. A cobalt complex electrolyte was investigated in parallel to the triiodide investigation, using the RGB analysis method. Iron and copper substrate were found to be vulnerable, despite the cobalt electrolyte being heralded as a non-corrosive electrolyte.

Since NHC compounds were not seen to reduce the degradation of the examined vulnerable substrates, inhibition techniques such as blocking layer and NHC's were trialled, with analysis made on their affect compared with the previous study. The structure of the NHC's were discovered to be critical to the inhibition effect and from this, a number of theories for the corrosion inhibition mechanism were suggested.

Acknowledgements

Firstly, I would like to acknowledge KESS and the European Social Fund (ESF), in addition to Tata Steel Colours, for funding this work. This research would not have been possible without the of the SPECIFIC project facilities and the support of my colleagues at Swansea University. I would also like to acknowledge and thank Dr Kirsi Yliniemi of Aalto University, Finland, for all her help with the work presented in *Chapter 4* of this thesis.

I am in the debt of Prof. Dave Worsley and Dr Trystan Watson, who without their support, guidance (and extreme tolerance...) I would not have got to where I am today. This project was challenging to work on and I am glad I was able to complete it at Swansea University.

Thanks also go to Dr Matt Carnie, Dr Ian Mabbett, Dr Bruce Philip, Dr. Cecile Charbonneau, for specific help and the rest of the PostDoc team for guidance and advice throughout my PhD. I would also like to mention the inhabitants of my office, 2012-2013 (you know who your are), for making the last three years interesting. Thank God you never got me to sing!

Finally, I would like to thank my family for their support throughout the last few years, and for always giving me a place to come home to.

David Alexander Wragg

February 2015

Dedication

This thesis is dedicated to three brilliant people:

(Grandpa) ***Philip Theo Wragg*** *(7th December 1928 - 26th July 2013), respected, loved and terribly mischievous.*

and

Benjamin John Bland *(2nd January 1990 - 28th May 2014), my best mate and an inspiration. You will be greatly missed.*

and

(Grandad) ***Thomas Scott Atchison*** *(23rd March 1928 - 18th May 2014), inspiring, fun, pretty much indestructible and a proud Scot.*

List of relevant publications

Watson, T., Reynolds, G., Wragg, D., Williams, G., & Worsley, D. (2013). "*Corrosion Monitoring of Flexible Metallic Substrates for Dye-Sensitized Solar Cells*". *International Journal of Photoenergy.*

Wragg, D. A., Watson, T. M., & Worsley, D. A. (2013). "*Monitoring the effect of N-heterocyclic compound additives in dye sensitized solar cell electrolytes for corrosion inhibition*". *Meeting Abstracts* 12, 600.

Wragg, D. A., Yliniemi, K., Watson, T. M., & Worsley, D. A. (2013). "*Platinised counter electrodes for dye sensitized solar cells through the redox replacement of a low power electrodeposited lead sacrificial template*". *ECS Transactions,53*(24), 11-17.

Yliniemi, K., Wragg, D., Wilson, B. P., McMurray, H. N., Worsley, D. A., Schmuki, P., & Kontturi, K. (2013). "*Formation of Pt/Pb nanoparticles by electrodeposition and redox replacement cycles on fluorine doped tin oxide glass*". *Electrochimica Acta, 88*, 278-286.

List of publication contributions

Charbonneau, C., Hooper, K., Carnie, M., Searle, J., Philip, B., Wragg, D., Watson, T. and Worsley, D. (2013), "*Rapid radiative platinisation for dye-sensitised solar cell counter electrodes*," Prog. Photovolt: Res. Appl. doi: 10.1002/pip.2368

Yliniemi, K., Wragg, D., Watson, T. M., Worsley, D. A., McMurray, H. N., Wilson, B. P., Schmuki, P. & Kontturi, K. (2012), "*Conversion Kinetics and Characterisation of Pt/Pb Nanoparticles on Fluorine Doped Tin Oxide Glass*," *ECS Meeting Abstracts* 26, 2387-2387

Vyas, N., Wragg, D. A., Charbonneau, C., Carnie, M., & Watson, T. M. (2013). "*Low Cost TCO Less Counter Electrodes for Dye-Sensitized Solar Cell Application*," *ECS Transactions, 53*(24), 39-46.

Conferences

Electrochem 2012: Electrochemical Horizons, Dublin (Poster)

RSC Great Western Electrochemistry Meeting 2012 - Bath (1x Presentation)

UK-ISES PVSAT-9 Photovoltaic Science Applications and Technology Conference, 2013, Swansea (Poster)

ECS 223rd Meeting 2013 - Toronto (2x Presentations)

Posters

SLRR-based deposition of platinum for Dye Sensitized Solar Cell counter electrodes - D. Wragg, K. Yliniemi, T. Watson, D. Worsley, Swansea, Electrochem 2012

Low Power Electrodeposition of Platinum of Dye Sensitised Solar Cell Counter Electrodes - D. Wragg, K. Yliniemi, T. Watson, D. Worsley, PVSAT-9, 2013

List of Figures

List of tables

Contents

1 Introduction

A study by the International Energy Agency (IEA) showed that the total world consumption of energy was estimated to be 8677 million tonnes oil equivalent (Mtoe), or $1.0091351e10^{14}$ kWh, of which electricity consumption makes up 17.7%, from 2010 statistics [1]. This need will grow over the next century as the global population and industrial base increases. Furthermore, there is an increasing need to turn to other energy generation methods in order to conserve limited fossil fuel resources, as a recent BP study has estimated that only 52.9 years of oil production remain [2]. This study also promotes the efficient utilisation of abundant natural sources such as wind, tidal and solar power, with nuclear power also included in these alternative options. However since the Fukushima Daiichi accident in 2011, there has been a marked decrease in the development of nuclear infrastructure, falling from the 2006 peak of 2660TWh, to 2346TWh in 2012, a drop of 12% [3]. Several countries including Germany have opted to phase out and close their nuclear program fully over the next decade [4]. This uncertainty over nuclear power and its total phase out in a number of countries, coupled with the increasing price of oil and gas, has enabled a resurgence in renewable electricity generation.

The most visible type of renewable is wind power, with large onshore and offshore wind farms built both in the UK and many European countries [5]. The issue with wind power is that it is intermittent and very difficult to predict, this coupled with the difficulty in storing energy and the increased infrastructure needed to attach offshore wind farms to the grid, leads to the conclusion that wind power will not easily play a large part in meeting future energy needs, unless the mismatch between fluctuating daily power requirements and generation can be balanced [6][7]. However, if power storage technology improves then wind could play a vital role in the energy generation of many countries [8][9][10]. Tidal generation or wave power are other interesting technologies, however due to the hostile sea water environment and again the increased infrastructure in placement and grid connection of these sources, this resource so far remains out of reach for current large scale or base load generation needs [11].

Solar power is a much studied and publicised technology with massive potential for large scale energy generation, with 2012 showing massive growth in PV capacity, achieving *ca.* 102GW installed capacity [12]. As of 2013, Silicon cells typically made up the bulk of manufactured commercial devices due to their high power conversion efficiency and stability, though the amount of CIGS or CdTe modules produced is climbing as the

technology improves [13]. Unfortunately, these have several drawbacks such as high processing costs and the production of hazardous waste products. They also produce electricity at a higher cost than traditional generating technologies such as fossil fuels, though this is mitigated somewhat by feed in tariffs put in place by governments [14]. The potential for large scale uptake and commercialisation of photovoltaic technologies is high, especially considering recent public opinion on nuclear power and the projected scarcity of fossil fuels over the next century. Despite the high initial setup costs of solar power, the balance of system (BOS) infrastructure is much less than wind or tidal generation. The field of solar cell research is vast, with several different technologies reaching commercial viability and higher efficiencies over the last 20 years [15]. Thin film photovoltaic PV technologies use thin layers of PV materials to reduce the cell bulk and BOS needs, such as support for crystalline silicon roofing panels. Furthermore, thin films allow for continuous processing methods to be utilised rather than slower and more costly batch processing [16], [17].

Research on thin film photovoltaics has increased over the last 20 years, in order to improve upon standard polycrystalline silicon cells and to increase overall PV performance. One of the first thin film technologies was amorphous silicon (a-Si) [18]. Amorphous silicon cells are constructed using chemical vapour deposition (CVD) growth onto the required substrate. The materials used are known as P-type and N-type semiconductors, where the N-type has a large concentration of electrons and the P-type has an abundance of electron spaces, known as holes. The "P" and "N" refer to the positive and negative of the hole and the electron. A P-type semiconductor is created through the doping of silicon with electron accepting elements such as boron. This group XIII element has one less electron than the group XIV silicon and results in a substrate with a large positive charge that is able to accept electrons from a donor source. The N-type material is created through the addition of electron donating elements such as phosphorus or arsenic. These are group XV elements that will give the semiconductor a higher concentration of electrons than holes and an overall negative charge. Figure 1.1 illustrates a typical P-N junction and the energy levels involved in a typical silicon PV cell. Schematic 1 and 2 illustrate the movement of electrons and holes before and after the P and N material are joined. Schematics 3 and 4 show the change in energy levels of Schematics 1 and 2 respectively. Figure 1. shows a schematic of an amorphous silicon PV cell. As the material is illuminated by light with a higher energy than the band gap, charge carriers are excited and are free to move through the material.

Charge separation will occur due to band bending in the interface between P and N type materials.

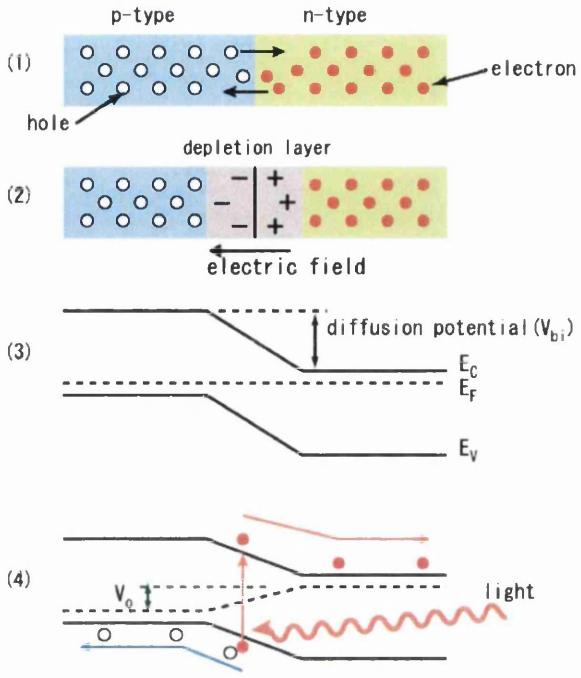

Figure 1.1: Energy level diagram for a p-n junction solar cell [19]

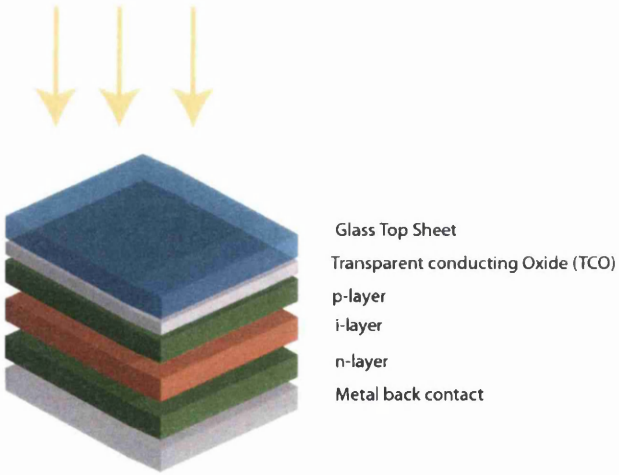

Figure 1.2: Schematic of an amorphous

This technology is less costly than traditional bulk silicon, though the efficiency is lower due to defects in the film that affect the film much more than the bulk material [20]. Amorphous silicon solar cells are currently commercially available from suppliers such as **"Sungen"** [21] and "HyET Solar" [22], and can be applied to building roofing, walls and blinds using a foil type architecture. Further uses of this in building-integrated

photovoltaics (BPIV) are as semi-transparent window glazing that can act as an aesthetic tint, as well as generating electricity [23].

The current highest performing single cell thin film solar cells have reached 29.1% using a gallium arsenide thin film cell (GaAs), Figure 1.3, at AM1.5 conditions, though this cell and its high performance come at increased cost [24]. Another attractive thin film solar cell technology is the $Cu(InGa)Se_2$ or CIGS cell. This type of cell uses a conducting glass or polymer and metal substrates with the active material in a sandwich configuration between, Figure 1.4. Repins *et al.* reported a glass based CIGS cell reaching an efficiency of 19.9% [25], though the current CIGS single cell record is now at 23.3% [24].

Cadmium Telluride (CdTe), Figure 1.5, is perhaps the most versatile thin film technology, due to its ideal band gap of 1.5eV that leads to an optimal conversion of photons from solar radiation to electricity [26], [27]. There are several drawbacks to this cell type, first is that the tellurium needed in this cell is mined as a by-product in other processes, gold and copper extraction, and as a result there is no large stockpile [28]. Further to this, the cadmium needed is toxic and banned by several countries leading to problems with commercialisation and eventual recycling of the product [28]. First Solar, a company heavily invested in this technology has developed recycling processes and has factored the cost of this and waste transport into their estimated cost of electricity [29]. Furthermore an independent review of the CdTe technology by the French Ministry of Ecology Energy and Sustainable Development indicated that the stability, efficiency and end life measures of CdTe cells, in particular First Solar was high and that, despite the materials problem the CdTe cells are a viable PV technology for use [30]. To date, there are several large CdTe installations worldwide: In 2008 an 835kW roof was installed in Germany; also a 2.4MW roof was installed in S. California and a large 40MW system was planned for installation in Germany [31].

Following on from this, the third generation of solar technologies includes photoelectrochemical (PED) and organic solar cells (OPV), which are currently under development. However, in comparison with first and second generation technology, large scale commercialisation has yet to be made a reality. There are current projects such as G24 Power Ltd in Cardiff [32]; the Swansea University SPECIFIC project and a variety of international programmes that are attempting to realise the dream of mass produced low cost solar power using these third generation developments [33].

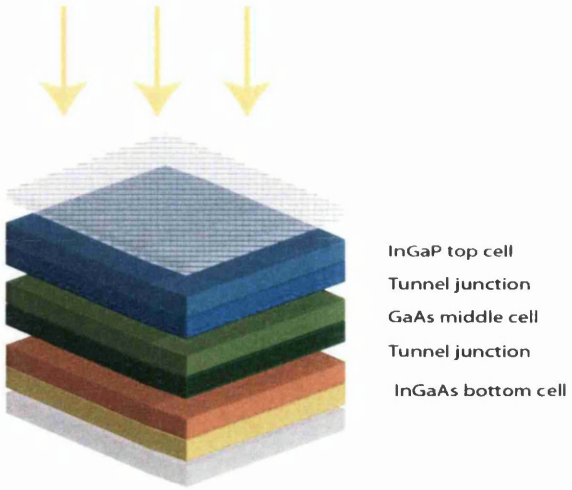

Figure 1.3: Schematic of a Gallium Arsenide (GaAs) Cell

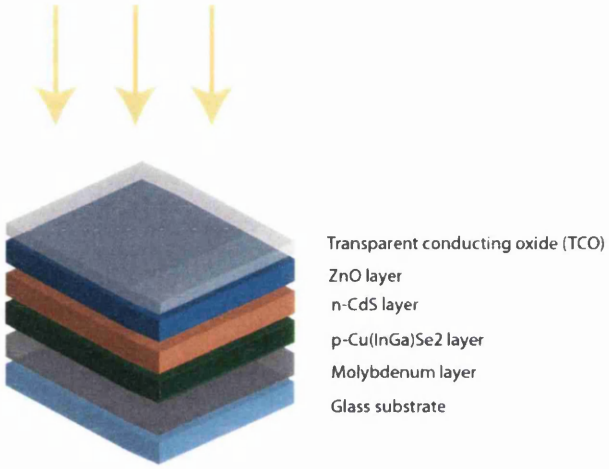

Figure 1.4: Schematic of a CIGS solar cell

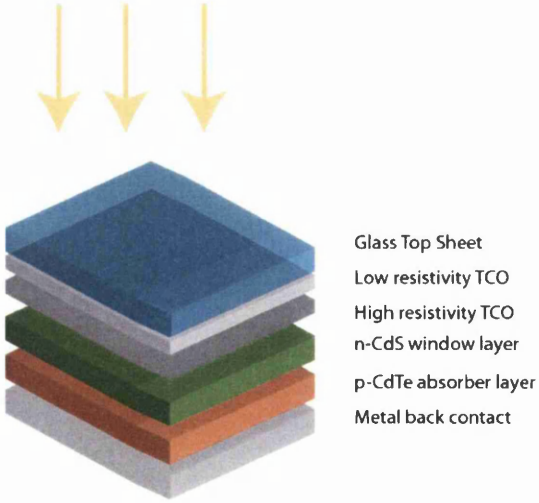

Figure 1.5 Schematic of a Cadmium Telluride (CdTe) solar cell

Dye sensitised solar cells (DSCs) are a type of photoelectrochemical thin film cell introduced by O'Regan and Grätzel in 1991 [34]. These have serious potential to be a contender in the low cost PV market due to the use of highly abundant, low cost and non-toxic materials. Before this can be realised, there is a need to progress from lab and batch processes to a mass producible device using low cost substrates such as metals and polymers. The change in substrates has engendered a requirement for fast and low temperature processing methods. In addition, there is increasing interest in building integrated photovoltaics (BIPV) and with this a requirement to produce cells on lightweight metallic substrates for use on roofing or as building cladding.

Currently, the highest performing DSCs are created in research centres and universities and use a traditional liquid electrolyte containing a redox couple (iodide/triiodide or cobalt complex ions) [35]. Unfortunately, the iodine based redox mediator is known as being highly aggressive, with the tendency to corrode several key industrial metals such as iron and aluminium and conductive connections such as silver and copper [36][37][38], [39]. Furthermore, the electrolyte requires a specially designed, expensive platinum nanoscale catalyst to accelerate the charge transfer reaction at the counter electrode [40]. Another type of cell, the perovskite solar cell, is also under development and hopes to avoid the current issues facing dye solar cells using liquid electrolytes, through the introduction of a solid perovskite photoactive material on a mesoporous scaffold such as TiO_2 or Al_2O_3 nanoparticles [41].

This work focuses on two of the most pressing issues facing the scale up of liquid state DSCs [42][43]: The need to produce a fast low temperature method of platinisation for iodide/triiodide electrolyte DSCs and the eventual need to for an *in situ* monitoring method for DSC production and quality for a mass production process. The low temperature platinisation issue will be addressed through the development of an electrodeposition technique, initially for FTO glass, with the eventual goal of usage on conducting polymers.

A further study was built out of the device observation work, looking at methods to mitigate the aggressiveness of high performing redox electrolytes towards the metal substrates preferred in the mass production of DSCs on a roll to roll production line, rather than batch sampling or destructive testing of devices. In order to mitigate electrolyte aggressiveness, this study will also assess the benefits of certain performance enhancing compounds, nitrogen containing heterocyclics, to ascertain their impact and viability for production DSCs.

1.1 Dye sensitised solar cells

This section covers DSC operation, components and electrochemistry, both current literature and industrial developments.

One of the earliest studies of photoelectrochemical solar cells was performed by Moser in 1887 employing an erythrosine dye to sensitise silver halide electrodes [44]. A more modern version of dye sensitised solar cell was developed further through a device patented by Chen *et al.* for an N-methylphenazinc methosulfate dye sensitised titanium dioxide (TiO_2) layer [45]. This early concept was unfortunately restricted to a monolayer of dye, resulting in a low surface area for the absorption of light and therefore low device efficiency. Desilvestro *et al.* then presented a paper on highly efficient sensitisation of TiO_2, using colloidal anatase TiO_2 particles, thus providing a method of increasing the surface area available for the dye [46]. This was taken further through the seminal report by M. Grätzel and B. O'Regan in 1991, who produced a highly efficient solar cell using a high surface area network of sintered TiO_2 particles as the semiconductor [34]. Over the last 20 years, this design has been improved upon and the current DSC efficiency record is over 12% using a cobalt electrolyte and an engineered organic dye [35].

1.1.1 Operation

A liquid state DSC can be described as having four main components: The TiO_2 semiconductor, the sensitising dye, the counter electrode redox catalyst and the redox mediator containing electrolyte [19]. There are other components, such as the sealing gasket used to join the electrodes, or the conductive paste used to enhance the cell contact points. These however are general components which vary according to the experimental procedure followed and the nature of the work to be performed.

The operational cycle of a DSC device is better explained in a diagrammatic format, Figure 1.6, with both components and basic electrochemical cycle identified. When illuminated, photons of light pass through the front transparent conducting substrate and interact with the sensitising dye which is adsorbed onto the TiO_2 semiconductor. The transfer of photon energy "$h\nu$", where "h" is Planck's constant and "ν" is the frequency of the electromagnetic waves, to the dye molecule shifts it to an excited state. The electrons then move from the highest occupied molecular orbital (HOMO) to the lowest unoccupied molecular orbital (LUMO). This excitation allows the molecule to undergo a metal to ligand charge transfer (MLCT) process where the electron density shifts from the central metal complex ion to the ligands surrounding this ion. Due to this shift, these electrons can then be injected into the

TiO_2 conduction band, where they diffuse through the mesoporous TiO_2 network to the TCO layer. This layer facilitates passage to the external circuit with minimal resistive and recombinative loss of electrons [19].

Once work has been done in the external circuit, the electron return is facilitated by the redox catalyst at the counter electrode, which promotes the reduction of triiodide to iodide. This species migrates through the electrolyte to the working electrode where it is oxidised through transferral of an electron to the oxidised form of the dye molecule, thus returning it to its neutral state. It should be noted that these electrochemical redox reactions at the working and counter electrode occur simultaneously and serve to aid charge separation and reduce recombination losses [19].

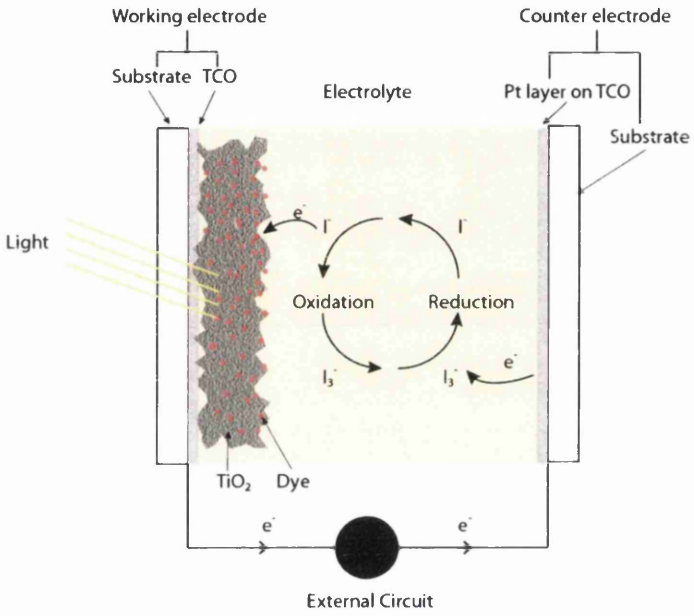

Figure 1.6: Schematic representation of DSC operation

The processes within the DSC can be summarised by Equations 1.1 - 1.3:

$$S + h\nu \rightarrow S^* \ (Photoexcitation\ of\ dye\ sensitiser) \qquad (1.1)$$

$$S^* \rightarrow S^+ + e^-_{cb} \ (TiO_2\ Charge\ Injection) \qquad (1.2)$$

$$2S^+ + 3I^- \rightarrow 2S + I^-_3 \ (Dye\ Sensitiser\ Regeneration) \qquad (1.3)$$

Understanding the processes that occur in the electrochemical cell is crucial when attempting to improve the device performance and understand how to best optimise the cell architecture to facilitate mass production.

1.1.2 Semiconductor

The active semiconductor used in most common DSCs is titanium dioxide, TiO_2 is known for having high stability as well as low toxicity. The most promising factor however, is that compared to other photovoltaic materials, such as silicon or cadmium telluride, it is very low cost and highly abundant. TiO_2 exists in three main forms, rutile, anatase and brookite. Due to the tri-phase nature of the TiO_2, extensive investigations into the performance of each of the TiO_2 phases have been reported in literature [47]. Generally, anatase type TiO_2 is used due its electrical activity and pyramidal form that maximises the surface area available for the adsorption of a sensitizing dye, see Figure 1.7. Titanium dioxide has a wide band gap of 3.6eV, which limits its optical activity to the UV portion of the optical spectrum, an unfortunate limitation for a solar cell. Therefore, further optimisation is needed so a larger range of the optical spectrum can be utilised.

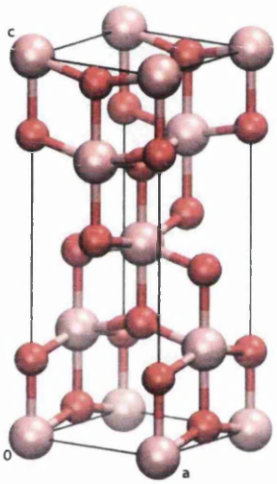

Figure 1.7: Anatase TiO_2 crystalline structure; Titanium (red), Oxygen (grey) [48]

The initial structures used for the semiconductors in photoelectrochemical solar cells are comprised of simple flat compact layers with low surface areas [49]. A radical change was needed to increase the surface area available and thus improve device performance. A development of an anatase type TiO_2 cell using a sintered TiO_2 colloid to manufacture a connected mesoporous network of particles was achieved in the 1980s, through the work of Moser, and then Desilvestro [50][51]. This process produced an electrode with a much larger surface area for dye adsorption than was previously possible and gave a large boost to DSC performance. Grätzel and O'Regan pushed this transformation further in their study on dye sensitised TiO_2 mesoporous networks, achieving a highly efficient DSC device [34].

During their investigation, it was determined that the performance of the TiO_2 semiconductor could be affected in several ways. Five key factors at the forefront of the analyzed literature were:

- Surface morphology
- Porosity
- Particle size
- Film thickness
- Sintering temperature

In the majority of devices, the TiO_2 should have a particle spacing large enough to allow the unhindered diffusion of the chosen electrolyte species into the TiO_2 mesoporous network [52]. This factor should be carefully balanced with surface area control and selection of particle size, to ensure the maximum surface area is available for dye adsorption. Small particles with an average size of 20nm are considered the best choice for this, although reports from literature recommend the inclusion of large particles, *ca.* 400nm, to act as light scattering particles to raise the incident photon to electron conversion efficiency (IPCE) and increase device performance [52]. Furthermore the film thickness should be optimised to avoid resistive losses in the electrode and reduce the migration distance of injected electrons, thus reducing the risk of recombination with the electrolyte charge carrying species [47], [53]–[55].

Titanium dioxide is usually applied in paste form, either from a commercial source, Dyesol, Solaronix or Sigma-Aldrich; or is produced from base materials such as P25 TiO_2 powder with the inclusion of binders and surfactants of the chemists' choice, this process also must utilise a complex autoclave process in order to produce the correct chemistry anatase powder and the specific TiO_2 paste required for DSC devices [56]. No matter the source of materials or application method, printing or doctor blade, the majority of literature sources use a sintering process of 450°C for *ca.* 30 minutes to remove the organic binder and surfactant and to produce an excellent level of particle connectivity and TiO_2/substrate adhesion [57]. This high temperature has unfortunately limited the use of DSCs to materials that could withstand this high processing temperature. There have been numerous attempts to produce a low temperature TiO_2 photoanode, which typically has resulted in weakened particle interconnectivity [58], [59]. This has, in turn, resulted in lower electrical contact between TiO_2 particles. In addition, the high temperature sinter is applied over 30 minute, which is not a viable timescale for a roll to roll process.

Different methods of sintering have been trialled in an attempt to keep the advantages of the high temperature sinter, but allow the use of temperature sensitive substrates. Vigil *et al.* reported a method using a microwave reactor for the deposition of TiO_2 onto conducting glass. The low power and fast application time was able to produce a good quality TiO_2 layer that could be applied to a DSC substrate [60]. A further radiative process was proposed by Guitierrez-Tauste *et al.*, reporting a UV decomposition of a TiO_2 precursor to deposit a thick porous TiO_2 film [61]. The method was successfully trialled on conducting polymer, ITO-PET, and FTO glass. The efficiency of the DSCs produced with this method only reached 2%, however this was for a non-optimised cell to prove the viability of the method.

An additional radiative technique was introduced by Watson *et al.* reporting the use of a near infrared heating process (NIR) to sinter the TiO_2 [62]. This method was developed out of the need for a rapid sintering method for TiO_2, in order to better suit the needs of commercial production. The NIR method was applied to FTO glass substrate or metallic substrates similar to those needed for a flexible roll to roll fabrication process. The FTO conductive layer will absorb the NIR radiation and the increase in temperature will burn off the solvent, binder and cause TiO_2 particle sintering to occur, Figure 1.8. In the case of metal substrates, the NIR method directly heats the metal substrate in order to sinter the TiO_2, the timescale reported in this study was 12.5s at varying power levels [62]. The test efficiencies reported were up to 2.9% on un-optimised cells for this sintering method.

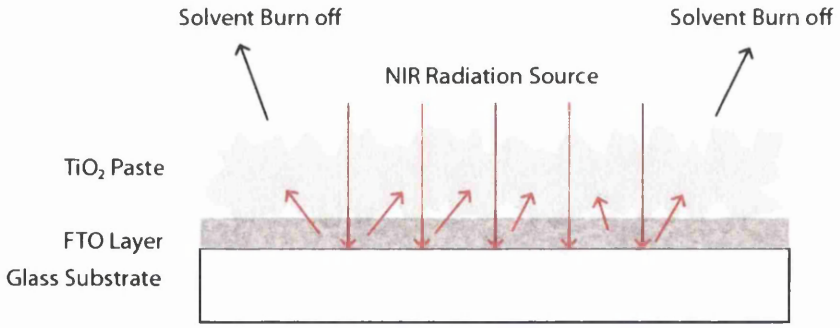

Figure 1.8: NIR sintering of TiO_2 paste on FTO glass substrate

In this study, the TiO_2 will be applied through the standard convection sinter method at 450°C due to the current developmental nature of this process. However, this method has been included to give recent background into the developments surrounding DSC scale up and commercialisation. The studies by Kalyanasundaram & Grätzel and Barbé *et al.* are

recommended for further information into the properties and structure of the TiO_2 semiconductors used in DSC devices [11, 14].

1.1.3 The dye sensitiser

The most common sensitising dye, and the one used throughout this work, is a ruthenium complex, the most widely used is N719, It has the formula "cis-Di(thiocyanato)bis(2,2'-bipyridyl)4,4'-dicarboxylate)ruthenium(II)" the structure of which is exhibited in Figure 1.9. This dye adsorbs to the TiO_2 surface using the carboxyl groups on the outside of the molecule, in addition providing orientation to the molecule to improve its operation. These provide a strong anchoring point, as well as acting as the pathway for the electron transfer that proceeds *via* a mechanism known as metal to ligand charge transfer (MLCT). As light is absorbed, the charge density between the ruthenium complex ion and the carboxylate ligand changes, thus electron transfer to the TiO_2 conduction band becomes possible. The N719 dye is a wide spectrum absorber, which maximizes the range of the optical spectrum which the DSCs can utilize [64], [65].

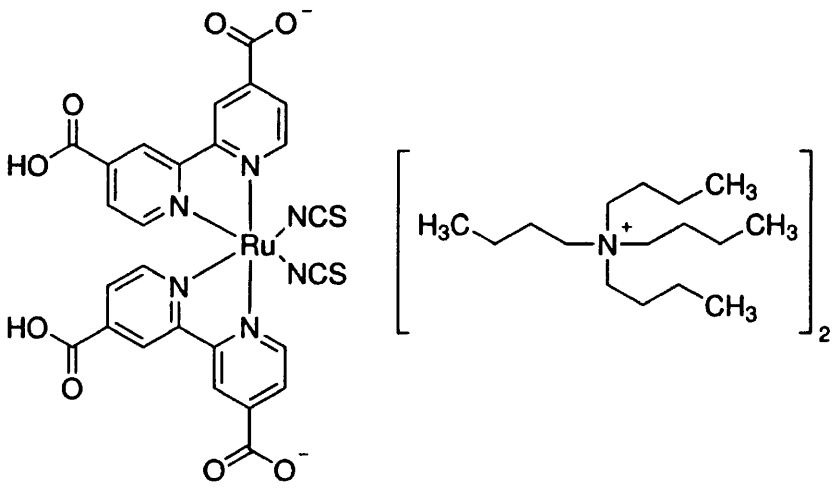

Figure 1.9: N719 sensitiser dye [66]

In the last decade there has been a drive to develop dyes that encompass a wider portion of the optical spectrum. Research has also been undertaken into the co-sensitisation of TiO_2 using two or more dyes tailored for different absorption ranges. There has also been a large movement toward organic dyes, rather than ruthenium based ones, in order to reduce the overall device cost [3, 14-15].

The performance of these sensitising molecules is usually measured using a parameter known as the incident photon to electron conversion efficiency (IPCE) [69]. This gives a

value for the quantity of incident radiation that can be converted to electrons for a given wavelength of light. Figure 1.10 compares the different IPCE values of a variety of dyes, N3 [$RuL_2(NCS)_2$], N749 [$RuL'(NCS)_3$] and Z907 [$RuL_2[Ru(bpy)_2(CN)_2]_2$], with that of unsensitised TiO_2.

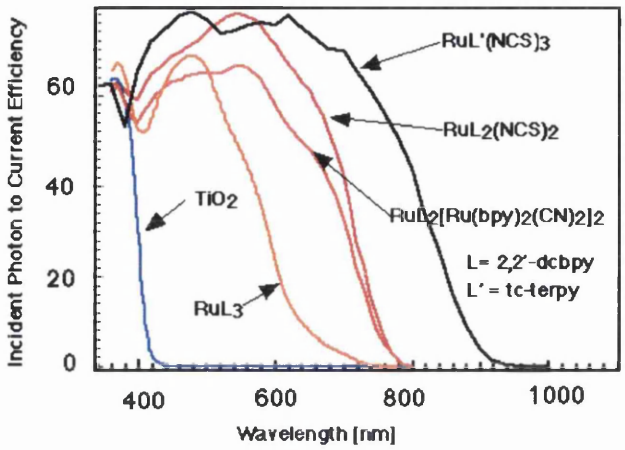

Figure 1.10: IPCE spectra for TiO_2 and sensitised TiO_2 [70]

Figure 1.11 compares the popular N719 dye with the black N749, where the N719 IPCE is *ca.* 80% for the 450nm to 550nm range mostly the visible light region, which is ideal for DSC operation.

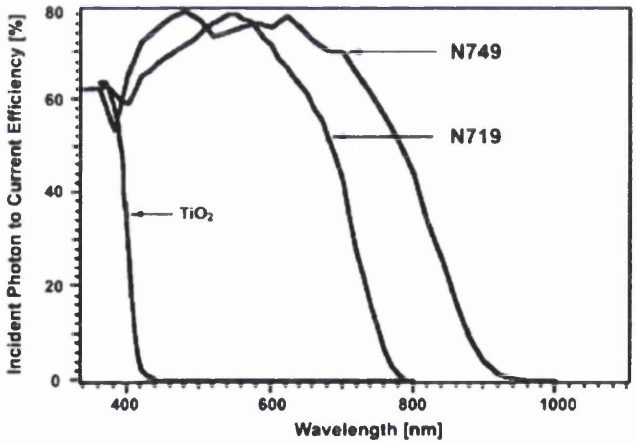

Figure 1.11: IPCE comparison between N719 and unsensitised TiO_2 [71]

The remaining 20% concerns the loss through absorption and reflection by the supporting substrates and transparent conducting oxide (TCO) layer. At the least used wavelengths, i.e. the red light portion of the spectrum from 700-900nm the IPCE is very low or non-existent. However, this can be improved through the inclusion of larger TiO_2 nanoparticles that act as a scattering layer; or through the use of tailored dye mixtures [72].

Grätzel *et al.* suggested a set of ideal properties that a dye sensitiser should possess to attain maximum cell performance [73].

- They should absorb all possible light below a recommended threshold of 900-920nm
- They should strongly adsorb to the TiO_2 surface with minimum external interference
- They need a redox potential that is compatible with the redox electrolyte, to allow easy dye regeneration
- They should be highly stable and be able to sustain operations for *ca.* 20 years

The dyes should exhibit excellent light harvesting performance with these properties, to produce a large photocurrent and thus provide an increase in device performance. The aspect that has direct relevance to this work is the compatibility with the redox electrolyte. In common DSCs, the relationship between ruthenium complex dyes and the high performing iodide/triiodide redox couple is well documented, see Section 1.1.4 further in this text. However, with the advent of new dyes and new electrolytes, in addition to the recent developments in solid state DSC this point bears close consideration. In particular, the redox potential of the dye must reach a high enough positive value with respect to the chosen redox couple to facilitate the efficient reduction of the oxidised dye. This will involve tailoring the HOMO and LUMO dye levels through changes in the structure and choice of groups attached to the molecule [64], [65].

1.1.4 The redox electrolyte

The interaction of the electrolyte with DSC components is the main focus of this study. In a liquid state DSC, it is a critical component as it facilitates the transfer of charge carriers between the working and counter electrodes, so regenerating the oxidised dye molecules. In addition, spacing between the redox potential of the electrolyte and the Fermi level of the TiO_2 controls the V_{oc} of the cell, making the choice of electrolyte a key factor in device performance [19]. The redox potential of this couple must be thermodynamically favourable to the dye sensitiser and have a large diffusion co-efficient.

The solvent of choice is also critical, as this will influence cell kinetics especially when using larger redox species such as large complex ions. A series of key factors were reported in the study by Stanley *et al.*

These should be followed when choosing a high performing electrolyte for a DSC device [74]:

- Low Viscosity Solvent
- Low Volatility Solvent
- Redox couple must be soluble in the chosen solvent
- The redox couple or solvent should not attack the dye sensitiser or other cell components
- The solvent should be non-toxic or exhibit low toxicity
- Low cost of chemicals

The solvent should not be extremely volatile as this will reduce the DSC stability and result in performance degradation over time. However, Papageorgiou *et al.* showed that the fairly volatile solvent, acetonitrile (ACN), and water provide the most facile kinetic performance in a DSC due to their low viscosity [40]. The industry standard solvent in use is methoxypropionitrile (n-MPN), or the variant 3-MPN, which is much less volatile than ACN [75]. Unfortunately, there is a corresponding increase in viscosity which will result in diffusion limitation of the redox species if the spacing between the photoelectrode and counter electrode exceeds 50μm, or the concentration of the I_3^- is too low. There are several further ideal characteristics which can aid in the choice of redox couple for a DSC electrolyte.

The iodide/triiodide redox couple is the most commonly used and until recently, the highest performing redox couple for DSCs [35]. This redox couple consists of I^- ions and I_3^- ion in a suitable solvent, such as ACN or 3-MPN. The transfer of charge from working to counter electrode is facilitated through the reduction of I_3^- ions on the platinum catalyst deposited on the counter electrode and electrons are returned to the dye *via* oxidation of I^- at the working electrode. A key reason for the success of the iodide/triiodide couple is the kinetically slow reduction of triiodide at FTO or bare TiO_2 interfaces, reducing the recombination loss at the electrolyte/conductive substrate interface [76].

This recombination loss can occur in several ways in a DSC device; electrons from the TiO_2 with the oxidised dye; these electrons with the triiodide species in the electrolyte or from the FTO layer to the triiodide [76]–[80]. This last pathway however, is kinetically the least favourable. Though the iodide/triiodide electrolyte has proved to give high performance in liquid based DSCs, it has several major drawbacks, which will unfortunately limit its use. The main issue is that it is highly aggressive and is known to corrode certain metals.

As previous studies have shown, there is a variety of redox couples used throughout the literature, each using different counter-ions and solvents optimised for each couple. A study by Wang *et al.* offered an electrolyte using a disulfide/thiolate redox couple, resulting in an efficiency of 6.4% under standard testing conditions (STC) in addition to exhibiting less corrosive behaviour [81]. Another alternative uses a cobalt based complex, which has gained widespread use in liquid electrolyte based DSCs. A device using this couple has recently set the efficiency record for liquid state DSC devices at 12% using a $Co^{(ii/iii)}$tris(bipryidyl)-based redox couple matched to a specially synthesised zinc porphyrin sensitising dye (YD2-*o*-C8) [35]. A thorough review of alternative redox electrolytes was performed by Yu *et al.* and details several alternative formulations to compare with the traditional iodide/triiodide redox electrolyte [82].

Equations 1.5 to 1.8 below represent the stoichiometric electrochemical reactions that occur in a DSC using an iodide/triiodide electrolyte. This is a multi-step, multi-electron process, aided by slow kinetics of the recombination of electrons injected into the TiO_2 conduction band with the iodide species (I^-) and the corresponding fast reduction of triiodide (I_3^-) at the counter electrode [52].

$$\mathrm{Dye} + h\nu \rightarrow \mathrm{Dye}^+ + \mathrm{e}_{\mathrm{CB}}^- \quad (1.5)$$

$$\mathrm{Dye}^+ + \frac{3}{2}\,\mathrm{I}^- \rightarrow \mathrm{Dye} + \frac{1}{2}\,\mathrm{I}_3^- \quad (1.6)$$

$$\frac{1}{2}\mathrm{I}_3^- + 2e^- \rightarrow \frac{3}{2}\mathrm{I}^- \quad (1.7)$$

$$\mathrm{I}_3^- + 2\mathrm{e}^- \rightarrow 3\mathrm{I}^- \quad (1.8)$$

The above reaction only holds for the standard ruthenium sensitiser used in conjunction with an iodide/triiodide redox couple. There are more exotic sensitising dyes or photoactive structures that can inject more than one electron for the same quantity of photons absorbed [83], [84]. In addition, the reaction will change if alternative redox couples are used. The reaction illustrated in Equations 1.9 to 1.12 are a key examples of this.

Equations 1.9 to 1.11 show a cobalt complex redox couple that operates *via* a one electron transfer from the Co^{2+} species to the oxidised dye and simultaneously the Co^{3+} species is reduced at the counter electrode, as per Equation 1.12 [77].

$$\text{Dye} + h\nu \rightarrow \text{Dye}^+ + e^-_{CB} \quad (1.9)$$

$$e^-_{CB} + \text{Dye}^+ \rightarrow \text{Dye} \quad (1.10)$$

$$\text{Co(II)} + \text{Dye}^+ \rightarrow \text{Co(III)} + \text{Dye} \quad (1.11)$$

$$e^-_{CB} + \text{Co(III)} \rightarrow \text{Co(II)} \quad (1.12)$$

This cobalt complex electrochemical process is summarised schematically in Figure 1.12.

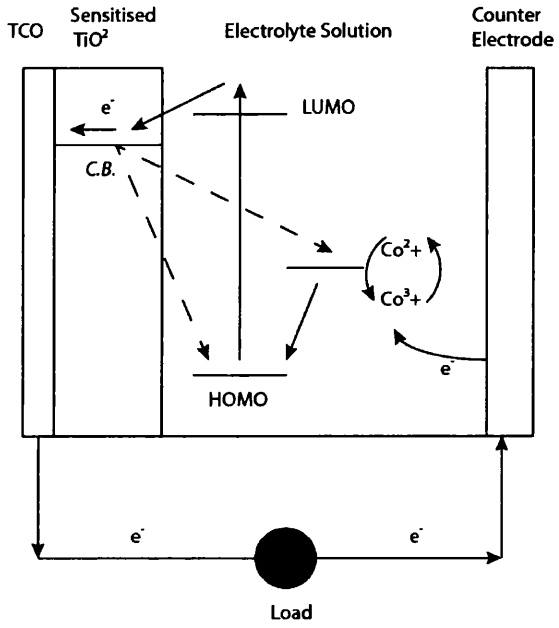

Figure 1.12: Schematic diagram of electron transfers in a DSC using a Co2+/3+ redox couple. (C.B = Conduction band; Co^{2+}/Co^{3+} = redox couple; ----- = Recombination pathways) [85][86]

Nusbaumer *et al.* reported on an efficient cobalt pyridine complex electrolyte to rival the iodide/triiodide based couple [87]. The complex used was bis[2,6-bis(1'-butylbenzimidazol-2'-yl)pyridine]cobalt(II) complex redox mediator in anhydrous ACN/ethylene carbonate (60:40) as the solvent. To create the redox couple, solid $NOBF_4$ was used to partially oxidise *ca.* 10% of Co(II) to Co(III), rather than creating two separate compounds. During this oxidation process, problems were reported where increasing electrostatic binding of the cobalt complex to the TiO_2 occurs as the Co(II) is converted to Co(III). This was shown to inhibit the regeneration of the sensitiser and as a result, reduce the performance of the DSCs. The paper suggested that changing the dye to one with a neutral charge – i.e. one with less carboxyl groups, could produce an increase in current [87]. The cobalt pyridine

complex (Co-(dbbip)$_2^{2+}$) used by Nusbaumer is illustrated in Figure 1.13. Nusbaumer *et al.* used a thin TiO_2 layer treated with $TiCl_4$ to form a thin TiO_2 blocking layer on the FTO substrate and a variety of custom ruthenium sensitizers. Due to the fast outer-sphere, one electron transfer process used by $Co^{2+/3+}$ couples, a compact TiO_2 blocking layer was required in order to reduce recombination loss from the FTO to the electrolyte.

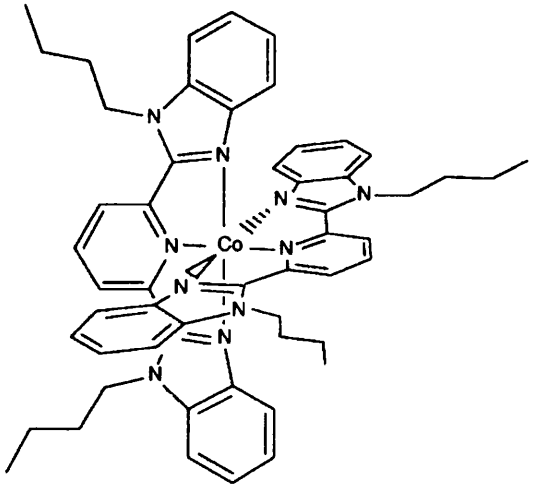

Figure 1.13: bis[2,6-bis(1'-butylbenzimidazol-2'-yl)pyridine]cobalt(II) complex (Co-(dbbip)$_2^{2+}$)

The use of cobalt complex electrolytes was further investigated by Sapp *et al.*, who reported that tailored complexes demonstrated in previous literature were difficult to synthesize, due chiefly to the unavailability of speciality ligands. As a result, Sapp *et al.* constructed their complexes using commercially available ligands [88]. The aim was to synthesise a cobalt complex with performance equal to I^-/I_3^- rather than attempting to create a "hero cell" with very high performance. This study utilised a standard N3-dyed-TiO_2 photo-electrode and compared a variety of catalysts such as Pt, Au and glassy carbon, with the latter two surpassing the platinum catalyst. The paper reported that cobalt complexes could easily be synthesised using widely available commercial compounds and then matched with standard DSC components in order to give a stable device. This should provide many advantages such as non corrosiveness, low volatility and low light absorbance when illuminated through the counter electrode.

Each of the previous literature sources investigated a pyridine type complex, though it was remarked by Sapp *et al.* that the cobalt complexes are amenable to tailoring into other structures through the use of different ligands [88]. A bipyridyl-type complex, rather than a pyridine complex was analysed by Klahr and Hamann and covered the methods by which DSC performance would be affected when using cobalt complex electrolytes [85]. The

positive conclusion was that, to their knowledge, DSCs using cobalt mediators are not limited by dye regeneration, though they are restricted by recombination kinetics, which will reduce the IPCE of cobalt based electrolytes.

The use of different redox mediators has thus far focused on obtaining comparable performance to that of the iodide/triiodide electrolyte. This target was surpassed by Yella *et al.* through the use of a custom designed zinc porphyrin dye (YD2-*o*-C8) in combination with a $Co^{(II/III)}$tris(bipyridyl)-based electrolyte [35]. This configuration resulted in a record efficiency of **12.3%**, though it should be noted that this was through the use of a co-sensitised film with both YD2-*o*-C8 and Y123 dyes. This setup increased the absorbance across the visible spectrum and obtained an IPCE (450nm-680nm) of over 80%. However, there is a slight reduction at 530nm (green) which was then covered through the co-sensitisation treatment. The J_{sc} achieved was 17.3mA/cm^2, which is much higher than the 11-13mA/cm^2 normally expected for the ruthenium sensitised, iodide/triiodide based DSC. The paper states that the performance difference stems from the high voltage loss attained in iodide/triiodide based cells during dye regeneration.

A further issue to consider when utilising the cobalt based complex, or any outer sphere one electron redox species, was how the structure of the dye affects device performance. Adding long chain molecules causes the inhibition of the electrolyte access to the TiO_2 surface – thus reducing the recombination rate and increasing performance [89]. This study utilises four octyloxy groups attached to the dye molecule. The combination of a custom dye with the cobalt sensitiser allows large V_{oc} of over 0.8V to be obtained; this is due to the high reduction potential of the Co complex compared with I_3^-. The custom dye also results in a larger overall light harvesting efficiency (LHE), therefore increasing the photocurrent and resulting in higher cell efficiencies.

Due to the bulky nature of the cobalt complexes compared to the standard iodide/triiodide couple, the mass transport of this couple has become an issue, resulting in increased recombination losses and slow dye regeneration. Several authors have endeavoured to study this aspect of electrolyte development in order to better understand and improve upon this type of redox couple. Kim *et al.* submitted a study on improving the mass transport of cobalt complexes in DSCs, by changing the TiO_2 nanostructure [90]. This study focused on increasing the porosity of the TiO_2 film rather than changing the dye or cobalt complex structure. The results obtained showed a definite improvement in DSC performance when a thin 6μm TiO_2 film with porosity around 60% and a pore size of *ca.* 24

nm is used, rather than a thick film with smaller pores and lower porosity. It should be noted that, despite the lower level of adsorbed dye for the more porous film, the performance, in particular the J_{sc}, still shows a considerable increase. This was attributed to the enhancement of mass transport for the bulky electrolyte, which as a result will enhance the dye regeneration rate.

Despite the milestone reported by Yella *et al*, this was only achieved through custom synthesised critical cell components, the dye and electrolyte [35]. In comparison, the paper by Liu *et al.,* reported a study of cobalt mediators with common ruthenium based dyes, in the form of the sensitizers N719 and Z097 [91]. This study uses EIS and *in-situ* NIR transmittance measurements to explain the difference in performance exhibited between two Ru-based dyes using the same Co-based electrolyte. DSC performance for the Z907 & Cobalt electrolyte is: J_{sc}=14mA/cm^2; V_{oc}=0.74V; FF=62% and η=6.5%. The N719 & Cobalt electrolyte give much lower results: J_{sc}=3.8mA/cm^2; V_{oc}=0.62; FF=76% and η=1.8%. In comparison, the efficiency for the Ru dye combined with the standard I^-/I_3^- is 7.7% for Z907 and 8.0% for N719. The main conclusion obtained here is that N719 & I^-/I_3^- performs better than Z907 & I^-/I_3^-, and that the reverse is true when using a Co-complex redox mediator. The study builds on the work reported by Felt *et al.* and Yella *et al.* which suggested that the bulky dye structures, such as the alkyl chains found on the Z907 dye would reduce recombination and so improve performance. The nonyl chains attached to the Z907 dye increase the electron diffusion length "L_n", shown by EIS measurements, which is explained by the study as a sign of inhibited recombination, rather than faster electron transport through the device. When using a one-electron outer-sphere redox mediator such as cobalt (II/III), inhibited electron recombination is a crucial factor, as previous works have shown the recombination time to be fast in comparison to that of the I_3^- species [92][93].

The reasoning behind the introduction and development of the cobalt redox couple was because it is composed of less aggressive species than the iodide/triiodide electrolyte. As a result it lends itself for study on metallic substrates cells for possible roll to roll line manufacturing. This work will analyse a particular cobalt complex, tris-(2,2'-bipyridine)cobalt(II/III) di(hexafluorophosphate) or $Co(bpy)_3(PF_6)_n$ in order to discover how it interacts when in contact with industrial metal substrates.

1.1.5 The counter electrode & redox catalyst

The counter electrode or DSC cathode forms the interface with the electrolyte where electrons are returned from the external surface. This usually consists of a conductive substrate such as FTO glass, ITO PET or a metal that is covered with a high specific area catalytic material, with its performance tailored to the choice of redox electrolyte. A catalyst is needed to enhance electron transfer across the interface, and to reduce overpotential and resistive losses at the counter electrode. The original catalyst use in the 1991 paper is not mentioned. However, further work has reported the use of a 2μm thick mirror layer of sputtered platinum as the catalyst material and to reflect back light from the counter electrode and increase the light harvesting capacity of the cell [94].

Further improvements to this device involved the use of a nano particulate structure for the catalyst, which so far, has produced the highest performance in catalysing the reduction of triiodide. The first nanostructured Pt catalyst for DSCs was introduced by Papageorgiou *et al.* who reported a thermally decomposed Pt nanocluster catalyst formed through the thermal decomposition of a 5mM chloroplatinic acid solution at 385-400°C [40]. The presence of this catalyst shown to be vital, as the study by Suzuki *et al.* showed, producing a DSC cell of 0.1% efficiency when bare FTO/glass was used as the substrate [95].

There are several application methods for this catalyst material, with the most stable and consistent being the previously reported thermal decomposition method. However, with the drive towards cheaper materials and mass production, there is a need to find low temperature alternatives to allow the use of polymeric substrates to act as a counter electrode, especially for industrial metal working electrode cells, where the counter electrode acts as the top-sheet of the device. To that end, there have been many reported methods in literature focused into three main groups: Chemical, electrochemical and vacuum methods.

Chemical platinisation uses the chemical reduction of a chloroplatinic acid precursor to deposit the platinum nanoparticles, though due to the chemical reaction involved, precise control of the deposit will be issue. Several reducing agents can be utilised, though sodium borohydride is the most commonly used in the platinisation of counter electrodes , though with this reducing agent, the boron constituent can result in the poisoning of the DSC if it remains on the counter electrode [96], [97]. The reduction process was explained by Sheppard *et al.*, with the main advantage of this reduction pathway being that it operates at low temperature suitable for the platinisation of polymeric counter electrodes [98]. The

main DSC studies to utilise this method were Park *et al.,* Jun *et al.* and Kang *et al.*, reducing chloroplatinic acid with 60mM sodium borohydride [99][100][101]. Of particular interest was the comment by Jun *et al.,* stating that chemically applied Pt was found to be unstable, giving poor adhesion to the substrate, compared to the high temperature thermal Pt method on glass [100]. Furthermore, the chemical reduction method would require large quantities of hazardous reducing agents, which in an industrial setup would increase the cost and effort required, in addition to adding large quantities of hazardous chemical to the production line.

A different method, one utilising D.C. magnetron sputtering has also gained attention, due to the high performance and stability of the deposited catalyst and the speed of manufacture. Unfortunately, this method suffers from several shortcomings when considering large scale production, requiring vacuum conditions, the equipment of which is expensive to setup and maintain. In addition, the equipment geometry is limited which affects the size and shape of the work piece – so not a particularly viable solution for mass production processes. However, the advantages of this process are fine control of the deposit and low contamination issues with the counter electrode, due to the vacuum environment and the pure Pt source used for the process. DSCs utilising this method have shown good performance when compared to the thermal Pt catalyst, though it is dependent on the layer thickness of the coating [102]. One of the critical findings when comparing the sputtered, chemical and thermal methods, was that each resulted in a different structure with varying performance [103], [104]. This is a crucial factor that must be investigated when analysing the platinisation methods developed in this work

Electrochemical deposition is the main focus of Chapters 3&4, in the hope of producing a viable low temperature, low cost and fast deposition process for use on FTO glass substrate. The intention is to develop a method that could be transferred onto conducting polymer substrate. Chapter 1.3 covers the background of electrodeposition and its usage as a viable technique for use in DSC devices and will summarise current research into this area of study. A previous study has compared the chemical, thermal and sputter deposited Pt catalysts in more detail [105], showing the current electrochemical superiority of the sputtered coating at 0.5nm and illustrating the material reduction and robustness compared with the more common thermal and chemically applied catalysts. Unfortunately, the sputtered Pt method has drawbacks when industrialising the process due to is requirement for vacuum conditions. The next section illustrates several areas that require development for industrialisation of DSCs to become a reality.

1.2 Industrialisation of dye sensitised solar cells

The scale up of laboratory devices with an active area of mm^2 to cm^2, to modules and panels in the m^2 range is an important area of research, and so far has only proved possible and commercially viable for high efficiency silicon and thin-film technology solar panels commonly found on building roofs. Of additional value is decreasing production times from the hours/days per cell in lab scale processing, in order to obtain a commercially viable product. The production process can be separated into its constituent parts in order to optimise the stages for in line processing. Figure 1.14 shows the breakdown and timescale of a typical lab scale DSC construction cycle with general timescales.

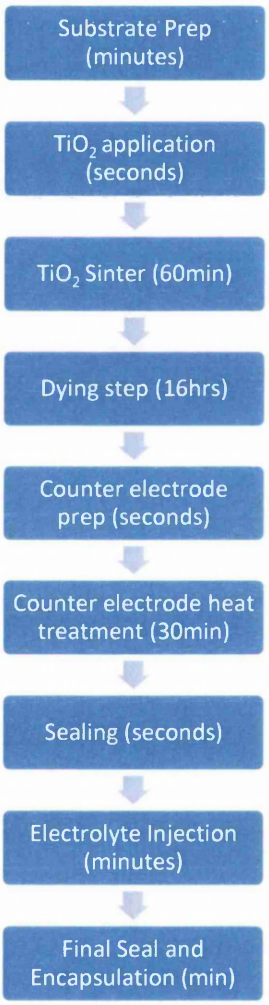

Figure 1.14: DSC manufacturing process and typical process times

The main hindrance to a fast production process is the sixteen hour dying time required to fully sensitise the TiO_2 layer. Recently, there have been several studies that investigated the dyeing process, uptake and sensitisation time. A study by Watson *et al.* studied two techniques for assessing dye uptake *in situ*, rather than using destructive testing methods

to analyse the cell, allowing for a rapid assessment of individual cells, and possible for in line quality control for eventual continuous processing lines [106]. Further studies regarding the dye loading of sensitised TiO_2 were undertaken using spectroscopic analysis, showing variation in dye loading with immersion time from seconds to 24 hours [107]. This study showed that 5 hours was sufficient to see a change using a typical immersion technique, rather than the longer times used in other reports. Recent studies by Holliman *et al.* assessed the ultra-fast sensitisation of DSCs, whereby the dyeing time was reduced from the typical 16-24 hours to 5 minutes using a pumped dye method. This resulted in DSCs with no recorded performance loss compared with the cells dyed for 18 hours [108]. A further study supported this result, with rapid dyeing in 5 minutes, and showing the performance gain in using multiple dyes to facilitate the absorption of more of the solar spectrum, thus increasing $1cm^2$ test cell efficiency to 7.5% [72].

A second production bottleneck is the TiO_2 sintering stage, taking 30 minutes for sintering, with an additional pre and post 15 minute treatment at a lower temperature (250°C) in order to remove the solvent and reduce the thermal shock to the substrate. A further 15 minutes at 250°C is also required post-sinter to allow the substrate to cool thus reducing thermal shock and damage to the sintered TiO_2 particle network. Reducing sinter time and temperature has garnered much interest ever since the inception of the DSC device by Grätzel. Several studies have shown that low temperature deposition of TiO_2 is possible, though the particle adhesion to the substrate and interconnectivity of the mesoporous network is much lower than for the high temperature sinter. These lead to a photoelectrode with much lower performance. A recent study has shown the potential of NIR as a method for rapidly sintering the TiO_2 in 12.5 seconds, reporting comparable performance to that of traditional 450°C TiO_2 cells [62].

The platinised counter electrode preparation stage will add a further 30 minutes to the manufacturing process, due to time needed for the decomposition of chloroplatinic acid to platinum, and for the platinum to form stable strongly adhered nanoclusters [109]. Temperature and time are critical in this case, as the counter electrode envisioned for mass produced DSCs are constructed from conducting polymers that are temperature sensitive and cannot withstand the standard thermal deposition temperature of 385-400°C for platinum catalyst deposition [40]. As a result, several alternative catalysts were studied, with examples such as PEDOT:PSS and several metal carbides and nitrides at the forefront of the investigations [110]–[112]. Due mostly to the early stage of this research and the

already established nature of the Pt catalyst, it was decided to use platinum as the focus catalyst of the study in Chapters 3 & 4.

Different forms of deposition have also been compared, in order to reduce the temperature and decrease the amount of platinum used in each cell. Several of these, such as chemical reduction and sputter deposition, have been widely reported in the literature and also studied in previous work [105]. Further to this, there have been investigations into the rapid thermal decomposition of the chloroplatinic acid precursor solution using near infrared radiation (NIR). This heats the FTO or ITO conductive layer on the glass or polymer substrate, causing the thermal deposition of the Pt particles [113].

In this thesis, the primary focus is alternative low temperature platinisation techniques using electrodeposition. This method is already in use commercially for the application of metallic coatings on metal sheets, such as galvanisation, in addition to the production of electronics components, particularly in battery manufacture. Our interest is in the availability of large electrolyte tanks used in previous roll to roll coating processes, such as galvanising. These are set up in such a way as to have high potential for adaptation to large scale electrochemical platinisation. If successful, the technique could pave the way for the production of polymeric counter electrodes for flexible dye sensitised solar cell devices.

1.2.1 Building Integrated Photovoltaics (BIPV)

One of the main goals behind the need for scaled up devices is the growing popularity of building integrated devices where the power or heat generation is integrated into the architecture of the building. In the case of building integrated photovoltaics (BIPV), higher efficiency panels mean that for the same area, more power is generated, or that less panel area is needed to produce the required power [42]. In addition, the integration of PV with building architecture should reduce the balance of system (BOS) that is the supporting, strengthening and connecting materials that are needed for conventional solar systems. BIPV was mentioned by Grätzel *et al.* as one of the main areas of application for DSC devices [52]. The scale up of DSC manufacture, both glass-based and flexible, is taking place on an international scale. Germany has several projects, known as ColorSol and InnoCo, that are focused on the large scale production of glass DSC devices, with the aim of module development for facades and PV windows [114].

Oliver *et al.* focused on the evaluation of BIPV in terms of economic analysis and compares it to conventional energy sources [115]. They report that, at the time of writing, PV energy supply had significant environmental benefits, but the economic cost of PV was much

higher than other energy sources. BIPV does reduce this cost somewhat, as long as there is a reduction in the supporting systems required. They also conclude that BIPV would be come more economically viable due to the dynamic nature of the PV industry as new technology becomes available. Jelle *et al.* reviewed the current state of the art of BIPV, including work on all forms of PV panel such as silicon, windows, foil PV and summarising the manufacturers involved [116].

Printed or thin film solar panels are ideal for BIPV, as they are generally flexible and easy to apply to existing buildings. Furthermore, due to the use of flexible materials such as sheet metal and polymers, the cells weigh much less than conventional devices, allowing them to be used without the need for large scale reinforcing of the roofing. These thin film devices are also much lower in cost than conventional bulk material devices, due to a reduction in both the material required purity [117]. It is the development of metal/polymeric solar cells that this study is intended to facilitate, in order to make roll to roll produced DSCs a reality.

1.2.2 Requirements and stability

When constructing liquid state-DSCs for commercial applications, there are several criteria that should be adhered to in order to produce viable devices. Those listed here are adapted from thin film cell criteria:

- Thermal stability. Including cycling, humidity and light soaking (1000hrs)
- Mechanically robust to withstand exposure and processing
- Chemically stable to avoid performance and material degradation
- Life time of *ca.* 20 years to match building roof or 10^8 redox turnover events [118]

Since solar cells are exposed to the elements on building roofs or walls, they need to be stable for a set period of time to be economically viable. Kato *et al.* achieved an improvement in DSC stability by utilising a solvent free electrolyte. This will reduce the vapour pressure in the liquid state DSC devices in addition to removing the degradation susceptible solvent from the cell [119]. Their conclusion stated that the resulting cell would be stable for an estimated 15 years outdoor usage. Further negative effects were found to be influenced by the quantity of water in the electrolyte. Sinke *et al.* reported that the inclusion of a nitrogen containing heterocyclic has a positive effect on stability through the protection of the cells from the destructive effects of water on the dye sensitiser, in addition to suppressing recombination [75].

Liquid state DSCs require a seal between the counter and working electrodes, this also acts as a separator, with the electrolyte injected into the resulting 25μm or 50μm cavity. This seal is based on a thermosetting polymer, commonly Surlyn or Bynel, from DuPont. This seal must provide a barrier against moisture ingress from the outer environment and also attack from the electrolyte (solvent or redox couple). Furthermore, it must be a good enough seal to withstand the change in vapour pressure as the device warms and cools in its daily operational cycle. Glass frit, a low melting point glass that is used like solder, can also be used as a sealant and separator for glass based devices [120], [121]. This type of cell was reported to be more durable and increased cell stability. Unfortunately, it will be difficult to use in flexible cells or in roll to roll fabrication.

A particular danger is from the degradation of DSCs through long term exposure to outdoor conditions such as temperature extremes, UV radiation and intense periods of illumination. The study by Pettersson *et al.* indicates that encapsulation and cell protection are critical requirements for the reproducible manufacture of DSC devices [122]. The study also acknowledged that the modules required a UV filter when outside to avoid degradation. Following this Hinsch *et al.* reported the use of an MgI_2 addition to the electrolyte which acts as a stabiliser by either faster hole reduction by iodide, or the formation of MgO as a surface layer to prevent unwanted side reactions. In addition, this study also used UV filters to enhance cell stability [120]. Carnie *et al.* reported that DSCs exposed to UV-A radiation failed within 400 hours due to the photocatalytic oxidation of the triiodide on the TiO_2 photoelectrode [123]. However, this was shown to be preventable through the use of a UV filtering top sheet, though a corresponding loss of efficiency was reported [124]. Cell stability is a critical issue to consider when constructing DSCs, especially when attempting the scaling up the process from lab devices to a roll to roll or large scale batch process. Any measures needed must be able to be processed or easily included in the device or they will drastically increase cost and materials usage.

The substrates used for both the working and counter electrode must be able to withstand varying environmental conditions, such as changes in temperature and humidity. The substrates must also be stable when in contact with the liquid electrolyte and other cell components. Certain metals, such as iron, are susceptible to corrosion in the electrolyte, and several polymers have been found to degrade following prolonged contact with electrolytes or exposure over time to UV light [125].

It was reported that the platinum nanoparticle catalyst was vulnerable to dissolution in the iodide/triiodide based electrolyte. Papageorgiou *et al* reported that electrochemically deposited Pt is prone to dissolution in iodide electrolyte, a finding of interest to this study due to the focus on electrodeposition of Pt in Chapters 3 and 4 [109]. This finding was explored further by Olsen *et al.* who reported on the stability of vapour deposited Pt on FTO-Glass [126]. They suggested that the dissolution of Pt through the formation of PtI_4 compounds was thermodynamically favourable. Interestingly, the study showed that only the vapour deposited Pt, rather than the solid Pt wire showed dissolution activity, leading to the conclusion that the deposition technique has an influence on the stability of the catalyst. Furthermore, the thermal Pt deposition reported by Papageorgiou *et al.* also reported high stability in the DSC electrolyte. It is critical then, that care must be taken in the choice of deposition and production of counter electrodes for commercial DSCs, as failure will drastically reduce cell efficiency and, lifetime.

The performance of the counter electrode can be studied through EIS characterisation, or cyclic voltammetry assessment of the counter electrode limiting current density. The degradation reported by literature was thought to be caused by poor adhesion of Pt to the conductive substrate and further problems could also be caused by the transport of loose Pt to the working electrode, causing sites of increased recombination loss.

1.2.3 Processing methods

Laboratory scale devices are normally constructed using a batch process and high temperatures to gain the best possible performance per device. However, this is not suitable for industry since batch processing is costly and limits the quantity of product per run. The most viable mass production process which could be used for thin film solar cells, such as CIGS and DSC would use roll to roll production, where flexible substrates such as metal sheets and polymers are coated with the required material on a continuous processing line.

A roll to roll manufacturing line is a highly controllable processing method, with each process stage optimised to give consistent performance [127]–[129]. This should allow for a high productivity process with much lower capital costs than the batch process used for bulk material or rigid solar cells. Typical coil coating processes run at up to 1000m/min for activities such as hot or cold rolling. A galvanising line will typically run at 200m/min and a coating line at 150m/min. If this is adapted for manufacturing DSC many factors need to be accounted for, such as dwell times between each stage, either for sintering, drying or dying

times depending on the process step. Flexible materials are preferred for mass production, as they will enable the use of a coil line, in addition to weighing less than the glass substrate typically used in DSC devices. In a BIPV system, the weight is a critical factor so as to not stress the building architecture or require extensive balance of system (BOS) expenditure to support it. Furthermore, flexible substrates allow the PV system to conform to the structure of the building, improving the appearance of the structure and allowing for varying architectural choices.

1.3 Electrochemical deposition

Electrochemical deposition, also known as electrodeposition or electroplating, is a versatile technique that uses an imposed current to deposit metal, from an electrolyte containing metal ions, on the surface of a substrate. This is a potentially low cost method for platinisation, as it will enable control of material quantity through careful optimisation of electrical parameters and electrolyte concentration. It also will avoid the high temperatures, vacuum conditions or reducing chemicals necessary for other common platinum deposition techniques. When considering the electrodeposition methodology, there are two type of electrochemical cell in use for lab based experimentation. These cells can be a variety of sizes or shapes, as long as there is provision for electrical contact to the work piece and an appropriate counter electrode to complete the circuit. The simplest form is a two electrode cell, containing an anode and a cathode which is connected to a potentiostat, Figure 1.15.

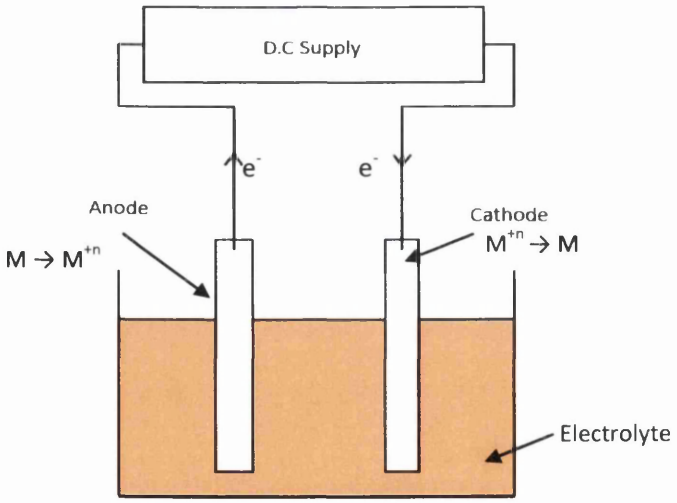

Figure 1.15: Diagram of a basic two electrode electrochemical cell

The electrodes are placed into an electrolyte solution containing a source of the required metal ions and an inert supporting electrolyte to minimise the Ohmic drop during

deposition and counter the depletion of metal ions as the deposition progresses [130]. The supporting electrolyte provides a source of ions to combat any IR drop during the process, chosen so that it takes no active part in the deposition process. The potentiostat provides the impetus for the reaction, or acts to negate any electrolyte reactions between the electrodes and the solution. In some cell set ups, the anode dissolves into the electrolyte solution to keep the concentration of ions constant.

The other type of deposition cell introduces a third electrode commonly known as a reference electrode. A reference electrode normally contains an ionic solution that is separate from, but ionically connected to the deposition solution [131]. This is placed near to the working electrode in order to give a localised, accurate reading of the cell potential, Figure 1.16.

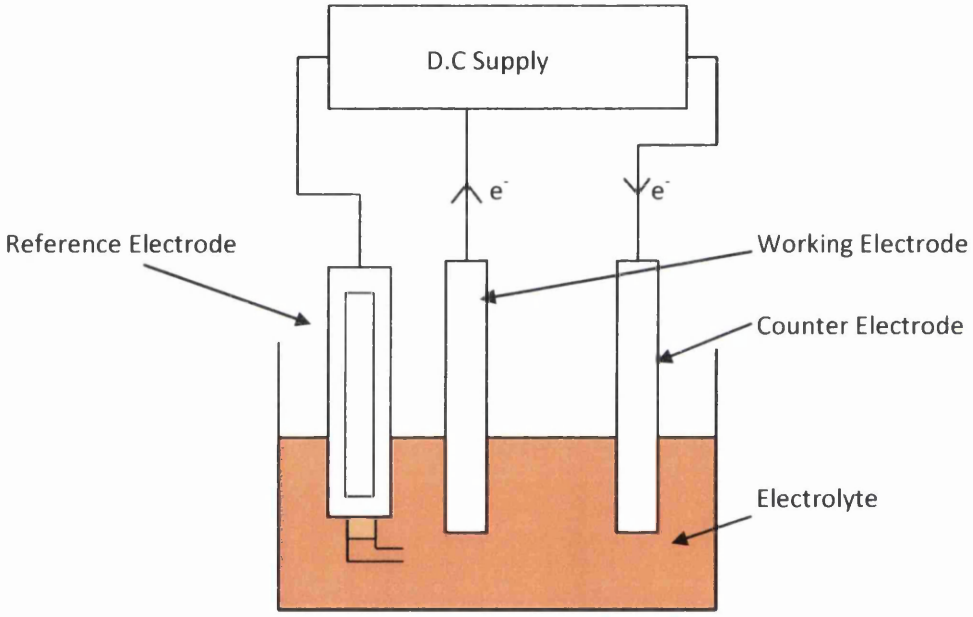

Figure 1.16: Three electrode electrochemical cell set up

The most common reference solutions are the Calomel electrode or an Ag/AgCl system. A three electrode cell is much more controllable than a two electrode set up as it allows for a more reliable reading of the solution potential and conditions.

1.3.1 Supporting electrolytes

In an electrochemical solution, a supporting electrolyte is used to increase the conductivity of a solution. The ionic species it contains should not be electroactive in the conditions used for the experiment and usually has a larger ionic strength than the active species in

solution. They are also used to eliminate the transport of the electroactive ions through migration in the electric field.

1.3.2 Electrochemical solutions

In an active electrochemical solution, the charge difference between the electrodes will form a distribution of ion charge throughout the solution. This takes the form of a gradient, with the largest concentration being adjacent to the electrodes. In this way, an electrode acts similar to a capacitor, as when the electrode potential changes, the amount of charge stored at the electrode/electrolyte interface also changes. However, this will not happen instantaneously due to the solution having an intrinsic resistance. Therefore the electrolyte/electrode interface can be represented as a resistor and capacitor in parallel. The situation at this interface is known as a double layer that includes the double layer capacitance (C_{dl}) and the solution resistance (R_D), and there have been several models developed to explain this.

The basic model is known as the Helmholtz model, where the ions in solution form a monolayer at the electrode surface, which equally balances the charge on the electrode, Figure 1.17. The double layer capacitance here is independent of the applied potential.

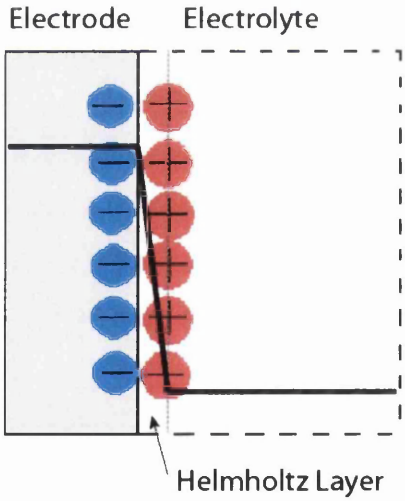

Figure 1.17: Helmholtz model of the electrochemical double layer. Solid black line indicates the steep potential distribution from the electrode to the solution

The Helmholtz model predicts that the entirety of the potential is reduced in the monolayer of ions at the electrode surface, with no residual potential in the bulk electrolyte. The next model, the Gouy-Chapman model, increases the complexity from a simple surface monolayer of ions, to a random atmosphere of ions at the electrode surface, Figure 1.18. Closer to the surface of the electrode, the atmosphere, i.e. the concentration of oppositely

charge electrodes is higher and the concentration of similar charge to the electrode is much less. As the distance from the electrode is increased, the reverse is true.

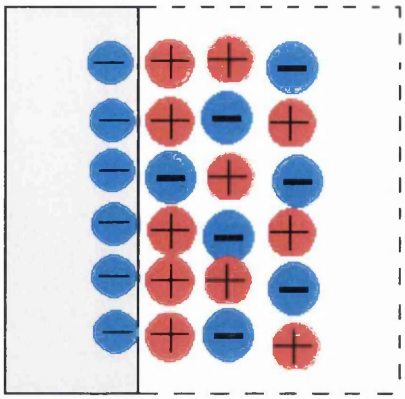

Figure 1.18: Gouy-Chapman model of the double layer (Grey=Electrode, White=Electrolyte)

The third model is known as the Stern model, Figure 1.19, which explores the middle ground between the extremes of the Helmholtz and Gouy-Chapman models. This model proposes that most of the charge on the electrode is balanced by the Helmholtz layer, while the remainder is taken by the diffuse layer theorised by the Gouy-Chapman model.

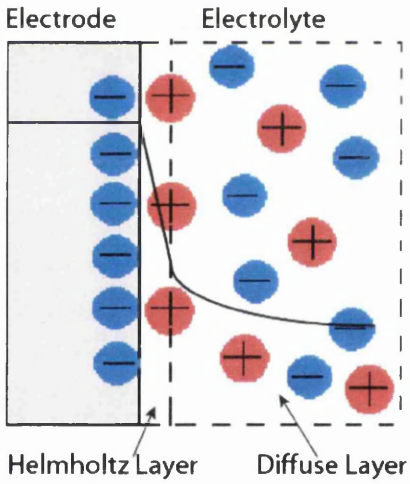

Figure 1.19: Stern model of the double layer, with solid line indicating potential distribution

There is a fourth model known as the Grahame triple-layer model. This final refinement includes species specific behaviour, where ions in solution will have different sizes and strengths, so introducing chemistry into the model of the electrode/electrolyte interface. The ion specific behaviour is dependent on the condition of the anions. If these are dehydrated, they can move close to the electrode surface, the degree of dehydration will control the type of interaction. If fully dehydrated, then short range bonding forces will dominate in addition to the expected electrostatic forces. In Figure 1.20, this difference in

bonding distance is represented by the inner and outer Helmholtz planes added to the Stern model [131].

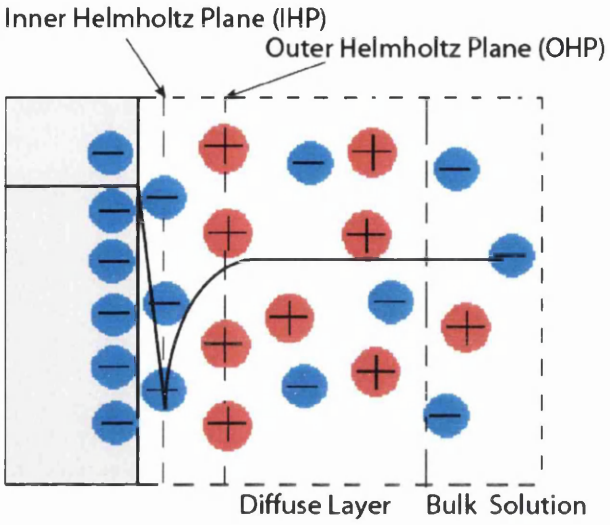

Figure 1.20: Triple layer model of the electrode/electrolyte interface

Modelling the behaviour at the electrode surface is crucial when considering surface processes such as catalysis and electrodeposition, in addition to unwanted processes such as corrosion. These models also illustrate how the conditions in a solution or electrochemical cell will change its behaviour through the movement and placement of ions.

1.4 Electrochemical control

Deposition control is achieved by applying a controlled current or potential difference between the working and counter electrode. This can take the form of a constant value, a pulsed or oscillating waveform or another specified profile. Simple waveforms include pulsed, square wave, sine etc. More complex forms include pulse reverse, where the amplitude of the first pulse is reversed for the second pulse and so on. There are other types, where a short high amplitude pulse is superimposed onto a background waveform. It is one of these pulsed waveforms that forms the basis of the method used in Chapter 4. The most common type used in industry is a pulsed waveform, an example of which can be seen in Figure 1.21.

This wave profile has been previously used in DSC and fuel cell research to deposit catalytic materials such as platinum, resulting in a variety of depositions [132]–[135]. Ayyadurai *et al.* produced deposits of varying agglomeration, depending on the chemical wetting agent added to the deposition solution [133]. Comparatively, Ye *et al.* produced spherical clusters

to 100-200nm crystal aggregations depending on the solution utilised [132]. However, in each of these methods so far, the Pt deposits have been discrete and spherical, rather than dendritic or layered, both of which would decrease the surface area of the catalyst. Chandrasekar *et al.* investigated several pulse deposition types, reviewing the advantages and disadvantages of each [134]. In particular, the report stated that the pulse current methodology would produce fine grained structures, which would be advantageous for a catalyst.

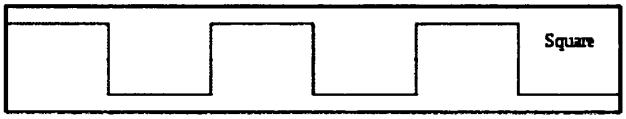

Figure 1.21: Example of a pulsed square waveform

In assessing the literature, it was seen that the pulsed waveform was thought to increase control over the deposit formation through the accurate tailoring of deposit quantity. In addition, it also allows the control of solution charging to enable the replenishment of the ion layer adjacent to the work piece and so avoiding areas of low ion concentration during deposition.

Once the wave profile has been determined, the potential or current to be applied will depend very much on the material to be deposited. This value can be found using the half cell potential of the material or by analysis of the deposition solution by cyclic voltammetry. The cyclic voltammetry scan, run from rest to positive and negative points will determine the electrochemical behaviour of the solution on the work piece material and will assist in optimising the values for the deposition run. Cyclic voltammetry analysis of a deposition solution is explained further in Chapter 2.2.3. Previous literature has shown that platinum is favourably deposited at -0.6V, which provides a starting point for the studies in this work [103].

1.4.1 Pulse width

The pulse width is defined by the t_{on} and t_{off} values and controls the shape of the deposition waveform and as a result has a serious impact on the nucleation and growth behaviour of the deposit. Longer t_{on} values will increase the deposit size and general morphology. In the case of a platinum catalyst, a small deposit size is recommended to maximise the surface area, therefore a short pulse (t_{on}) should be applied. Typical values for t_{on} in the literature are: 100-600ms [136]. The t_{off} time, or the time for which the applied current/voltage is

zero or at open circuit (OCP) is also of critical importance. The schematics in Figure 1.22 and Figure 1.23 display an example of different t_{on} and t_{off} lengths over the deposition cycle.

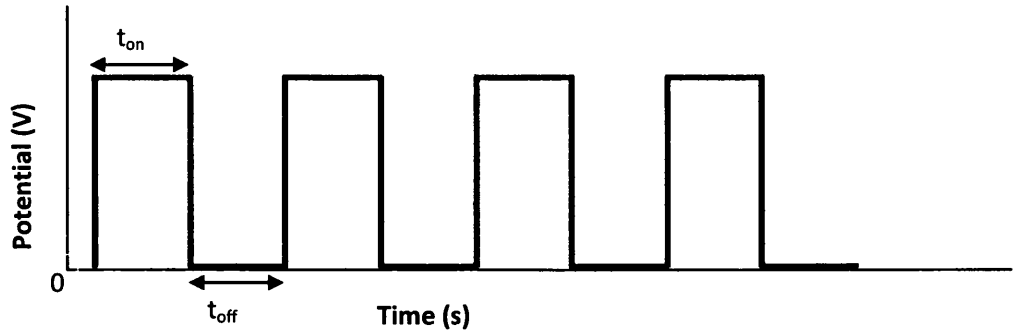

Figure 1.22: Cycle using a long t_{on} and t_{off} time

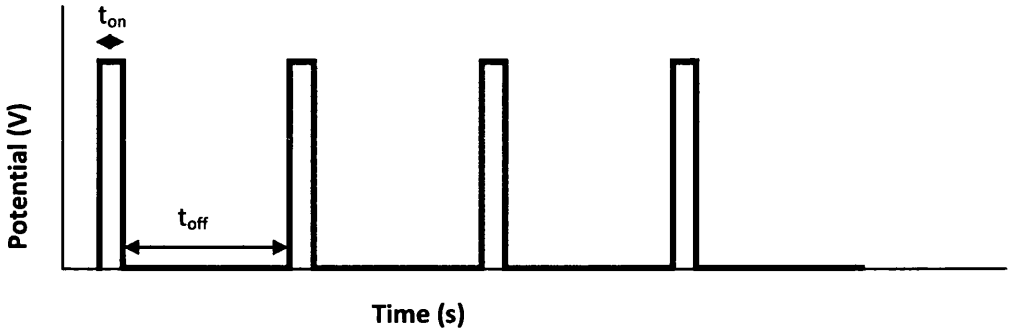

Figure 1.23: Cycle using a short t_{on} and a long t_{off}

As a current is applied to the work piece, an electrical double layer is charged adjacent to the surface, restricting the flow of metal ions to the work piece from the bulk solution. As the metal ions in the diffusion layer are depleted, the current density decreases and the deposit characteristics change. The t_{off} period allows for full or partial discharging of this layer, permitting the uninhibited passage of ions on the next deposition cycle [137].

1.4.2 Duty cycle

This is the percentage of total time of a cycle and is a rate determining step in pulsed electrodeposition [138]. Equations 1.13 - 1.14 below show the relationship between the t_{on} and t_{off} times, where *f* is the frequency and is given by 1/t, the reciprocal of the cycle time:

$$Duty\ Cycle = \frac{t_{On}}{t_{On}+t_{Off}} = t_{On}f \qquad (1.13)$$

Therefore:

$$Frequency = \frac{1}{t_{On}+t_{Off}} = \frac{1}{t} \qquad (1.14)$$

When the duty cycle is 50%, the t_{on} and t_{off} times are equal, changing the ratio of t_{on} to t_{Off} affects the pulse profile, and as a result will affect the resulting deposit. It was reported by several sources that the duty cycle has a large impact on deposit structure as the T_{on} time controls the nucleation and growth stage, and t_{off} influences diffusion and dissolution stages [139].

1.4.3 Temperature

Changing the temperature of the electrolyte will change its conductivity by making the solution less viscous. The ions in solution will have more energy and find it easier to diffuse to the work piece. This usually increases the speed of deposition, decreasing the pulse amplitude and duty cycle needed. There are varying examples in the literature of the temperature of deposition; there are a range of temperatures used dependent on the deposition solution – the most common and economic temperatures are in the range 25°C to 45°C.

1.4.4 Solution concentration

The concentration of the solution controls the quantities of ions available for deposition in solution. This will control the limiting current of the solution and the current density. However, this also depends on the area of the work piece and the applied current/voltage. Widely varying solution concentrations have been reported in the literature for use in DSC devices: 5, 10, 20mM [140]–[142]. The reviewed papers all use a form of aqueous chloroplatinic acid, with different additions or supporting electrolytes. Increasing the concentration of Pt ions in solution will result in variations in the deposit morphology or allow the reduction in applied potential, as more ions are available to deposit over time in high concentration solutions than low concentration. In addition, the formation of low specific area dendritic structures is reduced in high concentration solutions, as the concentration gradient from the electrode to the bulk solution will remain shallow for a longer period during the deposition activity.

1.4.5 Solution components

Aside from the desired compound or metal to be deposited, there are several other components that can be added to the electrolyte to influence the deposition behaviour and morphology. A simple change reported by Chen *et al.* was the choice of aqueous or non-aqueous solution, where an aqueous solution led to larger particle formation [142]. As a result of this, care should be taken to control the potential so that the deposit size is

decreased. Physical control additives such as viscous inert surfactant, i.e. Triton-X or poly(ethylene glycol) (PEG) can be used to control the rate of diffusion and the pattern of the deposit [38, 50]. Chemical control additives such as lead acetate, acids or supporting electrolytes are used to change the conditions under which the metal ions will deposit [144]. Wetting agents in particular are favoured additions, Ayyadurai *et al.* reported that the introduction of wetting agents to a solution $[PtCl_6]^-$ aided and accelerated the reduction of the ion to Pt metal [133]. The result was uniformly distributed spherical particles through the production of more nucleate Pt and the suppression of Pt particle growth. Supporting electrolytes are used to increase the conductivity of the electrolyte solution by adding an inert species into the solution which takes no part in the occurring reactions, this effectively eliminates the ohmic (IR) drop that occurs due to solution resistance [145].

1.4.6 Electrodeposition of platinum from chloroplatinic acid solution

Feltham and Spiro presented a mechanism by which platinum is electrodeposited from chloroplatinic acid solution, summarised in Equations 1.15 to 1.17 presented below [146]:

$$Pt^{4+}Cl_6^{2-} + 2e^- \rightleftharpoons Pt^{2+}Cl_4^{2-} + 2Cl^- \quad (1.15)$$

$$Pt^{2+}Cl_4^{2-} + 2e^- \rightleftharpoons Pt + 4Cl^- \quad (1.16)$$

$$Pt^{4+}Cl_6^{2-} + 4e^- \rightleftharpoons Pt + 6Cl^- \quad (1.17)$$

The paper recognises that all steps involve the breaking of Pt-Cl bonds, a kinetically slow process with low exchange current densities, an advantage for control purposes as this means no reactions should occur until a potential is applied to the electrodes.

In 1988, Baumgartner and Raub published a review of electrochemical deposition of platinum and platinum alloys. Their work brought together many techniques for the electrochemical deposition of platinum from the 20th century, focusing in particular on the variety of available electrolytes, i.e. chlorides, ammines, sulphate-nitrite and hydroxyl complexes [147]. The particular electrolyte used in this work uses aqueous chloroplatinic acid ($H_2PtCl_6.xH_2O$). The electrolyte used also determines the platinum ion used in the deposition, either Pt (II) or Pt (IV). Each has drawbacks, such as corrosion damage to metal substrates and hydrogen evolution due to high current density. In addition the oxidation state will decide the electrochemical effort required to reduce the ions to platinum metal Pt(0). The ion Pt(II) requires only two electrons, whereas Pt(IV) must gain four electrons to reduce it to platinum metal on a substrate surface. The choice will influence the efficiency of the deposition activity and affect the resulting morphology of the deposit.

1.5 Electrodeposition in DSCs

As stated previously, electrodeposition is an ideal process for in-line platinisation of counter electrodes, chiefly due to Tata's prior experience with ED lines for galvanising steel and large scale production. This process is attractive due to highly controllable depositions through varying the time, temperature and deposition voltage or current density. Changing the electrolyte composition also plays a significant role in determining the deposit characteristics and the performance of the catalyst.

Electrodeposited platinum catalysts have been previously used in several DSC studies, though the early iterations were used chiefly as comparison techniques for other platinisation methods and cell architecture [40]. Since the inception of the flexible DSC in the early 1990's, there have been several papers that investigate electrodeposited platinum as a low temperature alternative to the thermal platinisation method introduced by Papageorgiou *et al* in 1991 [40].

Kim *et al.* reported the first use of direct and pulsed current deposition techniques to deposit an efficient platinum catalyst for use in dye sensitized solar cells [136]. The catalyst consisted of 40nm clusters of 3nm nanoparticles and concluded that pulsed deposition dramatically increases the platinum surface area by *ca.* 1.86 times, though it seems the quantity of Pt is larger than the thermally deposited catalyst presented by Papageorgiou *et al.* The efficiency of DSC devices including this electrodeposited Pt on FTO-glass was stated to be in the range 3.68-5.03%, whereas on a flexible substrate the efficiency was 0.86%, due chiefly to the low temperature application of TiO_2. The deposition solution used in this study was chloroplatinic acid (H_2PtCl_6), which is typically used for thermal and chemical platinisation. In this method, the solution concentration was increased to 10mM and 10mM KCl electrolyte was added as a source of Cl^- ions. The study compares pulse and direct current deposition profiles and uses the control of current over time, rather than potential control in order to deposit the platinum. As previously mentioned, pulse current demonstrates a considerable advantage in the control of the deposit morphology and properties.

In comparison, direct current was shown to produce dendritic crystals due to ion limitation near the electrode substrate surface that requires diffusion of Pt ions from the bulk solution. These structures have a much lower specific area for catalyst than the pulse current structures, as the pulse allows the replenishment of ions from the bulk to the substrate. The direct deposition electrochemically favours growth of existing structures on

the substrate surface, however due to the replenishment activity allowed by pulse deposition, more nucleation is allowed and therefore smaller more distinct deposition will form with a higher specific area. This was proven electrochemically using impedance spectroscopy measurements which proved that the pulse current method produces a counter electrode with a lower charge transfer resistance and therefore a much higher catalytic efficiency than the direct current method. The use of impedance measurements will be detailed in Chapter 2 for the characterisation of DSC devices and counter electrode performance. In addition, this paper uses cyclic voltammetry to qualitatively ascertain if the catalyst is active toward the triiodide/iodide redox couple, showing the reduction and oxidation peaks referred to by Equation 1.7 and 1.8.

Adding complexity to this method, Yoon *et al.* reported on a technique of introducing a physical addition, in the form of the non-ionic surfactant, octaethylene glycol monohexadecyl ether ($C_{28}H_{58}O_9$) to the plating bath [148]. In contrast to Kim *et al.,* this method used potential control deposition at a value of -0.06V *vs.* Ag/AgCl reference electrode. The surfactant was used as a liquid crystal template to form a regular platinum deposit on the substrate surface. The end result was a high surface area deposit of spherical granules and some clusters. Similarly to Kim *et al.*, cyclic voltammetry was utilised to assess the catalyst behaviour toward the triiodide/iodide redox couple, though they also reported an additional technique known as chronoamperometry to verify the CV analysis. The DSC efficiency of cells using ED-Pt counter electrodes was reported as 7.6%, in comparison to the 6.4% reported for DSCs with thermally or sputter deposited platinum catalysts. The high efficiency was reported to be the result of a tailored deposit surface, showing an increased active surface area and decreased sheet resistance (R_s). In addition, these cells were only tested under forward illumination and used a thick platinum layer with a high reflectance – enhancing the light harvesting of the cell. This study differs from Kim *et al.* as it seeks to use the solution composition rather than the deposition parameters and profile to control the deposit morphology.

Tsekouras *et al.* reported a technique that builds on the previous study by Kim et al, utilising a short overpotential pulse of -0.6V followed by a constant potential of -0.4V to deposit the Pt [103]. The aim of the overpotential pulse was to activate the majority of nucleation sites on the substrate material. The direct current method produced large, *ca.* 600nm, particles similar to those produced by Kim *et al.* In comparison, the use of an initial overpotential pulse reduced the particle size to *ca.* 40nm with several larger agglomerations at *ca.* 350nm. The pulse and constant potential electrodeposition method

achieved a low R_{ce} value of 0.6Ωcm^{-2}, which is half that of the sputtered and constant potential methods presented in this paper. In terms of DSC performance, the low R_{ct} value results in a high fill factor that surpasses the compared sputtered method. The I_{sc} and V_{oc} values were comparable with DSCs using sputtered platinum CE's. Cell efficiencies reported were *ca.* 6.5%, compared with *ca.* 6.2% of the sputtered method. In addition, the electrodeposited catalysts were shown to degrade slower over a period of 21 days than the sputtered method.

It is interesting to note the variety of potentials used in these papers, though all used similar cell set ups and the H_2PtCl_6 based deposition electrolytes. Potential control seems to be the favoured method of deposition, as is the monitoring of charge density to act as the deposition cut off point rather than a specified time.

In contrast to previous studies, Li *et al.* used a nanoparticle colloid solution for the electrodeposition [149]. The deposition of already formed nanoparticles was performed at 2V, a larger value than the -0.6V or -0.4V used by Tsekouras *et al.* or Kim *et al,* though since the nanoparticles were already in solution there will be no detrimental reactions such as hydrogen adsorption or evolution to hinder the deposition activity. The mean particle size was reported to be 20-30nm and uniform and the coating on the FTO glass was thought to have less platinum loading than the comparison thermal and electroplating. DSC efficiency using these counter electrodes ranged from 3.81% for the 10 minute deposition time, to 6.41% efficiency after 40 minutes. Little improvement was seen when the deposition time was increased further to 20 minutes, as the efficiency remained at *ca.* 6.4%. Similar trends were also reported for the J_{sc}, V_{oc} and fill factor parameters. The drawback to this method is the reported high sheet resistance of the counter electrode at 9.3Ωcm^{-2} and the need to sinter the electrode at 450°C after deposition, a requirement that electrodeposition is supposed to circumvent.

A recent paper by Ko & Kwon returned to the traditional electrodeposition method, investigating the nucleation mechanism behind electrodeposited platinum on FTO glass [140]. Using cyclic voltammetry to analyse the deposition, they reported that the onset of Pt deposition occurs at *ca.*0.14V, when using a potassium tetrachloroplatinate solution, which contains the Pt(II) ion rather than the Pt(IV) of H_2PtCl_6 used by most other report literature in this chapter. The CV scan reported an increase in current when the deposition begins, followed by a drop at 0.01V said to be where $PtCl_4^{2-}$ ion depletion occurs at the electrode surface. Hydrogen absorption was shown to occur on the deposited platinum at

-0.14V which will compete with and limit further deposition activity. Hydrogen evolution was shown to occur at a more negative onset potential of -0.2V. It seems that regardless of deposition conditions, the particle size of the deposit rises with increasing deposition time, due to the amount of charge passed during the process. This paper also goes on to identify the nucleation mechanisms and show that there is a change from progressive to instantaneous nucleation on the simultaneous increase of the deposition overpotential and the concentration of ions [140]. Of particular interest was the conclusion that the deposited particle surface roughness increases with the overpotential. This seemingly combines the previously mentioned dendritic growth effect, with the already deposited high surface area particles, in order to increase the specific area of the catalyst.

The paper continues, stating that nucleation sites have different activation energies for nucleation, confirming the method used by Tsekouras *et al.* where they utilised an initial pulse to form many Pt nucleation centres before applying a potential in order to control the particle growth [103]. These can be saturated under certain applied potentials, -0.15 to -0.2V, where there will be no increase in particle density due to the activation and saturation of almost all the available nucleation sites. However, the particle size was reported to increase with overpotential. They go on to say that decreased particle size is closely associated with increased particle density when the overpotential is high. This was reported to be due to the overlap of diffusion zones around the nucleated platinum particles. This reduces the flux density of $PtCl_4^{2-}$ ions and thus reduces the particle size. The movement from low to high overpotential produces a change in the morphology of the deposits from smooth to rough, which was then shown, using cyclic voltammetry to increase the surface area. It should be noted that similar effects are not seen when only the concentration is changed. This agrees with the results reported previously by Chen *et al* in their paper on pulse deposition of Pt on carbon nanotubes, though they controlled diffusion using physical additives rather than electrochemical effects (CNT) [142].

Lin *et al* demonstrated highly efficiency DSCs with a low charge transfer resistance (R_{ct}), using an electrodeposited counter electrode fabricated in a 10mM $PtCl_6$ solution supported by 0.05M HCl [141]. A fast 30 second direct current deposition procedure was followed and 3-(2-Aminoethylamino)propyl-methyldimethoxysilane (*Me-EDA-Si*) was added to the electrolyte as a possible deposition control method. This is similar to the study by Yoon *et al.* who utilised octaethylene glycol monohexadecyl ether as a deposit control agent [148]. Coarse, high surface area deposits were found when Me-EDA-Si was used, in contrast to the inhomogeneous deposition when no Me-EDA-Si was added to the solution. In addition, no

dendritic deposits were seen where the growth phase has predominated over the nucleation phase, solving the issue found by Kim et al when purely DC deposition was employed with no additive chemicals in solution [136]. At high additive concentrations, the morphology was reported as rough, nodular with rod like grains. If the additive concentration is kept at 0.01vol%, a dispersed nodular structure is obtained with less aggregation than a solution containing 0.05 vol% Me-EDA-Si, so therefore the reduction promotes an active surface area increase. Me-EDA-Si was thought to inhibit the semicircular particle growth, as seen in other deposition methods. The paper goes on to report a low R_{ct} of 1.39Ωcm^{-2} for the solution containing 0.01 vol% of Me-EDA-Si. This low value indicates a facile electron transfer between the counter electrode and the triiodide species, attributed to a well-dispersed nodular structure with minimised aggregation. A comparison sputtered platinum counter electrode gave an R_{ct} value of 2.03Ωcm^{-2}. Interestingly, the trend in R_{ct} did not follow that of increasing platinum loading, possible reasons being a lack of active sites or lack of Pt in general at the surface. A major result was that the efficiency of the DSC was seen to decrease as the platinum loading increased, with the explanation given that increased particle agglomeration drastically reduces the efficiency of the catalyst and therefore the performance of the cell. The DSC efficiency using 0.01 vol% Me-EDA-Si addition was 7.39% with a low platinum loading of *ca.* 4.76$\mu g cm^{-2}$.

Throughout the literature, the pulse deposition method for platinisation has become more popular due to its increased control over the deposit morphology. One of the earlier reports using this method in DSCs was submitted by Yang *et al.* A pulse electrodeposition method was compared to a sputtered platinum counter electrode, the end result being a 6.0% DSC using the electrodeposited counter electrode [150]. An interesting factor in this method is the use of Triton X-100 surfactant as an additive. This work compares well with prior art such as Yoon *et al* and Lin *et al*, where a surfactant was utilised to reduce agglomeration in solution and provide a liquid crystal template for deposit control [148]. However, Yang *et al.* do not mentioned why the surfactant was added in this paper. The studies conclusion is that the pulse deposition method produces a catalyst with a high activity, surpassing that of the sputtered and direct current deposited platinum comparison samples. The cycle time used was 0.5s, with a duty time of 0.2s.

A more recent development applied a polystyrene template onto FTO glass, whereupon Pt was electrodeposited into the pores in the film [151]. The result was a high performing DSC with a J_{sc} of 18.94mA/cm^2 compared with a standard cell of 16.63mA/cm^2. This type of

physical template has been reported in several fields for the production of catalyst material.

1.6 Templated electrodeposition and galvanic replacement

Templated deposition can refer to several types of technique, as mentioned in the previous section. This can comprise of physical templates, liquid crystal agents, physical additives or the use of sacrificial material deposits to be replaced. Template electrodeposition allows for targeted and controlled deposition using the voids or holes in an insulating layer on the target substrate [152]. If necessary, the template can be removed post deposition, leaving the deposit on the surface.

A development of this method is known as double templating, and involves the placement of a physical template on a substrate surface, which acts as a template for the final material deposition. Ghanem *et al.* utilised this method in the electrodeposition of metal nanodots, where the secondary template consisted of electrodeposited macroporous polypyrrole which in turn was formed through self assembled polystyrene spheres on a substrate [153]. This technique was also used by Yin *et al.* in the synthesis of Pt nanomaterials for oxygen reduction [154]. It is a versatile process, however is complex and does not lend its self to inclusion in a roll to roll process.

As the previous sections report, electrodeposition is a viable route for the low temperature preparation of DSC catalysts. However, due to the non-uniform topography of the FTO surface layer, the deposition process is not straightforward. An interesting technique that may facilitate this action was the templated deposition of platinum thin films through single layer redox replacement (SLRR) by Brankovic *et al.* [155]. A sacrificial metal is underpotentially deposited onto the substrate, in the cited paper an Au(111) surface. This is achieved through a short pulse stage, giving maximum control over the deposit structure. The second stage involves transferring the templated substrate to a second bath of the required metal salt, and holding at open circuit potential. At OCP the more noble metal ions dissolve and replace the sacrificial metal template on the surface, due to the difference in redox potentials, which is known as galvanic replacement. The process is known as "single-layer" as only a monolayer of template metal is underpotential deposited on the substrate surface.

Brankiovic's procedure is built on the technique of galvanic, or "redox" replacement, where the differences in equilibrium potentials of two elements drives the replacement of one by

another. It is based around the standard electrode potentials that describe the individual potentials of reversible ionic reactions, Equations 1.18 and 1.19 [156]:

$$Pb^{2+} + 2e^- \rightarrow Pb \quad (E = -0.1251V) \qquad (1.18)$$

$$Pt^{2+} + 2e^- \rightarrow Pt \quad (E = 1.188V) \qquad (1.19)$$

The positive difference "ΔU" between electrode potentials of the more noble metal, in this case Pt and the Pb layer, drives the replacement process. It should be noted that the substrate must be more noble than the reactants in order to remain inert. Brankovic *et al.* summarised this process using Equation 1.20 [155]:

$$M^0_{UPD} + \left(\frac{m}{z}\right) P^{z+} \Longrightarrow M^{m+} + \left(\frac{m}{z}\right) P^0 \qquad (1.20)$$

Where M^0_{UPD} represents the sacrificial metal deposit; P^{z+} is the more noble metal cation and M^{z+} is the metal cation in solution following the oxidation of the sacrificial metal. P^0 represents the noble metal deposited through this process. The paper reported that this deposition activity is an irreversible process, which indicates good adhesion of the deposit to the substrate.

Surface limited replacement was also utilised for the production of bimetallic catalysts, illustrating the versatility of the method and the different materials that could be used. Mkwizu *et al.* studied the electrodeposition of ruthenium and platinum nanoclusters, with copper used as the sacrificial material [157]. Interestingly, spontaneous co-deposition of the catalyst elements Pt and Ru also occurred at open circuit without the sacrificial Cu being present. This should be assessed in any practical application of this technique as it will change the morphology of the catalyst in unanticipated ways. The end use was electrocatalysts of reactions such as oxygen reduction in a fuel cell, demonstrating that this method allows the fabrication of highly catalytic and versatile nanoparticles.

The combination of electrodeposition and electroless deposition was utilised by Papadimitriou *et al.* for the fabrication of Pt/Pb coatings on carbon and platinum substrates [158]. When a Pb coated substrate was immersed in Pt solution, it was spontaneously replaced by the Pt, resulting in a combined Pt/Pb electrode on carbon or Pt substrate, Figure 1.24. The unfortunate side effect is that there is remaining Pb template material, which may cause issues for its application area, in addition increasing the material waste.

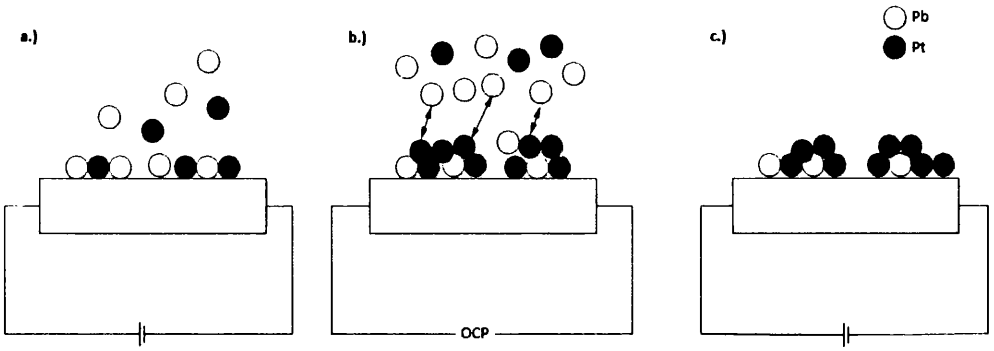

Figure 1.24: SLRR electrochemical deposition process schematic

The original technique reported by Brankovic *et al.* was refined further by Viyannalage *et al.* who reported the use of a single electrolyte bath containing both the sacrificial template metal salt, and the required replacement metal [159]. In contrast to Brankovic, this paper used Pb as the sacrificial material for growth of Cu layer on Au(111) and Ag(111). The original techniques reported by Brankovic and initially by Viyannalage used several solution baths, which left the electrode exposed to air, and the solutions in different stages of de-oxygenation. This was reported to be a serious issue, as the oxygen reduction reaction competes with the redox replacement reaction. The one pot process was developed in order to ensure the solution remains at a minimum oxygen concentration. In addition, the solution contains a high concentration of sacrificial ions, to ensure that only as short pulse would be required to form a layer. Furthermore, the replacement metal ions were kept at a low concentration, to control the amount that would simultaneously deposit on the deposition of the sacrificial metal.

A similar SLRR technique was reported by Rettew *et al*, however this study analysed the use of Ni, rather than Pb as the sacrificial metal, for the deposition of Pt onto Au substrate [160]. Interestingly, this study utilised chloroplatinic acid, a Pt(IV) solution, rather than the previously reported Pt(II) solutions due to the 1:2 stoichiometry that deposits more Ni on a surface than the equivalent Pt. Therefore, two nickel atoms will be required for every Pt replacement event - thus adding further control to the Pt deposition quantity, Equation 1.21:

$$Pt^{4+} + 2Ni_{surface} \rightarrow Pt_{surface} + 2Ni^{2+} \qquad (1.21)$$

This study also noted that under potential deposition techniques did not necessarily need to be used for SLRR to be successful.

Gocken *et al* further reported on the SLRR method, showing that the choice of replacement anion is important in controlling the stoichiometry of the reaction. The study showed that in a Cu/Pt reaction, four Cu atoms are replaced by one Pt - a factor that will influence the coverage of the adatoms on the substrate [161]. Similar to the study by Viyannalage *et al.*, Fayette *et al.* utilised Pb as the sacrificial metal instead of Cu, and included Pt^{2+} as the replacement ion in acidic conditions [162]. Their results showed the formation of a network of Pt clusters on the substrate surface, in this report a Au(111) surface. Interestingly, they also found that the adsorption of OH^- species on the substrate surface or the formation of PtOH compounds can increase the positive charge of the deposition system, and result in increased deposition of the Pt species outside of the experimental control. Further exploration of this effect suggested this could produce a non stoichiometric Pb to Pt exchange ratio. The Pt deposits were said to be in the Pt(111) crystallographic orientation, which agrees with a study submitted by Zhang *et al.*, where it was found that Pt(111) was the crystallographic orientation that favours the highest catalytic activity [163].

These methods have been used for the formation of thin films on organised, uniform metal surfaces, such as Au(111), Ag(111) and glassy carbon. However, the methods were used for the successful formation of catalyst materials and as a result it is believed this will make a viable route for development in the field of dye solar cells.

1.7 Corrosion and corrosion prevention methods

In order for flexible, mass produced DSCs to become a reality, they need to be viable on flexible substrates such as polymers and sheet metal, in order to reduce device cost and support structures [164]–[166]. However, unlike the beneficial catalytic reaction that occurs at the counter electrode, the electrolyte interaction between the iodide/triiodide and certain metal substrates results in degradation of the electrolyte or corrosion of the substrate. In order to ensure the stability of metal substrate dye solar cells during operation, the interaction at metal electrode substrates requires investigation.

1.7.1 General corrosion

Corrosion generally occurs at thermodynamically favourable sites on metal substrates. These "active sites" have a lower bonding energy than the surrounding metal, which increases the ease of any reactions occurring on the surface. The most common type of corrosion, for bare metals in a liquid environment, is through redox reactions where ionic species in solution attack the surface of a substrate and form corrosion products. The

attack usually occurs at "active sites", these are points on the surface that can accept or donate an electron, i.e.: dangling bonds, cracks, pits or defects in the material. An example reaction can be seen in the interaction between iron and oxygen, Equations 1.22 and 1.23:

$$Fe(s) \rightarrow Fe^{2+} + 2e^{-} \quad (1.22)$$

$$O_2(g) + 4e^{-} + 2H_2O \rightarrow 4OH^{-} \quad (1.23)$$

Corrosion prevention falls into several categories:

- Additives, such as corrosion inhibitors
- Sacrificial materials or coatings
- Electrochemical passivation
- Coatings.

Anti corrosion coatings have been widely used in the protection of vulnerable metal substrates, especially in the rolled steel industry as a large quantity of these products are used for environmental protection, i.e. roofing, and cladding of buildings. Coatings are an active measure, forming a barrier against any corrosion agents. These are mostly polymeric or colloidal coatings such as anti-rust paints. Recent research has suggested the use of metal nitride particles combined with a polymer such as polyimide. This coating has the potential to both conduct and protect a vulnerable metal substrate from corrosion, which has much use for the conducting substrate in DSC devices [167][168].

Anti corrosion treatments using sacrificial material are not a viable solution in DSC cells, as this will reduce device performance through depletion of charge carriers though corrosion of the sacrificial material, in addition to the inclusion of a vulnerable material into the device that could poison the cell or form recombination centres, so reducing V_{oc} and J_{sc}. Physical anti-corrosion measures are further made difficult due to the restricted architecture of the DSC devices. As a result, this fostered interest into chemical corrosion inhibition.

1.7.2 Corrosion inhibition in industry

There are many forms of additives used by industry for corrosion inhibition on common industrial metals in aggressive environmental conditions. In-organic inhibitors are the most common; such as chromate additions in chrome coatings were a popular anti corrosion additive, however, the use of this compound is now restricted for public health reasons.

Organic compounds, in the form of aliphatic or aromatic compounds can also be used. Aliphatic compounds, such as aliphatic amines are particularly of use in acidic environments [169], [170]. Aromatic compounds are also used, with compounds such as nitrogen-containing heterocyclics used to prevent corrosion of metal in acidic or similarly aggressive media [171]–[173]. Heterocyclic compounds are used as performance enhancing additives in dye solar cells, and as a result it was decided to restrict this study to this type of organic compound.

The reviewed studies on nitrogen containing heterocyclics report that these additives can bond *via* two mechanisms to a metal substrate. The first type, physisorption, involves the electrostatic attraction between molecule dipoles and the substrate surface at the metal/electrolyte interface. Chemisorption is the second mechanism, where charge is shared between molecule and substrate to create a coordinate bond. Many types of organic compound are used in industry, such as imidazoles, benzimidazoles and pyridine compounds [174], [175]. The study by Riggs *et al.* summarised the possible additive effects for corrosion inhibition [176]:

- Changing the electropotentials of the substrate or reactants
- Altering the corrosion product nature
- Chemisorption and physical blocking
- Changing electrolyte resistance.

These are suggested mechanisms for organic molecule inhibition action for metal substrate in contact with corrosive media such as HCl. It is hoped that the basic nature of NHC molecules will allow them to passivate metal substrate active sites through surface bonding and so restrict the interaction between the triiodide species and the metal in a DSC device. It is also thought that the addition of large complex molecules could hinder the movement of triiodide towards the metal surface, providing further corrosion protection to the metals and reducing triiodide depletion. The addition of NHC molecules is not designed to have a negative influence in performance and careful study of prior work has ensured that the compounds chosen have a corresponding positive effect on DSC devices, through other electrochemical mechanisms.

1.7.3 Corrosion in metal substrate DSC cells

It is well known that corrosion in liquid state DSCs with metal substrates is due to the highly aggressive nature of the iodide/triiodide electrolyte or more particularly the attack on the metal by the triiodide ion (I_3^-) [38][177], [178], shown by the Equation 1.24 below, when the number of electrons "n" is 2:

$$M + I_3^- \rightarrow M^{n+} + 3I^- \qquad (1.24)$$

This interaction will cause substantial loss of performance in the DSC through the reduction of charge carriers; furthermore the loss of I_3^- will be visible as a colour change from yellow/brown to clear as the triiodide attacks the metal substrate, thus making DSC production on metal substrates somewhat problematic. So far corrosion inhibition studies for DSCs have focused on the use of barrier coatings, or the development of none-corrosive or low-corrosion electrolytes, such as the cobalt based complexes analysed by Sapp *et al.* and Nusbaumer *et al* [88], [179]. Cobalt based electrolyte corrosion behaviour will be investigated further in Chapter 6. Several studies have explored the stability of metal substrates for DSC cells. Toivola *et al.* discussed the use and suitability of several industrial sheet metals such as zinc-coated steel and stainless steel, in addition to conductors such as copper [38]. Their study focused on soaking and encapsulation tests using relatively large volumes of electrolyte compared with that of standard DSC cells, a feature recognised that would give different degradation performance to the thin layer DSC reality. An important realisation made by this paper was that the corrosive action reduces the amount of triiodide in the cell, leading to a detrimental loss of performance. This was found to be a more important factor than the loss of the zinc protective coating on the tested zinc-coated carbon steel. An important conclusion was that stainless steel appeared to be resistant to degradation after 12 months of storage when used as a counter electrode substrate. One of the drawbacks of this technique is that, the usage of large electrolyte volumes does not accurately represent the conditions in a DSC where the electrolyte is only present

Miettunen *et al.* also reported on the stability of stainless steel when used as a counter electrode or a working electrode in contact with the electrolyte [180]. Their results showed that standard 304 stainless steel produced high performing cells with 4.7% efficiency with no cell degradation reported, a much higher efficiency than reported by Toivola *et al.* A critical difference between these two studies is the latter utilises thin layer DSCs, rather than the bulk volumes used by Tsekouras, thus the result will be more representative of the response of DSC cells. A prior study on industrial metals, though not DSC substrates, by

Tsukaue *et al.* reported that stainless steel 304: and 316L exhibited pitting corrosion in wet air containing slight amounts of iodine, the cause of which is believed to be the concentration of triiodide [181]. This indicates that control over the composition of the DSC electrolyte will be critical in the inhibition of corrosion on a metallic substrate.

A further paper by Miettunen *et al.* studied stainless steel, Inconel 600 and titanium for feasibility as dye solar cell counter electrode substrates [182]. Their study reported the degradation of stainless steel and Inconel 600 through the thermal platinisation process as the high temperatures utilised in the deposition cause the accelerated oxidisation of the metal. Corrosion products and a loss of electrolyte colour were observed following the 1000h study. Titanium was found to be the only stable metal in this study. However, the study also found that a thick 20nm film of Pt was able to improve metal stability for all metals, apart from Inconel - surmised to be due to the high reactive nickel content in the metal.

1.7.4 Use of additives in photovoltaics

The use of electrode surface modification treatments by the inclusion of additive compounds has been used for photo-electrochemical cells for several years. An early example was reported by Canfield and Parkinson who studied the passivation of exposed edge planes on nWSe_2 crystals by using 4-*tert.*-butylpyridine (4-tBP) [183]. The method involved the treatment of the crystal surface with neat 4-tBP at 60°C with the result that it increased V_{oc} and J_{sc} of the cell and reduced the dark current. The mechanism was thought to be one of intercalation, where the pyridine group of 4-tBP would bind between the crystal layers at exposed edges. Then the *tert.*-butyl segment of the molecule was said to provide a steric anchor preventing any further penetration of the TBP into the crystal lattice, thus confining the interaction area to the edge of the crystal structure.

In 1993, Nazeeruddin *et al.* explored the benefit of additives to DSC performance [184]. Their study exposed a sensitised TiO_2 electrode to a solution containing 4-*tert*-butylpyridine, in a similar manner to Canfield and Parkinson, before testing its effect on the performance in a standard DSC cell containing an iodide/triiodide electrolyte. They found that the 4-tBP suppressed the recombination, or dark current, reaction at the TiO_2/electrolyte interface, Equation 1.25:

$$I_3^- + 2e_{cb}^-(TiO_2) \rightarrow 3I^- \qquad (1.25)$$

Thus improving V_{oc} causing an increase in the fill factor and DSC cell efficiency.

The reduction of triiodide ions by interaction with injected electrons in the TiO_2 conduction band was originally said to occur through crossing the dye layer due to its small molecular size. However, more recent studies have shown that the reaction occurs at bare sites on the TiO_2, where no dye has adsorbed [185]. The 4-tBP compound decreases the reduction rate of triiodide, by adsorbing onto the TiO_2 surface at active sites, thought to consist of Ti(IV) ions [186]. These are areas of high Lewis acidity, prone to interacting with basic molecules, such as pyridine compounds, *via* nitrogen lone pairs. However, other studies such as Suzuki *et al.,* observed that pyridine (not quite 4-tBP) was physisorbed through electrostatic attraction, or Van der Waals force in a parallel orientation to the TiO_2 surface. It was reported that the bond originated between the charged Ti active sites and the charge located on the pyridine ring [187]. The nitrogen lone pair was said to increase the attraction, but was not the main bonding point.

The effect of 4-tBP on DSC performance was studied further by Huang *et al.* They studied how the compound influenced recombination kinetics and cell performance [79]. They also investigated two further additives, 2-vinylpyridine and poly(2-vinylpyridine) to assess their performance. The evaluation confirmed the conclusion reached by Nazeeruddin *et al.,* in that TBP and other pyridine compounds increase the V_{oc} and efficiency of DSCs and illustrated the dependence of V_{oc} on the recombination kinetics of DSC devices. They did not however, explore the possibility of energy level changes through the introduction of these N-containing heterocyclic compounds. These questions were discussed by Schlichthörl *et al.* in the same year, through the analysis of the band edge movement in DSCs using intensity modulated photovoltage spectroscopy (IMVS) showing that treating the TiO_2 with 4-tBP or NH_3 caused a band edge movement and resulted in a more negative V_{oc} for the device [188]. The suggested mechanism was that TBP and NH_3 deprotonate the TiO_2 surface, which is partially protonated during dye adsorption at the surface. Deprotonation shifts the conduction band (V_{cb}) in a negative manner, thus increasing the photovoltage of the device.

Greijer *et al.* used resonance Raman scattering to study several mechanisms in DSC operation. The study mainly focused on dye ligand exchange mechanisms. However, the technique studied was also used to observe the role of 4-tBP in a DSC device. One of the results obtained was that the thiocyanate group on the sensitising dye was seen to be unaffected by the addition of 4-tBP, which is an important factor when considering cell stability. The study suggested that, as pyridine is known to react with iodine, there will be a drop in the I_3^- concentration and thus an increase in stability of the device through

preservation of the thiocyanate ligand on the dye molecule. The improvement of DSC performance was an additional beneficial effect, which has not been previously explored in the literature. Several other sources analysed the interaction between iodine species (I_3^-) and pyridine compounds (Py). Kebede *et al.* has published two possible routes for the relationship between iodine species and pyridine in acetonitrile solution. These are shown in Equations 1.26-1.27 [189]:

$$Py + I_3^- \leftrightarrow PyI_2 \quad (1.26)$$

$$2Py + I_3^- \leftrightarrow Py_2I^+ + 2I^- \quad (1.27)$$

If these remain true for 4-tBP in a DSC electrolyte, Greijer *et al.* suggested that the following reactions would thus occur due to the electron donating ability of the lone pair on the nitrogen included in the pyridine compound, Equations 1.28-1.29 [190]:

$$(4TPB) + I_3^- \leftrightarrow (4TBP)I_2 + I^- \quad (1.28)$$

$$2(4TBP) + I_3^- \leftrightarrow (4TBP)_2I^+ + 2I^- \quad (1.29)$$

This reaction could then reduce the I_3^- concentration in the electrolyte and increase the amount of I^- present in solution. It was also suggested that the drop in triiodide concentration would increase the concentration of electrons in the TiO_2 electrode, thus provoking a rise in V_{oc} by reducing the probability of interaction between I_3^- and injected electrons. Returning to Kebede *et al.*, the study further suggested that the bonding between an excess quantity of pyridine (Py) and either the I_2 or I_3^- species would form a sterically bulky complex ion, which would be less capable of approaching close to the TiO_2 surface [189]. Their conclusions suggested that the increase of DSC performance was due to the formation of the dipyridine complex ion, shifting the reaction equilibrium to reduce the concentration of I_2 and other electron scavenging species in solution. Their study was based around the previous work on pyridine iodine bonding by Reid & Mulliken [191] and Tassaing & Besnard [192], and the earlier work on voltammetry studies of iodine species in acetonitrile solutions undertaken by Popov & Geske in 1957 [193].

Pyridine based compounds containing only one nitrogen atom one of several additive forms that have been considered for use in DSC devices. The 2005 study by Kusama *et al.* catalogued the behaviour of heterocyclic compounds containing more than one nitrogen atom in their structure and their effect on dye solar cells when included in the electrolyte solution [185]. This study was used to benchmark the additives possible for use in this

thesis. Figure 1.25 shows several structures for nitrogen-containing heterocyclic (NHC) candidates for use in this study.

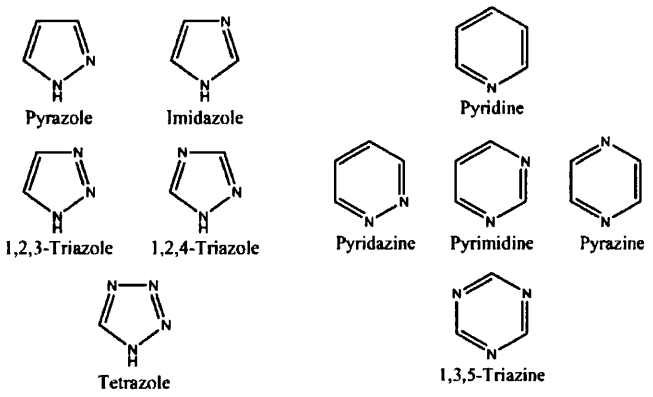

Figure 1.25: Nitrogen containing heterocyclics studied for use in DSC devices [185]

Kusama *et al.* showed that the V_{oc} of DSCs was greater with NHC additives included, than for devices containing no additive in the electrolyte [185]. There were, however, some exceptions: The compounds: 1,2,3-triazole; tetrazole and pyridazine *reduced* the device V_{oc}, and J_{sc} values. The exceptions appeared, from their data, to be due to the smaller (more positive) lowest partial charge of the N atom in the molecule. In addition, the paper also stated that nitrogen molecules in the 1, 3 or 2, 4 or 1, 4 positions will not be able to interact with the TiO_2 surface. Therefore there will be less NHC adsorption to free areas on the TiO_2 surface, which will reduce their effectiveness. Despite these exceptions, the cell fill factor improved as the majority of the NHC's studied were added to the electrolyte formulations, thus increasing device efficiency. This study further reported a decrease in dark current and an increase in V_{oc} as the lowest partial charge of the nitrogen atom in the compound increased. This value was said to give an estimate of the donating ability of the nitrogen's lone pairs; a factor considered previously by Greijer *et al.* [190] .

The results suggested that the NHC's were adsorbed onto the bare areas of the TiO_2 electrode, thus increasing V_{oc} through the decrease in recombination losses. This result supports the previous findings of Nazeeruddin *et al.* and is further supported through IPCE studies undertaken by Lindstrom *et al.* Here, a pyridine compound was adsorbed onto the TiO_2 surface at un-dyed TiO_2 sites, thus causing a higher IPCE value through blocking of the TiO_2 surface, or through the passivation of recombination sites [184], [194]. This was also said to lead to more efficient collection of electrons from further away from the conducting substrate [194].

They continued describing the relationship between the TiO_2 surface states and the additive compounds [185]. They suggested that the atoms of the additive compound with the lowest partial charge would provide preferential sites for bonding and adsorption on the TiO_2 electrode surface, due to the bare Ti^{4+} site being Lewis acidic. Therefore the lower the partial charge of the nitrogen atom, the easier and more frequently it will adsorb to the surface of the TiO_2 at un-dyed, or "active", sites. In addition, this study uses a relationship between the flat band potential (V_{FB}) and the redox potential of the electrolyte (V_{red}) to explain the change in V_{oc} when including N-containing heterocyclic additives in the electrolyte, Equation 1.30:

$$V_{oc} = V_{FB} - V_{red} \tag{1.30}$$

In previously reported literature, Schlichthörl *et al* confirmed that the inclusion of additives or nitrogen-containing heterocyclics to the electrolyte move the flat band potential, due to their adsorption to the TiO_2 surface [188]. The redox potential was said to be negligibly affected by these additions, therefore the increase in V_{oc} was attributed to the movement of V_{FB}. The reduction in J_{sc} was then suggested to be due to the negative movement of the TiO_2 conduction band, which unfortunately decreases the rate of electron injection from the dye to the semiconductor. The final factor reported in this study was the effect of nitrogen lone pair donating ability for each compound.

These studies build on the work of S. F. Nelsen who investigated the effect of additional groups attached to an N-heterocyclic ring [195]. The study concluded that as larger alkyl or other groups are added, the ionisation potential of the compound will decrease. Kusama *et al.* used this feature to explain the behaviour of different compounds on the performance of DSC devices. The analysis by Kusama *et al.* also agreed with the previous work of Kebede *et al.* and Greijer *et al.*, showing that the heterocyclic compounds react with iodine or triiodide in the electrolyte, forming charge transfer complexes [189], [196]. The bond here is between the nitrogen lone pair and the triiodide or iodine atoms as illustrated in Equation 1.31:

$$NHC + I_3^- \rightarrow NHC(I_2) + I^- \tag{1.31}$$

As mentioned previously, this reaction will reduce the quantity of I_3^- in the electrolyte and increase the concentration of iodide (I^-). This should improve hole collection at the working electrode and reduce the recombination of injected electrons with triiodide (I_3^-).

Further papers by Kusama *et al.* investigated the interactions of a large variety of heterocyclic compounds for use in dye sensitised solar cell devices [197]–[202]. These studies gave a good account of the performance benefits and limitations of each of the molecules investigated, and were an invaluable tool for informing the selection of electrolyte additives for this study.

The simplest form of reported additive is a pyridine compound, illustrated in Figure 1.26, and as previously mentioned in this chapter, the typical additive most commonly introduced to DSC electrolytes in literature is the pyridine derivative, 4-*tert*-butylpyridine (4-tBP). This is followed closely in popularity by n-methylbenzimidazole (n-MBI), see Figure 1.27.

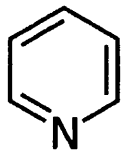

Figure 1.26: A simple nitrogen containing heterocyclic compound. "Pyridine"

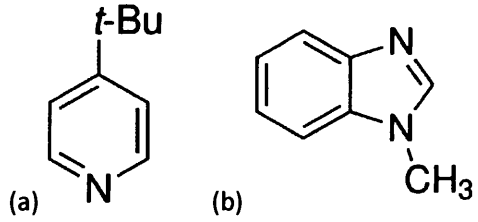

Figure 1.27 : Nitrogen containing heterocyclic compounds commonly used as performance enhancers in DSCs (a) 4-TBP, (b) 1-MBI

In order to select additional compounds for testing in this study, the reports on performance enhancing compounds by Kusama *et al.* were used as a guide [185], [201], [203]. Earlier studies into corrosion inhibition in other areas of industry were used to aid in the formulation of mechanisms and testing regimes for the selected compounds.

1.8 Monitoring methods

In order to investigate corrosion and corrosion inhibition behaviour and the characteristics of electrolytes and additives in the 2nd part of this work, a monitoring technique needed to be developed to accurately assess and record any variation over a large number of samples. Current non-destructive assessment of DSCs involves several electrochemical testing techniques or a passive absorption spectra analysis. Watson *et al.* presented two methods for the *in* situ monitoring of the dye uptake in dye sensitised solar cells[106]. The spectrum analysis method monitors used UV-VIS reflectance spectroscopy to show the wavelength

change as the dye is adsorbed to the TiO_2 surface. The second method involves the use of a camera/RGB sensor to analyse the colour change as the dye is adsorbed. This method is fast and accurate and correlates well to the UV-VIS study and shows the colour change or change in average intensity over long term or short term studies, depending on the requirements of the study and the limitations of the hardware used. The UV-VIS reflectance study has been adapted to study the corrosion of different industrial metals in contact with thin electrolyte layers by Reynolds *et al.* [204]. Encapsulation cells using different industrial metal substrates were exposed to thin electrolyte layers and analysed using this method. The report indicates different results to those previously submitted by Toivola *et al.* due to the thin electrolyte layers used rather than bulk electrolyte solution. The results by Reynolds *et al.* showed that in this setup, only titanium has complete corrosion resistance, whereas other metals such as zinc corroded in seconds.

UV-VIS and colour change studies were also used by Carnie *et al* for the assessment of UV photocatalytic oxidation of triiodide in DSC devices [123]. Their work showed that UV radiation photocatalyses the oxidation of triiodide causing electrolyte discolouration. An interesting conclusion was that cells degraded faster under loading, through triiodide consumption through increased hole availability. This factor has a large impact on future cell stability work, as it was initially thought that a passivation current through an active DSC would inhibit corrosion of metal substrate. Fortunately, this increased degradation can be mitigated through the use of UV protection measures, and the study also found that a reverse bias applied to the device could restore some of the cell performance following UV degradation.

Asghar *et al.* also assessed ageing through UV exposure and temperature, through using an RGB colour analysis technique [205]. They indicated that it was the interaction between electrolyte and TiO_2 that was a cause of electrolyte bleaching and that the dye layer was able to slow degradation, as seen through the photographic observation of cell colour change. The study also showed that it was possible to relate electrolyte colour to iodine concentration, an important factor for applying the result to later studies. The conclusion is of great interest as it indicates that the monitoring method is viable for large scale and long term observation. In addition, it also stresses that a stable background environment is required to make this method quantative and comparable. It is this RGB method that will be adapted for use in this study for the analysis of the corrosion inhibition efficiency of nitrogen-containing heterocyclics in DSC electrolytes.

1.9 Literature Conclusions 1

- Electrochemical platinisation is a viable route of study for the large scale solution processing of DSC counter electrodes
- There have been several problems, such as low performance and lack of adhesion to the substrates in previous experimental reports
- Platinum will be utilised over the newer, lower cost catalysts as it is better understood and to reduce the number of variables in this investigation
- There is a large variety in the deposition morphology between electrodeposition methods
- Only basic direct and pulse waveform deposition has been used for DSC counter electrode production
- There are other catalyst formation methods available to the electrochemist
- The most promising of these electrochemical methods, uses a low cost template material to form the initial deposit structure. Followed by electroless deposition of the required metal
- The electrochemical deposition methods have high potential for mass production, as an already templated substrate could be introduced into a running mass production line for electroless deposition, resulting in reduced manufacturing complexity for the process

1.10 Literature Conclusions 2

- There is a lack of *in-situ* monitoring methods that are viable for use in the quality assessment and control of mass produced DSC devices and current methods rely on small batch or individual studies that are slow to feed back into the process
- UV-VIS, in particular, has been an important technique in the analysis of DSC devices, however, the analysis of colour change (RGB value) for *in situ* monitoring has been utilised for the study of dye uptake in DSC devices and has potential for large scale monitoring of DSC production
- It is thought that the RGB analysis method should be investigated further especially on metal substrates for the investigation of corrosion and degradation of metal substrate cells
- Since the most viable method of DSC mass production will require the use of metal substrate, work will be required to assess the stability of the most common materials to be used in thin layer DSCs

- To that end these substrates should be trialled in a test environment mimicking that of DSC devices - though without the active TiO_2 and catalyst to complicate the study of substrate with electrolyte
- Commercially available non-iodide electrolytes should also be observed in a parallel study
- The degradation of metal substrates in triiodide electrolyte is a well known phenomenon in DSC cells
- Traditional anti-corrosion methods are known to affect the performance of the cell through chemical (poisoning) or physical (reduction in component performance, i.e. conductivity) effects
- It is possible that several chemical components of DSC cells could be used as corrosion inhibitors, in particular are those components already in use as inhibitors in industry such as organic compounds or heterocyclics
- It is suggested that traditional additives in DSC electrolytes could provide metal substrate a measure of protection
- In addition, this review has found that several alternative electrolytes are less aggressive toward metallic substrates than the triiodide/iodide redox couple.
- Little work has been done, to date, on the effect of these redox couples on metals.

1.11 Aims and Objectives

This thesis will first investigate the counter electrode/electrolyte interaction through the analysis and development of rapid electrochemical platinisation methods through the adaptation of existing methodology, these results will be compared against current platinisation methods. Following this, an alternative electrodeposition technique will be investigated, to discover its viability for use in DSC devices for batch and continuous processing.

Secondly, the working electrode/electrolyte interaction will be analysed using mass observation and analysis methods adapted for this usage. The interaction specified is between the triiodide/iodide electrolyte and a series of metallic substrates, chosen due to their potential as flexible materials for roll to roll produced DSCs. This will also be used to observe and analyse how the stability of these observation cells is affected by the inclusion of additives in the electrolyte. Finally, this technique will be trialled on a cobalt based electrolyte, thought to be less aggressive than the iodide/triiodide redox couple. The study is designed to assess this and ascertain the metals that are viable DSC substrate candidates.

Chapter 3: The intention of this thesis is to further develop and characterise simple electrochemical platinisation methods to ascertain if they are able to be adapted for fast usage for mass produced DSC cells, as a low temperature replacement for the high performance thermal deposition or the chemical reduction platinisation methods.

Chapter 4: This chapter looks at the development of an alternative electrodeposition method using a low cost templating process, which, was adapted from a surface layer redox replacement method to produce a platinum catalyst. First developed on FTO-glass and then characterised through physical and electrochemical analysis, before the being applied to FTO-glass based DSC cells.

Chapter 5: This section of research focused on the electrolyte reaction at the working electrode substrate and the detrimental corrosion of candidate metallic substrates for industrially produced DSC substrates. In mass production, quality assurance is critical in ensuring that the process runs efficiently and constantly. To that end, an RGB image analysis method was developed and compared with a currently available spectrophotometric method for the *in situ* monitoring of DSC devices. Of particular importance was the monitoring of cell degradation through the corrosion of the metal substrate when exposed to the aggressive iodide/triiodide electrolyte. In the process of characterising metal/electrolyte interaction, it was noticed that several electrolyte additives had corrosion inhibiting effects. This resulted in a secondary study into the performance of several nitrogen containing heterocyclic additives when included in a simple DSC electrolyte. A critical consideration was that these compounds should not be detrimental to performance when included in the electrolyte solution.

Chapter 6: Another solution to the corrosion issues of triiodide/iodide electrolyte is the use of one of the many reported electrolytes developed recently. In this study, a cobalt complex redox couple was exposed to several crucial metal substrates and analysed using the RGB analysis method developed in Chapter 5. Further to this, several corrosion inhibition methods were also trialled in the event that the less corrosive cobalt complex reacted poorly with any of the metal substrates.

Chapter 7: After reporting the experimental work in Chapters 3-6, this chapter looks at future work, adaptations and possibilities of the techniques put forward in this thesis.

1.12 References

[1] IEA, "IEA - Key World Energy Statistics 2012," 2012.

[2] BP, "BP Statistical Review of World Energy 2013," 2013.

[3] M. Schneider, A. Froggatt, K. Hosokawa, S. Thomas, Y. Yamaguchi, J. Hazemann, and A. Stanback, "World Nuclear Industry Status Report 2013," Paris, London, Kyoto, 2013.

[4] IAEA, "Nuclear Technology Review 2012," 2012.

[5] G. Corbetta, I. Pineta, J. Moccia, and J. Guillet, "The European offshore wind industry - key trends and statistics 2013," 2014.

[6] S. Bassi, A. Bowen, and S. Fankhauser, "The case for and against onshore wind energy in the UK," 2012.

[7] P. Breeze, *Power Generation Technologies*, 2nd ed. Newnes, 2014.

[8] G. V. Chilingar, M. Lackpour, F. J. Hormozi, and R. M. Hodel, "Cost Effectiveness of Energy Storage to Manage Wind Variability's Impact on the Electrical Grid," *J. Sustain. Energy Eng.*, vol. 2, no. 1, pp. 41–51, 2014.

[9] S. Heier, *Grid Integration of Wind Energy: Onshore and Offshore Conversion Systems*, 3rd ed. John Wiley & Sons, Ltd, 2014.

[10] J. P. Barton and D. G. Infield, "Energy Storage and Its Use With Intermittent Renewable Energy," *IEEE Trans. Energy Convers.*, vol. 19, no. 2, pp. 441–448, 2004.

[11] A. S. Bahaj and L. E. Myers, "Fundamentals applicable to the utilisation of marine current turbines for energy production," *Renew. Energy*, vol. 28, no. 14, pp. 2205–2211, Nov. 2003.

[12] F. Photovoltaics, "GLOBAL MARKET," 2013.

[13] "Photovoltaics Report," 2014.

[14] A. Campoccia, L. Dusonchet, E. Telaretti, and G. Zizzo, "An analysis of feed in tariffs for solar PV in six representative countries of the European Union," *Sol. Energy*, vol. 107, pp. 530–542, Sep. 2014.

[15] NREL, "NREL - Best Research Cell Efficiencies," 2013. [Online]. Available: http://www.nrel.gov/ncpv/images/efficiency_chart.jpg. [Accessed: 04-Mar-2014].

[16] A. Shah, J. Meier, A. Buechel, U. Kroll, J. Steinhauser, F. Meillaud, H. Schade, and D. Dominé, "Towards very low-cost mass production of thin-film silicon photovoltaic (PV) solar modules on glass," *Thin Solid Films*, vol. 502, no. 1–2, pp. 292–299, Apr. 2006.

[17] M. A. Green, "Consolidation of Thin-film Photovoltaic Technology: The Coming Decade of Opportunity," *Prog. Photovoltaics Res. Appl.*, vol. 14, pp. 383–392, 2006.

[18] D. E. Carlson and C. R. Wronski, "Amorphous silicon solar cell," *Appl. Phys. Lett.*, vol. 28, no. 11, 1976.

[19] K. Kalyanasundaram, "Photochemical and Photoelectrochemical Approaches to Energy Conversion," in *Dye Sensitized Solar Cells*, 1st ed., EPFL Press, Lausanne, 2010, p. 8.

[20] M. A. Green, "Crystalline and thin-film silicon solar cells : state of the art and future potential," *Sol. Energy*, vol. 74, pp. 181–192, 2003.

[21] "Sungen International Ltd," 2009. [Online]. Available: www.sungen.com/. [Accessed: 01-Apr-2012].

[22] H. Solar, "HyET Solar." [Online]. Available: http://www.hyetsolar.nl/. [Accessed: 04-May-2013].

[23] J.-H. Yoon, J. Song, and S.-J. Lee, "Practical application of building integrated photovoltaic (BIPV) system using transparent amorphous silicon thin-film PV module," *Sol. Energy*, vol. 85, no. 5, pp. 723–733, May 2011.

[24] M. A. Green, K. Emery, Y. Hishikawa, W. Warta, and E. D. Dunlop, "Solar cell efficiency tables (version 44)," no. version 44, pp. 701–710, 2014.

[25] I. Repins, M. A. Contreras, B. Egaas, C. Dehart, J. Scharf, C. L. Perkins, B. To, and R. Noufi, "19.9% efficient ZnO/CdS/ CuInGaSe 2 Solar Cell with 81.2% Fill Factor," *Prog. Photovoltaics Res. Appl.*, vol. 16, no. February, pp. 235–239, 2008.

[26] D. A. Cusano, "CdTe solar cells and photovoltaic heterojunctions in II–VI compounds," *Solid. State. Electron.*, vol. 6, no. 3, pp. 217–218, 1963.

[27] B. Goldstein, "Properties of Photovoltaic Films of CdTe," *Phys. Rev.*, vol. 109, no. 2, pp. 601–603, Jan. 1958.

[28] V. M. Fthenakis, "Life cycle impact analysis of cadmium in CdTe PV production," *Renew. Sustain. Energy Rev.*, vol. 8, no. 4, pp. 303–334, Aug. 2004.

[29] First Solar, "First Solar - The Recycling Advantage," 2014. [Online]. Available: http://www.firstsolar.com/en/technologies-and-capabilities/recycling-services. [Accessed: 06-Feb-2013].

[30] D. Lincot, R. Gaucher, E. Alsema, A. Million, and A. Jager-Waldau, "Environmental, Health and Safety (EHS) Aspects of First Solar Cadmium Telluride (CdTe) Photovoltaic Systems," 2009.

[31] First Solar, "First Solar - Projects," 2014. [Online]. Available: http://www.firstsolar.com/About-Us/Projects. [Accessed: 13-May-2013].

[32] G. P. Limited, "G24 Power Ltd," 2014. [Online]. Available: http://gcell.com/. [Accessed: 15-May-2012].

[33] SPECIFIC, "SPECIFIC - Swansea University," 2014. [Online]. Available: http://www.specific.eu.com/. [Accessed: 02-Jan-2013].

[34] B. O'Regan and M. Gratzel, "A low-cost, high-efficiency solar cell based on dye-sensitized colloidal TiO2 films," *Nature*, vol. 353, no. 6346, pp. 737–740, Oct. 1991.

[35] A. Yella, H.-W. Lee, H. N. Tsao, C. Yi, A. K. Chandiran, M. K. Nazeeruddin, E. W.-G. Diau, C.-Y. Yeh, S. M. Zakeeruddin, and M. Grätzel, "Porphyrin-Sensitized Solar Cells with Cobalt (II/III)-Based Redox Electrolyte Exceed 12 Percent Efficiency," *Science (80-.).*, vol. 334, no. 6056, pp. 629–634, Nov. 2011.

[36] A.-F. Kanta and A. Decroly, "Stainless steel electrode characterizations by electrochemical impedance spectroscopy for dye-sensitized solar cells," *Electrochim. Acta*, vol. 56, no. 27, pp. 10276–10282, Nov. 2011.

[37] A.-F. Kanta and A. Decroly, "An investigation of the electrolytic solution effects on stainless steel electrode for dye-sensitized solar cells," *Mater. Chem. Phys.*, vol. 130, no. 3, pp. 843–846, Nov. 2011.

[38] M. Toivola, F. Ahlskog, and P. Lund, "Industrial sheet metals for nanocrystalline dye-sensitized solar cell structures," *Sol. Energy Mater. Sol. Cells*, vol. 90, no. 17, pp. 2881–2893, Nov. 2006.

[39] M. Toivola, "Dye Sensitized Solar Cells on Alternative Substrates," Aalto University, 2010.

[40] N. Papageorgiou, S. Haruyama, K. Fujimoto, H. Konno, B. R. Pearson, M. Nagayama, N. Kagaku, T. Technology, and R. S. Alwitt, "An Iodine / Triiodide Reduction Electrocatalyst for Aqueous and Organic Media," *J. Electrochem. Soc.*, vol. 144, no. 3, pp. 876–884, 1997.

[41] J. Burschka, N. Pellet, S.-J. Moon, R. Humphry-Baker, P. Gao, M. K. Nazeeruddin, and M. Grätzel, "Sequential deposition as a route to high-performance perovskite-sensitized solar cells.," *Nature*, vol. 499, no. 7458, pp. 316–9, Jul. 2013.

[42] A. Henemann, "BIPV: Built-in solar energy," *Renew. Energy Focus*, vol. 9, no. 6, pp. 14–19, Nov. 2008.

[43] H. Desilvestro, M. Bertoz, R. Harikisun, P. Murray, P. Infelta, S. Tulloch, and G. Tulloch, "Packaging , Scaling Up and Commercialization of Dye Solar Cells," 2009.

[44] J. Moser, "Notiz über die Verstärkung photoelectrischer Ströme durch optische Sensibilisierung," *Monatsh. Chem.*, vol. 8, p. 373, 1887.

[45] S.-N. Chen, S. K. Deb, and W. H., "Dye - Titanium dioxide photogalvanic cell," 4,080,4881978.

[46] J. Desilvestro, M. Gratzel, L. Kavan, and J. Augustynski, "Highly Efficient Sensitization of Titanium Dioxide," *Society*, vol. 432, no. 5, pp. 2988–2990, 1985.

[47] N.-G. Park, J. van de Lagemaat, and A. J. Frank, "Comparison of Dye-Sensitized Rutile- and Anatase-Based TiO2 Solar Cells," *J. Phys. Chem. B*, vol. 104, no. 38, pp. 8989–8994, Sep. 2000.

[48] J. Moellmann, S. Ehrlich, R. Tonner, and S. Grimme, "A DFT-D study of structural and energetic properties of TiO2 modifications.," *J. Phys. Condens. Matter*, vol. 24, no. 42, p. 424206, Oct. 2012.

[49] H. Gerischer, M. E. Michel-Beyerle, F. Rebentrost, and H. Tributsch, "Sensitization of charge injection into semiconductors with large band gap," *Electrochim. Acta*, vol. 13, no. 6, pp. 1509–1515, 1968.

[50] J. Moser and M. Graetzel, "Photosensitized electron injection in colloidal semiconductors," *J. Am. Chem. Soc.*, vol. 106, no. 22, pp. 6557–6564, Oct. 1984.

[51] J. Desilvestro, M. Graetzel, L. Kavan, J. Moser, and J. Augustynski, "Highly efficient sensitization of titanium dioxide," *J. Am. Chem. Soc.*, vol. 107, no. 10, pp. 2988–2990, May 1985.

[52] M. Gratzel, "Solar Energy Conversion by Dye-Sensitized Photovoltaic Cells," *Inorg. Chem.*, vol. 44, no. 20, pp. 6841–6851, Oct. 2005.

[53] L. Hu, S. Dai, J. Weng, S. Xiao, Y. Sui, Y. Huang, S. Chen, F. Kong, X. Pan, L. Liang, and K. Wang, "Microstructure design of nanoporous TiO2 photoelectrodes for dye-sensitized solar cell modules.," *J. Phys. Chem. B*, vol. 111, no. 2, pp. 358–62, Jan. 2007.

[54] J. van de Lagemaat, N.-G. Park, and a. J. Frank, "Influence of Electrical Potential Distribution, Charge Transport, and Recombination on the Photopotential and Photocurrent Conversion Efficiency of Dye-Sensitized Nanocrystalline TiO 2 Solar Cells: A Study by Electrical Impedance and Optical Modulation T," *J. Phys. Chem. B*, vol. 104, no. 9, pp. 2044–2052, Mar. 2000.

[55] J. Sheng, J. Karasawa, and T. Fukami, "Thickness dependence of photocatalytic activity of anatase filma by magnetron sputtering," *J. Mater. Sci. Lett.*, vol. 6, pp. 1709–1711, 1997.

[56] T. Ohno, K. Sarukawa, K. Tokieda, and M. Matsumura, "Morphology of a TiO2 Photocatalyst (Degussa, P-25) Consisting of Anatase and Rutile Crystalline Phases," *J. Catal.*, vol. 203, no. 1, pp. 82–86, Oct. 2001.

[57] K. Kalyanasundaram and M. Gra, "Applications of functionalized transition metal complexes in photonic and optoelectronic devices," *Coord. Chem. Rev.*, vol. 177, no. 1, pp. 347–414, Oct. 1998.

[58] S. Nakade, M. Matsuda, S. Kambe, Y. Saito, T. Kitamura, T. Sakata, Y. Wada, H. Mori, and S. Yanagida, "Dependence of TiO2 Nanoparticle Preparation Methods and

Annealing Temperature on the Efficiency of Dye-Sensitized Solar Cells," *J. Phys. Chem. B*, vol. 106, no. 39, pp. 10004–10010, 2002.

[59] M. Durr, A. Schmid, M. Obermaier, S. Rosselli, A. Yasuda, and G. Nelles, "Low-temperature fabrication of dye-sensitized solar cells by transfer of composite porous layers," *Nat Mater*, vol. 4, no. 8, pp. 607–611, Aug. 2005.

[60] V. E, L. Saadoun, J. A. Ayllon, X. Domenech, I. Zumeta, and R. Rodriguez-Clemente, "TiO2 thin film deposition from solution using microwave heating," *Thin Solid Films*, vol. 365, pp. 12–18, 2000.

[61] D. Gutierrez-Tauste, I. Zumeta, E. Vigil, M. Hernandezfenollosa, X. Domenech, and J. Ayllon, "New low-temperature preparation method of the TiO porous photoelectrode for dye-sensitized solar cells using UV irradiation," *J. Photochem. Photobiol. A Chem.*, vol. 175, no. 2–3, pp. 165–171, Oct. 2005.

[62] T. Watson, I. Mabbett, H. Wang, L. Peter, and D. Worsley, "Ultrafast near infrared sintering of TiO2 layers on metal substrates for dye-sensitized solar cells," *Prog. Photovoltaics Res. Appl.*, vol. 19, no. 4, pp. 482–486, Jun. 2011.

[63] C. J. Barbe, F. Arendse, P. Comte, M. Jirousek, F. Lenzmann, V. Shklover, M. Gra, and M. Grätzel, "Nanocrystalline Titanium Oxide Electrodes for Photovoltaic Applications," *J. Am. Ceram. Soc.*, vol. 71, pp. 3157–3171, 1997.

[64] S. M. Zakeeruddin, M. K. Nazeeruddin, P. Pechy, F. P. Rotzinger, K. Kalyanasundaram, M. Gra, V. Shklover, and T. Haibach, "Molecular Engineering of Photosensitizers for Nanocrystalline Solar Cells: Synthesis and Characterization of Ru Dyes Based on Phosphonated Terpyridines," *Society*, vol. 1669, no. 8, pp. 5937–5946, 1997.

[65] J.-H. Yum and M. K. Nazeeruddin, "Molecular Engineering of Sensitisers for Conversion of Solar Energy into Electricity," in *Dye Sensitized Solar Cells*, 2010, pp. 89–99.

[66] Sigma-Aldrich, "Di-tetrabutylammonium cis-bis(isothiocyanato)bis(2,2'-bipyridyl-4,4'-dicarboxylato)ruthenium(II)." [Online]. Available: http://www.sigmaaldrich.com/catalog/product/aldrich/703214?lang=en&region=GB .

[67] S. Hwang, J. H. Lee, C. Park, H. Lee, C. Kim, C. Park, M.-H. Lee, W. Lee, J. Park, K. Kim, N.-G. Park, and C. Kim, "A highly efficient organic sensitizer for dye-sensitized solar cells," *Chem. Commun.*, vol. 0, no. 46, pp. 4887–4889, 2007.

[68] A. Mishra, M. K. R. Fischer, and P. Bäuerle, "Metal-Free Organic Dyes for Dye-Sensitized Solar Cells: From Structure: Property Relationships to Design Rules," *Angew. Chemie Int. Ed.*, vol. 48, no. 14, pp. 2474–2499, Mar. 2009.

[69] J. Halme, P. Vahermaa, K. Miettunen, and P. Lund, "Device physics of dye solar cells.," *Adv. Mater.*, vol. 22, no. 35, pp. E210–34, Sep. 2010.

[70] M. Grätzel, "Conversion of sunlight to electric power by nanocrystalline dye-sensitized solar cells*1," *J. Photochem. Photobiol. A Chem.*, vol. 164, no. 1–3, pp. 3–14, Jun. 2004.

[71] J.-H. Yum, E. Baranoff, S. Wenger, M. K. Nazeeruddin, and M. Gratzel, "Panchromatic engineering for dye-sensitized solar cells," *Energy Environ. Sci.*, vol. 4, no. 3, pp. 842–857, 2011.

[72] P. J. Holliman, M. Mohsen, A. Connell, M. L. Davies, K. Al-Salihi, M. B. Pitak, G. J. Tizzard, S. J. Coles, R. W. Harrington, W. Clegg, C. Serpa, O. H. Fontes, C. Charbonneau, and M. J. Carnie, "Ultra-fast Co-Sensitization and Tri-Sensitization of Dye-Sensitized Solar Cells with N719, SQ1 and Triarylamine Dyes," *J. Mater. Chem.*, vol. 22, pp. 13318–13327, 2012.

[73] M. Grätzel, "Dye-sensitized solar cells," *Photochem. Photobiol.*, vol. 4, pp. 145–153, 2003.

[74] A. Stanley, B. Verity, and D. Matthews, "Minimizing the dark current at the dye-sensitized TiO2 electrode," *Sol. Energy Mater. Sol. Cells*, vol. 52, pp. 141–154, Mar. 1998.

[75] W. C. S. E. Rijnberg, J.M. Kroon, J. Wienke, A. Hinsch, J.A.M. van Roosmalen, "Long Term Stability of NC-DSSCs," *Power*, vol. 2, pp. 1–6.

[76] G. Boschloo and A. Hagfeldt, "Characteristics of the iodide/triiodide redox mediator in dye-sensitized solar cells.," *Acc. Chem. Res.*, vol. 42, no. 11, pp. 1819–26, Nov. 2009.

[77] S. Nakade, T. Kanzaki, W. Kubo, T. Kitamura, Y. Wada, and S. Yanagida, "Role of Electrolytes on Charge Recombination in Dye-Sensitized TiO 2 Solar Cell (1): The Case of Solar Cells Using the I - / I 3 - Redox Couple," *Society*, no. 1, pp. 3480–3487, 2005.

[78] K. Paulo and K. Lobato, "Charge Transport and Recombination in Dye-Sensitized Nanocrystalline Solar Cells," 2007.

[79] S. Y. Huang, G. Schlichthörl, a. J. Nozik, M. Grätzel, a. J. Frank, and G. Schlichtho, "Charge Recombination in Dye-Sensitized Nanocrystalline TiO 2 Solar Cells," *J. Phys. Chem. B*, vol. 101, no. 14, pp. 2576–2582, Apr. 1997.

[80] R. Katoh, "Kinetics and mechanism of electron injection and charge recombination in dye-sensitized nanocrystalline semiconductors," *Coord. Chem. Rev.*, vol. 248, no. 13–14, pp. 1195–1213, Jul. 2004.

[81] M. Wang, N. Chamberland, L. Breau, J.-E. Moser, R. Humphry-Baker, B. Marsan, S. M. Zakeeruddin, and M. Grätzel, "An organic redox electrolyte to rival triiodide/iodide in dye-sensitized solar cells.," *Nat. Chem.*, vol. 2, no. 5, pp. 385–9, May 2010.

[82] Z. Yu, N. Vlachopoulos, M. Gorlov, and L. Kloo, "Liquid Electrolytes for dye-sensitized solar cells," *Dalt. Trans*, vol. 40, pp. 10289–10303, 2011.

[83] J. B. Sambur, T. Novet, and B. A. Parkinson, "Multiple Exciton Collection in a Sensitized Photovoltaic System," *Sci.* , vol. 330 , no. 6000 , pp. 63–66, Oct. 2010.

[84] R. J. Ellingson, M. C. Beard, J. C. Johnson, P. Yu, O. I. Micic, A. J. Nozik, A. Shabaev, and A. L. Efros, "Highly Efficient Multiple Exciton Generation in Colloidal PbSe and PbS Quantum Dots," *Nano Lett.*, vol. 5, no. 5, pp. 865–871, Mar. 2005.

[85] B. M. Klahr and T. W. Hamann, "Performance Enhancement and Limitations of Cobalt Bipyridyl Redox Shuttles in Dye-Sensitized Solar Cells," *J. Phys. Chem. C*, vol. 113, no. 31, pp. 14040–14045, Aug. 2009.

[86] M. Liberatore, L. Burtone, T. M. Brown, a. Reale, a. Di Carlo, F. Decker, S. Caramori, and C. a. Bignozzi, "On the effect of Al[sub 2]O[sub 3] blocking layer on the performance of dye solar cells with cobalt based electrolytes," *Appl. Phys. Lett.*, vol. 94, no. 17, p. 173113, 2009.

[87] H. Nusbaumer, S. M. Zakeeruddin, J.-E. Moser, and M. Grätzel, "An alternative efficient redox couple for the dye-sensitized solar cell system.," *Chemistry*, vol. 9, no. 16, pp. 3756–63, Aug. 2003.

[88] S. A. Sapp, C. M. Elliott, C. Contado, S. Caramori, and C. A. Bignozzi, "Substituted polypyridine complexes of cobalt(II/III) as efficient electron-transfer mediators in dye-sensitized solar cells.," *J. Am. Chem. Soc.*, vol. 124, no. 37, pp. 11215–22, Sep. 2002.

[89] S. M. Feldt, E. A. Gibson, E. Gabrielsson, L. Sun, G. Boschloo, and A. Hagfeldt, "Design of organic dyes and cobalt polypyridine redox mediators for high-efficiency dye-sensitized solar cells.," *J. Am. Chem. Soc.*, vol. 132, no. 46, pp. 16714–24, Nov. 2010.

[90] H.-S. Kim, S.-B. Ko, I.-H. Jang, and N.-G. Park, "Improvement of mass transport of the [Co(bpy)3](II/III) redox couple by controlling nanostructure of TiO2 films in dye-sensitized solar cells.," *Chem. Commun. (Camb).*, vol. 47, no. 47, pp. 12637–9, Dec. 2011.

[91] Y. Liu, J. R. Jennings, Y. Huang, Q. Wang, S. M. Zakeeruddin, and M. Gr, "Cobalt Redox Mediators for Ruthenium-Based Dye-Sensitized Solar Cells : A Combined Impedance Spectroscopy and Near-IR Transmittance Study," pp. 18847–18855, 2011.

[92] H. Nusbaumer, J.-E. Moser, S. M. Zakeeruddin, M. K. Nazeeruddin, and M. Grätzel, "Co(II)(dbbip)2, 2+ Complex Rivals Tri-iodide/Iodide Redox Mediator in Dye-Sensitized Photovoltaic Cells," *J. Phys. Chem. B*, vol. 105, no. 43, pp. 10461–10464, Nov. 2001.

[93] S. M. Feldt, G. Wang, G. Boschloo, and A. Hagfeldt, "Effects of Driving Forces for Recombination and Regeneration on the Photovoltaic Performance of Dye-Sensitized Solar Cells using Cobalt Polypyridine Redox Couples," *J. Phys. Chem. C*, vol. 115, no. 43, pp. 21500–21507, Nov. 2011.

[94] M. K. Nazeeruddin, A. Kay, R. Humphry-Baker, E. Muller, P. Liska, N. Vlachopoulos, and M. Grätzel, "Conversion of Light to Electricity by cis-X2Bis(2,2'-bipyridyl-4,4'-

dicarboxylate)ruthenium(11) Charge-Transfer Sensitizers (X = Cl-, Br-, I-, CN-, and SCN-) on Nanocrystalline Ti02 Electrodes," *J. Am. Chem. Soc.*, no. 4, pp. 7863–7863, 1993.

[95] K. Suzuki, M. Yamaguchi, M. Kumagai, and S. Yanagida, "Application of Carbon Nanotubes to Counter Electrodes of Dye-sensitized Solar Cells," *Chem. Lett.*, vol. 32, no. 1, pp. 28–29, 2003.

[96] J. H. Park, Y. Jun, H.-G. Yun, S.-Y. Lee, and M. G. Kang, "Fabrication of an Efficient Dye-Sensitized Solar Cell with Stainless Steel Substrate," *J. Electrochem. Soc.*, vol. 155, no. 7, p. F145, 2008.

[97] W. Yao, J. Yang, J. Wang, and Y. Nuli, "Chemical deposition of platinum nanoparticles on iridium oxide for oxygen electrode of unitized regenerative fuel cell," vol. 9, pp. 1029–1034, 2007.

[98] S.-A. Sheppard, S. a. Campbell, J. R. Smith, G. W. Lloyd, F. C. Walsh, and T. R. Ralph, "Electrochemical and microscopic characterisation of platinum-coated perfluorosulfonic acid (Nafion 117) materials†," *Analyst*, vol. 123, no. 10, pp. 1923–1929, 1998.

[99] J. H. Park, Y. Jun, H.-G. Yun, S.-Y. Lee, and M. G. Kang, "Fabrication of an Efficient Dye-Sensitized Solar Cell with Stainless Steel Substrate," *J. Electrochem. Soc.*, vol. 155, no. 7, p. F145, 2008.

[100] Y. Jun and M. G. Kang, "The Characterization of Nanocrystalline Dye-Sensitized Solar Cells with Flexible Metal Substrates by Electrochemical Impedance Spectroscopy," *J. Electrochem. Soc.*, vol. 154, no. 1, p. B68, 2007.

[101] M. Kang, N. Park, K. Ryu, S. Chang, and K. Kim, "A 4.2% efficient flexible dye-sensitized TiO2 solar cells using stainless steel substrate," *Sol. Energy Mater. Sol. Cells*, vol. 90, no. 5, pp. 574–581, Mar. 2006.

[102] A. Hauch and A. Georg, "Diffusion in the electrolyte and charge-transfer reaction at the platinum electrode in dye-sensitized solar cells," *Electrochim. Acta*, vol. 46, pp. 3457– 3466, 2001.

[103] G. Tsekouras, A. J. Mozer, and G. G. Wallace, "Enhanced Performance of Dye Sensitized Solar Cells Utilizing Platinum Electrodeposit Counter Electrodes," *J. Electrochem. Soc.*, vol. 155, no. 7, pp. K124 – K128, 2008.

[104] H. Bönnemann, N. Waldöfner, H.-G. Haubold, and T. Vad, "Preparation and Characterization of Three-Dimensional Pt Nanoparticle Networks," *Chem. Mater.*, vol. 14, no. 3, pp. 1115–1120, Mar. 2002.

[105] D. A. Wragg, "Application and Optimization of the Platinum Catalyst in Dye Sensitised Solar Cells - MRes Thesis," Swansea University, 2010.

[106] T. Watson, P. Holliman, and D. Worsley, "Rapid, continuous in situ monitoring of dye sensitisation in dye-sensitized solar cells," *J. Mater. Chem.*, vol. 21, no. 12, p. 4321, 2011.

[107] E. Dell'Orto, L. Raimondo, A. Sassella, and A. Abbotto, "Dye-sensitized solar cells: spectroscopic evaluation of dye loading on TiO2," *J. Mater. Chem.*, vol. 22, no. 22, pp. 11364–11369, 2012.

[108] P. J. Holliman, M. L. Davies, A. Connell, B. V. Velasco, and T. M. Watson, "Ultra-fast dye sensitisation and co-sensitisation for dye sensitized solar cells," *Chem. Commun.*, vol. 46, no. 38, pp. 7256–7258, 2010.

[109] N. Papageorgiou, "An Iodine/Triiodide Reduction Electrocatalyst for Aqueous and Organic Media," *J. Electrochem. Soc.*, vol. 144, no. 3, p. 876, 1997.

[110] S. Caramori, V. Cristino, R. Boaretto, R. Argazzi, C. A. Bignozzi, and A. Di Carlo, "New Components for Dye-Sensitized Solar Cells," *Int. J. Photoenergy*, vol. 2010, pp. 1–16, 2010.

[111] T. Muto, M. Ikegami, and T. Miyasaka, "Polythiophene-Based Mesoporous Counter Electrodes for Plastic Dye-Sensitized Solar Cells," *J. Electrochem. Soc.*, vol. 157, no. 8, p. B1195, 2010.

[112] M. Wu, X. Lin, Y. Wang, L. Wang, W. Guo, D. Qi, X. Peng, A. Hagfeldt, M. Grätzel, and T. Ma, "Economical Pt-free catalysts for counter electrodes of dye-sensitized solar cells.," *J. Am. Chem. Soc.*, vol. 134, no. 7, pp. 3419–28, Feb. 2012.

[113] C. Charbonneau, K. Hooper, B. Philip, D. Wragg, T. Watson, and D. Worsley, "Rapid Radiative Platinisation for dye-sensitised solar cell counter electrodes," *Prog. Photovoltaics*, 2013.

[114] S. Beucker, A. Hinsch, H. Brandt, W. Veurman, K. Flarup Jensen, C. Lang-Koetz, and M. Stabe, "Scaling-up of glass based DSC-modules for applications in building integrated photovoltaics," *2009 34th IEEE Photovolt. Spec. Conf.*, pp. 000937–000941, Jun. 2009.

[115] M. Oliver and T. Jackson, "Energy and economic evaluation of building-integrated photovoltaics," *Energy*, vol. 26, no. 4, pp. 431–439, Apr. 2001.

[116] B. P. Jelle and C. Breivik, "State-of-the-art Building Integrated Photovoltaics," *Energy Procedia*, vol. 20, no. 1876, pp. 68–77, Jan. 2012.

[117] B. H. Zervos, B. Kahn, and D. Park, "Printed and Thin Film Photovoltaics and Batteries."

[118] A. Hagfeldt and M. Gratzel, "Molecular Photovoltaics," *Acc. Chem. Res.*, vol. 33, no. 5, pp. 269–277, 2000.

[119] N. Kato, K. Higuchi, H. Tanaka, J. Nakajima, T. Sano, and T. Toyoda, "Improvement in long-term stability of dye-sensitized solar cell for outdoor use," *Sol. Energy Mater. Sol. Cells*, vol. 95, no. 1, pp. 301–305, Jan. 2011.

[120] A. Hinsch, J. M. Kroon, R. Kern, I. Uhlendorf, J. Holzbock, A. Meyer, and J. Ferber, "Long-term stability of dye-sensitised solar cells," *Prog. Photovoltaics Res. Appl.*, vol. 9, no. 6, pp. 425–438, Nov. 2001.

[121] G. Hashmi, K. Miettunen, T. Peltola, J. Halme, I. Asghar, K. Aitola, M. Toivola, and P. Lund, "Review of materials and manufacturing options for large area flexible dye solar cells," *Renew. Sustain. Energy Rev.*, vol. 15, no. 8, pp. 3717–3732, Oct. 2011.

[122] H. Pettersson and T. Gruszecki, "Long-term stability of low-power dye-sensitised solar cells prepared by industrial methods," *Sol. Energy Mater. Sol. Cells*, vol. 70, no. 2, pp. 203–212, Dec. 2001.

[123] M. Carnie, D. Bryant, T. Watson, and D. Worsley, "Photocatalytic Oxidation of Triiodide in UVA-Exposed Dye-Sensitized Solar Cells," *Int. J. Photoenergy*, vol. 2012, pp. 1–8, 2012.

[124] M. Carnie, D. Bryant, T. Watson, and D. Worsley, "UV Filtering of Dye-Sensitized Solar Cells: The Effects of Varying the UV Cut-Off upon Cell Performance and Incident Photon-to-Electron Conversion Efficiency," *Int. J. Photoenergy*, vol. 2012, pp. 1–8, 2012.

[125] P. M. Sommeling, "Long-term stability testing of dye-sensitized solar cells," *J. Photochem. Photobiol. A Chem.*, vol. 164, no. 1–3, pp. 137–144, Jun. 2004.

[126] E. Olsen, "Dissolution of platinum in methoxy propionitrile containing Li/I 2," *Sol. Energy Mater. Sol. Cells*, vol. 63, pp. 267–273, 2000.

[127] M. Izu and T. Ellison, "Roll-to-roll manufacturing of amorphous silicon alloy solar cells with in situ cell performance diagnostics," *Sol. Energy Mater. Sol. Cells*, vol. 78, no. 1–4, pp. 613–626, Jul. 2003.

[128] R. Søndergaard, M. Hösel, D. Angmo, T. T. Larsen-Olsen, and F. C. Krebs, "Roll-to-roll fabrication of polymer solar cells," *Mater. Today*, vol. 15, no. 1–2, pp. 36–49, Jan. 2012.

[129] K. Miettunen, M. Toivola, G. Hashmi, J. Salpakari, I. Asghar, and P. Lund, "A carbon gel catalyst layer for the roll-to-roll production of dye solar cells," *Carbon N. Y.*, vol. 49, no. 2, pp. 528–532, Feb. 2011.

[130] C. Rao and D. Trivedi, "Chemical and electrochemical depositions of platinum group metals and their applications," *Coord. Chem. Rev.*, vol. 249, no. 5–6, pp. 613–631, Mar. 2005.

[131] M. Paunovic and M. Schlesinger, *Fundamentals of Electrochemical Deposition*. Wiley, 2006.

[132] F. Ye, L. Chen, J. Li, J. Li, and X. Wang, "Shape-controlled fabrication of platinum electrocatalyst by pulse electrodeposition," *Electrochem. commun.*, vol. 10, no. 3, pp. 476–479, Mar. 2008.

[133] S. M. Ayyadurai, Y.-S. Choi, P. Ganesan, S. P. Kumaraguru, and B. N. Popov, "Novel PEMFC Cathodes Prepared by Pulse Deposition," *J. Electrochem. Soc.*, vol. 154, no. 10, p. B1063, 2007.

[134] M. Chandrasekar and M. Pushpavanam, "Pulse and pulse reverse plating—Conceptual, advantages and applications," *Electrochim. Acta*, vol. 53, no. 8, pp. 3313–3322, Mar. 2008.

[135] Y.-J. Song, J.-K. Oh, and K. Park, "Pt nanostructure electrodes pulse electrodeposited in PVP for electrochemical power sources.," *Nanotechnology*, vol. 19, no. 35, p. 355602, Sep. 2008.

[136] S. Kim, Y. Nah, Y. Noh, J. Jo, and D. Kim, "Electrodeposited Pt for cost-efficient and flexible dye-sensitized solar cells," *Electrochim. Acta*, vol. 51, no. 18, pp. 3814–3819, May 2006.

[137] S. U. C. Dept., *Southampton Electrochemistry Summer School Course Material.* Southampton University Chemistry Dept., 2011.

[138] K. H. Choi, H. S. Kim, and T. H. Lee, "Electrode fabrication for proton exchange membrane fuel cells by pulse electrodeposition," *J. Power Sources*, vol. 75, no. 2, pp. 230–235, Oct. 1998.

[139] N. Ibl, "Some theoretical aspects of pulse electrolysis," *Surf. Technol.*, vol. 10, no. 2, pp. 81–104, 1980.

[140] Y.-S. Ko and Y.-U. Kwon, "Electrochemical deposition of platinum on fluorine-doped tin oxide: The nucleation mechanisms," *Electrochim. Acta*, vol. 55, no. 24, pp. 7276–7281, Oct. 2010.

[141] C.-Y. Lin, J.-Y. Lin, C.-C. Wan, and T.-C. Wei, "High-performance and low platinum loading electrodeposited-Pt counter electrodes for dye-sensitized solar cells," *Electrochim. Acta*, vol. 56, no. 5, pp. 1941–1946, Feb. 2011.

[142] X. Chen, N. Li, K. Eckhard, L. Stoica, W. Xia, J. Assmann, M. Muhler, and W. Schuhmann, "Pulsed electrodeposition of Pt nanoclusters on carbon nanotubes modified carbon materials using diffusion restricting viscous electrolytes," *Electrochem. commun.*, vol. 9, no. 6, pp. 1348–1354, Jun. 2007.

[143] A. Gomes and M. I. da Silva Pereira, "Pulsed electrodeposition of Zn in the presence of surfactants," *Electrochim. Acta*, vol. 51, no. 7, pp. 1342–1350, Jan. 2006.

[144] M. Saitou, "Electrochemical characterization of platinum black electrodeposited from electrolyte including lead acetate trihydrate," *Surf. Coatings Technol.*, vol. 201, no. 6, pp. 3611–3614, Dec. 2006.

[145] A. D. McNaught and A. Wilkinson, *IUPAC. Compendium of Chemical Terminology, 2nd ed. (the "Gold Book").* Blackwell Scientific Publications, Oxford, 1997.

[146] A. M. Feltham, M. Spiro, I. Introduction, C. Efficiency, D. S. Pretreatment, A. D. Appearance, B. D. Growth, V. S. Area, A. E. Determination, C. Reproducibility, and R. P. Procedures, "Platinized Platinum Electrodes," vol. 1970, no. 1895, 1970.

[147] B. M. E. Baumgartner and C. J. Raub, "The Electrodeposition of Platinum and Platinum Alloys," *Platin. Met. Rev.*, vol. 32, no. 4, pp. 188–197, 1988.

[148] C. Yoon, J. Lee, W. Chae, and K. Kim, "Enhanced performance of a dye-sensitized solar cell with an electrodeposited-platinum counter electrode," *Electrochim. Acta*, vol. 53, no. 6, pp. 2890–2896, Feb. 2008.

[149] P. Li, J. Wu, J. Lin, M. Huang, Z. Lan, and Q. Li, "Improvement of performance of dye-sensitized solar cells based on electrodeposited-platinum counter electrode," *Electrochim. Acta*, vol. 53, no. 12, pp. 4161–4166, 2008.

[150] C.-C. Yang, H. Q. Zhang, and Y. R. Zheng, "DSSC with a novel Pt counter electrodes using pulsed electroplating techniques," *Curr. Appl. Phys.*, vol. 11, no. 1, pp. S147–S153, Jan. 2011.

[151] C.-C. Wang, J.-G. Chen, K.-C. Huang, H.-W. Chen, Y.-C. Wang, C.-Y. Hsu, R. Vittal, J.-J. Lin, and K.-C. Ho, "A platinum film with organized pores for the counter electrode in dye-sensitized solar cells," *J. Power Sources*, vol. 239, pp. 496–499, Oct. 2013.

[152] W. Schwarzacher, O. I. Kasyutich, P. R. Evans, M. G. Darbyshire, G. Yi, V. M. Fedosyuk, F. Rousseaux, E. Cambril, and D. Decanini, "Metal nanostructures prepared by template electrodeposition," *J. Magn. Magn. Mater.*, vol. 198–199, pp. 185–190, Jun. 1999.

[153] M. a. Ghanem, P. N. Bartlett, P. de Groot, and A. Zhukov, "A double templated electrodeposition method for the fabrication of arrays of metal nanodots," *Electrochem. commun.*, vol. 6, no. 5, pp. 447–453, May 2004.

[154] J. Yin, J. Jia, and L. Zhu, "Double-template synthesis of platinum nanomaterials for oxygen reduction," *Microchim. Acta*, vol. 166, no. 1–2, pp. 151–156, Jun. 2009.

[155] S. R. Brankovic, J. X. Wang, and R. R. Ad, "Metal monolayer deposition by replacement of metal adlayers on electrode surfaces," *Surf. Sci.*, vol. 474, pp. L173–179, 2001.

[156] A. J. Bard and L. R. Faulkner, "Appendix C - Reference Tables," in *Electrochemical Methods: Fundamentals and Applications*, 2nd ed., D. Harris, E. S. Swain, C. Robey, and E. Aiello, Eds. John Wiley & Sons, Ltd., 2001, pp. 808–809.

[157] T. S. Mkwizu, M. K. Mathe, and I. Cukrowski, "Electrodeposition of multilayered bimetallic nanoclusters of ruthenium and platinum via surface-limited redox-replacement reactions for electrocatalytic applications.," *Langmuir*, vol. 26, no. 1, pp. 570–80, Jan. 2010.

[158] S. Papadimitriou, a. Tegou, E. Pavlidou, G. Kokkinidis, and S. Sotiropoulos, "Methanol oxidation at platinized lead coatings prepared by a two-step electrodeposition–electroless deposition process on glassy carbon and platinum substrates," *Electrochim. Acta*, vol. 52, no. 21, pp. 6254–6260, Jun. 2007.

[159] L. T. Viyannalage, R. Vasilic, and N. Dimitrov, "Epitaxial Growth of Cu on Au (111) and Ag (111) by Surface Limited Redox ReplacementsAn Electrochemical and STM Study," no. 111, pp. 4036–4041, 2007.

[160] R. E. Rettew, J. W. Guthrie, and F. M. Alamgir, "Layer-by-Layer Pt Growth on Polycrystalline Au: Surface-Limited Redox Replacement of Overpotentially Deposited Ni Monolayers," *J. Electrochem. Soc.*, vol. 156, no. 11, p. D513, 2009.

[161] D. Gokcen, S.-E. Bae, and S. R. Brankovic, "Stoichiometry of Pt Submonolayer Deposition via Surface-Limited Redox Replacement Reaction," *J. Electrochem. Soc.*, vol. 157, no. 11, p. D582, 2010.

[162] M. Fayette, Y. Liu, D. Bertrand, J. Nutariya, N. Vasiljevic, and N. Dimitrov, "From Au to Pt via surface limited redox replacement of Pb UPD in one-cell configuration.," *Langmuir*, vol. 27, no. 9, pp. 5650–8, May 2011.

[163] B. Zhang, D. Wang, Y. Hou, S. Yang, X. H. Yang, J. H. Zhong, J. Liu, H. F. Wang, P. Hu, H. J. Zhao, and H. G. Yang, "Facet-dependent catalytic activity of platinum nanocrystals for triiodide reduction in dye-sensitized solar cells.," *Sci. Rep.*, vol. 3, p. 1836, May 2013.

[164] G. Smestad, C. Bignozzi, and R. Argazzi, "Testing of dye sensitized TiO 2 solar cells I : Experimental photocurrent output and conversion efficiencies," *Luminescence*, vol. 32, pp. 259–272, 1994.

[165] H. Greijer, "Environmental aspects of electricity generation from a nanocrystalline dye sensitized solar cell system," *Renew. Energy*, vol. 23, no. 1, pp. 27–39, May 2001.

[166] J. Goldstein, I. Yakupov, and B. Breen, "Development of large area photovoltaic dye cells at 3GSolar," *Sol. Energy Mater. Sol. Cells*, vol. 94, no. 4, pp. 638–641, Apr. 2010.

[167] N. Vyas, C. Charbonneau, M. Carnie, D. A. Worsley, and T. M. Watson, "An Inorganic/Organic Hybrid Coating for Low Cost Metal Mounted Dye-Sensitized Solar Cells," *ECS Trans.* , vol. 53 , no. 24 , pp. 29–37, Oct. 2013.

[168] N. Vyas, D. A. Wragg, C. Charbonneau, M. Carnie, and T. M. Watson, "Low Cost TCO Less Counter Electrodes for Dye-Sensitized Solar Cell Application," *ECS Trans.* , vol. 53 , no. 24 , pp. 39–46, Oct. 2013.

[169] C. a. Mann, "Organic Inhibitors of Corrosion," *Trans. Electrochem. Soc.*, vol. 69, p. 115, 1936.

[170] S. a Umoren, U. M. Eduok, and E. E. Oguzie, "Corrosion Inhibition of Mild Steel in 1 M H 2 SO 4 by Polyvinyl Pyrrolidone and Synergistic Iodide Additives," *Port. Electrochim. Acta*, vol. 6, no. 26, pp. 533–546, 2008.

[171] J. Aljourani, K. Raeissi, and M. a. Golozar, "Benzimidazole and its derivatives as corrosion inhibitors for mild steel in 1M HCl solution," *Corros. Sci.*, vol. 51, no. 8, pp. 1836–1843, Aug. 2009.

[172] J. Aljourani, M. a. Golozar, and K. Raeissi, "The inhibition of carbon steel corrosion in hydrochloric and sulfuric acid media using some benzimidazole derivatives," *Mater. Chem. Phys.*, vol. 121, no. 1–2, pp. 320–325, May 2010.

[173] N. Goudarzi, M. Peikari, M. Reza Zahiri, and H. Reza Mousavi, "Adsorption and corrosion inhibition behaviour of stainless steel 316 by aliphatic amine compounds in acidic solution," *Arch. Metall. Mater.*, vol. 57, no. 3, pp. 845–851, 2012.

[174] R. Holze, "The electrosorption of imidazole on a gold electrode as studied with spectroelectrochemical methods," *Electrochim. Acta*, vol. 38, no. 7, pp. 947–956, May 1993.

[175] M. A. Khalifa, M. El-Batouti, F. Mahgoub, and A. B. Aknish, "Corrosion inhibition of steel in crude oil storage tanks," *Mater. Corros.*, vol. 54, pp. 251–258, 2003.

[176] "Study of Organic Inhibitors For Hydrochloric Acid Attack on Iron.pdf." .

[177] T. Ma, X. Fang, M. Akiyama, K. Inoue, H. Noma, and E. Abe, "Properties of several types of novel counter electrodes for dye-sensitized solar cells," *J. Electroanal. Chem.*, vol. 574, no. 1, pp. 77–83, Dec. 2004.

[178] K. Miettunen, "Performance and Stability of Dye Solar Cells on Stainless Steel," Helsinki University of Technology, 2009.

[179] H. Nusbaumer, S. M. Zakeeruddin, J.-E. Moser, and M. Grätzel, "An alternative efficient redox couple for the dye-sensitized solar cell system.," *Chemistry*, vol. 9, no. 16, pp. 3756–63, Aug. 2003.

[180] K. Miettunen, J. Halme, M. Toivola, and P. Lund, "Initial Performance of Dye Solar Cells on Stainless Steel Substrates," *J. Phys. Chem. C*, vol. 112, no. 10, pp. 4011–4017, Mar. 2008.

[181] Y. Tsukaue, G. Nakao, Y. Takimoto, and K. Yoshida, "Initiation Behavior of Pitting in Stainless Steels by Accumulation of Triiodide Ions in Water Droplets," *Corrosion*, vol. 50, no. 10, pp. 755–760, Oct. 1994.

[182] K. Miettunen, I. Asghar, X. Ruan, J. Halme, T. Saukkonen, and P. Lund, "Stabilization of metal counter electrodes for dye solar cells," *J. Electroanal. Chem.*, vol. 653, no. 1–2, pp. 93–99, Apr. 2011.

[183] D. Canfield and B. A. Parkinson, "Improvement of energy conversion efficiency by specific chemical treatments of n-MoSe2 and WSe2 Photoanodes," *J. Am. Chem. Soc*, vol. 103, no. 14, pp. 1279–1281, 1981.

[184] M. K. Nazeeruddin, A. Kay, R. Humpbry, E. Miiller, P. Liska, N. Vlachopoulos, M. Gratzel, R. Rodicio, R. Humphry-Baker, and E. Muller, "Conversion of Light to electricity by cis-X2Bis(2,2'-bipyridl-4,4'-dicarboxylate)ruthenium(II)Charge-Transfer Sensitisers (X=Cl-, Br-, I-, CN- and SCN- on Nanocrystalline TiO2 electrodes," *J. Am. Chem. Soc.*, vol. 115, no. 14, pp. 6382–6390, 1993.

[185] H. Kusama, M. Kurashige, and H. Arakawa, "Influence of nitrogen-containing heterocyclic additives in I– I3–redox electrolytic solution on the performance of Ru-dye-sensitized nanocrystalline TiO2 solar cells," *J. Photochem. Photobiol. A Chem.*, vol. 169, pp. 169–176, 2005.

[186] M. Dürr, a. Yasuda, and G. Nelles, "On the origin of increased open circuit voltage of dye-sensitized solar cells using 4-tert-butyl pyridine as additive to the electrolyte," *Appl. Phys. Lett.*, vol. 89, no. 6, p. 061110, 2006.

[187] S. Suzuki, Y. Yamaguchi, H. Onishi, T. Sasaki, and K. Fukui, "Study of pyridine and its derivatives adsorbed on a TiO (110) – (1 Â 1) surface by means of STM , TDS , XPS and MD calculation in relation to surface acid – base interaction," vol. 94, no. 110, pp. 161–166, 1998.

[188] G. Schlichthorl, S. Y. Huang, J. Sprague, A. J. Frank, and G. Schlichtho, "Band Edge Movement and Recombination Kinetics in Dye-Sensitized Nanocrystalline TiO 2 Solar Cells : A Study by Intensity Modulated Photovoltage Spectroscopy," *J. Phys. Chem. B*, vol. 101, no. 41, pp. 8141–8155, 1997.

[189] Z. Kebede and S.-E. S.-E. Lindquist, "Donor–acceptor interaction between non-aqueous solvents and I2 to generate I-3, and its implication in dye sensitized solar cells," *Sol. Energy Mater. Sol. Cells*, vol. 57, no. 3, pp. 259–275, Mar. 1999.

[190] H. Greijer, J. Lindgren, and A. Hagfeldt, "Resonance Raman Scattering of a Dye-Sensitized Solar Cell: Mechanism of Thiocyanato Ligand Exchange," *J. Phys. Chem. B*, vol. 105, no. 27, pp. 6314–6320, Jul. 2001.

[191] C. Reid and R. S. Mulliken, "Molecular Compounds and Their Spectra. IV. The Pyridine-Iodine System," *J. Am. Chem. Soc.*, vol. 76, no. 15, pp. 3869–3874, 1954.

[192] T. Tassaing and M. Besnard, "Ionization Reaction in Iodine / Pyridine Solutions : What Can We Learn from Conductivity Measurements , Far-Infrared Spectroscopy , and Raman Scattering ?," vol. 5639, no. 96, pp. 2803–2808, 1997.

[193] A. I. Popov and H. Geske, "Studies on the Chemistry of Halogen and of Polyhalides. XIII. Voltammetry of Iodine Species in Acetonitrile," *J. Am. Chem. Soc.*, vol. 80, no. 20, pp. 5346–5349, 1958.

[194] H. Lindstrom, H. Rensmo, S. Sodergren, A. Solbrand, and S.-E. Lindquist, "Electron Transport Properties in Dye-Sensitized Nanoporous–Nanocrystalline TiO2 Films.pdf," *J. Phys. Chem.*, vol. 100, no. 8, pp. 3084–3088, 1996.

[195] S. F. Nelsen, "Ionization from nitrogen and oxygen lone pairs: a comparison of trialkylamine, dialkyl ether, tetraalkylhydrazine, and dialkyl peroxide photoelectron spectroscopic ionization potentials," *J. Org. Chem.*, vol. 49, no. 11, pp. 1891–1897, Jun. 1984.

[196] H. Greijer Agrell, A. Hagfeldt, H. G. Agrell, and J. Lindgren, "Degradation mechanisms in a dye-sensitized solar cell studied by UV–VIS and IR spectroscopy," *Sol. Energy*, vol. 75, no. 2, pp. 169–180, Aug. 2003.

[197] H. Kusama and H. Arakawa, "Influence of pyrimidine additives in electrolytic solution on dye-sensitized solar cell performance," *J. Photochem. Photobiol. A Chem.*, vol. 160, no. 3, pp. 171–179, Aug. 2003.

[198] H. Kusama and H. Sugihara, "Theoretical studies of 1:1 charge-transfer complexes between nitrogen-containing heterocycles and I2 molecules, and implications on the performance of dye-sensitized solar cell," *J. Photochem. Photobiol. A Chem.*, vol. 181, no. 2–3, pp. 268–273, Jul. 2006.

[199] H. Kusama and H. Sugihara, "Theoretical studies of charge-transfer complexes of I2 with pyrazoles, and implications on the dye-sensitized solar cell performance," *J. Photochem. Photobiol. A Chem.*, vol. 187, no. 2–3, pp. 233–241, Apr. 2007.

[200] H. Kusama and H. Arakawa, "Influence of alkylaminopyridine additives in electrolytes on dye-sensitized solar cell performance," *Sol. Energy Mater. Sol. Cells*, vol. 81, no. 1, pp. 87–99, Jan. 2004.

[201] H. Kusama and H. Arakawa, "Influence of benzimidazole additives in electrolytic solution on dye-sensitized solar cell performance," *J. Photochem. Photobiol. A Chem.*, vol. 160, no. 1–3, pp. 441–448, Mar. 2004.

[202] H. Kusama and H. Arakawa, "Influence of aminotriazole additives in electrolytic solution on dye-sensitized solar cell performance," *J. Photochem. Photobiol. A Chem.*, vol. 164, no. 1–3, pp. 103–110, Jun. 2004.

[203] H. Kusama, H. Sugihara, and K. Sayama, "Nitrogen-Containing Heterocycles' Interaction with Ru Dye in Dye-Sensitized Solar Cells," *J. Phys. Chem. C*, vol. 113, no. 48, pp. 20764–20771, Dec. 2009.

[204] G. J. Reynolds, T. M. Watson, G. Williams, and D. Worsley, "Corrosion Resistance of Metallic Substrates for the Fabrication Dye-Sensitized Solar Cells," *ECS Trans.*, vol. 33, no. 17, pp. 129–138, 2011.

[205] M. I. Asghar, K. Miettunen, S. Mastroianni, J. Halme, H. Vahlman, and P. Lund, "In situ image processing method to investigate performance and stability of dye solar cells," *Sol. Energy*, vol. 86, no. 1, pp. 331–338, Jan. 2012.

2 *Experimental*

2.1 Platinum deposition characterisation

In order to establish a baseline for the study of an electrochemical platinisation technique suitable for eventual use in a roll-to-roll DSC production process, several studies were undertaken to assess the nature of this method and what direction to move, in order to develop a viable process. The goals were: fast processing, low material use and ease of integration into a mass production process.

The initial investigation utilised cyclic voltammetry in a 3 electrode cell to qualitatively characterise the 0.5mM potassium tetrachloroplatinate, $K_2[PtCl_4]$ (99.9% K_2PtCl_4 powder, Sigma-Aldrich) deposition solution. The electrochemical cell consisted of a Pt mesh counter electrode (99.9%Pt, Goodfellow), an FTO-glass working electrode of $1cm^2$ exposed area (NSG, 15Ω/□) and an Ag/AgCl reference electrode (Sigma-Aldrich, 3M KCl and +0.230V ±10mV *vs.* SHE). The scan range (max and min values) was initially set at +1V and -1V to establish basic electrodeposition activity. Once this was achieved, the scan range was narrowed to -0.8V and 0.6V to obtain the best resolution of the electrochemical process. Furthermore, three different scan speeds were applied to establish if any kinetically restrictive processes were present.

Since the deposition events are known to take place under negative potential in this cell, the potential was cycled from 0V to the negative max range and then to the positive maximum range. A current will then be recorded flowing between the working and counter electrodes. This current represents the flow of ionic species towards the working electrode, where they are adsorbed and then reduced from platinum chloride ions to platinum metal. The CV scan will give several features, peaks and troughs that indicate electrochemical processes occurring in solution. From these features, an idea regarding the possible deposition potentials can be reached, as will the values required to avoid detrimental processes such as hydrogen adsorption on the working electrode or evolution from solution when increasingly negative potentials are applied.

To assess the potential of electroplatinisation of FTO glass, symmetrical cells were constructed using the method detailed in Section 2.5.4. A key feature to check in these CV scans is the symmetrical nature of the peaks, which will give an indication of the repeatability of the catalyst deposition method. However, the most important value obtained from these is the limiting current (J_{lim}), the value of which indicates the potential

where the catalytic performance becomes kinetically limited as species are transferred from the bulk electrolyte to the electrode. This is a good quantitative measure to compare the performance of catalyst material, which avoids the need to build full DSC devices until the best performing catalyst has been identified.

2.1.1 Direct electrodeposition

Simple direct electrodeposition of platinum onto FTO glass used novel rapid deposition times at several deposition potentials adapted from literature sources, which were compared against the CV scan taken of the Pt deposition solution. Tsekouras *et al.* and Ito *et* al. supplied the -0.6V and -1.8V respectively for the initial study of platinum electrodeposition [1][2]. A three electrode electrochemical cell was used, including an Ag/AgCl reference electrode (Sigma-Aldrich, 3M KCl and +0.230V ±10mV *vs.* SHE), platinum wire mesh counter electrode (99.9%, Goodfellow) and FTO-glass working electrode (NSG, 15Ω/□). The deposition solution was 5mM chloroplatinic acid ($H_2PtCl_6.xH_2O$, Sigma-Aldrich) in distilled water. The deposition event was controlled and monitored through a potentiostat (Ivium Technologies, CompactStat). The deposition times chosen were 1, 5, 10 and 20 seconds. After each deposition, the working electrode was removed from solution and rinsed with distilled water and dried at room temperature. Samples were stored in a desiccator under vacuum conditions in the dark until required for analysis or DSC construction.

2.1.2 Direct deposition characterisation

Since the nature of different deposition methods makes accurate comparisons difficult, these platinised FTO-glass samples were characterised using UV-Vis spectroscopy to give a point of reference between different methods. UV-VIS analysis will be described in detail in Chapter 2.6.4. Following UV-VIS characterisation, scanning electron microscopy (SEM) was used to understand more about the deposition quantity, morphology and coverage over the substrate. Once the better performing deposition parameters were obtained, counter electrodes were used in DSC devices to test their performance under full operating conditions. The method for DSC construction and characterisation will be described further in Chapter 2.4 and 2.5.

2.2 Lead template deposition and platinum redox replacement process

Following on from the direct platinisation study, this deposition method used a modification of the procedure reported by Fayette *et al.,* in this case using FTO glass rather than Au(111) as the deposition substrate surface [3]. In this study, the working electrodes were maintained at $1cm^2$ for electrochemical studies and 15mm x 25mm FTO glass when used for DSC counter electrodes. The glass electrodes were stored in a vacuum sealed desiccator following preparation and only immersed in the electrolyte solution immediately prior to deposition to avoid contamination. This process utilises a similar three electrode cell to that of the CV study: FTO glass working electrode (NSG, 15Ω/□) Pt mesh counter electrode (99.9% Goodfellow) and an Ag/AgCl reference electrode (Sigma-Aldrich). All potentials used in this study are quoted with respect to an Ag/AgCl reference electrode, with the electrode spacing held at *ca.* 20mm.

2.2.1 Lead & platinum one bath electrolyte preparation

The one pot electrolyte solution consisted of 0.1M $NaClO_4$ (>98%, ACS Reagent, Sigma-Aldrich), 1mM $Pb(ClO_4)_2.3H_2O$ (98%, ACS Reagent, Sigma-Aldrich), 0.5mM $K_2[PtCl_4]$ (99.9%, Aldrich) and 10mM $HClO_4$ (70%, Analytical reagent grade, Fisher Scientific) was measured and combined in distilled water, using sonication to ensure full dissolution of all constituents. The solution was purged with N_2 for 2 hours before the commencement of any experimental activity.

2.2.2 Redox replacement deposition process

The electrodeposition process was controlled via a potentiostat (Ivium CompactStat, Ivium Technologies) and consists of two steps, repeated immediately after each other until the set number of cycles was reached. The range of cycles tested was: 1, 5, 10 and 20. Step 1 (E_1) consisted of Pb deposition at a reducing potential of either -0.75V or -0.5V for one second. In Step 2 (E_2) the sample was held at open circuit conditions (OCP) for redox replacement of Pb by Pt to occur. The OCP stage was held until a pre-set OCP value was reached, or if 60 seconds had passed. This cut off time ensures that all samples remained comparable to each other. Holding OCP for a longer time will ensure that all Pb has been replaced by Pt. Cyclic voltammograms were used to select the E_1 voltages at -0.75V or -0.5V. The E_2 cut off voltages were set as 0.2V or 0.5V.

2.2.3 Cyclic voltammetry for redox replacement platinisation analysis

An electrochemical cell was set up using a platinum mesh counter electrode, Ag/AgCl reference electrode and a working electrode prepared from FTO/Glass, Figure 2.1. The working electrode consisted of an FTO glass of 10mm x 5mm where the area to be exposed was $1cm^2$, the rest of the electrode was covered by PTFE tape. For the study of Pb/Pt deposition in Chapter 4, the CV potential scan range was set at -0.8V to +0.6V, with the scan start at 0V to discover the potential range of the reaction. The initial scan rate was 25mV/s, then 50mV/s to discover kinetic variables in the solution. The CV electrolyte consisted of either 0.1M $NaClO_4$, 1mM $Pb(ClO_4)_2$ and 10mM $HClO_4$ for the study of Pb deposition; or 0.1M $NaClO_4$, 1mM $Pb(ClO_4)_2$, 0.5mM $K_2[PtCl_4]$ and 10mM $HClO_4$ for the study showing the interaction of Pb and Pt in solution as the deposition occurs. The electrode spacing here was *ca.* 20mm and an Ag/AgCl reference electrode was used, set using previous literature settings [4].

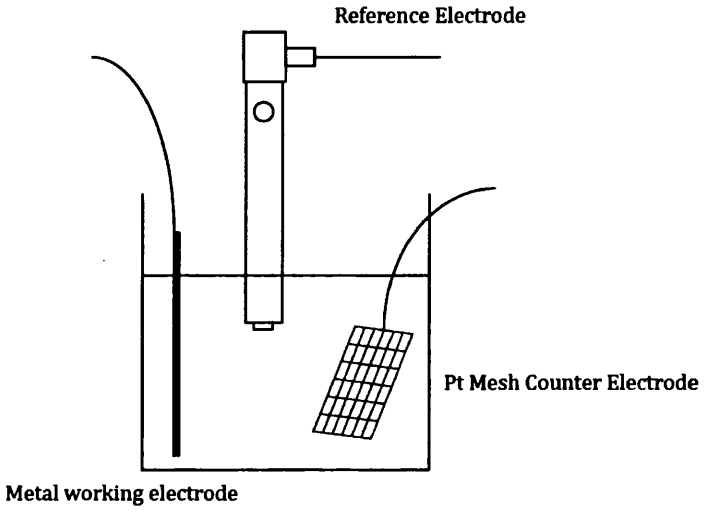

Figure 2.1: Three electrode cell schematic

The scan was run at scan speeds of 10, 20 and 50 mV/s and several scans were run per sample in order to discover any variation or process issues. In this study, 10 scans were run with the 1st and last used to characterise the deposition. A typical deposition scan will consist of several peaks, denoting the behaviour or change in ions in solution. The paper by Ko & Kwan was used as a reference source for this section, as they fully described the CV of platinum deposition from chloroplatinic acid, though in their paper they use compounds containing Pt^{4+} ions, rather than the Pt^{2+} compounds used in this work [5].

2.3 Fabrication of dye sensitized solar cells

2.3.1 Working electrode fabrication

The working electrodes were first prepared by cutting a 100mm x 25mm strip from FTO glass (NSG, 15Ω/□) and cleaning with mild detergent and ethanol. In addition, the glass was heat treated at 450°C to remove any organic contaminants on the substrate surface. After cooling to ambient, scotch tape was used to define a trough of *ca.* 1cm^2 in the centre of the glass strip, and then TiO_2 layer (DSL18NR-T or DSL NR-AO, Dyesol) was doctor bladed onto the surface using a glass rod. The scotch tape acted as both guide and TiO_2 layer thickness control. The FTO glass strip was then heat treated using a program of 150°C (15min) to 450°C (30min) to 150°C (15min) then covered and left to cool to ambient. The strip was then measured out to the required 15mm x 25mm lengths and then carefully cut to shape. Immediately prior to immersion in the dye, the TiO_2 photoelectrodes were shaped to 1cm^2 squares in the centre of the glass piece using a microscope slide and ruler to ensure repeatability. Finally, the working electrodes were immersed in a dye solution consisting of 0.3mM N719 dye (Dyesol, B2 dye) in a 1:1 solution of acetonitrile/*tert*-butanol for 16-24 hours to facilitate dye adsorption, Figure 2.2.

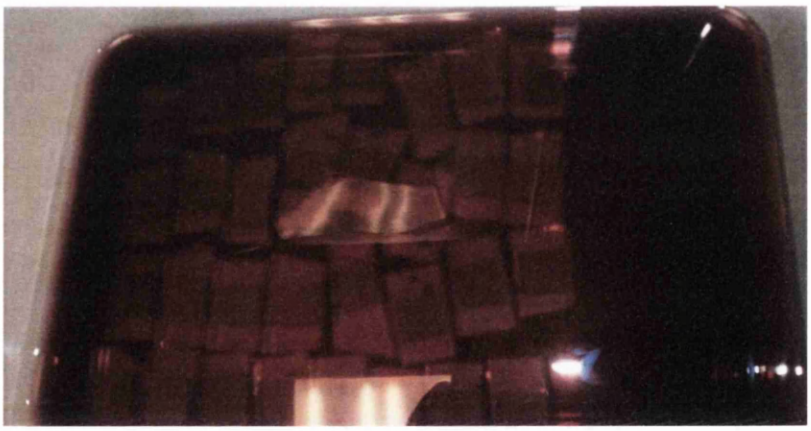

Figure 2.2: Sensitisation of TiO_2 photoelectrodes in N719 dye

2.3.2 Counter electrode fabrication

The counter electrode (CE) consists of platinised FTO glass cut to 25mm x 15mm to match the working electrode. An electrolyte filling hole was pre-drilled into the CE using a 0.5mm tungsten carbide drill bit. The glass was then cleaned using water and a mild detergent and then rinsed thoroughly with ethanol. The platinisation solution of 5mM chloroplatinic acid in 2-propanol was applied to the conductive side using a capillary tube and allowed to wet out to a thin layer. This must be carefully done when constructing reverse illuminated cells,

as increased thickness will start to restrict the illumination entering through a counter electrode in this type of cell. Figure 2.3, illustrates the procedure of applying chloroplatinic acid to the FTO-glass substrate.

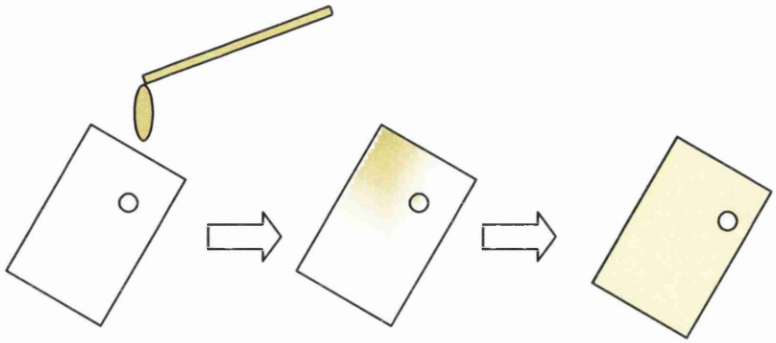

Figure 2.3: Chloroplatinic acid application process for a counter electrode

The counter electrodes were then heat treated at 400°C for 30 minutes to deposit the platinum nanocluster catalyst. Once heat treated, the CE's were covered and left to cool to ambient before being used on the same day. In addition to thermal platinisation, electrochemical platinisation was also used and is described in detail in Chapter 2.1. A completed thermally platinised electrode can be seen in Figure 2.4.

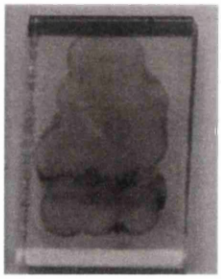

Figure 2.4: Thermally platinised counter electrode – excess applied to demonstrate Pt coverage

The platinum layer is usually barely visible to the naked eye. However in this example, an excess of precursor has been applied to illustrate the coverage, giving a grey/black layer across the FTO/glass surface. To chemically platinise this electrode the chloroplatinic acid coated electrode was dried in a furnace at 120°C for 20 minutes and then immersed in a 60mM solution of potassium borohydride for 60 seconds. The electrode was then dried at 130°C for 20 minutes before leaving to cool in a covered container. Sputter platinisation utilised the same 25mm x 15mm electrode substrate as the thermal and chemical platinisation methods. The electrode was fixed to a rotating stage inside the vacuum chamber of a Quorum Q150T vacuum sputter coater (Quorum Technologies Ltd). Once the vacuum was pulled, the sputter deposition was performed using parameters controlled by

the internal software. The target used was a 0.1mm platinum disc (SC502-314C, Quorum Technologies Ltd) and the layer thickness chosen was 0.5nm. Once coated, the electrodes can be used in a DSC device with no further processing.

2.3.3 Sealing, electrolyte injection and finishing

Following dye sensitisation, the working electrodes were removed from the dye and immersed briefly in either ethanol or ACN/*t*-butanol solution to remove any excess dye and to ensure the TiO_2 pores are clear. The counter and working electrodes were then dried with nitrogen or clean dry air to ensure no particles of dust or glass remained on the surface. The two electrodes were sealed together using 25µm Surlyn gaskets and a T-shirt press or a hot plate and flat weight, the Surlyn was cut to shape using a pre-made template and a scalpel. The temperature for both hot plate and press was 105°C found though trial sealing with sample materials. Immediately following sealing, the cells were checked for short circuits using a multimeter. A drop of the chosen electrolyte, see Section 2.4, was placed inside an O-ring set over the electrolyte filling hole, the cell was then placed in a desiccator and a vacuum was drawn to remove the air in the DSC electrolyte cavity. As the vacuum is reduced, the electrolyte was allowed to flow into the void in the cell. The cell was carefully cleaned of excess electrolyte and the hole was sealed using Surlyn and a 5mm diameter cover glass. Figure 2.5 shows an example of a standard cross shaped lab DSC.

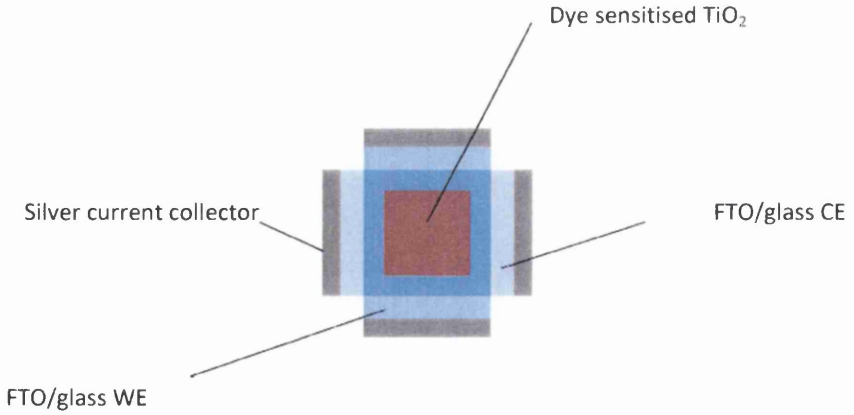

Figure 2.5: Schematic of DSC device

Silver paste was carefully applied to the exposed ends of the working and counter electrodes to give low resistance contact points on the cell. Care was taken that no silver came between either FTO glass electrodes, as this will cause a short circuit and render the DSC inoperable.

2.4 Electrolyte preparation

2.4.1 Preparation of a basic iodide/triiodide electrolyte

The basic iodide/triiodide electrolyte used for all corrosion studies and electrochemical measurements contains 0.5M Lithium Iodide (Sigma-Aldrich), 0.1M Iodine (Sigma-Aldrich) and 0.5M 4-tert-butylpyridine (4-TBP, Sigma-Aldrich) in 3-methoxypropionitrile (3-MPN, Sigma-Aldrich) and was sonicated for *ca.* 15 minutes to ensure that all components had dissolved in solution.

2.4.2 Standard DSC electrolyte

A typical DSC electrolyte was prepared using 0.8M 1-propyl-3-methylimidazolium iodide (PMMI, Dyesol Ltd), 0.1M iodine (Sigma-Aldrich), 0.05M guanidinium thiocyanate (GuSCN, Sigma-Aldrich) and 0.3M 1-Methylbenzimidazole (1-MBI, Sigma-Aldrich) in 20ml of 3-MPN (Sigma-Aldrich). The addition of GuSCN is used to suppress the recombination rate of electrons at the photoelectrode of the cell. The resulting solution was sonicated for 15 minutes to ensure all constituents were evenly dissolved in solution.

2.4.3 Preparation of an electrolyte with N-heterocyclic additions

A basic DSC iodide/triiodide electrolyte containing LiI and I_2, similar to that described in Section 2.4.1 was used as the starting point. Next, nitrogen containing heterocyclic additives (NHC's) were added, at concentrations of 0.25M, 0.5M and 1M creating a sample of each electrolyte, and one without NHC addition as a control. Additives selected for testing were 4-*tert*-butylpyridine (4-TBP) and 1-methylbenzimidazole (1-MBI) and 1, 3, 5-Triazine (135-T). The additives 4-TBP and 1-MBI have been used previously to increase DSC performance through the reduction of dark current and recombination processes. The third additive, 135-T, was chosen for its reported high effect as a performance enhancer by Kusama *et al.* [6] and due to the inclusion of 3 nitrogen atoms in the structure of the molecule compared to the 1 and 2 of 4-TBP and 1-MBI respectively.

2.4.4 Preparation of a cobalt complex redox electrolyte

This electrolyte used the compounds "tris-(2,2'-bipyridine)cobalt(II) di-(hexafluorophosphate)" or $Co(bpy)_3(PF_6)_2$ based complex and "tris-(2,2'-bipyridine)cobalt(III) tri(hexafluorophosphate)" also known as $Co(bpy)_3(PF_6)_3$ (Dyenamo AB, Sweden) [7]. A cobalt electrolyte solution was created with 0.2M of $Co(bpy)_3(PF_6)_2$ and 0.02M or 0.2M of $Co(bpy)_3(PF_6)_3$. A further compound, 0.1M $LiClO_4$, was also added to the

DSC electrolyte as a source of lithium ions to improve DSC performance. Previous literature reported that two main concentrations of 4-TBP were in use, 0.5M and 0.25M. Both concentrations were used in test DSC cells to optimise the electrolyte formulation. Due to the known stability of the 3-MPN solvent from literature concerning the iodide/triiodide electrolyte, this was used for the study of the cobalt complex electrolyte. However, due to the more viscous nature of 3-MPN, a higher concentration of Co^{3+} ions (0.2M) was utilised in addition to the literature recommended concentration of 0.02M in an attempt to avoid mass transport related losses in these devices.

The preparation method for the electrolyte used in the study of corrosion behaviour of the cobalt electrolyte was similar to that described previously. In this study, the NHC additives, 4-TBP and 1-MBI, were added at the concentrations 0.25M, 0.5M and 1M. A control electrolyte containing no additives was used for preparing control samples. Furthermore, in the corrosion cell, the $LiClO_4$ was not added in order to minimise interactions with the substrate and allow focus on the interactions of the $Co^{2+/3+}$ redox couple with the substrate.

2.5 DSC device characterisation

2.5.1 I-V testing

DSC testing was done on a Newport Oriel Sol3A class AAA Solar Simulator, see Figure 2.6. The equipment contains a 450W Xenon light source which is certified to IEC 60904-9 Ed 2 (2007), JIS C 8912 and ASTM E 927-05 standards. An NREL certified secondary standard silicon reference cell connected to the test rig was positioned under the stabilised lamp to calibrate the output of the lamp to 1 sun, using the provided sun level meter and a variable power supply. DSCs with an active area of $1cm^2$, as described in Section 2.3, were placed on a testing stage and carefully positioned in the centre of the illumination area. They were then connected to the Keithley 2420 Sourcemeter *via* four leads, see Figure 2.7. The leads and crocodile clips used as connectors are highly conductive and are connected using silver connection points on the cell. These can be further enhanced using copper tape. Prior experience has shown the crocodile clip connectors to be reliable for the purpose of lab scale DSC testing. The current-voltage (I-V) characteristics of the DSCs to be studied were recorded using the Keithley 2420 Sourcemeter and the Oriel IV software package provided with the instrument. Tests were programmed by using a designated recipe, with the user inputs: max reverse bias = -1.00V, max forward bias = 0.8V, a current limit = -50mA, sample area = $1cm^2$, number of sweep points = 200, pre-sweep delay = 1s and a dwell time per

point = 200ms; an additional parameter, the Sun Level, is also needed to aid in the calculation of cell parameters.

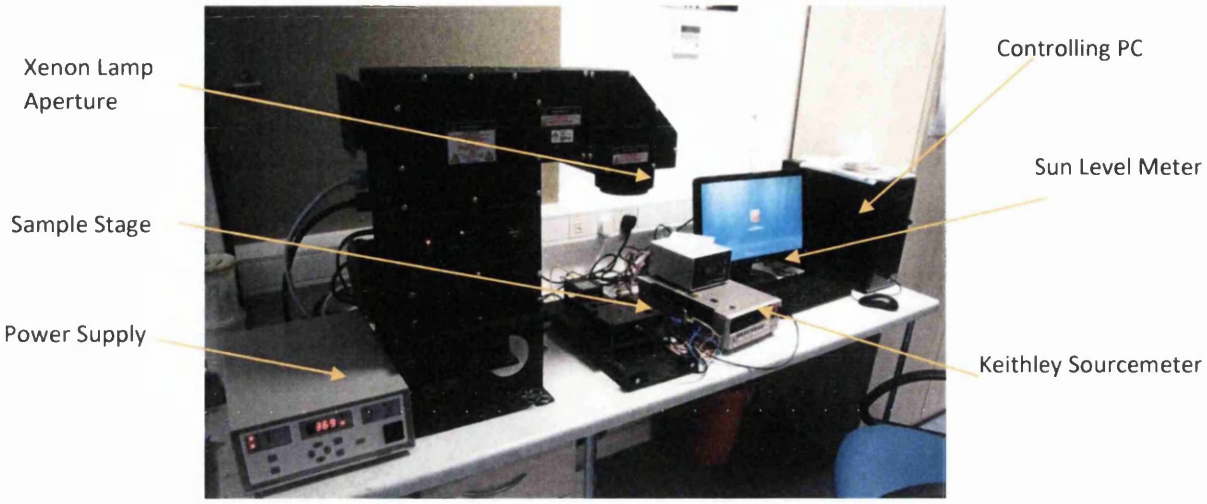

Figure 2.6: Newport Oriel Solar Simulator

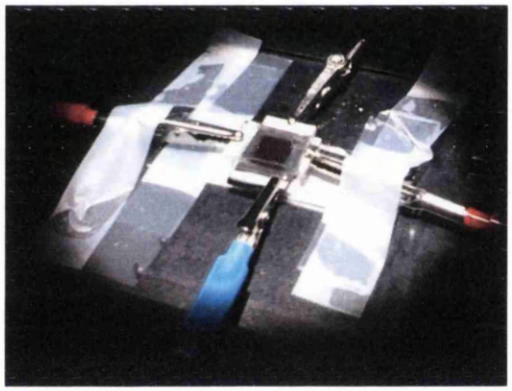

Figure 2.7: DSC connection setup

However, to ensure full understanding of the result, the testing theory was assessed before running analysis on the DSCs constructed in the process of this study.

2.5.2 I-V testing theory

The cells in this work were studied under standard testing condition (STC); that is AM1.5 terrestrial spectrum, a total irradiance of 1000Wm^{-2} and ca. 25°C [4-5]. The performance of DSCs was calculated using the current *vs.* voltage (I-V) response of each cell, where the specific performance parameters required were:

- Short Circuit Current Density (J_{sc})
- Open Circuit Voltage (V_{oc})
- Fill Factor (FF)
- Efficiency (η)

The Oriel software calculates the performance of each test cell within the software package. However, the basic equations are included below to facilitate understanding of the characterisation method:

The short circuit current density (J_{sc}) is the maximum current generated under short circuit conditions, at V=0, for a given cell area, under standard reporting conditions. The active cell area used for all DSC in this work was $1cm^2$, meaning that the more comparable parameter of short circuit current density (J_{sc}) was assumed to equal to the short circuit current (I_{sc}), as a result, J_{sc} is used from here on in this work, thus facilitating comparisons between cells in this work and by others.

The fill factor (FF) represents the comparison of the I-V curve to the response of an ideal diode. It illustrates the relationship between the actual and maximum power of a DSC, and as a result is a sensitive measure of performance losses in the DSC such as transfer resistance and diffusion problems. The fill factor is mainly influenced by the internal resistances of a DSC. The TCO resistance, electrolyte diffusion resistance and charge transfer resistance. This value was calculated through using the relationship with key cell parameters, as can be seen in Equation 2.1:

$$FF = \frac{P_{max}}{V_{oc} \times J_{sc}} = \frac{\eta \times A_c \times E}{V_{oc} \times J_{sc}} \qquad (2.1)$$

Where P_{max} represents the point of maximum power, V_{oc} is the open circuit voltage, η is the energy conversion efficiency (%), A_c is the surface area (m^2 or cm^2) and E is the irradiance (Wm^{-2} or Wcm^{-2}). A benchmark value for the fill factor of high performing cells is 0.7 or 70% for a cell of ca. $1cm^2$.

The final and most widely used comparative performance value is the energy conversion efficiency of the DSC, Equation 2.2:

$$\eta = \frac{P_{max}}{E \times A_c} = \frac{V_{oc} \times J_{sc} \times FF}{E \times A_c} \qquad (2.2)$$

Where P_{max} is the maximum power point on the I-V curve and the product of V_{oc}, J_{sc} and FF; E represents irradiance (Wm^{-2} or Wcm^{-2}) and A_c is the area available for light absorption (mm^2 or cm^2), in this case the area of TiO_2 is $1cm^2$ for all cells.

2.5.3 EIS characterisation of DSC device

Electrochemical impedance spectroscopy (EIS) scanning was used to study the interfacial properties of DSC cells, a detailed explanation of the process and theoretical background can be found in the work of Bisquert, Fabregat-Santiago and J. Halme [8]–[14]. A Gamry Reference 600 Potentiostat/Galvanostat/ZRA was used both to run the EIS measurement and record the data returned. Scans on full DSC devices were run in the light with a D.C voltage applied to the device to retain the cell at the maximum power point (M_{pp}). When testing symmetrical CECE cells no D.C potential needs to be imposed due to the absence of a working electrode. The imposed D.C voltage for DSC devices depends on the electrolyte used, as the open circuit potential differs for each redox couple. It is usually taken from I-V measurements made on the devices prior to EIS testing, as a result a DC voltage of -0.65V *vs.* E_{Ref} was used for iodide/triiodide cells. The frequency range used for all scans was 50000 Hz to 0.1Hz, using 10 points/decade.

A small amplitude AC voltage modulation is superimposed on the DV voltage applied to the cell, Equation 2.3, where E_t is the potential at time "t" and E_0 is the amplitude of the signal, ω is the frequency in radians:

$$E_t = E_0 sin(\omega t) \tag{2.3}$$

The resulting AC current response to this is measured over a set frequency range.

$$f = \omega / 2\pi \tag{2.4}$$

At different frequencies, the device interfaces respond with varying behaviour, corresponding to different interfacial properties, giving a varying current response, I_t , see Equation 2.5:

$$E_t = E_0 sin(\omega t) \tag{2.5}$$

Thus the impedance can be calculated as an analogue to Ohms law, Equation 2.6:

$$Z = \frac{E_t}{I_t} = \frac{E_0 sin(\omega t)}{I_0 sin(\omega t + \phi)} = Z_0 \frac{sin(\omega t)}{(\omega t + \phi)} \tag{2.6}$$

This allows the impedance to be expressed in terms of magnitude Z_0 and the phase shift Φ, further aiding in the graphical illustration of impedance for the assessed devices.

The interfaces and interactions found in a DSC are:

- TiO_2/Electrolyte
- Counter electrode/Electrolyte
- Conducting substrate/Electrolyte
- Diffusion of species in the electrolyte

Simple combinations of components such as resistors and capacitors are thus used to model certain interfaces. A resistor and capacitor pair in parallel is commonly used to model an electrode/electrolyte interface such as the one found in a DSC cell at the counter electrode, see Figure 2.8. The capacitance value represents the charging of the electrochemical double layer, often known as the Helmholtz layer for a simple analysis, or the combined Gouy-Chapman-Stern model for a more complex model, explanations of these models can be found in Chapter 1.3.2; and the resistor represents the charge transfer resistance at the interface. The impedance of a resistor is simply equal to the resistance or by the equation:

$$Z(\omega) = Z_0 e^{j\phi} \tag{2.7}$$

Whereas the impedance of a capacitor is represented by:

$$Z = \frac{1}{j\omega C} \tag{2.8}$$

To more accurately represent the interface, the capacitor can be replaced by a constant phase element (CPE), that accounts for the 3D nature of the interfacial double layer and returns more strongly representative value illustrating "real world" behaviour.

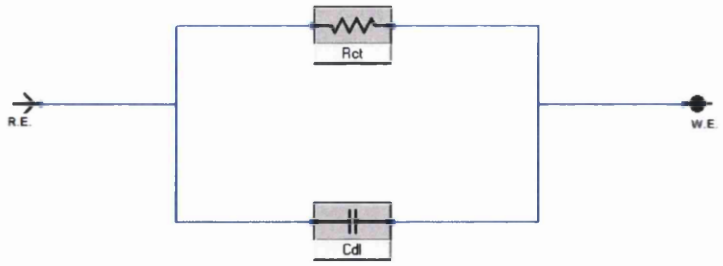

Figure 2.8: Modelling the interface (The Counter Electrode)

The addition of more elements and increased circuit complexity allow the modelling of many electrochemical systems. The Randles circuit and the transmission line model explored in this next section are examples of such modelling.

Impedance is defined as the measure of the opposition of a circuit to a current, when a voltage is applied. This is different to resistance, in that it is applicable to AC circuits and has both magnitude and phase, rather than just magnitude. The value "impedance" can be thought of as possessing a real and imaginary component, these can be plotted graphically with the "real" part is on the X-axis and the "imaginary" impedance is in the Y-axis. This graph is known as a Nyquist plot, such as the example found in Figure 2.9. The key thing to notice is that on a Nyquist plot, each point is the impedance at one frequency, high frequencies results are plotted on the left side and get lower as you progress along the X-axis. The drawback is that the exact frequency is not shown on this type of plot. Impedance is represented as a vector, where the length of the vector is the magnitude of the impedance. The angle between the vector and the X-axis is called the phase angle.

The diameter, or apex, is also where the resistive effect equals the capacitive effect. Either side of this point, the system is either acting in a more capacitive nature (vertical component) or a more resistive nature (horizontal component) - thus giving rise to the different paths found on a typical Nyquist curve.

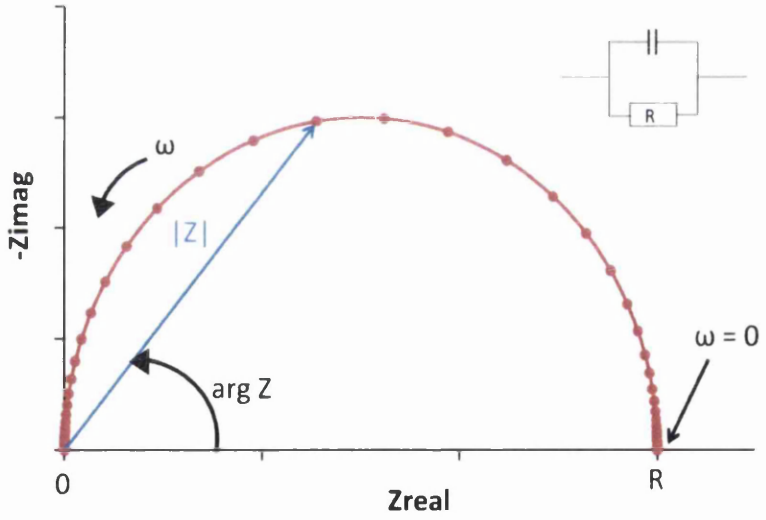

Figure 2.9: Graphical plot of a resistor and capacitor in parallel, known as a Voigt element

In order to record and assess the frequency, a different style of presentation is the Bode plot. In this, the log of the frequency is on the X-axis and the impedance and phase-shift are plotted on the Y-axis, Figure 2.10. Bode plots are usually used in parallel to Nyquist diagrams in order to capture the frequency response of the electrochemical system. There are two types of Bode plot: The phase plot and the magnitude plot which represent the phase shift at different frequencies and the magnitude of the frequency response.

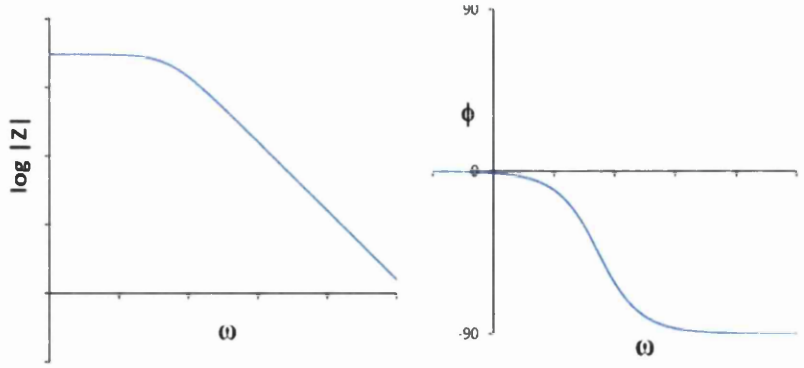

Figure 2.10: Standard Bode plots for the Voigt element a.) Magnitude plot and b.) Phase plot

Since the DSC device includes several elements, it requires a larger model than given by the Voigt element. Figure 2.11 shows a typical Nyquist plot for a standard DSC cell with a thermal deposited platinum counter electrode. The three semicircles represent the sections for cell series resistance (R_s), charge transfer resistance (R_{ct}) and TiO_2 resistance (R_r) are marked on the graph. The recombination resistance can also be written as R_{rc}, which is the terminology use throughout this work.

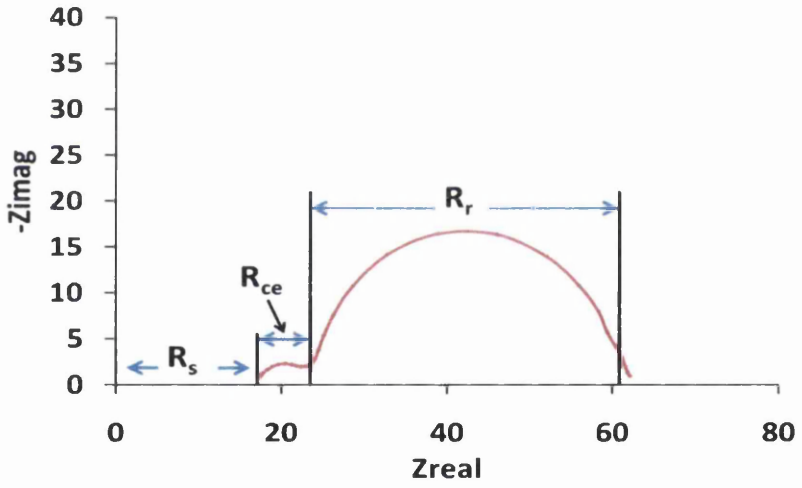

Figure 2.11: Standard EIS plot for an iodide/triiodide based DSC

Equivalent circuit modelling is then used to determine the values for R_s, R_{ct} and R_{rc} by fitting a curve to the dataset. In addition to the standard resistor and capacitor components, some theoretical components are also used, such as the constant phase element, which has attributes of both capacitors and resistors or the Warburg, which is used to model diffusion in porous electrodes. The simplest electrical equivalent model used to start modelling a DSC is the Randles circuit [14]. This consists of a resistor in series to a capacitor and resistor placed in parallel, see Figure 2.12. In some cases, the capacitor is replaced by a constant phase element, as most commonly used in DSC models due to the complicated and three

dimensional nature of the TiO_2 photoelectrode. An additional component, a Warburg element can also be used to model the diffusional aspect of a DSC porous electrode.

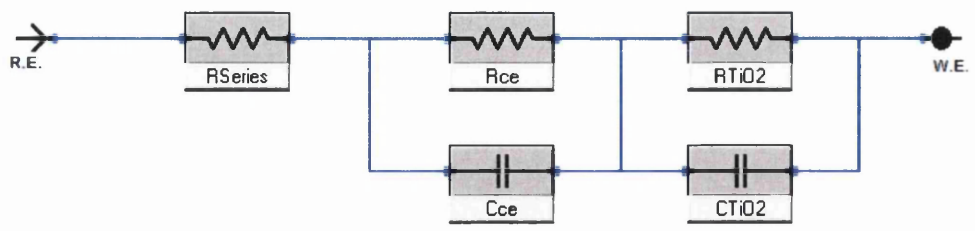

Figure 2.12: Randles Circuit Diagram

The R_s value represents the series resistance of the conductive substrate and is found on the Nyquist plot as the X-axis offset before the first small semicircle forms. This small radius semicircle (R_{ct}) represents counter electrode/electrolyte interface and can be modelled through a parallel capacitor/resistor combination. The capacitor can be replaced by a constant phase element or CPE which provides a better fit for DSC cells as the interface will not behave in an ideal manner – as modelled using a resistor and parallel capacitor. This is the critical value used to assess the performance of different redox catalysts in DSC devices, the smaller the value of R_{ct}, the more efficiently the charge transfer at the counter electrode, and the higher the fill factor of the cell. The final large semicircle represents the recombination resistance of the DSC (R_{rc}). In a high performing cell, this is expected to have a large radius, indicating low recombination losses in the device.

If the frequency range is set to encompass frequencies down to 0.01 Hz, there will be a third semicircle or part semicircle that represents the diffusion resistance of the electrolyte itself, known as R_D. This is represented in the Randles circuit by the Z_d impedance, commonly modelled as a Warburg element. This elements impedance depends on the applied frequency, thus at higher frequencies, the Warburg impedance will be small since the spacing between electrodes is low. Conversely, at low sampling frequencies, the reactants in the cell have to diffuse much further and will thus increase the impedance. Warburg elements come in several configurations: Bounded, infinite and porous to better represent the type of diffusion that is occurring in the system.

Due to the variability of the real world, these "ideal" components do not necessarily give the most accurate model of the dye solar cell system. An indication of this is usually obtained through a depressed or flattened semicircle on the EIS Nyquist plot. The need for

this element is normally caused through having a roughened or 3D surface, like that required by a high surface area catalyst material. The element known as a constant phase element (CPE) can be used in place of the capacitor, and is represented by Equation 2.9:

$$Z_{CPE} = \frac{1}{(j\omega)^{\beta} Q_0} \tag{2.9}$$

The Q_0 value is equal to the capacitance of the element and β represents the ideality of the CPE with respect to capacitance. If this exponent is equal to 1, the impedance will equal that of a capacitor, see Equation 2.10:

$$Z = \frac{1}{j\omega C} \tag{2.10}$$

In most cases, the equivalent capacitance can be calculated from the constant phase element parameters used in addition to the values for the resistor placed in parallel, see Equation 2.11:

$$C_{eq} = \frac{(R \times Q^0)^{1/\beta}}{R} \tag{2.11}$$

Understanding the methods and equations behind the data obtained from the EIS software facilitates a more comprehensive understanding of how cell architecture affects the results. To increase device performance, a larger surface area for light absorption is required, a mesoporous network of TiO_2 is utilised. This can be modelled in EIS by the use of a transmission line. Modelling a porous electrode interface is different from a planar surface as the volume of a pore is much smaller and access to the active surface will be limited, resulting in the diffusion of ions into and out of the pore becoming the rate limiting step. As a result, modelling must separate the regions of the porous material in order to encompass all the effects. In a standard liquid electrolyte DSC architecture, the conductive substrates are modelled as planar, where the reaction occurs on the surface to electrolyte interface. The porous material has several other interfaces: The outer surface/electrolyte and the active surface within the porous network, in addition the size and shape of the pores will also limit the flow of ions into and out of it, a factor than must also be accounted for.

As mentioned previously, the rate of ion diffusion within the pores is a rate limiting step in a DSC and must be modelled accordingly, hence a transmission line model. The model consists of several connected elements that describe the charge transfer resistance and capacitance, in series and parallel, that describe the outer layer of the porous structure and

the inner active surface within the porous network. This model was developed for DSC devices by Bisquert *et al.* [15], and is illustrated in Figure 2.13.

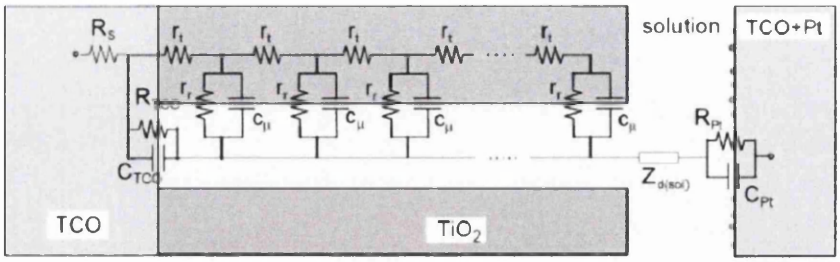

Figure 2.13: Transmission line model of a dye solar cell [11]

In this model, R_{TCO} denotes the charge transfer resistance at the transparent conducting oxide (TCO) back layer, C_{TCO} denotes the chemical capacitance for charge accumulation and recombination at the same interface. The transport resistance across the TCO layer is given by R_s, and the diffusion of the triiodide/iodide redox species is given as the impedance $Z_{D(sol)}$. C_μ denotes the chemical capacitance due to the change in electron density and R_t is the electron transport resistance. R_r is the charge transfer resistance related to recombination at the TiO_2 interface. R_{pt} is the counter electrode/electrolyte interface charge transfer resistance and C_{pt} is the interface capacitance at the same interface [8]. If the transmission resistance is less than the recombination resistance, a 45° line will appear in the region between the counter electrode and working electrode collected data. The Nyquist plot of that is described thus is shown in Figure 2.14; the length of this transmission line is described as 1/3 of the electron transport resistance.

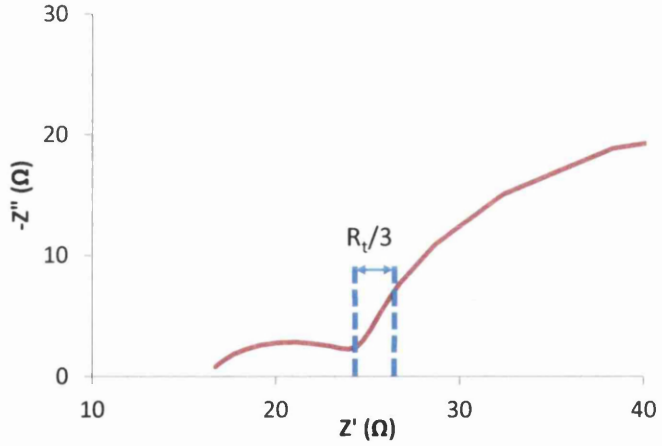

Figure 2.14: Nyquist plot showing the transmission line segment

This is a complete model of an active dye solar cell device. However, to reduce the number of parameters or depending on the cell behaviour, a simpler model such as a Randles circuit can be used.

2.5.4 Cyclic voltammetry for electrochemical analysis of symmetrical counter electrode cells

FTO glass electrodes were cut to 25mm x 15mm, marked and pre-drilled with a 0.5mm electrolyte filling hole similar to the counter electrode preparation method for DSCs in Section 2.3.2. The counter electrodes were then platinised using thermal, sputtered or electrochemical platinisation techniques. The two electrodes were assumed to be symmetrical in nature and were sealed together using a 25µm Surlyn Gasket. The electrolyte was vacuum backfill injected and the hole sealed with Surlyn and thin cover glass. A schematic of this cell set up can be seen in Figure 2.15, showing the key elements in a counter electrode cell. Figure 2.16 shows an image of a representative cell used in this study.

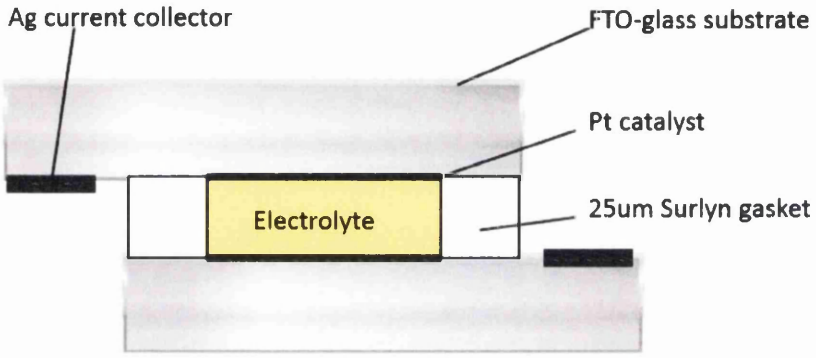

Figure 2.15: Symmetrical counter electrode cell

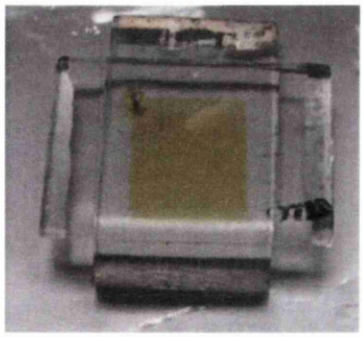

Figure 2.16: Standard CECE cell for catalyst testing in electrolyte

The key issues to note in this testing is that the effect of the TiO_2 will not be taken into account on any electrochemical measurements. Therefore, when taking measurements, this should be clearly stated and the results then compared with full DSC devices when and where possible.

The cyclic voltammetry (CV) scan was run within the operational limits for the solar cell, i.e. from 1V to -1V [16], care should be taken not to exceed these limits as the integrity of the cell will be compromised through the damage of the electrolyte, Figure 2.17.

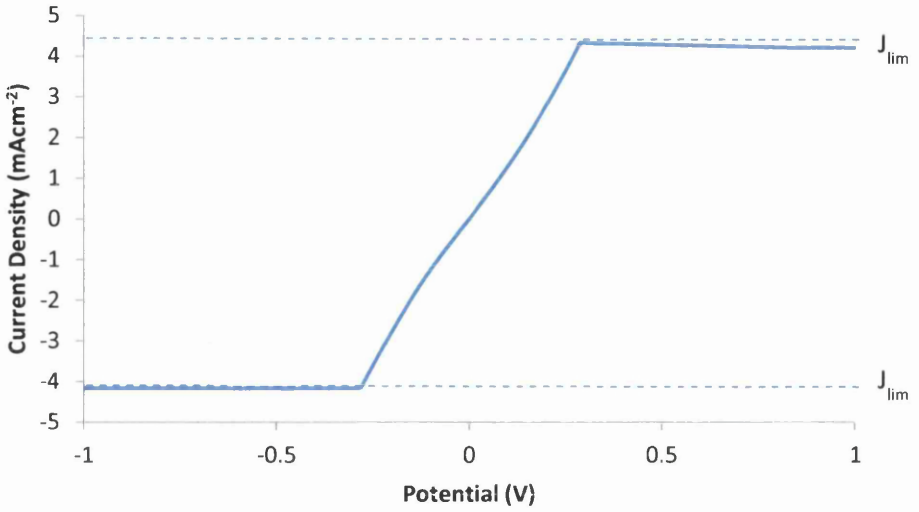

Figure 2.17: CV curve representing CECE cells (Ag / AgCl (3M KCl)

The scan rate was varied from 2mV/s to 50mV/s to ensure any variance due to diffusion limitations were visible and could be accounted for. A standard CECE cell will give an ohmic response with the current increasing in a steady relationship with applied potential, until a limit is reached and the current response becomes static no matter the applied potential. This value is known as J_{lim} and is a good indication and point of comparison for catalyst material – particularly in thin layer test cells. This value can be used alongside the previously discussed counter electrode charge transfer resistance (R_{ct}) value obtained from EIS characterisation in order to assess the performance of catalyst materials without the need to dismantle the devices and perform a physical analysis.

2.6 Corrosion testing

All metals used as corrosion cell substrates were purchased from Goodfellow Metals Ltd. Metals of different purity were initially assessed to determine the effect on corrosion behaviour, Table 2.1. Once this was achieved, the lower purity, lower cost metals were used for further corrosion testing. While copper is not a construction material, it is extensively used as a highly conductive contact in DSC devices, an as a result is utilised in the later corrosion inhibition testing of nitrogen containing heterocyclic compounds (NHC's) in Chapter 5.

Table 2.1: Metals used for corrosion cell substrates

Metals	Purity
Nickel	99.98% Ni
Aluminium	99.999% Al
	99.9% Al
Iron	99.5% Fe
Titanium	99.6% Ti
Molybdenum	99.9% Mo
Stainless steel 316	18%Cr, 10%Ni, 3%Mo
Stainless steel 304	18%Cr, 8%Ni
Zinc	99.9%Zn
Inconel 625	61%Ni, 22%Cr, 9%Mo, 5%Fe
Tungsten	99.95%W
Chromium	99.95%Ch
ECCS	N/A
Copper	99.9%Cu

2.6.1 Metal substrate preparation

Two types of corrosion cell were produced for this work, one for DR UV-VIS spectrophotometric observation and the other for time-lapse photographic monitoring and image analysis. Metal coupons of 50mm x 50mm x 2mm were prepared firstly by abrading the metal surface using 1200 grit silicon carbide paper to remove any oxide layer and surface impurities. The coupons were then washed with mild detergent and then ethanol before being air dried. In the case of aluminium, the surface must be activated through abrasion with 1200 grit paper and further polishing with Al_2O_3 and distilled water, the samples are cleaned in the same manner as the other metals. For the cobalt electrolyte corrosion study in Chapter 5, a thin titania blocking layer was applied to ascertain if this would give a physical anticorrosion effect, both by NHC augmented electrolyte and electrolyte containing no additive. The blocking layer was applied by immersing the metal substrate in a prepared $TiCl_4$ solution at 80°C for 30 minutes inside a fume cupboard.

2.6.2 Glass top sheet preparation

The top sheet consisted of 2mm thick plain non-conducting glass, cut to 50mm x 50mm, to allow clear observation of the behaviour of electrolyte on a metal substrate. Drill points for the electrolyte injection holes were marked in positions dictated by the placement of the electrolyte cavities in the Surlyn used to seal the cell. The necessary holes were drilled

using a 0.5mm drill bit and then the glass was cleaned using mild detergent and rinsed with ethanol.

2.6.3 Sealing and electrolyte filling

The UV-Vis corrosion cells were constructed from 50x50mm metal coupons and plain glass, a square of Surlyn 25µm thick and 50mm x 50mm in size was used as the spacer. The electrolyte void here was 25mm x 25mm in order to allow enough area for the reflectance measurement in the UV-Vis equipment. The time lapse photographic monitoring corrosion cells, use either a 25µm or 50µm Surlyn piece cut to 50mm x 50mm size and then 1cm^2 squares apertures were cut out the centre to create electrolyte cavities. Thinner Surlyn was used initially to create a cell sensitive to changes in the electrolyte. Once the cells had been successfully characterised using these two methods, the thicker 50µm Surlyn was used to better model actual DSC devices and electrolyte volumes.

The cell substrates were sealed together using a hot press set at 105°C, , to melt the Surlyn between the two substrates, thus creating the corrosion cell. It was found that pre-washing the Surlyn with ethanol and drying under enforced vacuum conditions improved its sealing behaviour, thus allowing cells to be manufactured promptly and minimising the exposure of the prepared metal surface to reaction with the atmosphere.

Figure 2.18: Hot press used for sealing substrates using thermosetting polymer gaskets

When the seal was complete, different electrolytes were then vacuum injected into the cavities. The injection holes were then sealed with Surlyn pieces and 5mm diameter cover glass. The iodide/triiodide electrolyte used as the basis for all corrosion investigations consisted of 0.1M LiI and 0.05M I_2 in 3-MPN. This is a simple three component electrolyte used in order to isolate the reaction of the iodide/triiodide electrolyte with the metal substrate. The nitrogen containing heterocyclic compounds (NHC's) chosen as additives for their possible corrosion inhibition properties were then added to samples of this basic

solution at the concentrations of: 0M, 0.25M, 0.5M and 1M, see Sections 2.4.3 for a detailed explanation of electrolyte preparation.

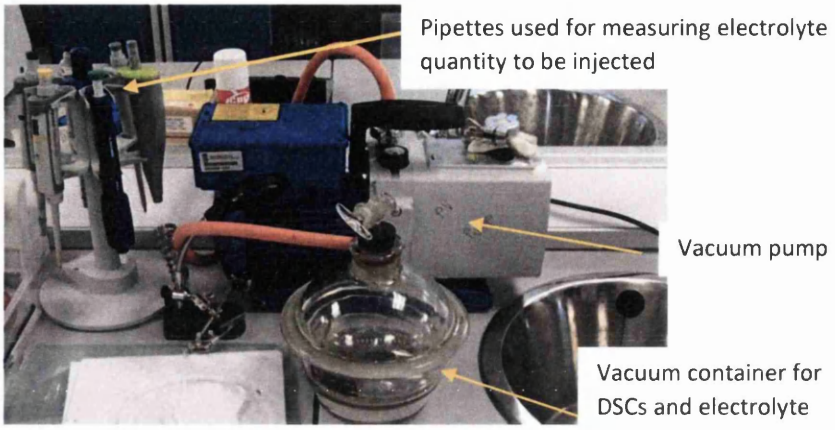

Figure 2.19: Vacuum pump set up for vacuum injection of electrolyte

In addition, the cobalt complex used in this study consisted of 0.2M Co^{2+} and 0.02M Co^{3+} in one cell and a higher quantity of Co^{3+} at 0.5M in a second cell, with 3-methoxypropylnitrile (3-MPN) chosen as a low volatility solvent. The additive 4-TBP was added in 0.25M and 0.5M concentration in two other cells in order to study the effectiveness of this additive on the behaviour of these corrosion cells. This NHC has previously been utilised as a performance enhancer in several cobalt electrolyte studies.

2.6.4 UV-VIS analysis for catalyst material and corrosion cells

UV-VIS analysis was performed using a Perkin Elmer Lambda 750S UV-VIS spectrophotometer and the product software package for analysis. In Chapters 3 & 4, this method is used to provide a means of characterising the platinum layer on FTO glass in order to allow comparison of different platinisation methods. A plain FTO glass counter electrode of 6.25cm^2 was used as a control sample.

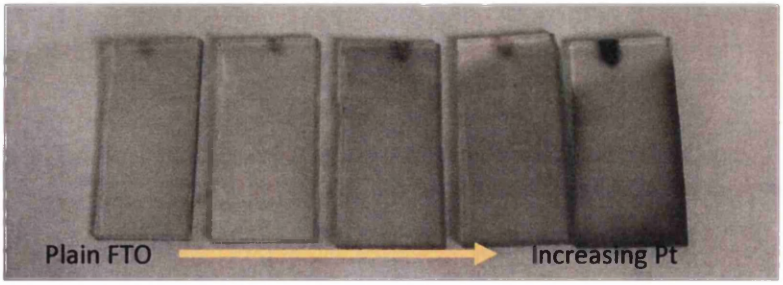

Figure 2.20: Different levels of platinisation for UV-VIS samples

The thermally platinised, chemically reduced and electrochemically platinised FTO glass were placed one after the other in the centre chamber of the 750S spectrophotometer in the forward light path (the back path was used as a reference point). The scan range used

was 250nmnm to 800nm in order to obtain a wide analysis spectrum. The platinum peak was thus recognised to be *ca.* 430-440nm, allowing several critical cell parameters, such as J_{sc}, efficiency, FF and V_{oc} and limiting current (J_{lim}) to be compared. Furthermore, the absorbance value can be used as a qualitative value for the quantity of platinum catalyst present on the FTO glass surface. A labelled example spectrum for platinum on FTO-glass can be seen in Figure 2.21.

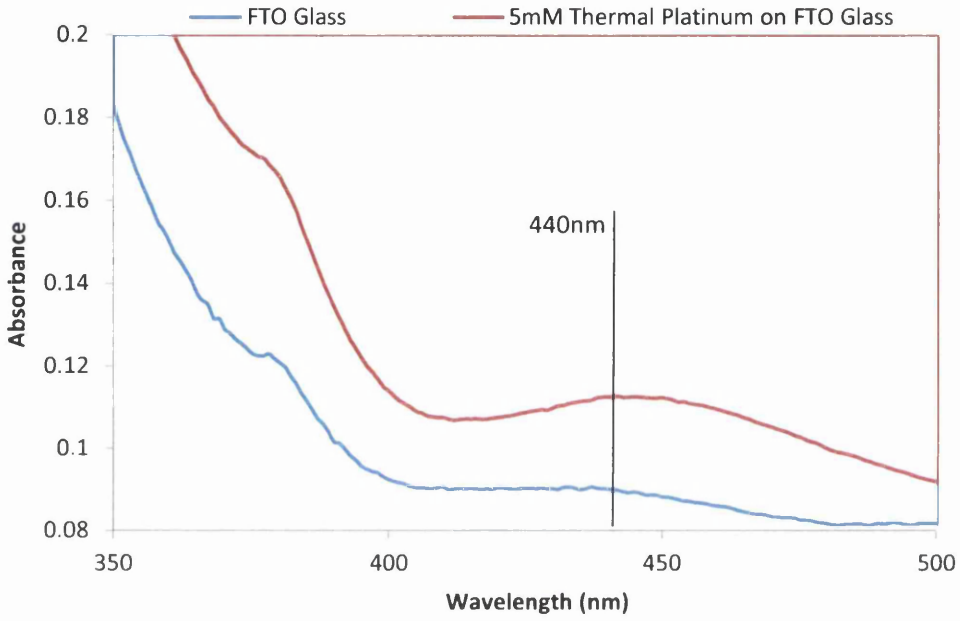

Figure 2.21: Example UV-VIS absorbance spectra for platinised FTO-glass

In Chapter 5 this method was used to study the corrosion of metal coupons when interacting with a triiodide/iodide electrolyte. This process uses the attached 60mm integrating sphere in the Lambda 750S equipment, which monitors the absorbance changes in the I_3^- redox mediator over a specified time frame when it is placed in contact with a prepared metallic substrate. The integrating sphere arrangement acts to direct the light beam to the sample, Figure 2.22. The encapsulation cell, described in Section 2.6, was thus placed in the reflectance aperture of the integrating sphere so that only the electrolyte region interacted with the beam path. The monochromatic light beam was able to pass through the 2mm glass top layer and 2µm thick electrolyte layer to reflect off the metal substrate surface. This reflected light is carried back to the detector where it was then analysed through the Perkin Elmer software package.

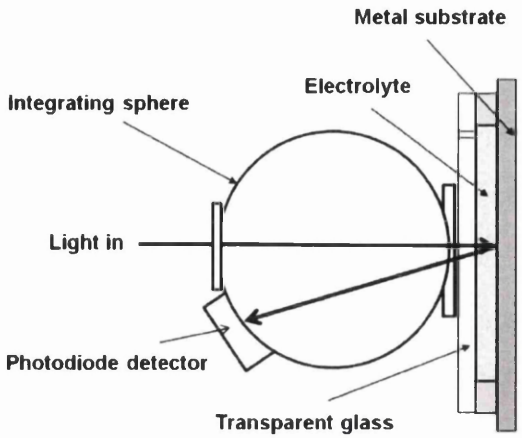

Figure 2.22: Integrating sphere schematic

All experiments were carried out *in-situ* using the time-lapse setting in the software package. Absorption spectra over a range between 300nm and 800nm were recorded every 5 minutes for 24 hours. These spectra were analysed, concentrating on the absorption wavelength of triiodide (*ca.*410nm) to give the rate of colour change, and thus the rate of I_3^- disappearance. If no corrosion had occurred, the metals were subjected to further testing over longer time periods.

2.6.5 Time-lapse photographic monitoring and image analysis

The time-lapse corrosion analysis was performed in an Ortery light box with a computer controlled Canon EOS600D acquiring the images, Figure 2.23 shows a schematic of this process.

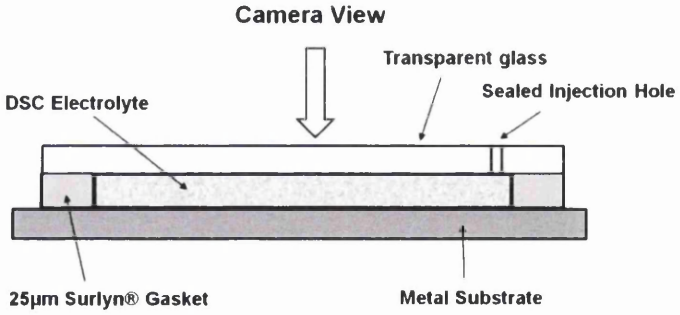

Figure 2.23: Schematic of time-lapse setup for image analysis

The lighting, focal length and sample position were constant throughout the experiment to ensure repeatability. Corrosion cells, as described in Section 2.6.1-2.6.3, were placed on the sample table and labelled to ensure accurate data analysis. The images were collected every 5 minutes with no initial delay for up to 1000 hours, or until no visible change occurred.

Figure 2.24 shows an example image of a corrosion cell captured *via* this set up. Once the images were collected, they were transferred to the Sigma Scan program and analysed using a purpose written macro to streamline data analysis process, and a region selection tool, an example of which is shown in Figure 2.24b. The output values required were the area analysed, average red, blue and green values and the average intensity (RGB colour). An example of the variation in these values is presented in Figure 2.25.

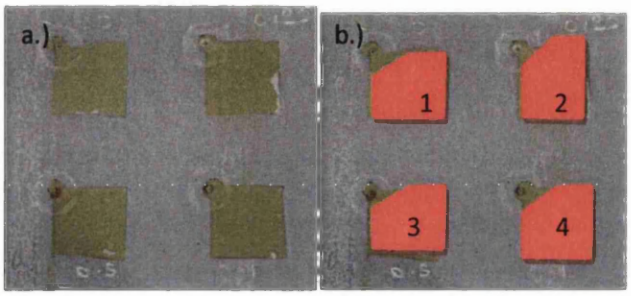

Figure 2.24: a.)Example corrosion cell image, b.)Area selection in Sigma Scan software

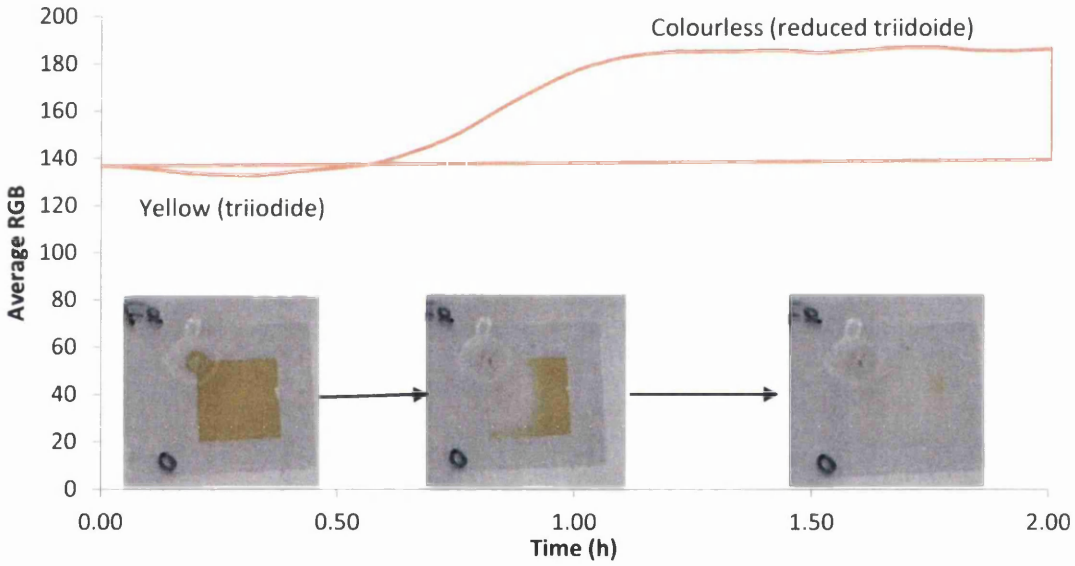

Figure 2.25: Graph showing the change in Avg. RGB *vs.*time for an example corrosion cell

The graph shows a change in the average colour of the observed cell as the corrosion proceeds over the observation time. Values in the range 40-100 denote a yellow/brown colour, an indication of the presence of triiodide. The 170 value indicates the complete loss of electrolyte colour. The numbers should be treated as relative values at this stage, since the metal background and variation in triiodide concentration between each cell will produce variations in the values. As a result, it is the change in value that is important to this study.

2.7 Scanning Electron Microscopy (SEM)

The field emission gun scanning electron microscope (FEG-SEM) used to characterise samples in this work was the Hitachi S4800. The equipment software was used to capture images at various accelerating voltages (V_{acc}) and working distances (W.D). An FEG is used to produce a coherent small diameter electron beam that can use a larger current density than a standard SEM, resulting in improved image resolution and a reduction in noise. This was considered an asset in this study, as it involved the imaging of nanoscale platinum particles.

Samples of $1cm^2$ were prepared on FTO glass and then mounted on the provided sample stage, carbon clips and copper clips were used to facilitate conduction from the conducting FTO to the stage in order to prevent charging and damage of the sample. The initial analysis should be done at an accelerating voltage V_{acc} of 10keV and a working distance (W.D) of 10mm, in order to orientate the sample and avoid damage to vulnerable samples through high power electron beam burning. The W.D and V_{acc} can be further optimised throughout the process to provide the best image quality. Figure 2.26 shows a sample image from a S4800 showing a bare FTO layer on a glass substrate. The FTO grains can be described as scale-like and several microns in size.

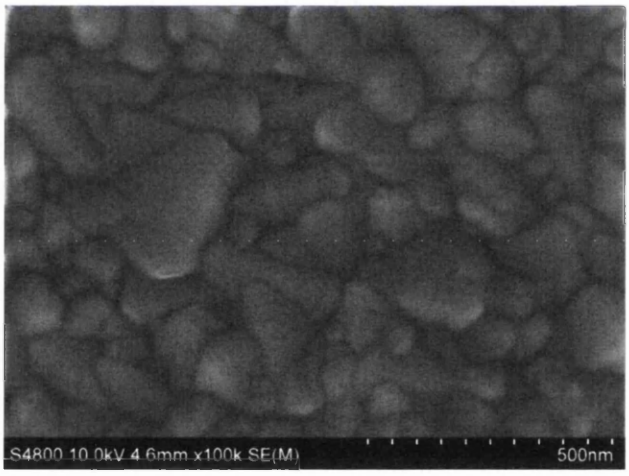

Figure 2.26: Sample image from an S4800 FEG-SEM

2.8 X-Ray Photoelectron Spectroscopy (XPS)

XPS spectra were obtained for electrochemically platinised samples using a Physical Instruments 5600 x-ray spectrometer. The Al K∝ radiation (1486.6eV, 300W) was used as the excitation potential and the target element spectra were measured with the pass energy of 23.50eV at 45°. Thickness calibration was achieved using a silicon wafer with a

top layer consisting of 100nm SiO_2. Atomic percentages were measured from an area of 800μm^2 at 1.3nm interval thickness, the pass energy here was 117.40eV. For atomic percentage determination, the peak areas were corrected with sensitivity factors of the instrument software (MultiPakV6.1A, Physical Electronics Inc., 1994-1999) which used photoionization cross sections of Scofield (σ) and the asymmetry parameter (β). The XPS spectra were analysed using the Origin 8.6 Pro software and used Gaussian algorithms to fit peaks to the spectra. The visible peaks were fitted using local maxima and hidden peaks were revealed using the 2nd derivative. A baseline for peak finding was formed using eight manually selected data points; this will be shown on each XPS spectra included in this work.

2.8.1 XPS theory

XPS is a method of using x-ray radiation to irradiate a material and recording the number and energy of the electrons that are released from the sample surface. The method requires a vacuum chamber and a beam energy of 200-2000eV, though there are sources such as from synchrotrons that are able to use a wider energy range up to 5000eV. An X-ray photoelectron spectrometer consists of an X-ray source, a vacuum chamber and collection and analytical tools for the electrons produced through the X-ray bombardment, Figure 2.27.

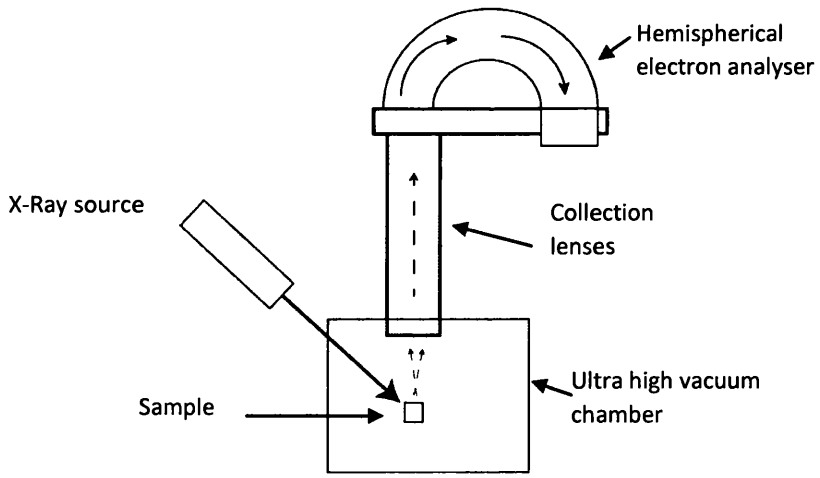

Figure 2.27: XPS schematic

The X-rays produced usually consist of several varying energy levels, called a non-monochromatic beam. However, to obtain accurate results, a monochromatic beam of one energy level is required. This is usually produced through the diffraction and focusing of the original beam off a crystalline quartz disc. The resulting beam is monochromatic and usually exhibits an energy of 1486.6eV, which corresponds to the aluminium Kα energy

level and has a wavelength of 0.83nm. This beam is then focused on the surface of a sample where it encourages the emission of electrons from the top 3-10nm when using the Al Kα x-ray radiation. This technique is used to measure the type and quantity of surface elements, discover any contamination and can discover the chemical states and bonding energies of surface atoms. The electrons that are excited from the material during X-ray bombardment "*hv*" are collected and then passed through an analyzer which measures the binding energy values. These are characteristic of the element and electron position in the atomic structure, such as the 1s, 2s, 2p, and other levels, Figure 2.28.

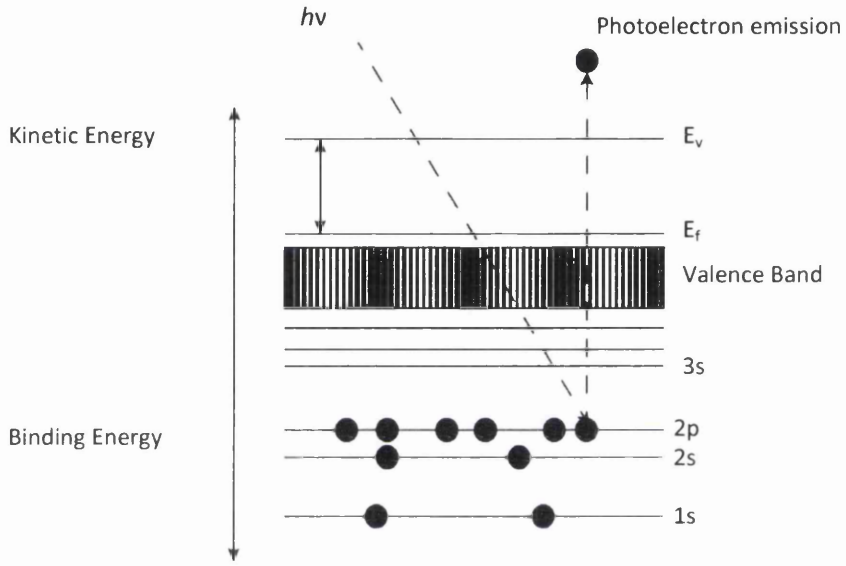

Figure 2.28: Energy level diagram for the operation of XPS

The number of electrons detected can be related to the quantity of that element in the surface of the sample under analysis. It is critical that this be performed under high vacuum, as this will minimise the amount of random electrons being detected and causing errors in the data. The collection of electron binding energies will form a spectrum, such as the example shown in Figure 2.29, where the binding energy is plotted versus the intensity, in counts per second, of those energies.

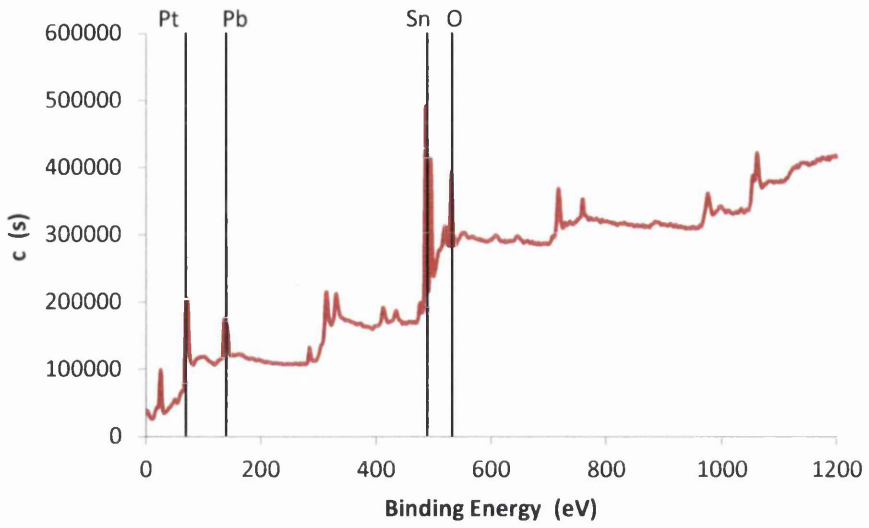

Figure 2.29: Example XPS spectra for Pt/Pb on FTO-glass substrate

Each peak represents the intensity of a certain binding energy, which can then be matched against known energy levels using either the software database integral to the XPS software, or literature sources [17]–[20]. The main peaks for this sample were at:

- 69.71eV for Pt4f
- 135.51eV for Pb4f
- 486.91eV for Sn3d5
- 530.91eV for O1s

When the spectrum is examined more closely, certain peaks can be broken down into two near identical peaks, known as doublet peaks. This feature is known as spin orbital splitting and is generally exhibited by electrons from the p, d and f shells [21]. These slight differences in peak value can give further identification to elements contained in the spectra. Spin orbital splitting is referenced through the use of fractional indices that are given after the shell notation, i.e. $p_{3/2}$ or $d_{5/2}$. The indices refer to the peak area ratio between the split peaks. Figure 2.30 shows the doublet peak for platinum using the data from Figure 2.29. The spin orbital splitting means that the binding energy peak for the Pt4f energy level has been split into two peaks, which using the local maxima characterisation method were found to be at 70.16eV and 73.45eV, referring to $Pt4f_{7/2}$ and $Pt4f_{5/2}$. When the NIST database is used value from 70.80 to 71.30eV are reported to be platinum metal, or Pt_0 [17].

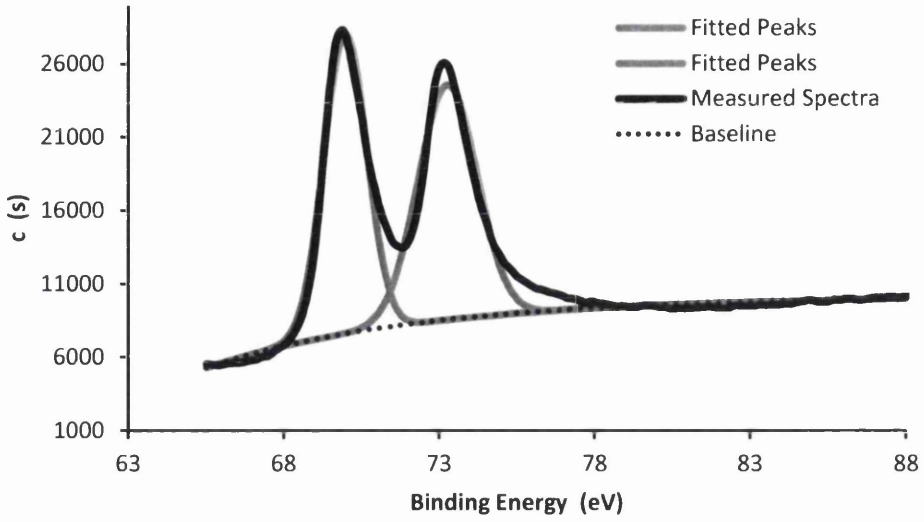

Figure 2.30: Doublet XPS peak for Platinum (Pt4f binding energy), with peak fitting and baseline indicated. Dark line represents measured data

This doublet, as previously mentioned, allows for a more accurate identification of the elements present in the XPS spectrum. This method only allows for the accurate characterisation of the samples surface. To analyse deeper, an ion gun is used to etch layers off the sample following each XPS measurement. The relative intensities of elements at each layer can then be compared using a thickness profile, giving more information regarding the atomic makeup of the sample, Figure 2.31.

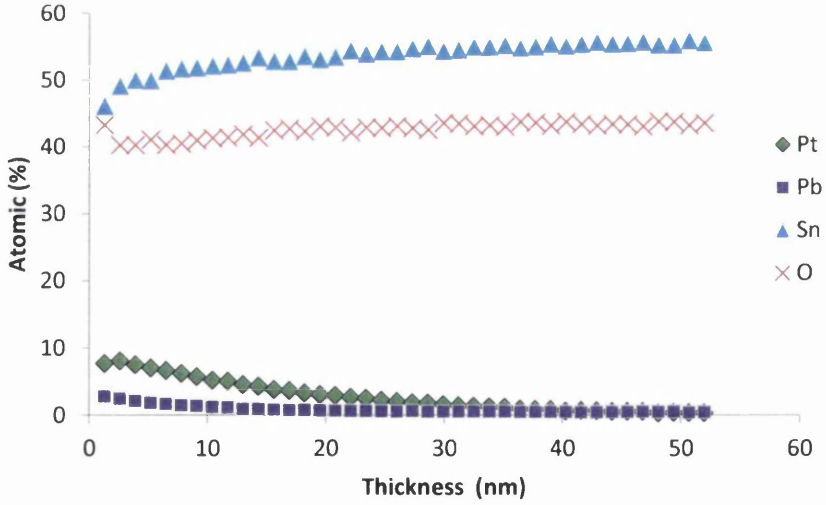

Figure 2.31: Example thickness profile for FTO-glass sample after Pb/Pt deposition

Care must be taken to ensure that the ion gun is fully calibrated, allowing for an accurate value for the depth etched from the sample.

2.9 References

[1] G. Tsekouras, A. J. Mozer, and G. G. Wallace, "Enhanced Performance of Dye Sensitized Solar Cells Utilizing Platinum Electrodeposit Counter Electrodes," *J. Electrochem. Soc.*, vol. 155, no. 7, pp. K124 – K128, 2008.

[2] S. Ito, N.-L. C. Ha, G. Rothenberger, P. Liska, P. Comte, S. M. Zakeeruddin, P. Péchy, M. K. Nazeeruddin, and M. Grätzel, "High-efficiency (7.2%) flexible dye-sensitized solar cells with Ti-metal substrate for nanocrystalline-TiO2 photoanode.," *Chem. Commun. (Camb).*, no. 38, pp. 4004–6, Oct. 2006.

[3] M. Fayette, Y. Liu, D. Bertrand, J. Nutariya, N. Vasiljevic, and N. Dimitrov, "From Au to Pt via surface limited redox replacement of Pb UPD in one-cell configuration.," *Langmuir*, vol. 27, no. 9, pp. 5650–8, May 2011.

[4] C. Yoon, J. Lee, W. Chae, and K. Kim, "Enhanced performance of a dye-sensitized solar cell with an electrodeposited-platinum counter electrode," *Electrochim. Acta*, vol. 53, no. 6, pp. 2890–2896, Feb. 2008.

[5] Y.-S. Ko and Y.-U. Kwon, "Electrochemical deposition of platinum on fluorine-doped tin oxide: The nucleation mechanisms," *Electrochim. Acta*, vol. 55, no. 24, pp. 7276–7281, Oct. 2010.

[6] H. Kusama, M. Kurashige, and H. Arakawa, "Influence of nitrogen-containing heterocyclic additives in I− I3−redox electrolytic solution on the performance of Ru-dye-sensitized nanocrystalline TiO2 solar cells," *J. Photochem. Photobiol. A Chem.*, vol. 169, pp. 169–176, 2005.

[7] S. M. Feldt, E. A. Gibson, E. Gabrielsson, L. Sun, G. Boschloo, and A. Hagfeldt, "Design of organic dyes and cobalt polypyridine redox mediators for high-efficiency dye-sensitized solar cells.," *J. Am. Chem. Soc.*, vol. 132, no. 46, pp. 16714–24, Nov. 2010.

[8] F. Fabregat-Santiago, J. Bisquert, G. Garcia-Belmonte, G. Boschloo, A. Hagfeldt, F. Fabregatsantiago, and G. Garciabelmonte, "Influence of electrolyte in transport and recombination in dye-sensitized solar cells studied by impedance spectroscopy," *Sol. Energy Mater. Sol. Cells*, vol. 87, no. 1–4, pp. 117–131, May 2005.

[9] J. Halme, P. Vahermaa, K. Miettunen, and P. Lund, "Device physics of dye solar cells.," *Adv. Mater.*, vol. 22, no. 35, pp. E210–34, Sep. 2010.

[10] L. Han, N. Koide, Y. Chiba, A. Islam, R. Komiya, N. Fuke, A. Fukui, and R. Yamanaka, "Improvement of efficiency of dye-sensitized solar cells by reduction of internal resistance," *Appl. Phys. Lett.*, vol. 86, no. 21, p. 213501, 2005.

[11] J. Bisquert and F. Fabregat-Santiago, "Impedance Spectroscopy: A General Introduction and Application to Dye-Sensitised Solar Cells," in *Dye Sensitized Solar Cells*, 1st ed., K. Kalyanasundaram, Ed. EPFL Press, Lausanne, 2010, p. 523.

[12] J. Bisquert, "Hopping transport in dye sensitized solar cells," *J. Phys. Chem. C Lett.*, 2007.

[13] Q. Wang, S. Ito, M. Grätzel, F. Fabregat-Santiago, I. Mora-Seró, J. Bisquert, T. Bessho, and H. Imai, "Characteristics of high efficiency dye-sensitized solar cells.," *J. Phys. Chem. B*, vol. 110, no. 50, pp. 25210–21, Dec. 2006.

[14] F. Fabregat-santiago, J. Bisquert, E. Palomares, L. Otero, D. Kuang, S. M. Zakeeruddin, and M. Gra, "Correlation between Photovoltaic Performance and Impedance Spectroscopy of Dye-Sensitized Solar Cells Based on Ionic Liquids," vol. 2, pp. 6550–6560, 2007.

[15] J. Bisquert, "Influence of the boundaries in the impedance of porous film electrodes," *Phys. Chem. Chem. Phys.*, vol. 2, pp. 4185–4192, 2000.

[16] H. Wang (Bath University), "Discussion with H. Wang on CV analysis of DSCs." Bath University, 2008.

[17] A. V. Naumkin, A. Kraut-Vass, S. W. Gaarenstroom, and C. J. Powell, "NIST X-ray Photoelectron Spectroscopy Database," *NIST X-ray Photoelectron Spectroscopy Database, Version 4.1 (National Institute of Standards and Technology, http://srdata.nist.gov/xps Gaithersburg, 2012);*, 2012. [Online]. Available: http://srdata.nist.gov/xps. [Accessed: 13-Aug-2012].

[18] J. F. Watts and J. Wolstenholme, *An Introduction to Surface Analysis by XPS and AES*, Illustrate. Wiley, 2003.

[19] G. Wang, Y. Lin, X. Xiao, X. Li, and W. Wang, "X-ray photoelectron spectroscopy analysis of the stability of platinized catalytic electrodes in dye-sensitized solar cells," *Surf. Interface Anal.*, vol. 36, no. 11, pp. 1437–1440, Nov. 2004.

[20] D. Briggs and M. P. Seah, *Practical Surface Analysis - Auger and X-ray Photoelectron Spectroscopy*, 2nd ed. Wiley, 1990.

[21] P. van der Heide, *X-ray Photoelectron Spectroscopy: An introduction to Principles and Practices*. Wiley, 2011.

3 *Investigation into fast electrochemical platinisation on FTO-Glass for potential use in a roll to roll fabrication process*

3.1 Introduction

Standard glass based DSCs have progressed to the stage where their high efficiency and durability allows them to be commercialised. However, the use of glass means that the resulting cells are expensive, due to the supporting infrastructure and require a batch type manufacturing process. However, there has been a recent drive to construct DSC devices using polymeric and metal sheet materials in an effort to reduce device costs and weight, in addition to allowing mass production on a roll to roll coating line.

A metal and polymer substrate cell, as previously mentioned in Chapter 1, consists of a flexible sheet metal substrate, such as titanium upon which a sensitised TiO_2 electrode is fixed. A conducting polymer such as ITO-PET or ITO-PEN is then platinised and sealed to the metal using the same Surlyn as used in standard glass cells. Electrolyte can be vacuum injected through holes left in either the metal or polymer electrode and then sealed.

The drawback of using the lower cost conducting polymers is that their low thermal tolerance precludes the use of high temperature processing such as the 385°C required for thermal platinisation, or the 450°C needed for sintering a TiO_2 photoelectrode. Low temperature processing is available for the application of the TiO_2 semiconductor. However, this process results in a poorly connected TiO_2 semiconductor and a less efficient DSC device.

In terms of the application of the catalyst, there are several high performing alternatives to thermal platinisation, see Chapter 1.1.5. Sputter deposition for example produces a highly catalytic platinum layer, which has been compared and contrasted with other methods in previous studies [1]. Unfortunately, this is a costly process that is limited to certain work-piece geometries and vacuum conditions [2]–[4]. A further low temperature alternative involves the chemical reduction of a chloroplatinic acid precursor. This has been investigated in previous literature [5]–[7], and further compared with thermal and sputter deposition in previous research [1]. Chemical platinisation (using sodium borohydride) provides a viable low temperature platinisation method, though it will introduce further hazardous chemicals and time sensitive processes to an already complex production line.

It was thought that the usage of electrochemical deposition, or "electrodeposition", would mitigate some of the disadvantages of other platinisation methods. Further, this would capitalise on the industry expertise of strip product manufacturers, such as Tata Steel Colours and in coating methods, electrodeposition and galvanising. In addition, the coating and galvanising industry has large solution tanks available that could be repurposed for electrodeposition of platinum on a roll to roll production line. As a result, electrochemical deposition seems to be an extremely viable option and has already been introduced for the production of fuel cell electrode and catalyst material [9, 10].

To avoid large performance losses in DSC devices, a specific deposit morphology and catalytic performance is required. The catalyst is thus defined by the active area, also known as the specific surface area of the catalyst. This can be assessed through electrochemical means such as cyclic voltammetry (CV) and electrical impedance spectroscopy (EIS). In electrodeposition, such a highly catalytic structure can only be created through fine control deposition parameters, such as potential, time and the deposition solution.

There have been many reports on the electrodeposition of platinum for the manufacture of the redox catalyst for dye sensitised solar cell counter electrodes, but most of these studies have used timescales from 30 seconds to several minutes [10]–[12]. While this has been reported to produce viable, high performing catalytic material, the longer timescales used are not considered practical for a rapid continuous manufacturing process. The primary study here analyses the adaptation of previously reported electrodeposition techniques, but using shorter, <1 minute timescales to ascertain if fast simple processing is possible on FTO-Glass substrate.

FTO-Glass was chosen instead of ITO-PET due to its stability and common use, a key quality for this initial study where we are analysing the deposit rather than the deposit/substrate interaction. This will also remove the complication of a flexing substrate from the construction and testing process. The widespread use of FTO-glass throughout DSC literature will allow a straightforward comparison with other common platinisation methods. FTO-glass will give a stable, but also a challenging surface for electrodeposition due to its scale like morphology rather than a consistent, smooth surface.

As typical literature methods use timescales over 30 seconds, the aim of this chapter is to improve several high performing published methods, to develop them to run at the high speeds required for a continuous coating line, i.e. under 30 seconds if possible. It is hoped

that this development will rival the application speed and performance of the chemical reduction platinisation method that is also under consideration for industrial use. Since the resources available do not permit the use of a full or pilot scale manufacturing plant, this study utilises lab-scale electrochemical analysis.

3.2 Experimental

The reaction mechanism for the electrodeposition of platinum from hexachloroplatinic acid [H_2PtCl_6 (aq)] are as follows [13]:

$$Pt^{4+}Cl_6^{2-} + 2e^- \rightleftharpoons Pt^{2+}Cl_4^{2-} + 2Cl^- \quad (3.1)$$

$$Pt^{2+}Cl_4^{2-} + 2e^- \rightleftharpoons Pt + 4Cl^- \quad (3.2)$$

$$Pt^{4+}Cl_6^{2-} + 4e^- \rightleftharpoons Pt + 6Cl^- \quad (3.3)$$

As previously mentioned in Chapter 1.5, the Pt-Cl bond cleaving is a kinetically slow process that should not occur until a potential is applied to the electrodes. This ensures that the deposition will be fully under external control and this will dictate the overall structure. However, once platinum is present on the surface, the process may auto-catalyse, increasing platinum deposition over the externally controlled amount. To control this, a positive potential should be applied following each deposition event.

The electrochemical deposition cell consisted of an Ag/AgCl reference electrode, platinum mesh counter electrode and a FTO glass working electrode. The initial deposition working electrode size was $1cm^2$. The deposition solution consisted of 5mM chloroplatinic acid in aqueous solution, with 50mM HCl used as the supporting electrolyte in order to control the ohmic drop in the solution and control mass transport effects, further to this its inclusion will control the pH throughout the deposition event.

Initially, constant voltage deposition potentials were used as this remains the simplest method of applying the necessary power needed to deposit the platinum material. The potentials used here are adapted from literature sources: The -0.6V potential, from Tsekouras *et al.* [14], lies at the high edge of the negative, or cathodic, region of the Pt CV curve, Figure 3.1, whereas -1.8V, taken from the report of Ito *et al.* [15], lies outside the presented CV curve. In this region hydrogen ions will adsorb to the working electrode substrate from solution or evolve on previously deposited platinum particles.

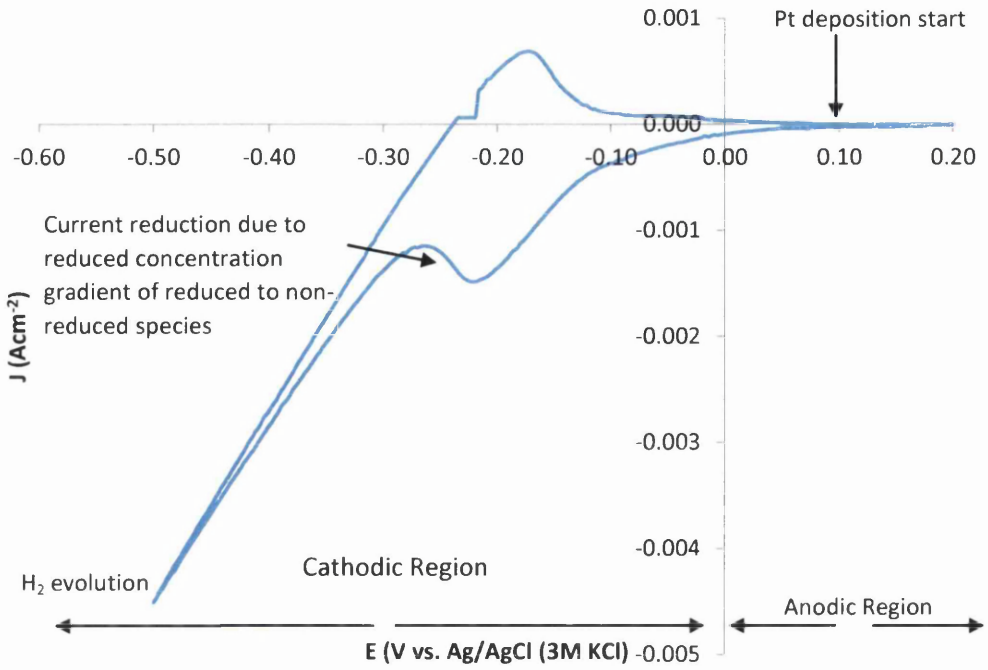

Figure 3.1: Example CV curve for the deposition of platinum from $H_2PtCl_{6\,(aq)}$

Competition will thus occur between deposition and hydrogen adsorption and it was theorised that this competition could reduce the platinum particle size. Deposition times from 1 second to 30 seconds were tested at each voltage to observe how the deposit was affected by voltage and time. In addition, the effects of pulse deposition was studied and compared to the constant potential methods in order to further understand the requirements needed for fast deposition of an efficient catalyst.

Throughout this study, the electrochemically deposited platinum catalyst was compared against thermal, chemical and sputter platinised FTO glass electrodes. These were produced through the methods detailed in Chapter 2.2.2. In summary, the thermal catalyst was applied using 5mM chloroplatinic acid in 2-propanol, heat treated on FTO-glass at 385°C for 30 minutes, as per the method introduced by Papageorgiou *et al.* The chemically platinised CE's utilised a 60mM sodium borohydride reducing agent to reduce 5mM chloroplatinic acid in 2-propanol that was dried onto the FTO-glass at 120°C for 20 minutes. The sputter platinised electrode was produced through vacuum magnetron sputtering to a layer thickness of 0.5nm, see Chapter 2.2.3.

3.3 Results and Discussion

3.3.1 Electrodeposition for platinum redox catalyst

It was known from the outset that shorter deposition times would be favourable for inclusion in a roll-to-roll process due to the reduction of process specific bottlenecks in in-line fabrication. As a result, this study favours rapid sub-minute deposition times when designing the experiments. In this initial study, a simple direct deposition technique using a potential of -0.6V from Tsekouras *et al.* [14], was first characterised using UV-VIS spectrophotometry to measure the change in absorbance as the deposition time was varied. Previous studies have shown that a thicker platinum layer would result in higher absorbance at certain wavelengths, specifically around 440nm [1]. This method was shown to allow comparison between counter electrodes produced through different platinisation methods and so will allow the comparison of this method. Increasing values for absorbance at a wavelength of 430-440nm, given in Figure 3.2, relate to Pt quantity on the FTO-glass substrate as deposition time increases.

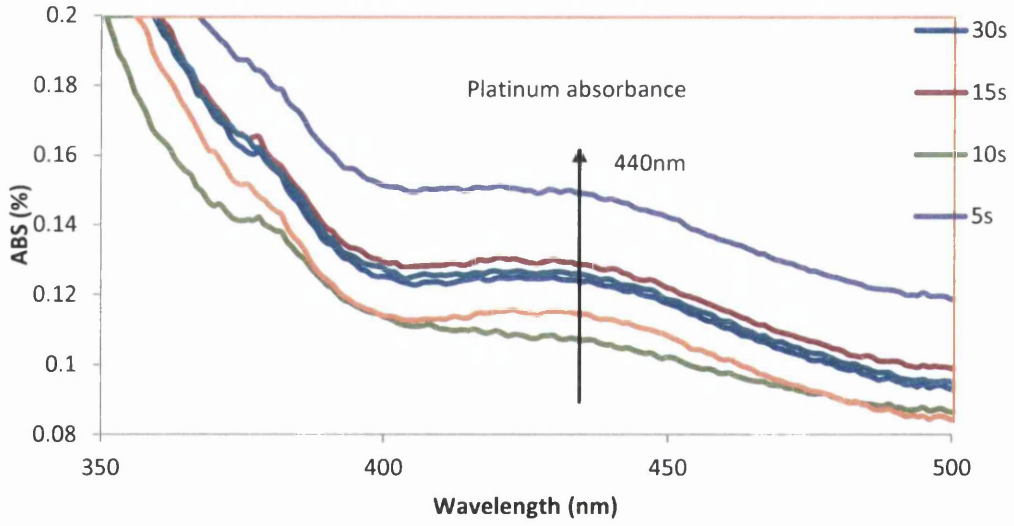

Figure 3.2: UV-Vis Spectra for potentiostatically deposited platinum at -0.6V for varying deposition times. The platinum absorbance peak can be seen at a wavelength of 440nm. (Average of three measurements)

The results were not as expected, with 30, 15 and 10s giving highly variable absorbance values from the expected increasing trend. The difference is believed to be due to the varying growth patterns on FTO substrate, in addition to dendritic and partial continuous layer formation on the FTO surface. This will be explored further in the text using SEM imagery.

Comparing the absorbance at 440nm allows for the comparison of different platinisation techniques, where different measures for deposition (temperature, time or measured thickness) are used, Figure 3.3. Fresh samples of 0.5nm sputtered platinum, 5mM concentration thermal platinum and 5mM concentration chemically applied platinum were produced in order to compare the more common platinisation method with the electrodeposition technique used in this chapter. These other methods are known to produce catalysts structures composed of small particles on the scale of 5-50nm, resulting in a much lower absorbance and scattering effect than seen for the electrodeposited CE.

There is a large increase in ABS from plain FTO-glass to the 0.5s value of 0.11, which is higher than the equivalent thermal or chemical platinisation electrodes. This indicates the growth stage of large particle of Pt has predominated, rather than nucleation of many small particles. This is supported by the work of Kim *et al.*, who stated that direct deposition favours the growth of existing structures and dendritic formations due to ion limitation at the electrode surface [16].

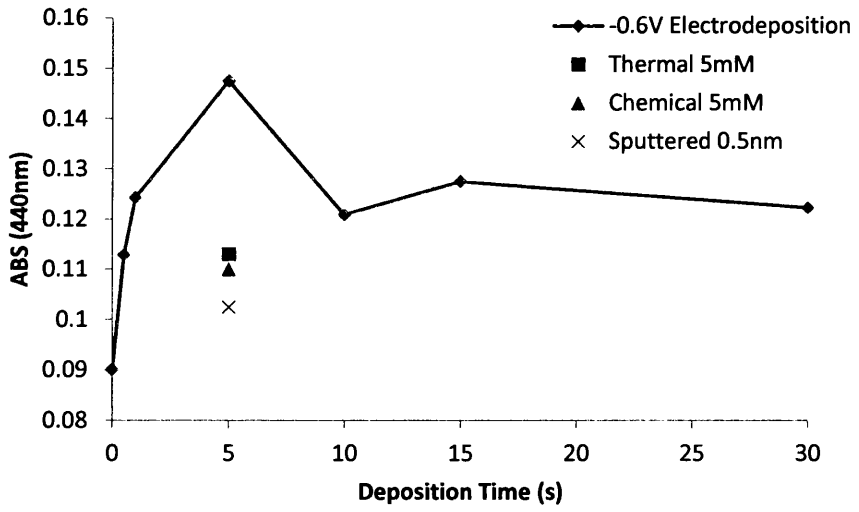

Figure 3.3: Absorbance of the platinum layer at 440nm versus deposition time at -0.6V (average of 3 measurements)

The peak in ABS value at 5s, for the electrodeposited counter electrodes, was thought to be due to the increasing growth of dendritic formations. The reduction at 10s was attributed to particle agglomeration or the formation of a continuous or near continuous layer with less scattering and absorbance ability than of discrete particles. It is known that once nucleation has occurred during direct deposition, growth of the original deposits will continue as long as the potential is applied. After a given time, suggested in Figure 3.3 to

be 5s, the small particles that have nucleated and grown on the FTO surface may begin to agglomerate, forming crystalline formations with less scattering and absorbance effects than a large quantity of faceted particles. It is also postulated that the difference in crystal morphology between electrochemically grown Pt and other common platinisation methods could be the cause of the increased absorbance of the ED-Pt, though later in this chapter, the scanning electrode microscope images indicate that the thermal, chemical and sputtered Pt clusters are smaller by several orders of magnitude than even the most rapidly electrodeposited Pt catalyst.

To provide a comparative study, further experiments were conducted using settings adapted from Ito *et al.* [15]. Their paper presented a 7.2% efficient DSC using titanium and polymer substrates and an electrodeposited platinum counter electrode. The electrodeposition in this chapter utilises the same potential of -1.8V, but it has been applied it using times of 15, 10, 5 and 1 seconds, the time noted in the Ito *et al* work was 15 seconds, tested in this study as a comparison point to ascertain how repeatable this technique is on FTO-glass. As Figure 3.4 shows, a relatively large increase in ABS value occurs from 1s to 10s, which is then followed by a plateau up to 15s. This trend illustrates the growth of the platinum layer on the substrate. The range from 10s to 15s is thought to be a brief plateau before further growth occurs. From this, it was suggested that the technique used by Ito *et al.* can be further improved and adapted to faster processing times.

As previously seen, only the most rapid deposition times of 1s has a comparable absorbance to the thermal, chemical and sputter platinised electrodes. As the time is increased, it was seen that the 5 second deposition gives a value approximately four times that of the thermal 5mM catalyst, Figure 3.4. The difference indicates that a larger quantity of Pt is deposited using this higher deposition potential. In a potential DSC counter electrode, this is unwanted as more material coverage will result in less light penetration through the electrode, a serious issue in reverse illuminated cells with a metal electrode. However, despite the high potential, the initial ABS values are comparable to that of the -0.6V potential study, lying in a similar ABS range of 0.11 to 0.17. It is only when the longer deposition times of 10, 20 and 30s are compared, that a large increase in ABS can be seen, compared with the lower potentials used previously. The large potentials facilitate increased deposition in the same timeframe due to the higher overpotential driving force for deposition.

The linear nature of the increase in absorbance, compared with that of platinum deposited at -0.6V, was unexpected. It was believed that the differences between these electrodeposition methods was due to increased competition at -1.8V with H_2 evolution and PtOH adsorption, as mentioned by Fayette *et al* [17]. This competition, in addition to the increased concentration gradient between the substrate and bulk electrolyte through fast ionic depletion, was believed to increase dendritic formation and layer thickness, resulting in a Pt layer that growth progressively with deposition time.

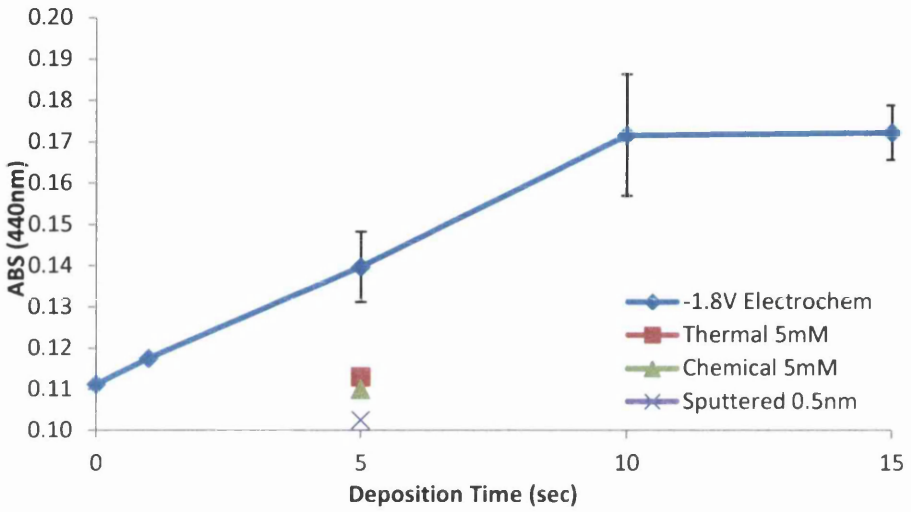

Figure 3.4: UV-VIS analysis of -1.8V electrochemically deposited platinum at 440nm for different deposition times (average of three measurements)

The UV-VIS technique can give a qualitative idea of the structure and formation of the Pt on FTO-glass. In order to obtain a clearer representation of catalyst performance for this study, a more accurate testing regime must be employed. Therefore, further CV studies using a simple iodide/triiodide electrolyte in a symmetrical cell setup were undertaken to record the limiting current density (J_{lim}). A typical CV scan for a symmetrical counter electrode cell containing iodide/triiodide electrolyte is shown in Figure 3.5.

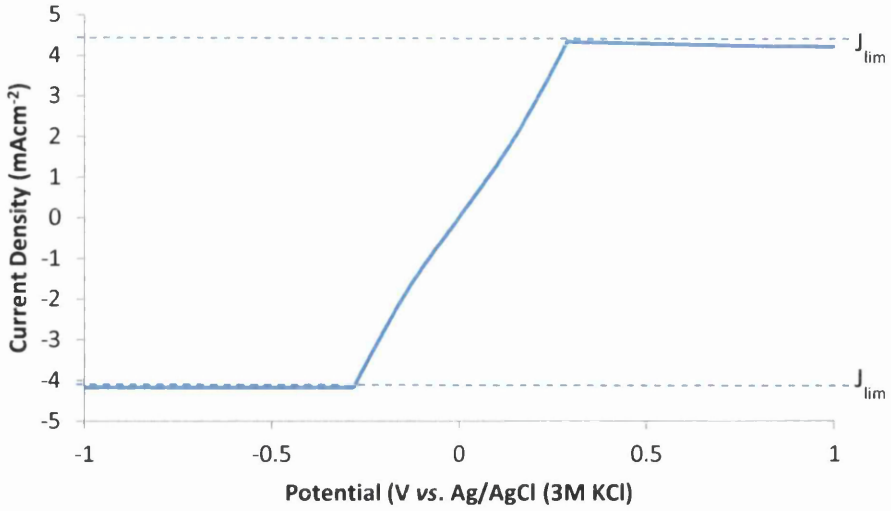

Figure 3.5: CV plot for symmetrical counter electrode cells prepared through different platinisation methods

The variation in J_{lim} with deposition time is displayed in Figure 3.6. As the potential is scanned from 0V to a maximum defined limit of 1.5V, the redox reduction of the triiodide species is forced to take place at the counter electrode catalyst defined by the polarisation of the scan (Positive or Negative). However, since this is a symmetrical cell, the response of either scan will be identical or near to identical. The J_{lim} value occurs where the potential is high enough that the species near the electrode have all been reduced and must be transferred in from the bulk solution. The rate of electron transfer of the minority species (I_3^-) in the cell will then become mass transfer limited, as the reaction becomes dependent on how fast species can diffuse from the bulk electrolyte to the electrode. In thin layer cells such as these, the triiodide depletes rapidly, causing a limiting current plateau to be visible on the CV scan. The higher the J_{lim} value, the more efficient the electron transfer reaction at the catalyst before the cell becomes mass transfer limited.

The thermal, chemical and sputter produced catalysts used as comparison values can be seen in Figure 3.6, which uses the absorbance (ABS) of Pt on FTO-glass to compare the J_{lim} of different platinisation method, the higher the absorbance, the longer the deposition time. They exhibit higher values for J_{lim} than any tested electrochemically platinised counter electrode. This is despite the higher Pt amount indicated by the high absorbance value. These lower values suggest that electrochemically produced platinum has a different reactivity and lower specific area than the more common platinisation methods. This also means that unless the crystal structure can be further controlled, a larger quantity of Pt will be required to produce a similar catalytic effect to rival the more common methods.

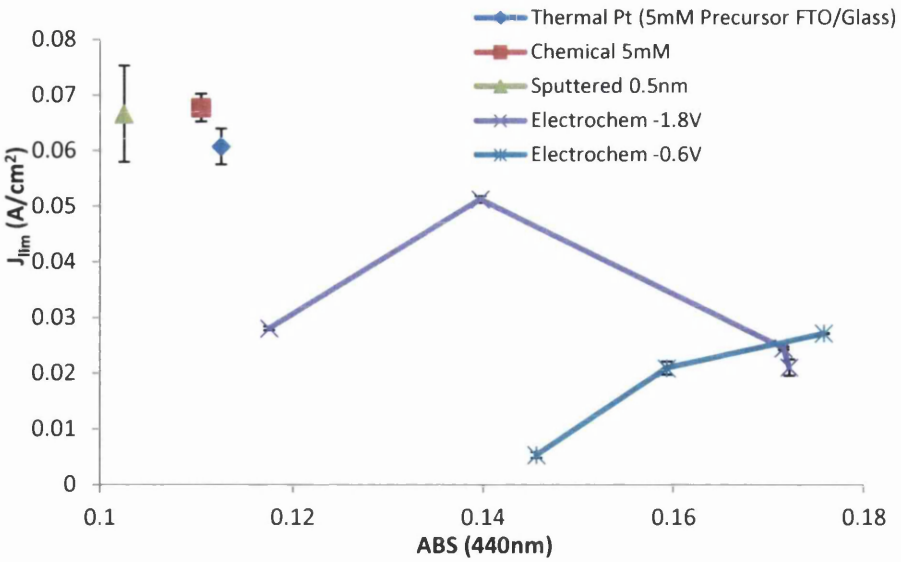

Figure 3.6: Absorbance (relative Pt quantity) *vs.* limiting current density for thin layer Pt/Pt cells (average of 3 measurements)

So far, the electrodeposition methods have been analysed using electrochemical or indirect analysis (UV-VIS). In order to better explain the results observed in Figure 3.6, SEM imagery of the deposition morphology was undertaken, Figure 3.7. The thermal Pt catalyst exhibits discrete deposits in the range of 5-50nm that are evenly distributed across the surface of the FTO glass substrate, Figure 3.7a.

The small size and uniform distribution (i.e. little agglomeration) lead to the low absorbance values returned in the UV-VIS analysis, Figure 3.3. Comparatively, the UV-VIS absorbance for the -0.6V and -1.8V potentiostatically electrodeposited platinum is around 1.5x greater, Figure 3.7b&c, explains this through the presence of large (*ca.* 100nm) clusters that have formed due to particle agglomeration and poorly controlled deposit growth. These structures are much thicker in aspect than the equivalent structures of the thermal and chemical alternatives so will absorb or reflect a much larger fraction of the incoming light when analysed using the UV-VIS technique.

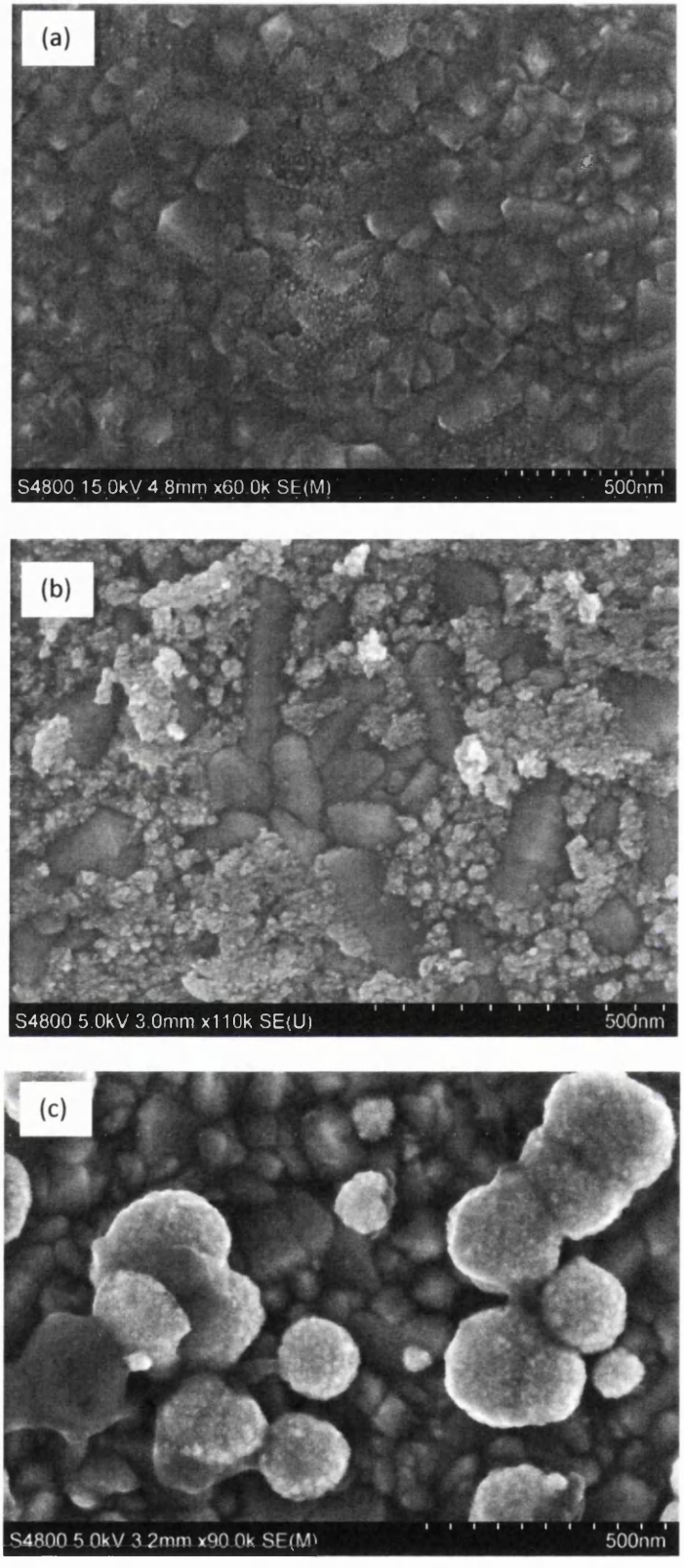

Figure 3.7: SEM imagery of (a) Thermal Pt; (b) -0.6 ED-Pt; (c) -1.8V ED-Pt, on FTO glass substrate

Figure 3.8 further illustrates how a long deposition time of 30 minutes will affect the catalyst structure. The SEM shows an irregular crystalline structure that has clearly undergone much agglomeration. Further to this, the dendritic "spike" morphology of the crystals indicates that the growth is occurring using ions from the bulk solution, as the layer adjacent to the electrode has been quickly depleted and not replenished due to the constantly applied potential. This formation will reduce the specific catalytic area of the platinum catalyst and will result in a counter electrode with an increased ability to absorb or scatter incoming light - a serious drawback if used in reverse illuminated DSCs.

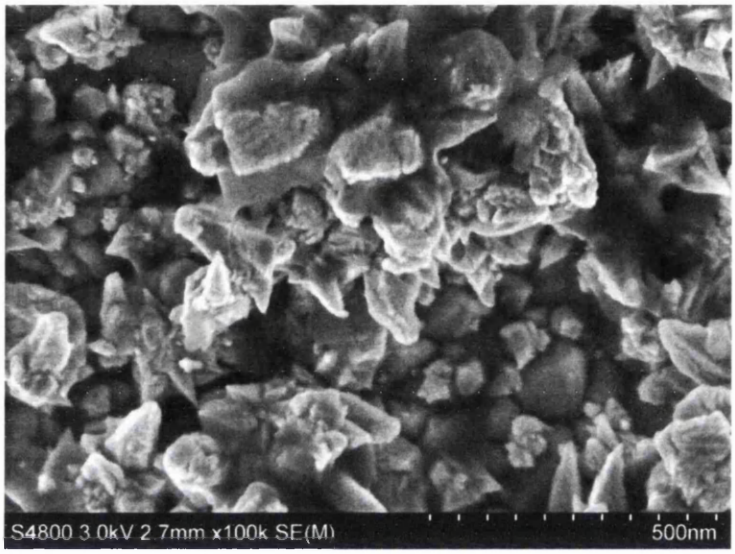

Figure 3.8: -1.8V deposition from 30 minutes; as a comparison with short timescale deposition of platinum

It was then necessary to construct example DSC test cells in order to evaluate the electrodeposited counter electrodes examined in this study. To that end, cells were constructed using counter electrodes platinised by potentiostatic deposition at -1.8V for deposition times of 1, 5, 10 and 30 second. After analysis of the UV-VIS and FEG-SEM images in addition to the cyclic voltammetry data, it was predicted that the device peak efficiency would lie around five seconds deposition, as this resulted in the peak J_{lim} value of $0.051A/cm^2$. Following this characterisation work, full DSC devices were constructed to obtain experimental performance values for DSC using potentiostatically platinised counter electrodes, see Table 3.1, with literature value from Tsekouras *et al* and Ito *et al.* included for comparison [14], [15]. The main observation made from this date, is that the DSCs using the electrodeposited platinum counter electrodes exhibits comparable performance to the control samples using thermal, chemical and sputter platinised counter electrodes. The thermal and chemically applied catalysts were produced using 5mM chloroplatinic acid

precursor, which in previous work showed balanced platinum quantity and specific activity for a standard liquid state DSC [1].

Table 3.1: DSC results from cells using -1.8V electrodeposited CE's (from an average of 3 test cells)

ABS (440nm)	Deposition Time (s)	V_{oc} (V)	J_{sc} (mA/cm^2)	FF (%)	η (%)
0.1722	15	0.71(±0.01)	8.60(±0.40)	56(±6.5)	3.4(±0.6)
0.1716	10	0.72(±0.02)	9.30(±0.37)	55(±5.4)	3.7(±0.2)
0.1397	5	0.71(±0.002)	8.80(±0.45)	57(±2.0)	3.6(±0.3)
0.1175	1	0.69(±0.01)	8.90(±0.92)	50(±2.6)	3.1(±0.3)
0.1125	Thermal 5mM	0.74(±0.002)	10.49(±0.40)	70(±6.0)	5.5(±0.7)
0.1105	Chemical 5mM	0.65(±0.002)	7.90(±0.12)	69(±0.006)	3.5(±0.04)
0.1025	Sputtered 0.5nm	0.75(±0.004)	8.10(±0.53)	68 (±1.3)	4.1(±0.3)
Ito *et al.*	15 (ITO/PEN)	0.78(N/A)	13.6(N/A)	68(N/A)	7.2(N/A)
Tsekouras *et al*	Various	0.80(N/A)	12(N/A)	67(N/A)	6.4(N/A)

The main conclusion that can be drawn here is that our adapted methods were not comparable to the optimised literature techniques of the original studies by Ito *et al.* and Tsekouras *et al.* Surprisingly though the performance of the DSCs using our adapted methods are within 0.5% efficiency of the lab produced cells using chemically platinised counter electrodes. However, the thermally platinised devices still exhibit much higher performance, Figure 3.9. It was further seen that increasing the platinum quantity through longer electrodeposition times does not produce an enhancement of performance relative to the quantity of platinum used, as the peak efficiency was seen to be at 5s and 10s deposition times, giving 3.6% and 3.7% respectively. It was thought that these deposition times give the best balance between platinum quantity and specific surface area when using un-optimised conditions and FTO/glass substrate.

DSC analysis has previously shown that the fill factor is the most direct way to obtain a representation of the counter electrode effect on DSC performance. The value can be quantitatively compared through the current density (J) - Potential (E) curves generated by solar simulator testing, Figure 3.10. The comparison samples: thermal, chemical and sputtered all return a fill factor of *ca.* 70%, which represents an efficient cell with little internal factors detrimentally affecting DSC internal resistance. In comparison, the electrodeposited Pt devices return a fill factor correspondingly lower in the range 50-60%. This reduction describes losses due to internal resistances in the DSC device. Since the electrolyte, TiO_2 and dye were produced at the same time and using the same batch, it was concluded that the decrease was due to the change in counter electrode specific activity,

due to the difference in Pt catalyst structure, as visible in the SEM images, Figure 3.7 and Figure 3.8.

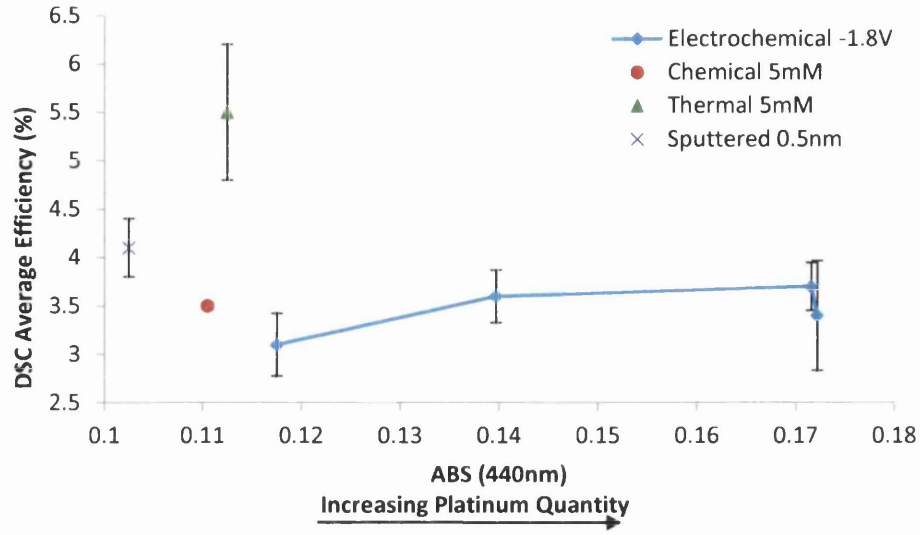

Figure 3.9: DSC efficiency comparison of cells using different counter electrode types (3 cell average)

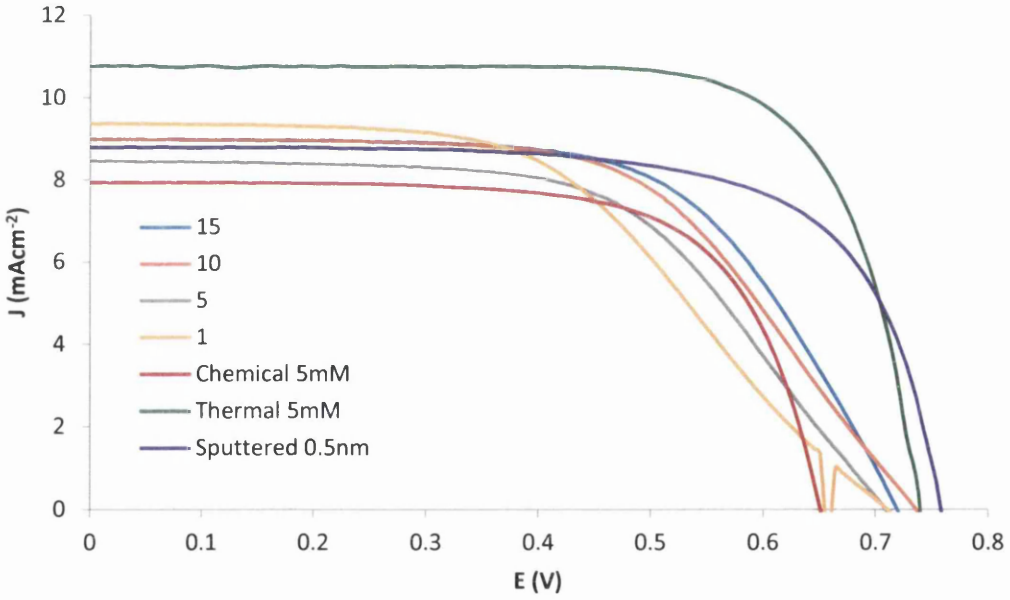

Figure 3.10: J-E curves for -1.8V deposited platinum using best performing DSC devices

Catalyst activity relates to the active area of the catalyst material where reactants can bond to the surface. Smaller particles are known to have a high specific surface area, therefore when comparing the relative sizes of the particles the electrodeposited material is clearly at a disadvantage due to their large size. The previous studies also indicate that the electrodeposited material may not be as catalytically active as the thermally or chemically applied material, though further work will be require to confirm this theory. However, it is

postulated that the nucleation and growth mechanism of electrodeposition does not produces the most viable crystal structure for catalysts, instead forming in the most favourable orientation for growth. Despite this, the surprisingly high DSC results for the cells using electrodeposited counter electrodes seem to suggest that, as least in small lab devices, the catalyst performance does not have as large an impact on device performance as expected.

To further explore this, these cells were also tested in the reverse orientation, where illumination enters through the counter electrode side to mimic the orientation of metal/polymer substrate cells. Here, the presence and absorbance of the platinum layer will have a crucial effect, see Table 3.2.

Table 3.2: Performance of reverse illuminated cells with electrodeposited counter electrodes

Pt Type	ABS	Deposition time (s)	V_{oc} (V)	J_{sc} (mAcm^{-2})	FF (%)	η (%)
ED	**0.1175**	**1**	**0.69(±0.01)**	**6.32(±1.1)**	**53(±0.7)**	**2.3(±0.4)**
ED	0.1397	5	0.70(±0.01)	5.63(±0.3)	61(±0.7)	2.4(±0.1)
ED	**0.1716**	**10**	**0.69(±0.01)**	**5.95(±0.6)**	**59(±5.7)**	**2.4(±0.01)**
ED	0.1722	15	0.71(±0.01)	5.49(±0.3)	62(±4.4)	2.4(±0.3)
Thermal 5mM	**0.1125**	**N/A**	**0.75(±0.001)**	**5.16(±0.09)**	**71(±1.4)**	**2.7(±0.01)**
Chemical 5mM	0.1105	N/A	0.74(±0.004)	5.09(±0.13)	67(±1.4)	2.6(±0.02)
Sputter 0.5nm	**0.1025**	**N/A**	**0.74(±0.003)**	**5.59(±0.54)**	**67(±1.6)**	**2.8(±0.28)**

Immediately visible is an overall reduction of *ca.* 1% efficiency, due to the reduction of the quantity of light reaching the photoelectrode and as a result a lower J_{sc} value from the decrease in excited electrons. The majority of this loss is caused through absorbance by the electrolyte solution, though there will also be an effect from the reflectance and absorbance of the platinum counter electrode. Therefore, when considering Pt application techniques, lower quantity techniques and parameters were sought wherever possible.

Direct deposition, it seems is not the most ideal method for platinisation of DSC counter electrode, as only the short 1s electrodeposition time produces a coating with similar absorbance to the comparison thermal, chemical and sputter platinisation methods. On analysis of the data, there is a slight reduction in J_{sc} as the deposition time increases giving a difference of 0.84mAcm^{-2} between 1s and 15s. This study concluded that the method does not allow for stringent control of the deposition quantity and morphology. The deposits were large, with a low specific surface area expected. As a result, the next technique uses a

modified literature methods from Tsekouras *et al.* to analyse if the nucleation and growth stages of electrodeposition can be further controlled.

3.4 Control of nucleation and growth

Tsekouras *et al.* reported that an initial -0.6V pulse followed by a constant potentiostatic step at -0.4V formed an efficient catalyst for use in DSCs [14]. The stated aim of the pulse was to create nucleation sites on the conductive substrate, and then the potentiostatic hold stage will enable these nucleation points to steadily develop into platinum clusters. It was thought that adapting this method but using shorter hold times could result in a higher specific surface area catalyst, rather than the large scale growth observed previously in purely potentiostatic deposition.

The pulse method is strongly recommended as it allows the replenishment of ions at the substrate surface by the bulk solution [18]. This reduces the concentration gradient that facilitates the unwanted dendritic growth. Removing the current also allows the nucleation of new platinum particles, which should promote the coverage of small, high surface area deposits over larger growth or agglomeration of Pt.

The absorbance of the electrodeposited coating was noticeably higher than the alternatives, leading to the conclusion that ED-Pt layers are thicker and cover more of the FTO/Glass substrate and that control of the -0.4V direct potential hold is critical. This will reduce the overall fraction of light reaching the working electrode under reverse illumination. The absorbance does not increase in a linear fashion with deposition time, as one might expect, see Figure 3.11. There is little overall change in ABS from 1 to 15 seconds, however as the deposition time is increased from 10s, a jump in ABS occurs, which is thought to represent the change from individual growth to amalgamation of clusters, thus increasing the coverage of the FTO/glass.

Now that the variation in platinum quantity was ascertained in comparison to conventional platinisation methods, cyclic voltammetry testing of ED-deposited counter electrodes in a symmetrical sandwich cell configuration was used to compare the catalyst performance or J_{lim} value against the thermal, chemical and sputter platinum catalysts, using the relative absorbance of the catalyst on FTO glass as a comparative aid, Figure 3.12.

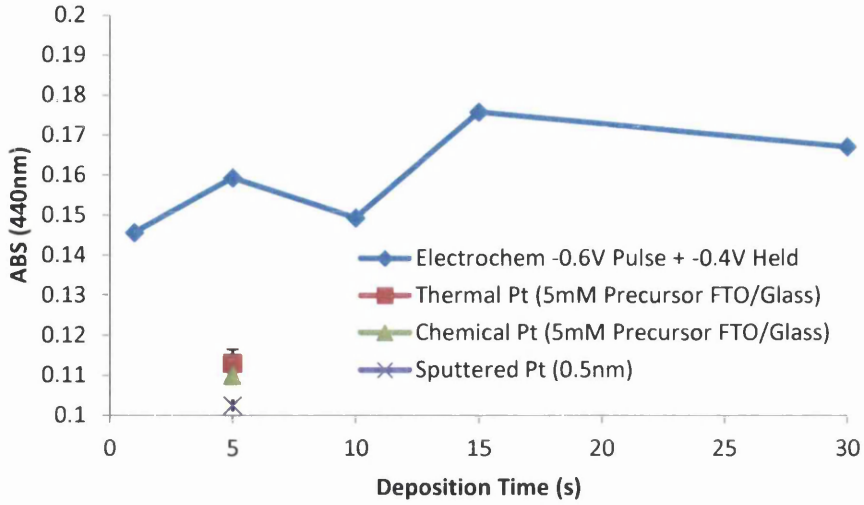

Figure 3.11: Comparison of the absorbance (440nm) of pulse + hold electrodeposited counter electrodes versus commonly used platinised counter electrodes

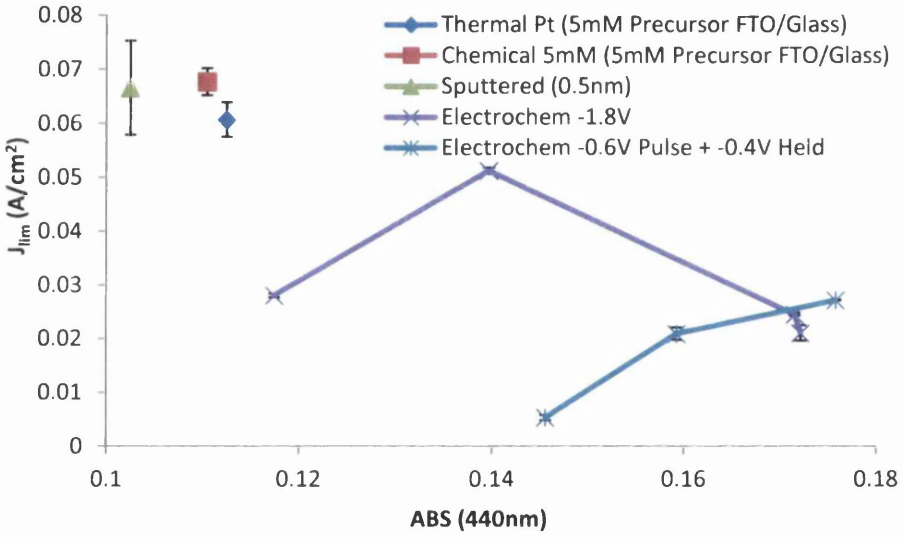

Figure 3.12: Comparison of J_{lim} for pulse + hold and other platinisation methods

Unfortunately, it was demonstrated that the J_{lim} values for electrodeposition using the adapted methods are much lower than for the more common platinisation techniques. However, both techniques produce variable results depending on deposition time. The pulse/potential hold method produces particularly poor results, which is believed to be due to the lower surface area dendritic growth caused by the potential hold stage. This is similarly thought to explain the poor activity of the -1.8V method. As a result of this study, one of our original theories regarding the control of deposition using the rapid depletion of the diffusion layer, will now be abandoned. This method will promote irregular crystal formations and growth and lead to poor control of the deposition and deposit morphology.

This now confirms our need to reduce the deposition time and further control the deposit morphology through solution and electrochemical controls. This will be addressed in the work presented in Chapter 4.

3.5 Conclusions

This initial chapter has adapted several previously reported electro-platinisation methods for DSC counter electrodes to ascertain the effect of decreased deposition times on the resulting counter electrode. This is an important feature when looking to develop a method for large scale fast continuous processing on an industrial roll to roll coating line. The performance of these catalysts is has been extremely variable and poor in comparison to the more commonly used thermal and chemical platinisation. Optimisation will be required in order to produce a viable counter electrode catalyst, when using direct or pulse deposition, due to the large amount of variables in the process.

A conclusion drawn from this data is that electrodeposited platinum requires much more material than the more established techniques due to the growth stage, and that if this can be removed or more thoroughly controlled, then the method could reach comparable performance with the standard platinisation methods. Whether this is due to the crystal structure of the deposit resulting in a lower specific area and specific catalytic activity, or through poor adhesion of the electrochemically produced catalyst to the substrate, is not yet understood. Due to the requirement for more controlled and directed deposition and a reduction in materials usage, the next section covers the development of a replacement process, where a low cost material is used as a template for replacement by platinum. The templating material deposit should be able to be optimised so that the morphology is one that gives the desired performance, in addition to remaining rapid enough for inclusion in a rapid continuous coating process.

As found through this study, the electrodeposition of platinum on FTO-glass substrate is far from simple, giving varying microstructures with poor catalytic activity compared to other low temperature platinisation methods.

Further work recommended is an assessment of the deposition potentials required when using lower deposition concentrations than 5mM. This should allow the development of a lower power and lower material deposition technique to use on FTO/glass, metal substrates and conducting polymers.

3.6 References

[1] D. A. Wragg, "Application and Optimization of the Platinum Catalyst in Dye Sensitised Solar Cells - MRes Thesis," Swansea University, 2010.

[2] X. Fang, T. Ma, G. Guan, M. Akiyama, T. Kida, and E. Abe, "Effect of the thickness of the Pt film coated on a counter electrode on the performance of a dye-sensitized solar cell," *J. Electroanal. Chem.*, vol. 570, no. 2, pp. 257–263, Sep. 2004.

[3] S. Mukherjee, B. Ramalingam, L. Griggs, S. Hamm, G. a Baker, P. Fraundorf, S. Sengupta, and S. Gangopadhyay, "Ultrafine sputter-deposited Pt nanoparticles for triiodide reduction in dye-sensitized solar cells: impact of nanoparticle size, crystallinity and surface coverage on catalytic activity.," *Nanotechnology*, vol. 23, no. 48, p. 485405, Dec. 2012.

[4] C.-P. Cho, H.-Y. Wu, and C.-C. Lin, "Impacts of sputter-deposited platinum thickness on the performance of dye-sensitized solar cells," *Electrochim. Acta*, vol. 107, pp. 488–493, Sep. 2013.

[5] C. Rao and D. Trivedi, "Chemical and electrochemical depositions of platinum group metals and their applications," *Coord. Chem. Rev.*, vol. 249, no. 5–6, pp. 613–631, Mar. 2005.

[6] W. Yao, J. Yang, J. Wang, and Y. Nuli, "Chemical deposition of platinum nanoparticles on iridium oxide for oxygen electrode of unitized regenerative fuel cell," *Electrochem. commun.*, vol. 9, pp. 1029–1034, 2007.

[7] C. C.-M. C.-H. Chen, T.-C. Wei, and S. Cherng, "Electroless deposition of platinum on indium tin oxide glass as the counterelectrode for dye-sensitized solar cells," *Mater. Chem. Phys.*, vol. 55, no. 1, pp. 1687–1695, Jul. 2010.

[8] H. Kim, N. P. Subramanian, and B. N. Popov, "Preparation of PEM fuel cell electrodes using pulse electrodeposition," *J. Power Sources*, vol. 138, no. 1–2, pp. 14–24, Nov. 2004.

[9] S. M. Ayyadurai, Y.-S. Choi, P. Ganesan, S. P. Kumaraguru, and B. N. Popov, "Novel PEMFC Cathodes Prepared by Pulse Deposition," *J. Electrochem. Soc.*, vol. 154, no. 10, p. B1063, 2007.

[10] H. M. Yasin, G. Denuault, and D. Pletcher, "Studies of the electrodeposition of platinum metal from a hexachloroplatinic acid bath," *J. Electroanal. Chem.*, vol. 633, no. 2, pp. 327–332, Aug. 2009.

[11] N. Fu, X. Xiao, X. Zhou, J. Zhang, and Y. Lin, "Electrodeposition of Platinum on Plastic Substrates as Counter Electrodes for Flexible Dye-Sensitized Solar Cells," *J. Phys. Chem. C*, p. 120123074250004, Jan. 2012.

[12] P. Li, J. Wu, J. Lin, M. Huang, Z. Lan, and Q. Li, "Improvement of performance of dye-sensitized solar cells based on electrodeposited-platinum counter electrode," *Electrochim. Acta*, vol. 53, no. 12, pp. 4161–4166, 2008.

[13] A. M. Feltham, M. Spiro, I. Introduction, C. Efficiency, D. S. Pretreatment, A. D. Appearance, B. D. Growth, V. S. Area, A. E. Determination, C. Reproducibility, and R. P. Procedures, "Platinized Platinum Electrodes," vol. 1970, no. 1895, 1970.

[14] G. Tsekouras, A. J. Mozer, and G. G. Wallace, "Enhanced Performance of Dye Sensitized Solar Cells Utilizing Platinum Electrodeposit Counter Electrodes," *J. Electrochem. Soc.*, vol. 155, no. 7, pp. K124 – K128, 2008.

[15] S. Ito, N.-L. C. Ha, G. Rothenberger, P. Liska, P. Comte, S. M. Zakeeruddin, P. Péchy, M. K. Nazeeruddin, and M. Grätzel, "High-efficiency (7.2%) flexible dye-sensitized solar cells with Ti-metal substrate for nanocrystalline-TiO2 photoanode.," *Chem. Commun. (Camb).*, no. 38, pp. 4004–6, Oct. 2006.

[16] S. Kim, Y. Nah, Y. Noh, J. Jo, and D. Kim, "Electrodeposited Pt for cost-efficient and flexible dye-sensitized solar cells," *Electrochim. Acta*, vol. 51, no. 18, pp. 3814–3819, May 2006.

[17] M. Fayette, Y. Liu, D. Bertrand, J. Nutariya, N. Vasiljevic, and N. Dimitrov, "From Au to Pt via surface limited redox replacement of Pb UPD in one-cell configuration.," *Langmuir*, vol. 27, no. 9, pp. 5650–8, May 2011.

[18] S. Kim, Y. Nah, Y. Noh, J. Jo, and D. Kim, "Electrodeposited Pt for cost-efficient and flexible dye-sensitized solar cells," *Electrochim. Acta*, vol. 51, pp. 3814–3819, 2006.

4 *Controlled electrodeposition - Use of templating deposits to control the size and shape of a platinum deposit*

4.1 Introduction

Chapter 3 demonstrated that the electrodeposition of Pt on to FTO-glass is not straightforward. Direct deposition was seen to lead to uncontrolled growth of the platinum material, producing a catalyst with lower specific activity for triiodide reduction than the alternative thermal and chemically produced catalysts, evidenced through the comparison of limiting current for the counter electrodes and the EIS comparison of DSC devices. In addition, the assessment of lower potential deposition and an attempt at nucleation control also resulted in low performing, high materials usage Pt catalyst. Therefore it was considered that the direct deposition of Pt was not the most viable method.

This chapter involves the novel production of platinum nanostructures *via* galvanic replacement of an electrodeposited Pb template through low power electrodeposition onto FTO-glass. The template material is thought to be able to aid in the control of deposit formation and morphology to a larger extent than direct deposition of Pt from solution. The redox replacement method was adapted from a previous study on *surface layer* redox replacement (SLRR) by Fayette *et al.* Their study focused on the deposition of Pt on Au through the replacement of underpotentially deposited Pb template material [1]. Fayette *et al.* in turn built on the work of Brankovic *et al.* on the replacement of a Cu monolayer on a simple Au(111) substrate [2].

For the work presented in this chapter, an FTO glass substrate, rather than the Au(111) used in the original study, is utilised as the deposition substrate. The aim was to optimise the deposition parameters and deposit morphology to produce a viable triiodide reduction catalyst suitable for dye sensitised solar cell devices (DSCs). The use of a single solution bath containing both Pb^{2+} and Pt^{2+} ions in a supported aqueous solution was adapted from the literature to ensure that there would be no multi stage or lengthy processing steps to scale up to pilot production [1], [3]. This will aid in reducing line length, line complexity and the number of stages in the DSC fabrication process.

The authors are aware of the toxic nature of the Pb sacrificial metal, however in the developmental stages it has been chosen to provide further understanding of the process as it is applied to FTO-glass. From this it is hoped that other metals will eventually replace Pb to give a low cost, non-toxic templating material.

4.2 Experimental

A one pot deposition electrolyte solution was adapted from the SLRR deposition study performed by Fayette *et al.* [1], and is described in detail in Chapter 2.2. Briefly, the electrolyte contains 0.1M $NaClO_4$ (>98%, ACS Reagent, Sigma-Aldrich), 1mM $Pb(ClO_4)_2.3H_2O$ (98%, ACS Reagent, Sigma-Aldrich), 0.5mM $K_2[PtCl_4]$ (99.9%, Aldrich) and 10mM $HClO_4$ (70%, Analytical reagent grade, Fisher Scientific), these were combined in distilled water. The solution was purged with N_2 for 2 hours before the commencement of any experimental activity.

Cyclic voltammetry (CV) measurements were performed in solution using FTO/glass working electrodes, to ascertain the correct parameters for the deposition. Several samples were then produced using the deposition process described in Chapter 2.2: A 1s cathodic pulse at either -0.75V or -0.5V to deposit Pb, followed by a potential and time controlled OCP stage where Pb is replaced by Pt. To fully characterise the deposits, working electrodes of $1cm^2$ FTO glass were produced and then characterised using SEM and XPS, as described in detail in Chapter 2.7 and 2.8. UV-Vis analysis was not utilised in this study due to the possibility of lead deposits causing errors in the reading. To assess the catalyst in an operational environment, DSC counter electrodes were produced using this deposition method. Full DSC devices were constructed according to the procedure described in Chapter 2.3 and were then tested under standard testing conditions (STC), using a AAA-class solar simulator, as per the method reported in Chapter 2.5.

4.3 Initial Pb/Pt deposition solution characterisation

Since the electrochemical characteristics of FTO-glass differ from the Au(111) surfaces used by the reference studies, CV analysis was run to determine the deposition potential for Pb (E_1) and an appropriate cut off potential for the open circuit potential redox replacement stage (OCP). The scans were run in both the absence and presence of Pt^{2+} ions to ensure that the correct potentials were chosen with respect to both Pb and Pt, and to assess the electrochemical behaviour of Pb^{2+} and Pt^{2+} ions in solution.

The deposition was experimentally observed to occur from -0.6V, shown on the scan profile in Figure 4.1. In this solution the reaction exhibits reversibility, as evidenced by a large peak at -0.4V on the anodic sweep, illustrating the stripping of Pb from the FTO surface back into solution. At potentials positive of -0.3V no reaction was seen to occur, indicating that holding the potential at $\geq$0.3V will inhibit any deposition activity on the FTO-glass electrode.

The CV profile also demonstrates the consistent behaviour of the Pb^{2+} solution (without Pt present) over multiple scans, as the majority of the deposited material is stripped back into the solution on the anodic sweep. There is a slight increase in the deposition and stripping peaks with each cycle, which is believed to be due to changes in the ion concentration adjacent to the working electrode over time. The ability to strip Pb allows the removal of any excess material after the deposition. This is a great benefit as Pb has the potential to act as a poison for the catalyst, as has been seen in automotive catalytic converters [4]. This will occur through the bonding of Pb with the iodide species in the electrolyte, or through migration to the TiO_2 surface where it will form recombination centres. Its removal will conserve the templating material in solution and benefit both cell performance and process efficiency. Previous literature has noted that the replacement reaction between Pb and Pt is an irreversible process [2], supporting the suggestion of stripping as a method of removing unwanted sacrificial metal from the substrate surface.

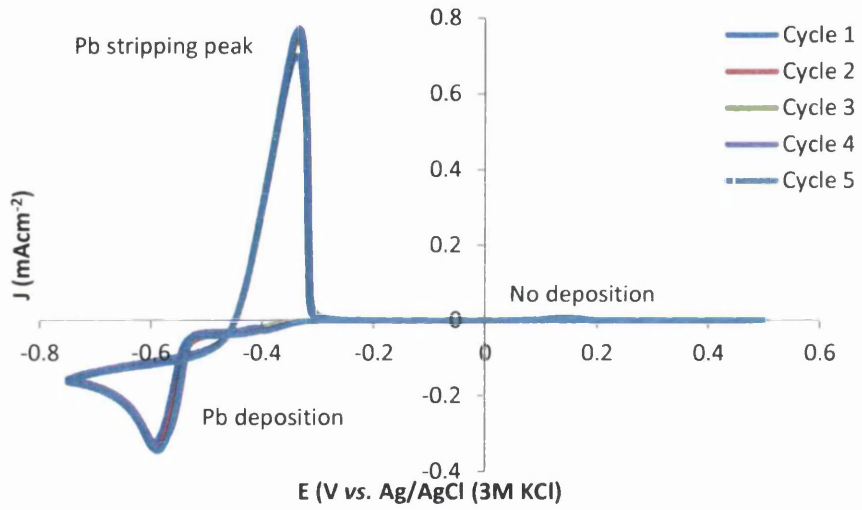

Figure 4.1: Cyclic Voltammetry Scan of FTO-Glass electrode in a supported Pb^{2+} solution (Pt mesh counter electrode, Ag/AgCl reference, Scan rate: 25mV/s)

On the introduction of Pt^{2+} ions into the deposition solution the CV profile changes are immediately visible through the absence of a stripping peak at -0.4V and the deposition peak at *ca.* -0.6V shifting to -0.5V after the initial scan, see Figure 4.2. The peak shift is believed to be due to the presence of Pt ions in solution. They may also auto catalyse the deposition of materials, as the presence of a catalyst material will reduce the activation energy for deposition reactions. The gap in readings at -0.4V is a the result of reading lag in the Ivium software, the feature itself "II" describes the first deposition peak for Pb^{2+} ions and it is also thought to cause minor Pt deposition due to the relatively large potential, as

confirmed by the work done in Chapter 3. Pt can deposit from solution at -0.4V. The second peak, labelled "III" also represents Pb^{2+} or Pt^{2+} reduction to lead [Pb(0)] or platinum [Pt(0)] metal. The potential continues to increase with the commencement of another peak, labelled "IV", from -0.75V, indicating the occurrence of hydrogen evolution rather than adsorption due to the presence of a current flow. Due to the visible presence of hydrogen and the commonly known ability of platinum to catalyse the reduction of hydrogen from solution, it was postulated that a small quantity of Pt, as well as Pb, co-deposited onto the FTO while the cathodic scan was in progress. Furthermore, a positive peak is visible at 0V, labelled "V", indicative of the re-absorption of hydrogen into the deposition solution thus further supporting this theory. This peak potentially represents a small amount of Pb stripping from the electrode surface, though in this scan it is thought to be mostly masked or out competed by hydrogen evolution from solution. Point "I" represents the start and finish of the CV scan at an anodic potential large enough to prohibit any deposition or other reaction occurring when not required, thus giving more control over the deposition mechanism.

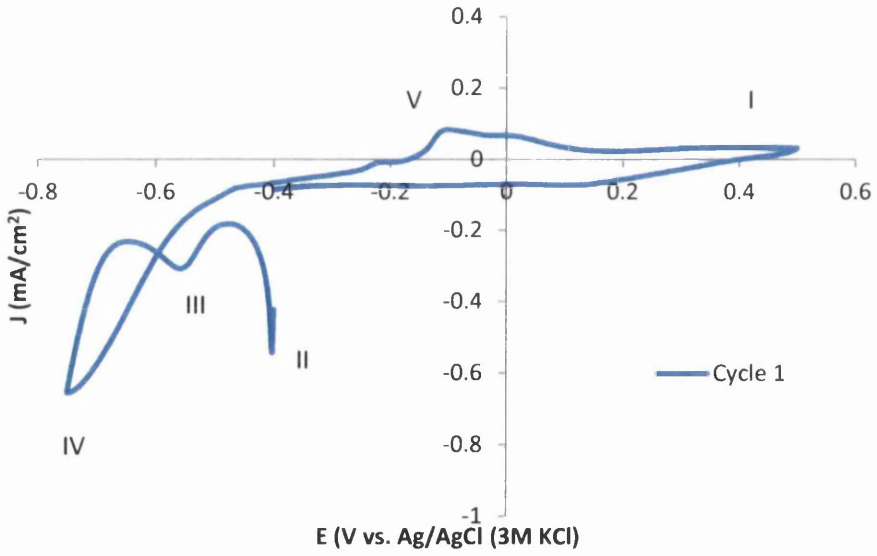

Figure 4.2: CV scan for deposition on FTO-glass - 1st cycle

The lack of a large Pb stripping peak, visible in both the 1st scan and all subsequent scans, Figure 4.3, when the solution contains Pt^{2+} ions is suggested to be due to the presence of the hydrogen reduction peak, which will grow as the quantity of catalytic Pt increases, this increases the competition between hydrogen reduction and the stripping of Pb. Further to this, the previously deposited platinum particles will act as low energy deposition sites and catalyse the deposition of further platinum metal, increasing the quantity deposited each

cycle more than the amount originally thought. On comparison of scans in the presence and absence of Pt ions, Figure 4.1 and Figure 4.2, a visible increase in cathodic current was seen at the start of the scan when Pt^{2+} ions are added. This combined with the known fact that hydrogen adsorption and evolution preferentially takes place on Pt, supports the theory for the co-deposition of Pb and a small amount of Pt.

There are other electrochemical factors involved in the activity seen in these scans. Several studies report Pb underpotential deposition (UPD) occurring on already deposited Pt, thus providing more Pb template material than controlled by the applied potential [1]. These CV scans, Figure 4.3, form the basis of the study of templated electrodeposition onto FTO-glass and provide comparison data for other electrodeposition studies encountered. Appropriate values for the deposition and redox replacement were chosen, where "E_1" represents the deposition potential and "E_2", the redox replacement or OCP cut-off potential. The two E_1 values represent the two maximum cathodic potentials used in this study. In addition, two cut off anodic potentials "E_2" were also studied.

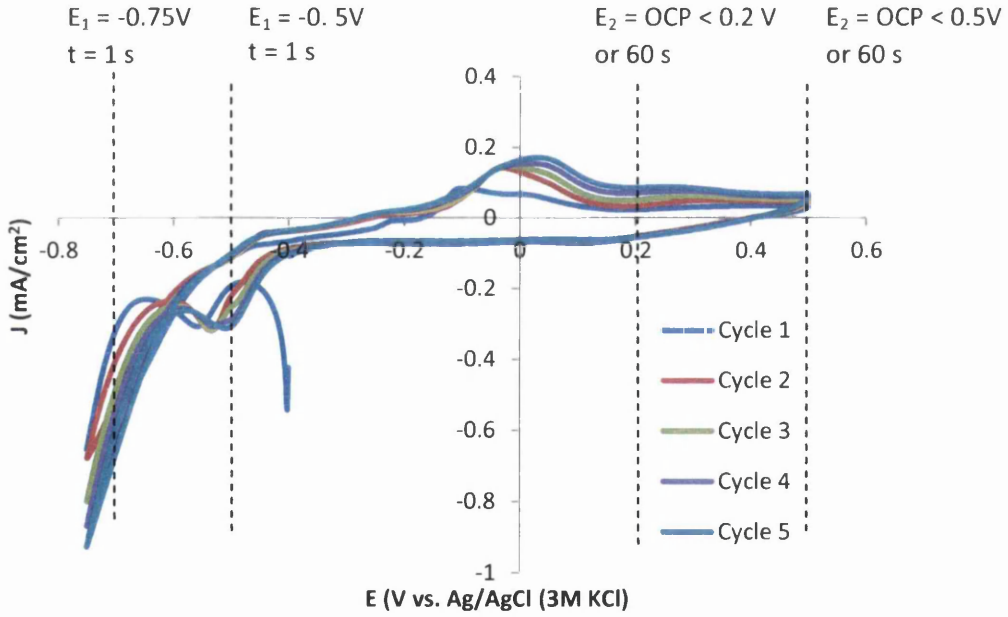

Figure 4.3: CV scan for FTO-glass in a supported Pb^{2+}/Pt^{2+} solution

Each different potential will return different deposition behaviour and allow for in-depth characterisation. A cut off time of 60s was programmed into the OCP stage of the deposition to ensure all sample were relatable through controlling the replacement stage, despite the varying parameters investigated through this study.

The high deposition overpotential (E_1) was set at -0.75V which was chosen as it sits outside the initial deposition peak – thus indicating that there is enough applied energy to activate the majority of active sites on the FTO [5]. Care was taken when choosing and applying this potential, as its large cathodic nature may cause hydrogen adsorption at already deposited Pt and thus competing with further deposition on the working electrode surface. The low deposition overpotential (E_1) chosen was -0.5V, which sits directly on the deposition peak shown in Figure 4.3. The cut off potentials, E_2, were chosen as either 0.2V or 0.5V. Where E_2 = 0.2V, this is positioned immediately after the exhibition of oxidation and stripping behaviour on the CV scan, which should give a shorter replacement step. The E_2 = 0.5V was chosen to study the effect of a longer replacement step on the final deposit morphology.

Now that the solution was fully characterised and the deposition parameters E_1 and E_2 were chosen, the next stage was to perform several deposition events on FTO-glass samples of 1cm^2 and examine the resulting deposits through Scanning Electron Microscopy (SEM) to ascertain the deposit morphology and the deposit constituents through X-Ray Photoelectron Spectroscopy (XPS). The aim was to establish how the final deposit makeup is influenced through deposition potential parameters.

4.4 Deposition of Pb/Pt

Deposition profiles were obtained from the potential *vs.* time data, which is presented in Figure 4.4 (a-d). These show visually the experimental behaviour and show how closely the reality matches the desired experimental outcome.

Figure 4.4a shows the outcome of utilising a high Pb deposition potential (E_1=-0.75V) that is then followed by a low replacement potential cut off stage (0.2V), or the 60s cut-off time. Figure 4.4b differs, showing a high replacement potential cut off (E_2=0.5V), or the 60s cut-off time. Figure 4.4c and Figure 4.4d indicate the result of using a low deposition voltage (E_1=-0.5V). However, a short replacement potential (E_2=0.2V) is used in Figure 4.4c and a long replacement potential cut-off (E_2=0.5V) is used in Figure 4.4d. For all experiments, the potential cut off may not be reached on all cycles, due to the slow increase in as OCP is held - hence the 60s imposed cut off for all samples.

A key point to note on Figure 4.4 a & c is that the time taken to complete each OCP replacement stage becomes longer with each competed deposition cycle, an unfortunate factor that could make rapid deposition on an in-line process problematic on a larger scale. This varying replacement stage length is suggested to be due to diffusion limitations in solution, caused by the increase of Pb on the surface of the FTO. The large scale

replacement of Pb by the Pt will create areas of low ion concentration adjacent to the working electrode surface as the Pt ions are depleted. Therefore, the deposition time will increase due to slow diffusion of ions from the bulk solution. In comparison, the OCP step where a long potential OCP cut-off of 0.5V is used appears regular, Figure 4.4b & d. This is suggested to be due the increase in time for Pt ions to diffuse into and replenish the double layer adjacent to the working electrode.

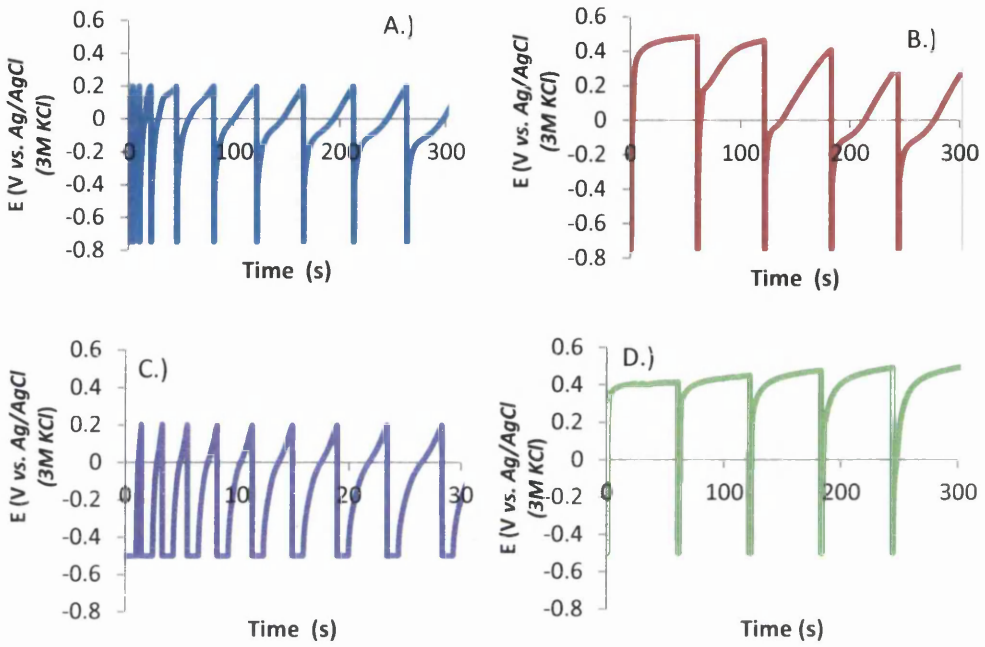

Figure 4.4: Deposition profiles on FTO-glass in a 3 electrode cell consisting of a Pt mesh counter electrode, Ag/AgCl reference; (a) E_1=-0.75V, E_2=0.2V; (b) E_1=-0.75V, E_2=0.5V; (c) E_1=-0.5V, E_2=0.2V; (d)E_1=-0.5V, E_2=0.5V, for all cells there is a 60s cut off for the E_2 stage, to keep samples relatable

This initial work has shown that Pb/Pt deposition and replacement is electrochemically feasible on FTO glass substrates. It had also indicated that a high degree of control must be exerted over the process to obtain the desired deposition and replacement events. This is not just controlled through the choice of potentials, but also in cycle time and through choosing conditions that stop electrochemical activity occurring when not needed and changing the deposit growth behaviour and final morphology.

After the successful production of electrodeposited Pt samples, these were further characterised in order to discover the material coverage and the effect on composition and morphology of differing the deposition potentials and cycles.

4.5 Effect of deposition profile on deposit morphology

The Pt/Pb coated FTO glass were further characterised through SEM imaging to determine the effect of changing the E_1 and E_2 parameters on the surface coverage and deposit morphology. The SEM images in Figure 4.5 (a-h) show the results of different deposition schemes on FTO-glass substrate. The left hand images are low magnification, and the right hand are high magnification images of the corresponding sample. A & B refer to Sample 1; C & D refer to Sample 2; E & F refer to Sample 3; and G & H refer to Sample 4. As a general description, the deposit was seen to consist of a varied distribution of both large and small diameter nanoparticles and clusters on the FTO surface. The FTO is visible as the large, *ca.* 100+ nm scale like formations in the background of the image.

The images show that the Pb deposition potential "E_1" and the OCP cut off time "E_2" have a large effect on the deposit morphology and coverage. A combination of a low deposition potential (E_1 = -0.5V) and a low cut off potential (E_2 = 0.2V) for Sample 3, gave the lowest coverage, shown in Figure 4.5e&f. The employment of a low potential causes a reduction in the amount of Pb deposition occurring during the application of E_1. This was theorised to be due to the reduction in activated nucleation sites on the FTO surface. Therefore, as less Pb is deposited, the Pt quantity will reduce in parallel to the replacement events. A low cut off voltage for the OCP replacement stage (E_2=0.2V) means that the growth of nanoparticles will also be limited. When the cut off potential "E_2" is increased, *a la* Sample 4, the coverage was seen to improve, confirming the influence of the growth stage of electrodeposition for improving the Pt layer.

Samples 1 and 2 use a larger E_1 potential of -0.75V, which results in excellent coverage of the FTO-glass, despite different E_2 cut offs of -0.2V and -0.5V respectively in Figure 4.5a&c. After comparison of the potential *vs.* time plots in Figure 4.4, it was initially thought that the higher E_1 value is able to activate more of the nucleation sites on the FTO surface [6], thus resulting in the increased coverage of small particles visible in Figure 4.5a&c, irrespective of cut off potential. Sample 4 also shows a large coverage of small particles, similar to the distribution of sample 1, but using a lower initial potential of -0.5V. It is possible that -0.5V is enough potential to activate the majority of nucleation points on the FTO surface, and the difference between particles on sample 3 and 4 is due to varying particle growth from the 0.2V cut off and the 0.5V cut off potentials.

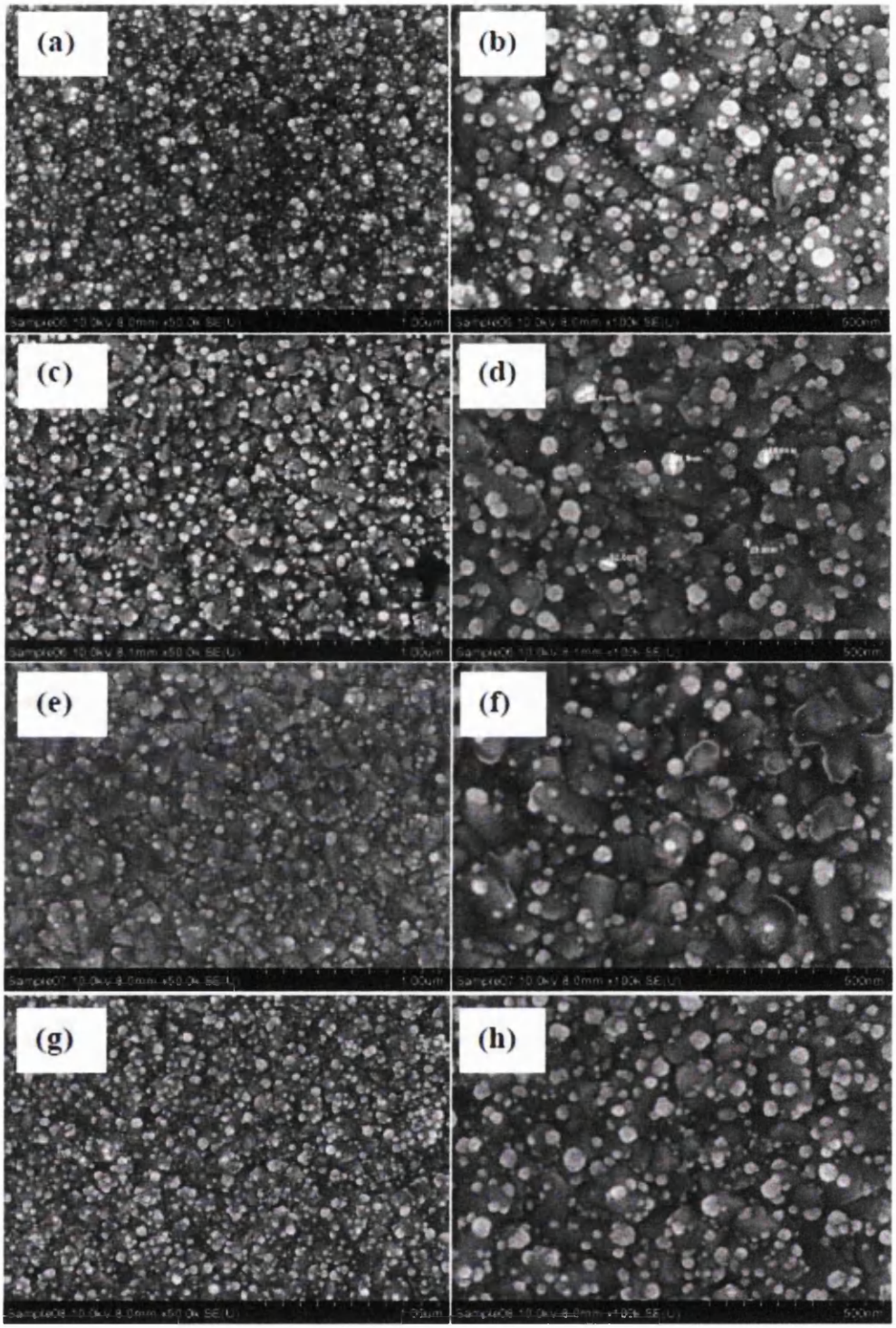

Figure 4.5: SEM images showing Pb/Pt nanoparticle deposit coverage and morphology on FTO-glass: (a) & (b) Sample 1: E_1=-0.75V, E_2=0.2V; (c) & (d) Sample 2 E_1=-0.75V, E_2=0.5V; (e) & (f) Sample 3 E_1=-0.5V, E_2=0.2V; (g) & (h) Sample 4 E_1=-0.5V, E_2=0.5V, for all cells there is a 60s cut off for the E_2 stage, to keep samples relatable

This conclusion was reached as the OCP replacement time or E_2 stage is approximately identical in size from the 4th cycle onwards due to the set cut off time of 60s set for all

cycles. The basic study of catalysis undertaken in Chapters 1.1.5 and Chapter 3 indicated that the most ideal structure for a highly efficient catalyst is small particles in great numbers. From the SEM images, it can be seen that the parameters of Sample 1, 2 and 4 produce large quantities of 20-50nm particles, which are believed to be good for use as a reduction catalyst in DSC devices.

4.6 XPS analysis of Pt/Pb nanoparticles deposit on FTO glass surface

Once the SEM imagery indicated the presence of nanoparticle and -cluster formations on the FTO-glass substrate, it was then necessary to discover what elements were present in order to determine the efficiency of this deposition method for the production of a Pt catalyst. Unfortunately, energy dispersive spectroscopy (EDS) analysis using a SEM-EDS detector proved not to have the sensitivity required in order to fully determine the elements present in the surface structures, therefore an alternative method was sought. X-Ray photoelectron spectroscopy (XPS), described in Chapter 2.8 was used to determine the exact nature of the surface and to further determine the effect of E_1 and E_2 on the structure of the deposit. FTO-glass samples of $1cm^2$ were assessed in layers from the top down, using an electron beam to etch away each layer down to the base FTO-glass conducting substrate. Thus, four samples were chosen for study using the potentials for E_1 and E_2 listed below, using 10 deposition cycles for each potential set as it was felt this deposited a viable amount of material for analysis:

S1: $E_1 = -0.75V$; $E_2 = 0.20V$

S2: $E_1 = -0.75V$; $E_2 = 0.50V$

S3: $E_1 = -0.50V$; $E_2 = 0.20V$

S4: $E_1 = -0.50V$; $E_2 = 0.50V$

A full XPS spectrum, while useful, does not lend itself to interpretation without further analysis, as Figure 4.6 demonstrates quite handily. Thus a table of known atomic binding energies was used to split the XPS data into peaks representing individual elemental spectra [7], this was further matched against the results obtained in past studies to verify their accuracy. The full spectrum indicates the presence of the element: Pt, Pb, Sn, O and C on the substrate surface.

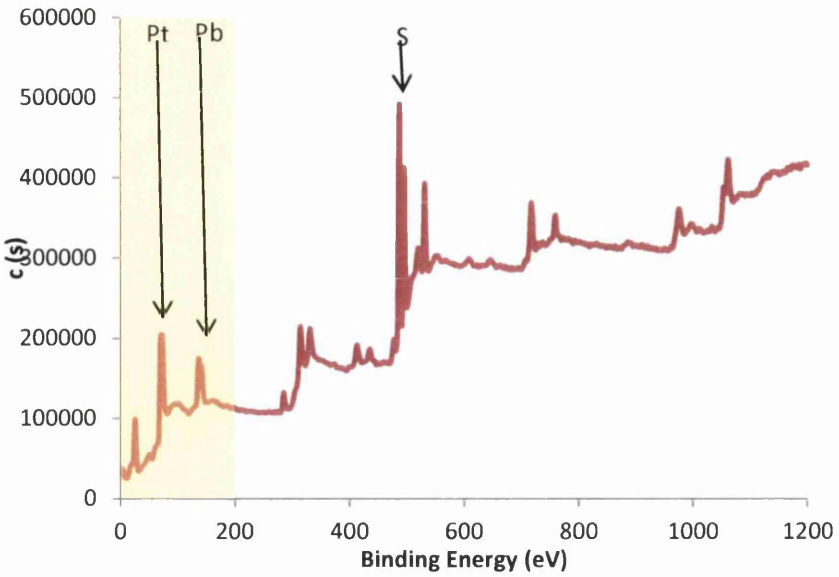

Figure 4.6: Example full XPS spectra of Sample 1 (S1) highlight represents the region of interest for Pt and Pb detection

The Sn peaks, Figure 4.7, were confirmed through literature to represent the FTO-glass electrode, the peaks 487.13 ±0.24eV corresponding to the $Sn3d_{5/2}$ peak; and 495.55 ±0.23eV for the Sn $3d_{3/2}$ peaks depending on the sample analysed [8][9].

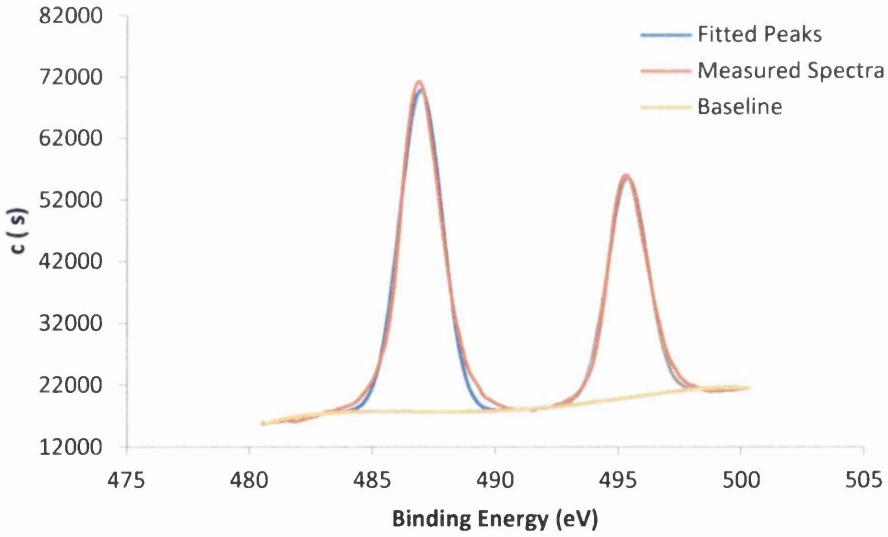

Figure 4.7: Example XPS spectra for Sn, using the Sn3d energy level. (Sample 1)

Figure 4.8 focuses on the spectral response of the platinum particles, using the Pt4f energy level, where images (a)-(d) refer to Samples 1-4 respectively. The presence of these spectra in all samples is both expected and reassuring, as is the consistency of the spectral response across all samples. The doublet peaks at *ca.* 71eV and 74eV represent $Pt4f_{7/2}$, indicating the presence of metallic platinum particles, denoted as Pt(0). The other smaller doublet peaks

at 72eV and 75eV represent other oxidation states of Pt, such as Pt(II) or Pt(IV) that indicate other platinum compounds such as PtO_2.

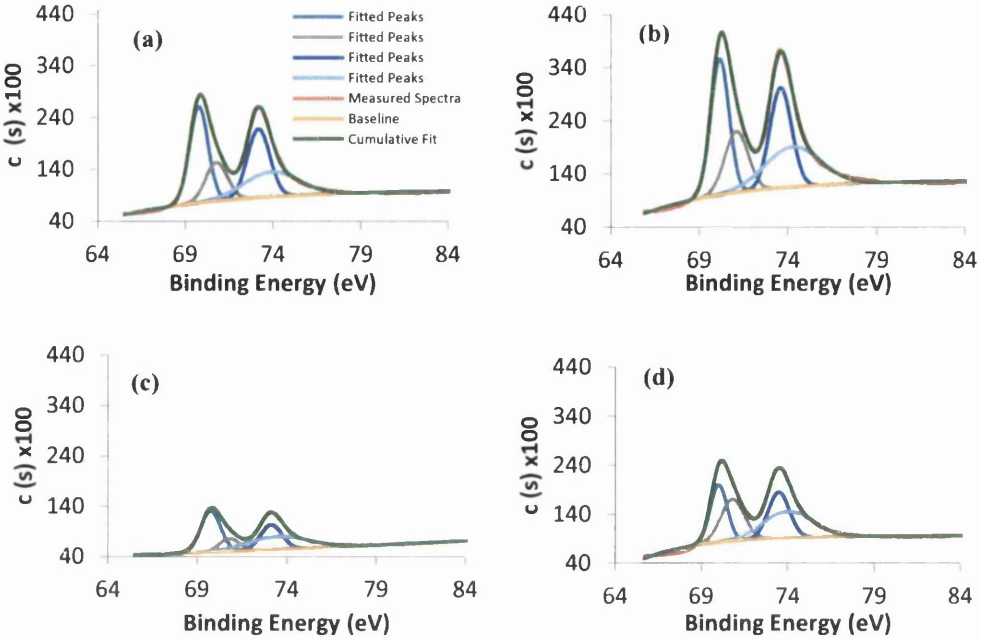

Figure 4.8: Comparison XPS Pt4f spectra (a) Sample 1, (b) Sample 2, (c) Sample 3, (d) Sample 4

Figure 4.9 shows XPS spectral comparison of Sample 1-4 in image (a)-(d) respectively. This set of data is interesting as it indicates that there is still Pb present on the surface of the prepared electrode, despite already being exposed to several replacement cycles during deposition. In these spectra, metallic Pb, Pb(0), is indicated by doublet peaks at 136.5 and 141eV respectively. Peaks at 138.9eV indicate Pb^{2+} oxidation states, whereas Pb^{4+} is represented at 137.7eV [10][11]. The presence of remaining Pb will present an issue in full DSC devices, as Pb can potentially act as a poison or facilitate unwanted processes that degrade cell performance. In addition, their presence increases the size of the catalytic particles and clusters on the substrate surface, reducing the specific surface area. The Pb also takes up surface sites that could potentially hold catalytic Pt. Further work suggested here is to further adjust the electrodeposition parameters and use XPS to ascertain those where the minimum Pb remains.

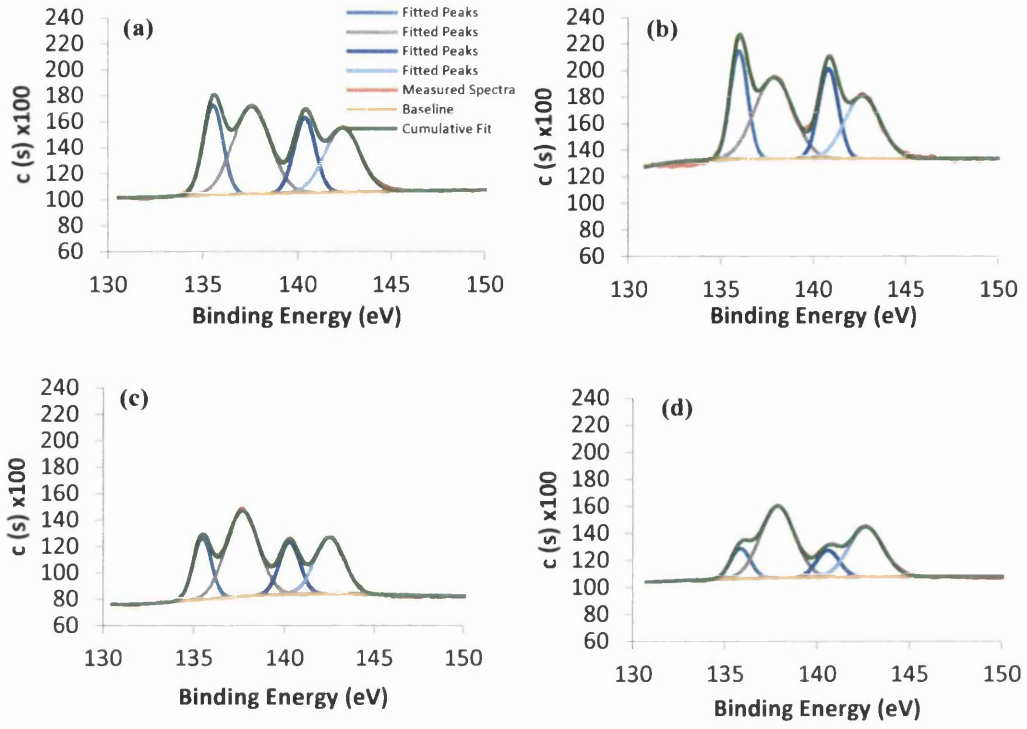

Figure 4.9: Comparison of XPS spectra for Pb4f, (a) Sample 1, (b) Sample 2, (c) Sample 3, (d) Sample 4

Figure 4.10 and Figure 4.11 show the presence of Pt and Pb using the 4f energy level peaks for Sample 1 (S1). These spectra indicate the presence of both the Pb template and the Pt replacement element after 10 cycles of deposition and replacement, when the high Pb deposition potential of -0.75V is coupled with a short cut off potential (E_2 = 0.2V). The larger deposition potential is known from literature to activate more nucleation sites on the FTO surface [12], as evidenced by the particle density seen in Figure 4.5a, initially resulting in a high quantity of Pb on the surface. When this is combined with the low E_2 replacement potential of -0.2V it is suggested to account for the presence of remaining Pb on the surface.

The presence of Pb was detected using the Pb4f energy, which shows up as visible peaks given at 135.73±0.28, 137.76±0.18, 140.53±0.32 and 142.56±0.17eV corresponding to samples 1-4 respectively. Each peak can be further matched to different oxidation states of Pb present at that point in the deposit. The peaks at 135.73±0.28eV and 140.53±0.32eV correspond to the $4f_{7/2}$ and $4f_{5/2}$ regions representing Pb^0 or non-oxidised Pb atoms. The peaks at 137.76±0.18eV and 142.56±0.17eV refer to high oxidation states of Pb, such as Pb^{2+} which is expected to be present from the $Pb(ClO_4)_2$ component of the deposition solution.

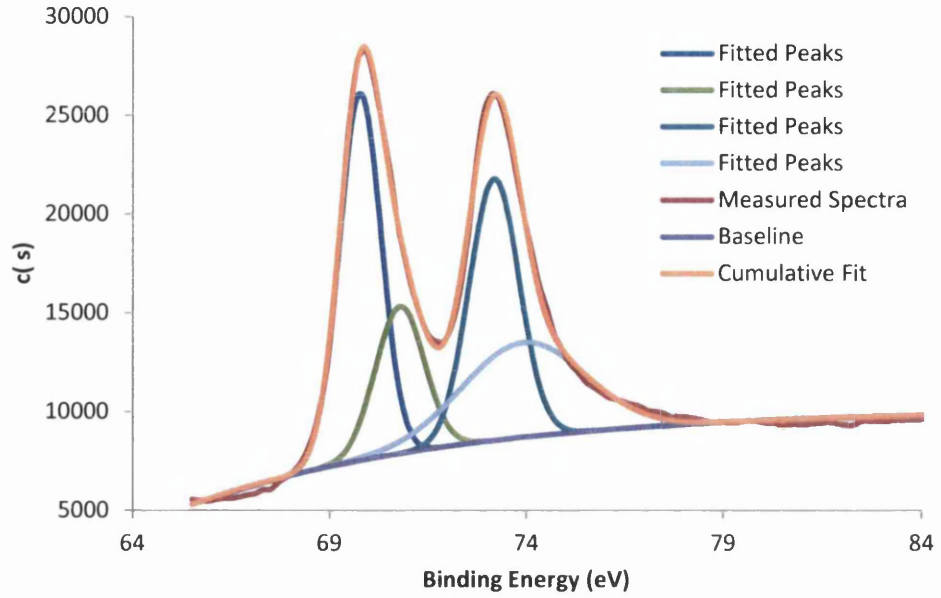

Figure 4.10: Pt spectra using the Pt4f peaks for Sample 1 (S1)

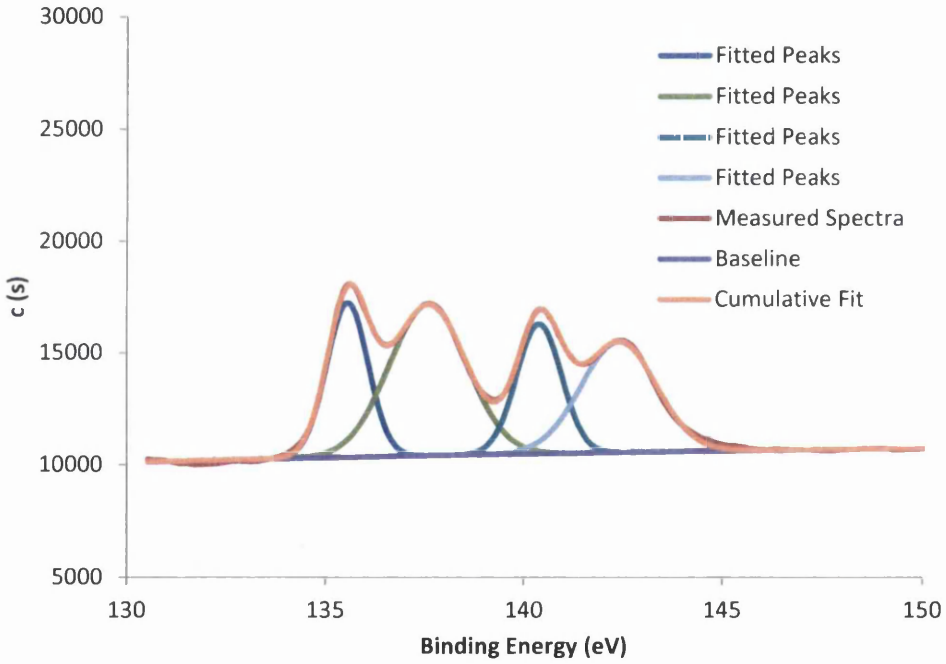

Figure 4.11: Pb spectra using the Pb4f peaks for Sample 1 (S1)

In order to find platinum, a 2nd derivative method was used which can find partially or fully hidden peaks. A partially hidden set of Pt^0 peaks, denoting free or non-combined Pt, was discovered at a value of 69.93±0.24eV and 73.36±0.25eV, this peak formation is also known as a doublet peak. The characteristic pattern is caused by a condition known as spin-orbit splitting in the Pt "*f*" shell. This is caused by the effective unbalancing of an *f* shell orbital due to the ionisation of an electron by the applied X-ray energy [13]. Further evidence of Pt at different oxidation states was seen through the respective peaks 70.88±0.22eV and

73.96±0.34eV, which could also be an indication of remaining $K_2[PtCl_4]$ from the deposition solution.

If local maxima are used to find and characterise XPS peaks, the centre of the two peaks in the Pt doublet are at 70.16±0.24eV and 73.45±0.25eV relating to $Pt4f_{7/2}$ and $Pt4f_{5/2}$. Using the NIST database for referencing the elemental binding energies, this states that peak values of 72.90 and 74.20eV relate to $K_2[PtCl_6]$ and values from 70.83-71.30eV can be seen as metallic platinum, or Pt_0 [7]. Thus using these values, the presence of Pt can be confirmed without the use of the 2nd derivative method or local maxima used here. The Pt4f spectra also gives a firm confirmation to the presence of Pt_0 and further higher oxidation states of Pt, here suggested to be Pt^{2+} from any $K_2[PtCl_6]$ deposition solution remaining on the surface of the sample.

Once the presence of Pt was confirmed on the FTO surface, it was necessary to examine the surface coverage of Pt and discover the ratio of Pt to remaining Pb. The ratio of Pt to Pb considers all forms of the element detected, at any oxidation state. The variation in the atomic percentage of tin (Sn) can be used as an indicator of Pt/Pb coverage, since higher Pt/Pb coverage will leave less Sn exposed. Table 4.1 summarises the previously described peak values for Pb and Pt and furthermore lists the ratio of Pt:Pb found on the surface of each sample in addition to the percentage of detectable Sn.

Table 4.1: Summary of Sn3d, Pb4f and Pt4f peak positions; Pt:Pb atomic ratio and Sn percentage on the sample surface

Sample	Sn 3d (eV)	Pb 4f (eV)	Pt 4f (eV)	Pt:Pb	Sn%
Sample 1	486.97	135.55; 140.38 (Pb^0)	69.77; 73.18 (Pt^0)	2.74:1	25.49
	495.39	137.58; 142.39 (Pb^{2+})	70.79; 73.93 (Pt^{2+})		
Sample 2	487.37	136.01; 140.85 (Pb^0)	70.18; 73.61 (Pt^0)	3.72:1	23.85
	495.79	137.90; 142.69 (Pb^{2+})	71.11; 74.30 (Pt^{2+})		
Sample 3	486.97	135.49; 140.30 (Pb^0)	69.777; 73.18 (Pt^0)	1.31:1	34.20
	495.39	137.70; 142.52 (Pb^{2+})	70.79; 73.93 (Pt^{2+})		
Sample 4	487.21	135.86; 140.60 (Pb^0)	70.02; 73.50 (Pt^0)	3.97:1	20.54
	495.65	137.87; 142.65 (Pb^{2+})	70.82; 74.04 (Pt^{2+})		

Samples 2 and 4 give the highest ratio of Pt:Pb with 3.72:1 and 3.97:1 respectively, showing that the E_2 value has a large impact on the final composition of the deposit and surface coverage. The lowest ratio is given by Samples 1 and 3 with 2.74:1 and 1.31:1 respectively.

If this is compared with the Sn% on the surface layer it gives the highest to lowest surface coverage as: Sample4 (Sn20%) > Sample 2 (Sn23%) > Sample 1 (Sn25%) > Sample 3 (34%).

The difference in the Pt:Pb ratio and the surface coverage indicated by the change in detectable Sn on the surface is due to the relationship between the E_1 and E_2 values used to control the deposition. The different E_1 values activate different numbers of nucleation sites and further control the size of these sites in the initial 1s deposition. The E_2 value, both the pre-programmed and one controlled through the cut off time of 60s will result in different levels of platinisation, which will vary for each sample and cycle. In addition, as platinum is deposited on the FTO surface it will affect the deposition conditions of the cell. At the larger potential of -0.75V, there is potential for hydrogen evolution on the deposited Pt to compete with the next cycle of Pb deposition.

Despite the observed variations, the Pt:Pb ratios remain comparable, believed to be due to the enforcement of the 60s cut-off time, which ensured that most deposition steps were as similar as possible. The higher ratios exhibited by Samples 2 & 4 have different E_1 values of -0.75V and -0.5V respectively. The higher ratio of Sample 4 was suggested to be due to the E_1 potential lying in the supposed UPD region of the deposited Pt surface layer and causing UPD deposition to occur. Thus this will give steady, regular deposition and replacement activity. The E_1 value of Sample 2 however is -0.75V which is a cathodic enough potential to allow hydrogen adsorption or reduction to occur on the surface of any deposited Pt. This will compete with Pb deposition and thus result in a smaller Pt:Pb ratio.

Another critical factor is the length of the deposition cycles. This is dictated by E_2 the OCP cut off potential, or the imposed 60s time limit on this stage. However, the potential is not always that as was dictated by the program. Sample 2 was seen to reach an OCP value of 0.4V at the start of the deposition, which gradually reduced to 0.25V after the 4^{th} cycle of deposition. Sample 4 however reaches the desired values, at 0.47-0.5V throughout the deposition event. The difference was thought to be due to the high E_1 potential depleting the ions closest to the electrode. As a result it will take time to replace these from the bulk, and since E_1 is repeated the depletion effect is cumulative, resulting in the cut off potential not being reached within the allotted 60s time limit. The lower potential used for Sample 4 would cause less depletion and as a result, solution can recover faster, resulting in a more rapid rise in recorded potential as OCP is held.

Samples 1&2 with the same E_1 value have a comparable deposition cycle profile after the 4^{th} cycle, as previously mentioned, which provide an explanation for the similar surface

coverage seen in the SEM imagery and in the XPS values discussed in this section. However, due to the different pre-set E_2 values between Sample 1&2 of 0.2V and 0.5V this will lead to the different Pt:Pb ratios seen in Table 4.1. Further evidence of this trend can be seen on examination of Sample 3, as the low surface coverage and Pt content are due to short replacement steps and the low pre-set OCP cut off potential of 0.2V being maintained throughout the deposition event in this case.

The values for coverage are taken from XPS analysis of the top surface layer of each sample. In order to further understand and characterise this deposition method, a thickness profile was measured using the XPS and ion etching as shown in Figure 4.12 to Figure 4.15. All samples have a high Pt value, independent of E_1 or E_2 though the amount of Pt at the final layer and the depth the Pt varies between samples.

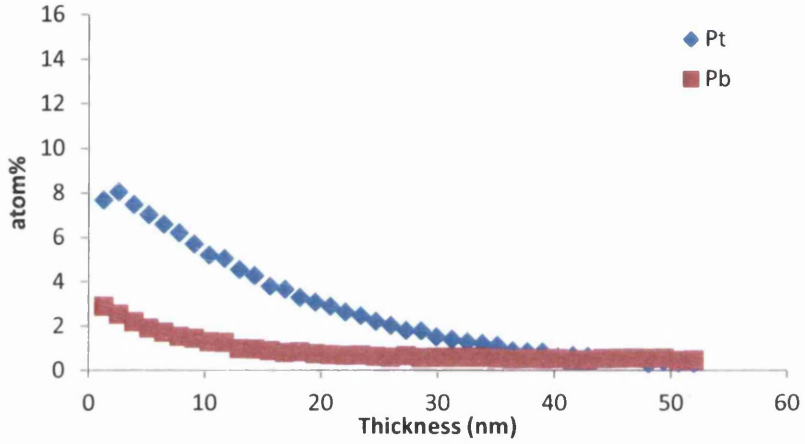

Figure 4.12: Varying atomic percentages of Pt and Pb with thickness, measured through XPS (Sample 1; E_1=-0.75V, E_2=0.2V)

Samples 2 and 4 appear to demonstrate similar layer growth, giving an increase in Pt quantity in the top 40-45nm depth. It was thought that this is the result of the long initial OCP replacement stage observed in Figure 4.4 b & c. In comparison, Samples 1 and 3 indicate that the shorter OCP Pt replacement time results in reduced Pt present directly on the FTO-glass surface. Thus the overall layer thickness for these samples is also reduced, giving *ca.* 35nm and *ca.* 25nm thickness values respectively. Finally, the Pt content of Sample 4 increases to over 14% and in Sample 2 the Pt content reaches 12%, thus showing that the E_1 value is also an important parameter for determining the structure of the deposit and Pt content.

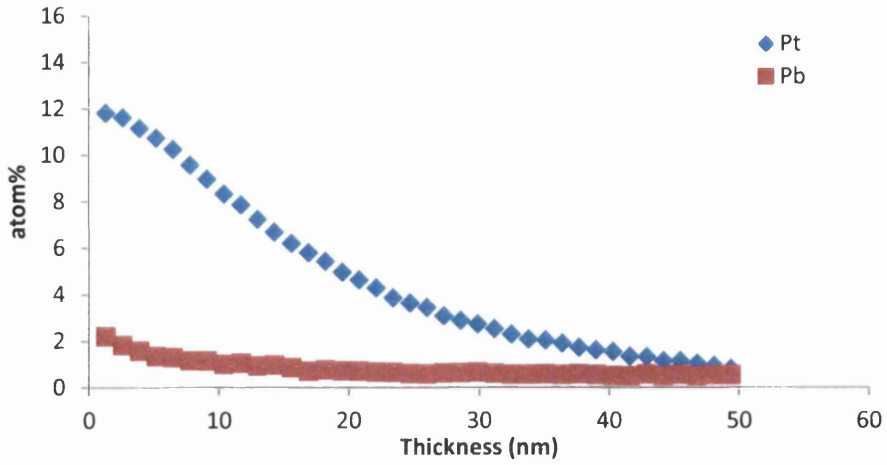

Figure 4.13: Variation in atomic percent of Pt and Pb as a function of layer thickness, measured through XPS analysis (Sample 2; E_1=-0.75V, E_2=0.5V)

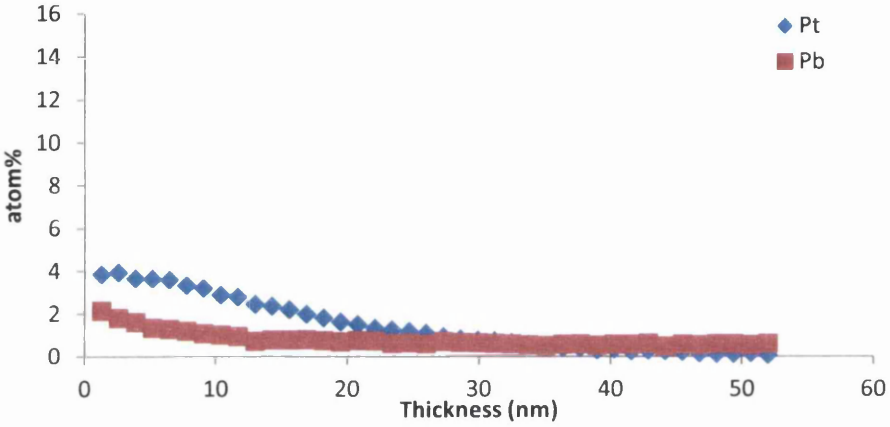

Figure 4.14: Variation of atomic percent of Pb and Pt with layer thickness. Measured by XPS analysis (Sample 3; E_1=-0.5V, $E_2$0.2V)

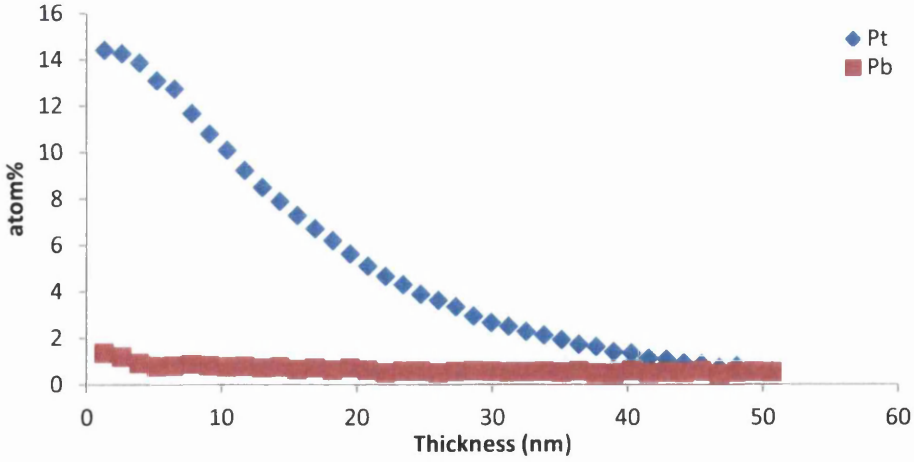

Figure 4.15: Variation in atomic percent of Pb and Pt with layer thickness, measured by XPS analysis (Sample 4; E_1-0.5V, E_2=0.5V)

The XPS data confirms the presence of Pt on all samples, and shows there is still Pb remaining on the surface, even following several deposition and replacement events. Samples 2 or 4 give the highest ratio of Pt:Pb at 3.72:1 and 3.97:1 respectively, though Sample 4 indicates the highest surface coverage, giving a reading of 20.54Sn% compared to Sample 2 at 23.85Sn% detected through surface analysis, the lower number indicates less FTO visible to the XPS surface scan at each layer, which agrees strongly with the SEM imagery in Figure 4.5g&h. Since the catalytic performance of electrodeposited Pt is known to be less than thermal or chemical, it was decided to select the parameters from Sample 4 (E_1=-0.5V, E_2=0.5V or 60s) as this will provide more Pt on the counter electrode for this developmental investigation. If this was proven to be successful, then future work would focus on limiting the size of Pt deposits through potential and chemical controls.

4.7 Use of electrodeposited counter electrodes in DSCs

Now that the catalyst deposit has been characterised, the next stage involves the manufacture of DSC counter electrodes containing an iodide/triiodide redox couple. The aim of this section is to assess this process for use as a low temperature, rapid alternative for current platinisation methods. The initial tests characterising the catalyst behaviour as a site for the reduction of triiodide was achieved using cyclic voltammetry to qualitatively assess the ability to reduce triiodide in solution. Following this, EIS measurements were made on symmetrical type cross cells as described in Chapter 2.5.4. DSC cells were then constructed using the electrodeposited counter electrodes and then tested under standard testing conditions (STC) using a simulated light environment, the testing setup and parameters are described in Chapters 2.5. The parameters chosen were as for Sample 4, using an E_1 value of -0.5V to deposit the Pb, and a potential cut off E_2 value of -0.5V. Further to this, the potential was held at 0.5V prior to the start of the deposition to ensure no electroless deposition occurred before the commencement of the study. The range of cycles used to deposit the catalyst was 1, 5, 10 and 20, chosen due to the particle size and distribution indicated in the previous characterisation stage. This should give the broadest useful idea of the catalyst performance in a DSC cell.

4.7.1 Cyclic Voltammetry in iodide/triiodide solution

Basic cyclic voltammetry allowed the qualitative assessment of the catalyst activity for the reduction of the triiodide species necessary in a DSC device. Figure 4.16 exhibits several peaks representative of the sought after reduction activity, thus confirming the catalyst viability for use in a DSC cell. A typical CV plot gives the current density "J" vs. the potential "E" with the potential given versus the reference electrode used in the electrochemical cell. Both the I_3^- reduction and I^- oxidation peaks are marked.

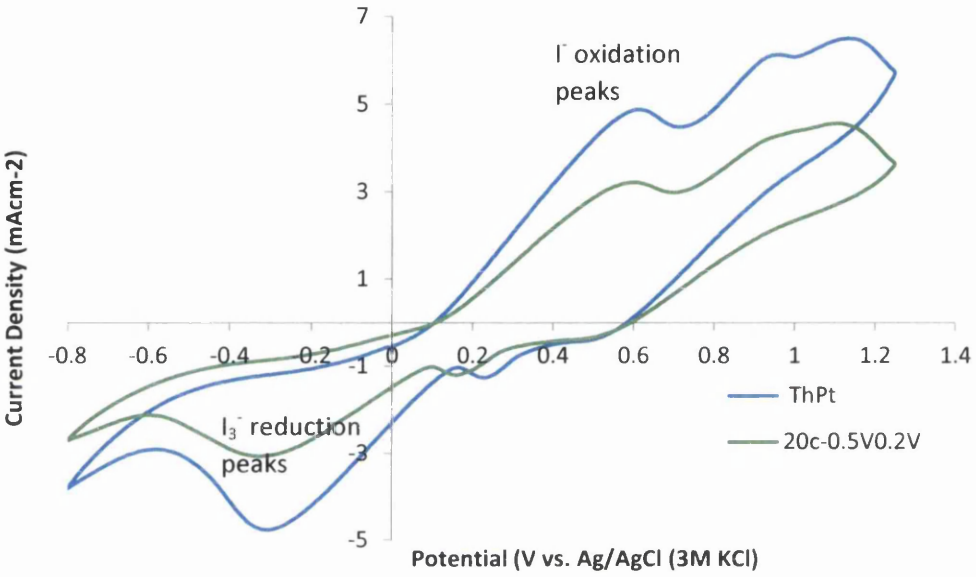

Figure 4.16: Cyclic voltammetry in a solution containing I_3^-/I^- ions. (3 electrode cell: Pt/FTO-glass working electrode, Ag/AgCl reference, Pt mesh counter electrode)

Obtaining quantative measurements from a CV scan is not a straightforward task. In the interests of streamlining this study and assessing different methods for potential use on scale up of this technology, electrical impedance spectroscopy (EIS) was next utilised to rapidly and accurately characterise the performance of the catalyst to allow for a quantitative comparison with the traditional thermal and chemical platinisation methods.

4.7.2 Electrical Impedance Spectroscopy (EIS) analysis

Electrical impedance spectroscopy and the theory behind the method was explained in Chapter 2.5.3, where it was detailed that the chief method of presenting DSC results was in the form of a Nyquist plot and Bode plots. The Nyquist plot can be separated into three distinct areas, each giving details of the different interfaces in a DSC device. The x-axis offset represents the series resistance of the conductive substrate (R_s). The 1st semicircle describes the interface between the counter electrode/catalyst and the electrolyte, called

the charge-transfer resistance (R_{ct}) and the 2nd semicircle describes the recombination resistance of the TiO_2 photoanode (R_{rc}), as detailed previously in Figure 2.9. To obtain the performance parameters, R_s, R_{ct} and R_{rc}, electrical equivalent circuit modelling is used, represented in this case by the model shown in Figure 4.17. Modelling theory is described in greater detail in Chapter 2.4.2. This model provides a good fit to the data sets, allowing the critical parameter "R_{ct}" to be calculated and used as a comparison of the catalytic efficiency of the different counter electrodes.

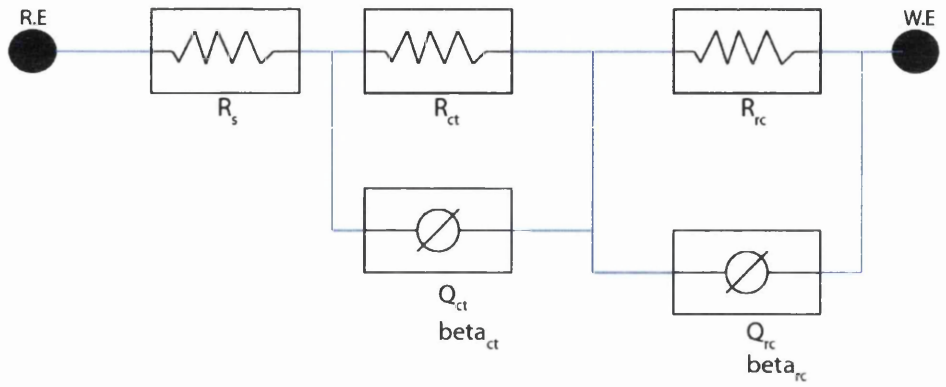

Figure 4.17: Equivalent circuit model of a DSC

The EIS data is presented in Figure 4.18 to Figure 4.21, where the main parameter used for the comparison of the counter electrodes is the R_{ct} value from the initial semicircle, indicating the efficiency of the electron transfer between the catalyst and the triiodide species. A higher R_{ct} value indicates poor catalytic ability and therefore reduced efficiency of the counter electrode. DSC devices containing a thermally or chemically platinised counter electrode are included for comparison, Figure 4.23 and Figure 4.23. The measurements were taken with the cells in the dark and a DC voltage of -0.65V applied to the cell to ensure that the cells are at the maximum power point when under measurement and comparable to each other as a deviation in V_{oc} will lead to different values of R_{ct} . Using this method, a clear difference will be able to be seen between a good and poor catalyst [14]. The frequency range used for this study was 50000Hz to 0.1Hz, using 10 points/decade and an AC perturbation of 10mV rms. The full experimental details can be found in Chapter 2, in addition to a theoretical background into the EIS study of dye solar cell devices.

In addition to the Nyquist plots, a Bode plot showing the magnitude of the impedance and the phase angle at different frequencies is also included. As mentioned in Chapter 2, the Bode plot imparts further information regarding the state of the cells undergoing testing as a function of the frequency. The Bode plots are generally in the form of peaks and troughs, indicating constant phase elements/resistor pairs shown in Figure 4.17.

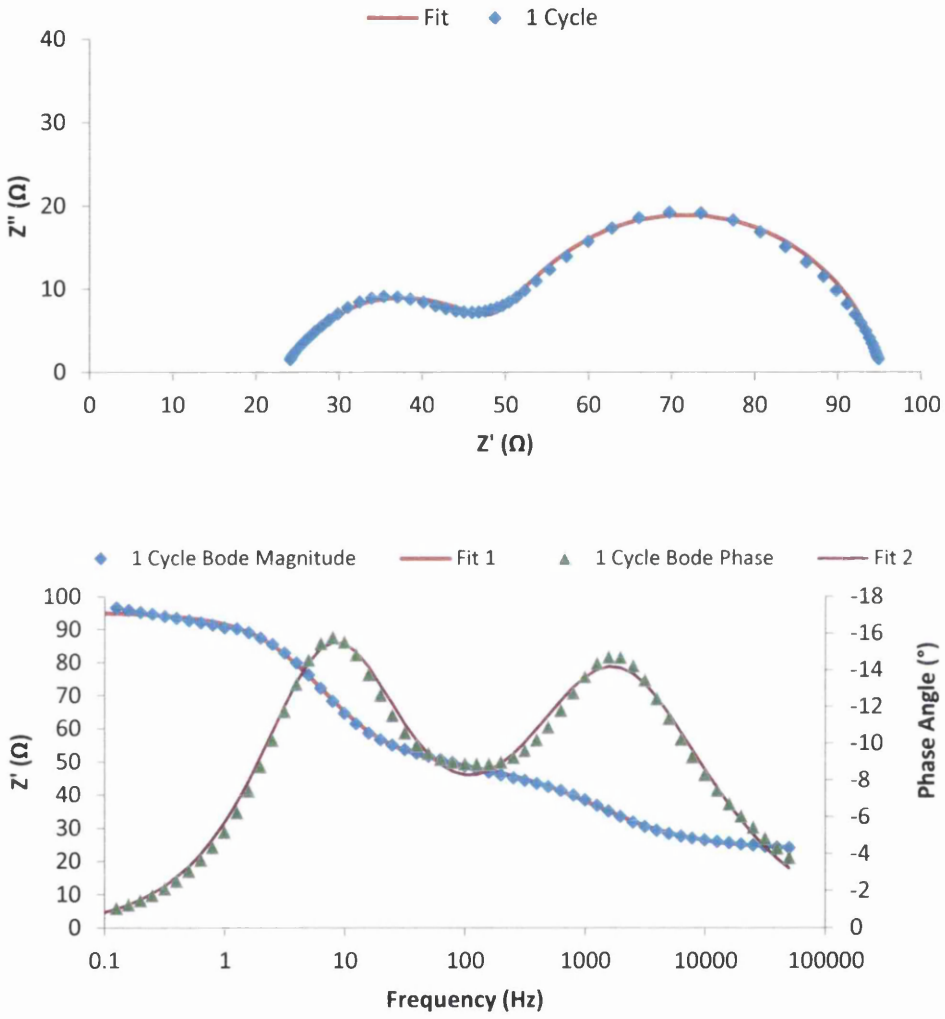

Figure 4.18: Nyquist and Bode plots with fitting for DSC cells using SLRR electrodeposited Pt counter electrodes at 1 cycle deposition

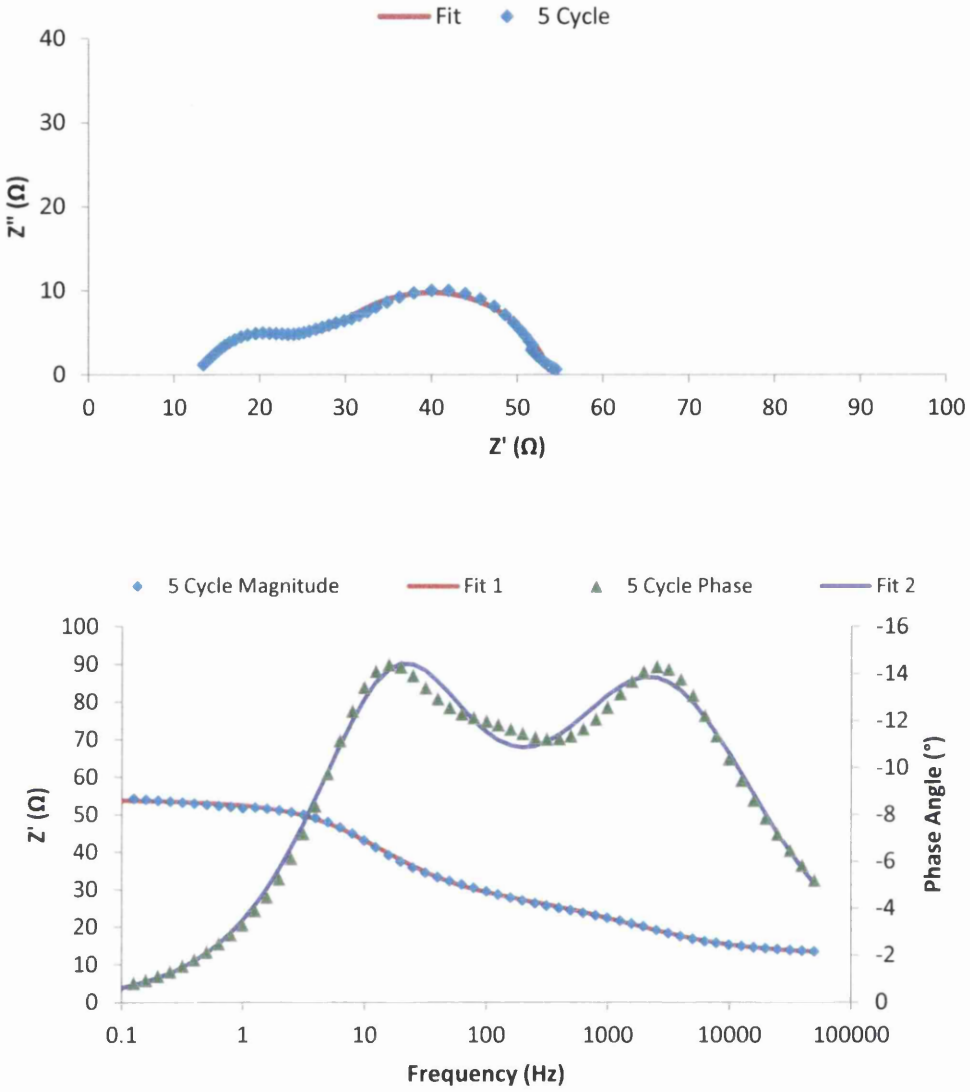

Figure 4.19: Nyquist and Bode plots with fitting for DSC cells using SLRR electrodeposited Pt counter electrodes at 5 cycles deposition

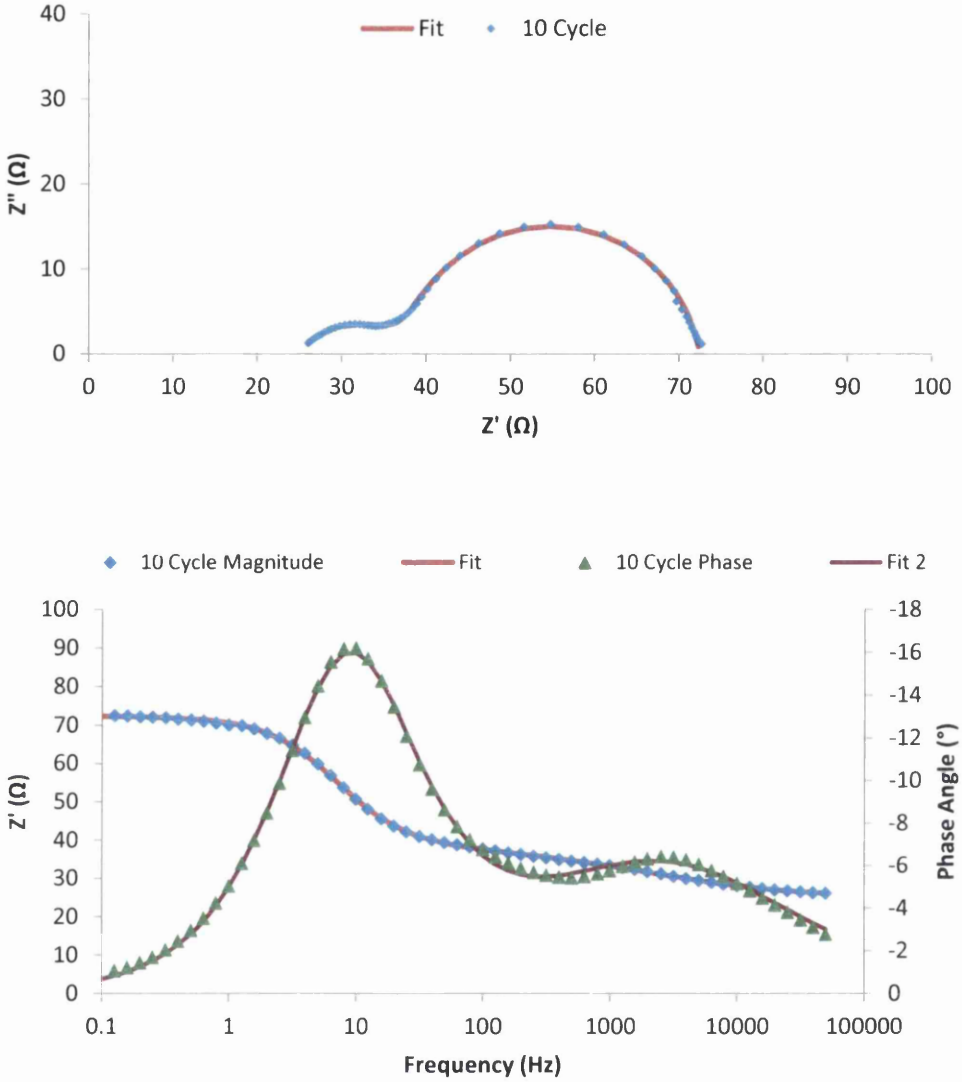

Figure 4.20: Nyquist and Bode plots with fitting for DSC cells using SLRR electrodeposited Pt counter electrodes at 10 cycles deposition

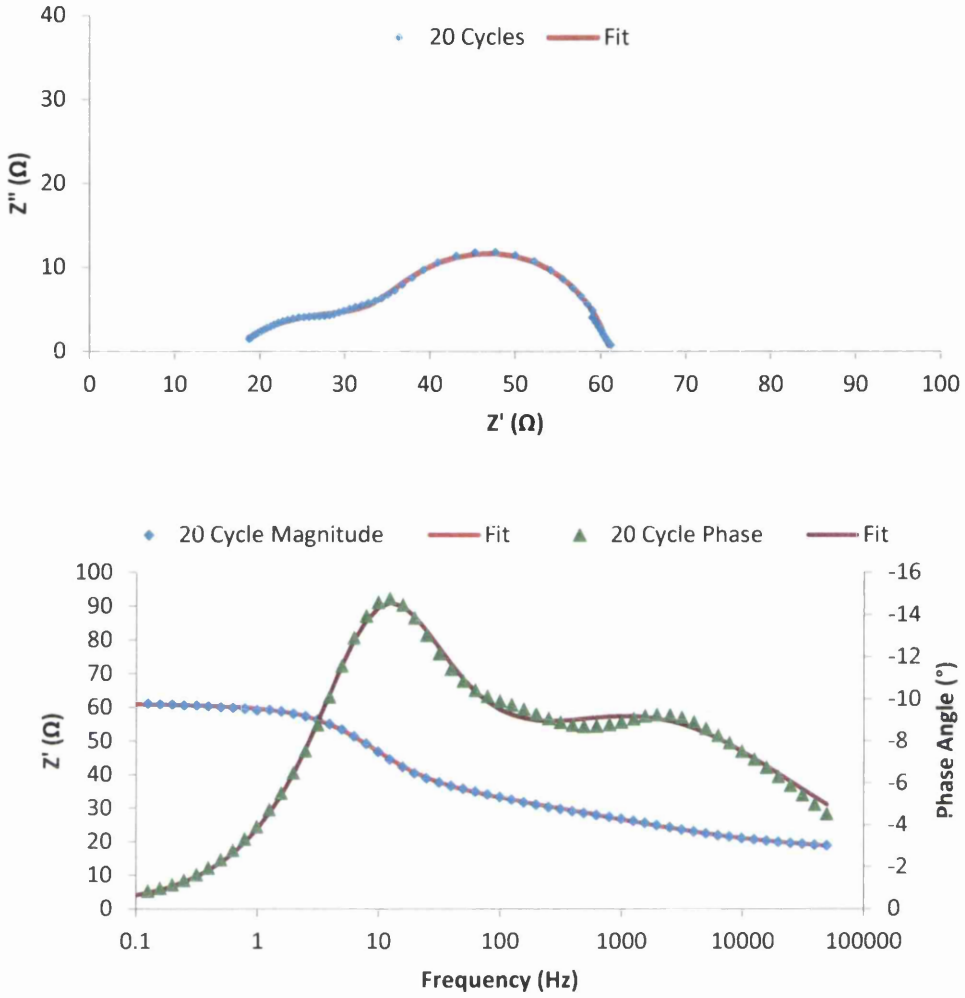

Figure 4.21: Nyquist and Bode plots with fitting for DSC cells using SLRR electrodeposited Pt counter electrodes at 20 cycles deposition

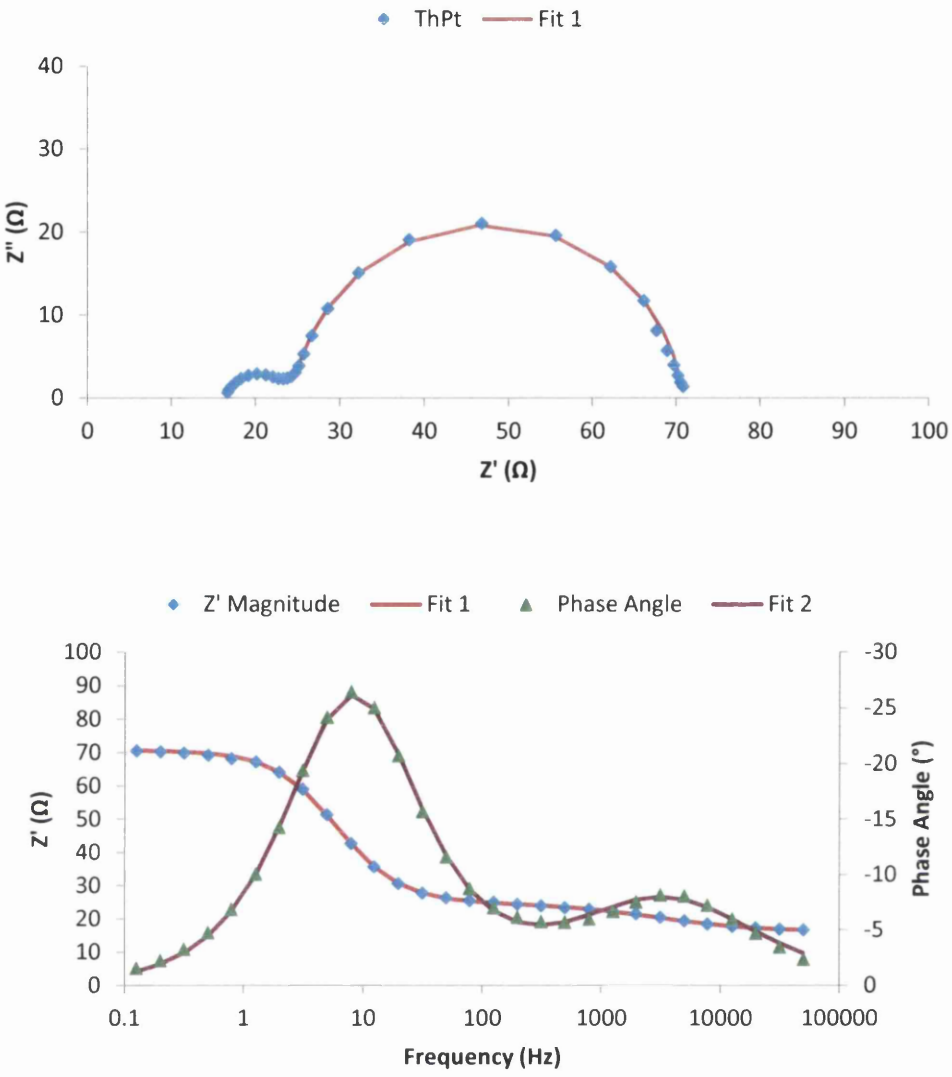

Figure 4.22: Nyquist and Bode plots with fitting for DSC cells with thermally deposited Pt counter electrodes

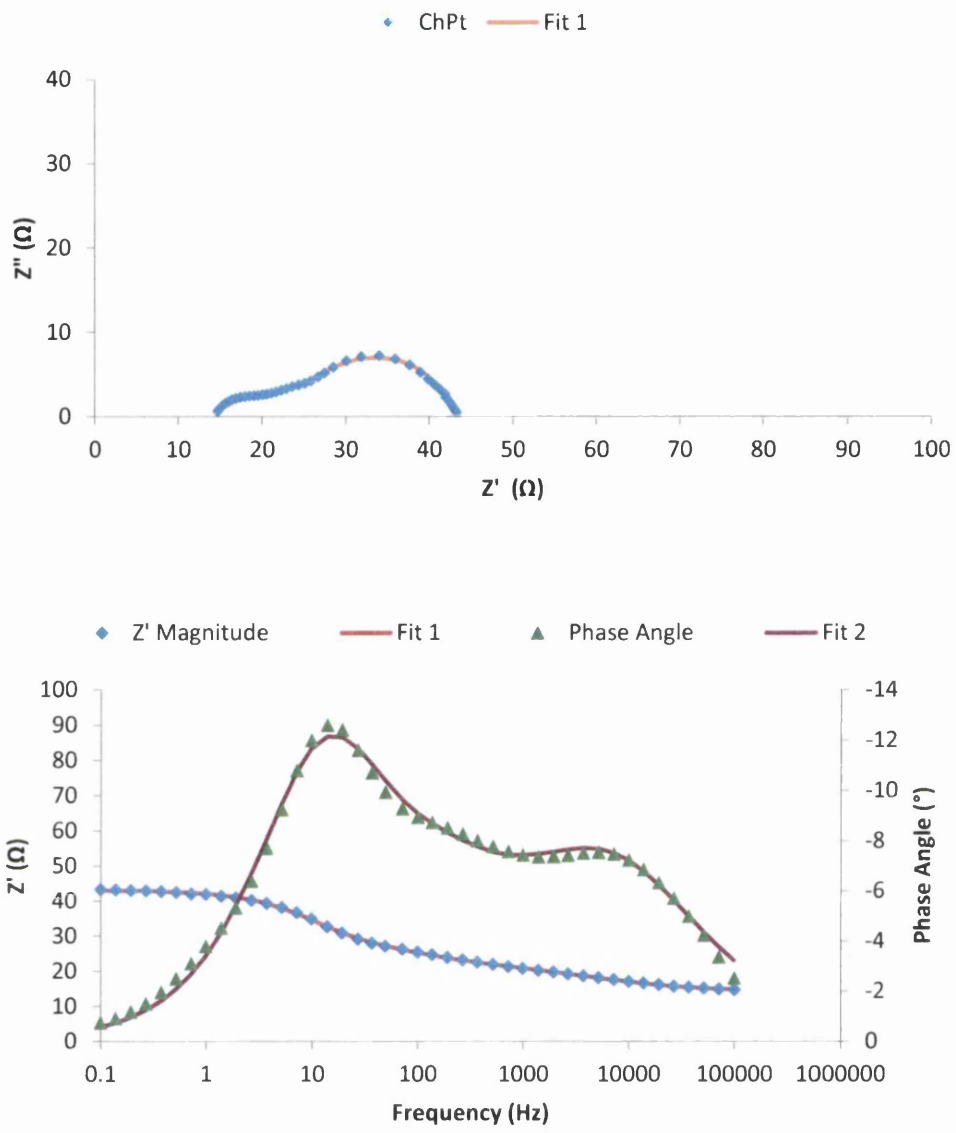

Figure 4.23: Nyquist and Bode plots with fitting for DSC cells with chemically deposited Pt counter electrodes

Figure 4.24 illustrates that ED-Pt counter electrodes have a much higher R_{ct} than the comparable thermal Pt and the chemically produced Pt catalyst when an average was taken of three DSC cells. A single cycle deposition exhibited an R_{ct} value of *ca.* 30 Ωcm^{-2} compared to the literature value for thermal platinum of *ca.* 4 Ωcm^{-2} [15], though our thermally produced Pt catalyst had an R_{ct} of **12.8Ωcm^{-2}**. As the number of deposition cycles was increased to 5 cycles, a drop was seen to occur in the R_{ct} to *ca.* 20 Ωcm^{-2} region. This suggests an increase in the specific surface area due to an increase in the number of platinum active sites. Furthermore, the increase in Pt will remove or counterbalance any remaining poorly catalytic Pb on the FTO surface further enhancing the performance.

There is very little variation in R_{ct} on increases to 10 and 20 cycles, suggesting a limit to the catalyst performance with this electrodeposition method. The limit was proposed to be due to the increase in catalytic particle and cluster size thus reducing the catalyst specific area at higher cycles. Furthermore, it is known that different methods of platinisation form different crystal structures of platinum. The Pt[111] facet has been demonstrated as the most highly catalytic with the Pt(411) and Pt(100) faces giving lower activity [16]–[18]. It is not yet known what orientation the electrodeposited method gives, though it is suggested that further work to examine this will allow for further catalyst optimisation.

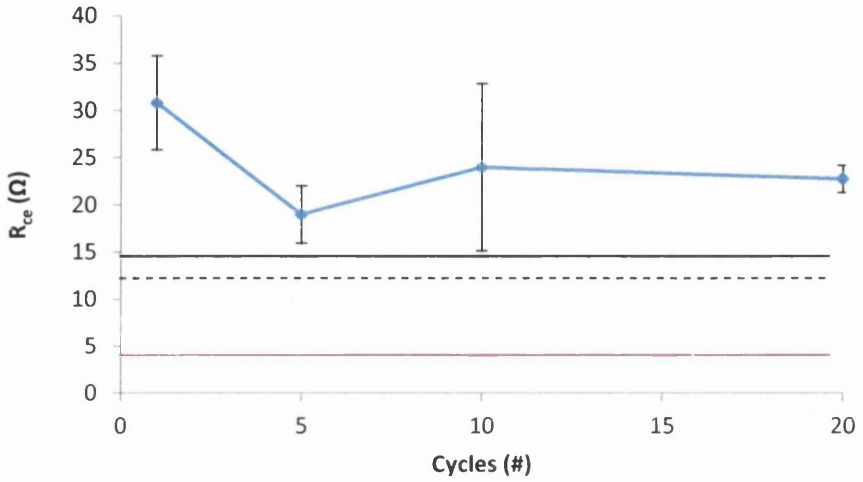

Figure 4.24: Comparison of charge transfer resistance (R_{ct}) for electrodeposited CEs, average of 3x DSCs per point (Key: *Solid line, average thermal Pt value; dashed line, average chemical Pt value; Red line, literature thermal Pt value* [19])

It was suspected that if Pb remained present in the DSC, it would affect the electrochemical performance of the DSC through interaction with the electrolyte species, reducing efficiency and through migration to the TiO_2 surface where it could form recombination sites, which will increase recombination activity.

4.7.3 DSC testing

Following the extensive characterisation and testing of the electrodeposited Pt coating on FTO through surface analysis and electrochemical means, counter electrodes were fabricated using this method and applied in the manufacture of complete DSC devices. The cells were exposed to a stimulated operating environment to assess their performance, the results were used to compare the electrodeposited cells with the standard DSCs using thermal and chemically platinised CE's. The EIS data presented in Figure 4.24 was thought to give an idea of the results to expect. The relatively high R_{ct} across all electrodeposited

cells will increase the overall cell resistance and appear as a reduction in the DSC fill factor. A summary of the average performance data for these devices can be found in Table 4.2, where 1 cycle represents the least platinum deposited, and 20 cycles as the most Pt deposited in this study. The I-V characteristics of the electrodeposited DSCs were seen to be highly comparable with standard DSCs, Figure 4.25, despite the low R_{ct} values given by the EIS analysis in Figure 4.24. The J-V data enabled several key performance parameters to be defined, that of V_{oc}, J_{sc}, FF and μ.

Table 4.2: DSC Average Performance Data

Cycles (#)	V_{oc} (v)	J_{sc} (mA/cm^2)	FF (%)	Efficiency (%)	R_{ce} (Ω/cm^2)
1	0.71 (±0.005)	8.09 (±0.6)	55.48 (±2.2)	3.18 (±0.4)	30.81 (±4.9)
5	0.70 (±0.013)	7.73 (±0.4)	49.87 (±10.6)	2.70 (±0.5)	18.99 (±3.0)
10	0.69 (±0.001)	8.39 (±0.1)	46.89 (±4.1)	2.70 (±0.2)	23.99 (±8.9)
20	0.68 (±0.023)	7.51 (±0.5)	63.34 (±5.4)	3.23 (±0.3)	22.76 (±1.4)
Thermal Pt	0.70 (±0.002)	10.49 (±0.4)	69.34 (±5.0)	3.97 (±0.7)	12.80 (±1.1)
Chemical Pt	0.65 (±0.0001)	7.86 (±0.1)	68.80 (±0.006)	3.53 (±0.04)	14.07 (±2.1)

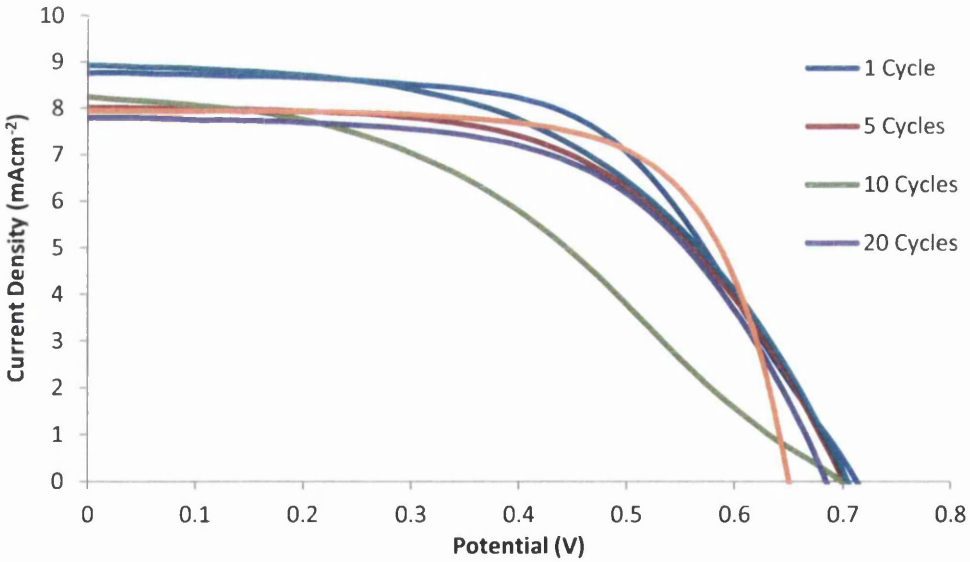

Figure 4.25: I-V curves for DSCs using electrodeposited counter electrodes, DSCs using thermally deposited Pt counter electrodes are used for comparison (Average of 3 DSCs per variable)

The key performance parameters for the comparison of counter electrodes are the fill factor (FF) and the efficiency.

The FF, as mentioned previously in Chapter 2.5.2 is a comparison of the ideal performance of a DSC versus the actual performance of the cell, taking into account resistive losses as well as manufacturing errors. Figure 4.26 compares the values for the ED-Pt with standard Th-Pt and Ch-Pt containing DSCs. A variable range from 46-63% was given by the FF, with a large standard deviation indicating inconsistencies in manufacture. Compared with the usual 60-65% FF of standard DSCs using thermal counter electrodes the FF is low and unstable with 10 cycles displaying the lowest value. The drop in FF is considered to be due to R_{ct} reduction when the catalyst specific area decreases with the growth of Pt deposit size. However, there is an increase at 20 cycles to *ca.* 60% which does follow the decreasing trend. This was attributed to the rise in overall catalyst material due to more Pb available for Pt replacement. The increase in material will offset the reduction in deposit specific area as the total surface coverage has doubled, as seen through XPS analysis.

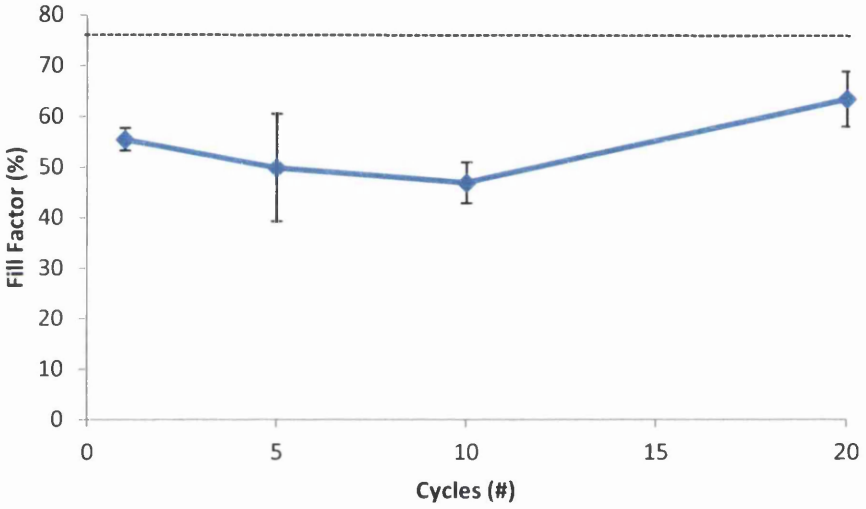

Figure 4.26: Fill factor (FF) of DSCs using electrodeposited counter electrodes for differing number of deposition cycles. (-------) indicates thermal Pt V_{oc} (Results average of 3 DSCs)

Efficiency, the other crucial parameter used for the assessment and comparison of solar devices, matches the variable trend of the FF results showing its reliance on fill factor changes, Figure 4.27. The conclusion can be made that the reduction in V_{oc} and increase of cell resistance exhibited by a lower FF are the main contributing factors to the reduced efficiency over that of the comparison devices using chemical and thermally produced counter electrodes. However, the small variation in efficiency with deposition cycles indicates that deposition cycles and quantity of catalyst have little impact. There is no doubt that the catalyst structure of the electrodeposited platinum is less catalytic than thermally deposited or chemically reduced Pt catalysts. This factor has been mentioned in

recent literature as facet dependent catalytic activity of platinum nanoparticles, where Pt(111) was found to have greater specific activity and therefore will give a lower R_{ct} than Pt(411) or Pt(100) facets [16].

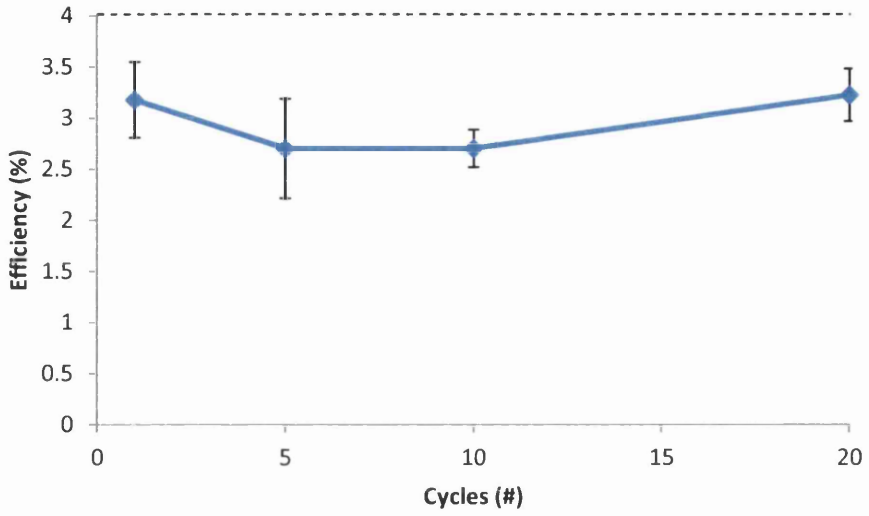

Figure 4.27: Efficiency (η) of DSCs using electrodeposited counter electrodes for differing number of deposition cycles. (-------) indicates thermal Pt V_{oc} (Results average of 3 DSCs)

The variation in V_{oc}, illustrated in Figure 4.28, reduces slightly as the number of deposition cycles is increased. However, there is a relatively large variation between the cells used for the average value, particularly for 20 deposition cycles. The V_{oc} is known to vary between devices due to the quality of the TiO_2 photoanode and the performance of the dye photosensitiser, which accounts for small variations. However, in the case of larger variations in cells of the same batch, there will be other factors influencing this value.

SEM and XPS characterisation have previously shown that the surface coverage and cluster size increases with number of deposition cycles, resulting in improvements in the R_{ct} and amount of catalytic material, see Figure 4.24.

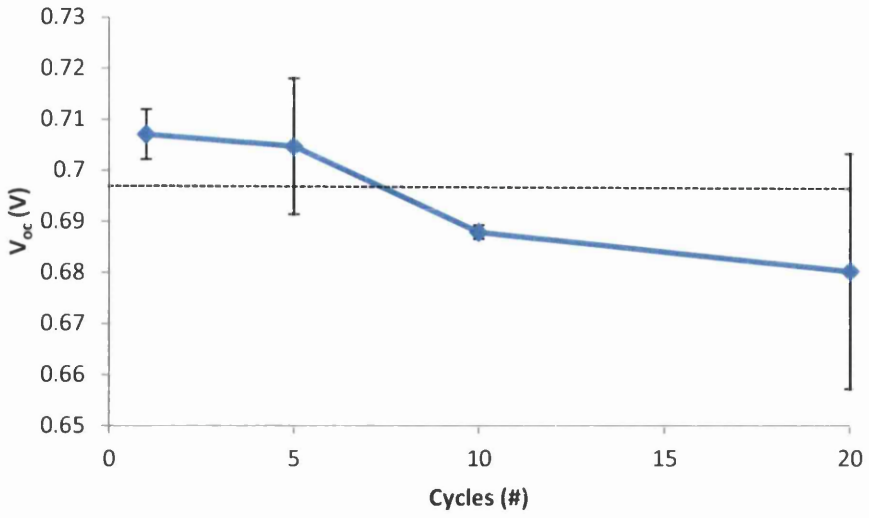

Figure 4.28: Open circuit voltage (V_{oc}) of DSCs using electrodeposited counter electrodes for differing number of deposition cycles, (-------) indicates thermal Pt V_{oc} (Results average of 3 DSCs)

The short circuit current density (J_{sc}) shown in Figure 4.29 does not show the same decreasing trend shown by the V_{oc} in Figure 4.28. Instead J_{sc} remains stable at *ca.* 8mAcm^{-2}.

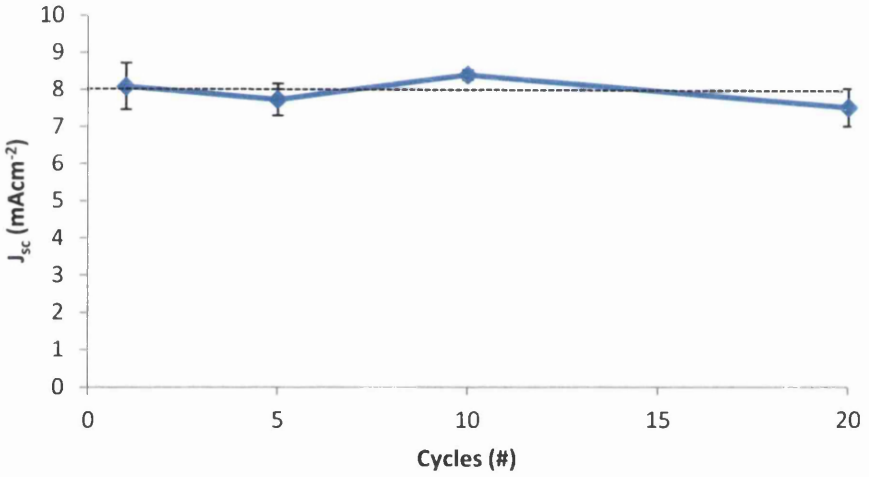

Figure 4.29: Short circuit current (J_{sc}) of DSCs using electrodeposited counter electrodes for differing number of deposition cycles. (-------) indicates thermal Pt V_{oc} (Results average of 3 DSCs)

This indicates that the amount of charge carriers in the electrolyte has changed little, contrasting with previous hypothesis that Pb-iodide bonding occurs, reducing the amount of charge carriers. Furthermore this also indicates that the remaining active components of the DSC, dye and TiO_2 remain stable. The J_{sc} was also discovered to compare favourably with our typical DSC, with either a chemical or thermal Pt counter electrode, a further indication that the active parts of the device were stable and fully functional.

Previous literature has studied the relative catalytic abilities of platinum, reporting that the crystal structure has a significant influence on the specific activity of the Pt catalyst [16]. It was clear from the results, that there is a disparity between the catalytic activity and that of the more common methods (thermal and chemical) which is believed to be due to the nucleation and growth deposition route of the electrodeposited catalyst. Therefore, in order to further optimise this deposition method, it must be altered to ensure the deposition of highly catalytic platinum at short deposition cycles to minimise material usage. In addition, further analysis needs to be done on the effect of Pb in the DSC system, to ensure that it will not adversely affect any of the dye cell components.

4.8 Conclusions and Further Work

The aim of this study was to develop a low temperature deposition method that would allow electrochemical platinisation to rival more traditionally produced Pt catalysts that would be suitable for use in DSC devices and adapted for use on a mass production line. Previous literature has already established that the amount of material deposited depends on the applied power and deposition time; therefore here we have used a low cost initial template, which is deposited through the application of brief high power stage. This enabled the control of Pt catalyst formation.

This study demonstrated that the application of repeat cycles of electrodeposition and OCP replacement stages to FTO glass could produce a homogenous distribution of Pb/Pt nanoscale particles on the FTO surface. An essential development was the use of a single solution for the entire process. Fast deposition of Pb was performed at a chosen potential "E_1", which was quickly followed by redox replacement by Pt at OCP. This process occurs through the oxidation of Pb by Pt^{2+} ions and then the replacement of Pb at the substrate surface. It was shown that this replacement step can be finely controlled through the cut off potential "E_2" or time limit, in this case 60s. It was further found that a small quantity of Pt co-deposits with Pb due the deposition potential chosen. This further increased the quantity of nucleation sites on the FTO for particle and cluster growth at OCP. Larger cut off potentials or time resulted in higher total coverage, therefore it was concluded that E_2 or an enforced cut off time play a significant role in determining the final coverage and structure when using this method. The E_1 was seen to affect the amount of Pb template available for replacement events at Stage 2, therefore this value must be cathodic enough to deposit material, but also must ensure that no other competing reactions are initialised, i.e. hydrogen evolution that may occur once Pt replacement occurs.

Despite the extra level of deposit structural control given by this method, the electrochemical behaviour was demonstrated to perform much lower than the standard thermally deposited Pt catalyst used for DSC devices. Whether this was due to poor particle connectivity or simply a function of the way in which the catalyst particles form remains to be studied. However, on the use of this method to manufacture DSC CE's, the performance found to remain comparable with the 3.9% cell efficiency exhibited by the standard thermally applied catalyst DSCs. The peak efficiency of 3.2% gained for electrodeposited CE devices was attained using both 1 and 20 deposition cycles. From this it was concluded that catalyst stability, more than electrochemical activity would dictate DSC performance. It was believed that a key point here was that the one cycle deposited catalyst was composed mostly of Pt, with little remaining Pb on the surface. Furthermore, the 20 cycle catalyst consisted of a high coverage of material which would contain mostly Pt. This was thought to account for the peak performance at 1 and 20 and led to the conclusion that both 5 and 10 cycles contained a less stable catalyst, possibly due to the presence of a larger amount of Pb remaining.

Despite the varying electrochemical and DSC performance given by this method, it has succeeded in proving to be a highly controllable deposition method, which through using a low cost lead template and reducing the concentration of expensive platinum in solution should result in an overall decrease in the cost of DSC counter electrode manufacture. In addition, this is a low temperature method which allows the use of polymeric substrates as the counter electrode. This would be of particular use in mass produced flexible DSCs were the working electrode is a metal substrate and there is a need for a flexible transparent top sheet as the CE. Now that this method has successfully been developed for us on FTO-Glass, future work should concentrate on the replacement of toxic Pb with other sacrificial metals. This could build on the prior work done by Rettew *et al.* who successfully utilised a Ni template instead of the Pb material used in this research. In addition, the electrolyte should be exposed to Pb in an isolation experiment to assess whether there is a change due to interaction between the Pb and the electrolyte species. The reaction should be visible through a colour change, noticeable on a UV-VIS scan. Further work could also be done to assess the affect of oxide layers on the prevention of electrolyte degradation - building on the knowledge that the strongly bonded oxide layer of titanium prevents cell degradation and corrosion in DSC devices when this substrate is used.

4.9 References

[1] M. Fayette, Y. Liu, D. Bertrand, J. Nutariya, N. Vasiljevic, and N. Dimitrov, "From Au to Pt via surface limited redox replacement of Pb UPD in one-cell configuration.," *Langmuir*, vol. 27, no. 9, pp. 5650–8, May 2011.

[2] S. R. Brankovic, J. X. Wang, and R. R. Ad, "Metal monolayer deposition by replacement of metal adlayers on electrode surfaces," *Surf. Sci.*, vol. 474, pp. L173–179, 2001.

[3] L. T. Viyannalage, R. Vasilic, and N. Dimitrov, "Epitaxial Growth of Cu on Au (111) and Ag (111) by Surface Limited Redox ReplacementsAn Electrochemical and STM Study," no. 111, pp. 4036–4041, 2007.

[4] M. Shelef, K. Otto, and N. C. Otto, "Poisoning of Automotive Catalysts," *Adv. Catal.*, vol. 27, pp. 311–365, 1979.

[5] Y.-S. Ko and Y.-U. Kwon, "Electrochemical deposition of platinum on fluorine-doped tin oxide: The nucleation mechanisms," *Electrochim. Acta*, vol. 55, no. 24, pp. 7276–7281, Oct. 2010.

[6] Y.-S. Ko and Y.-U. Kwon, "Electrochemical deposition of platinum on fluorine-doped tin oxide: The nucleation mechanisms," *Electrochim. Acta*, vol. 55, no. 24, pp. 7276–7281, Oct. 2010.

[7] A. V. Naumkin, A. Kraut-Vass, S. W. Gaarenstroom, and C. J. Powell, "NIST X-ray Photoelectron Spectroscopy Database," *NIST X-ray Photoelectron Spectroscopy Database, Version 4.1 (National Institute of Standards and Technology, http://srdata.nist.gov/xps Gaithersburg, 2012);*, 2012. [Online]. Available: http://srdata.nist.gov/xps. [Accessed: 13-Aug-2012].

[8] A. I. Martínez, L. Huerta, J. M. O.-R. De León, D. Acosta, O. Malik, and M. Aguilar, "Physicochemical characteristics of fluorine doped tin oxide films," *J. Phys. D. Appl. Phys.*, vol. 39, no. 23, pp. 5091–5096, Dec. 2006.

[9] Y. Masuda, T. Ohji, and K. Kato, "Facile Synthesis of Characteristic Tin Oxide Particulate Films in Aqueous Solution," *Int. J. Appl. Ceram. Technol.*, vol. 8, p. n/a–n/a, Jan. 2012.

[10] J. F. Román-Zamorano, M. Flores-Acosta, H. Arizpe-Chávez, F. F. Castillón-Barraza, M. H. Farías, R. Ramírez-Bon, J. F. Roma, and Æ. F. F. Castillo, "Structure and properties of lead and lead sulfide nanoparticles in natural zeolite," *J. Mater. Sci.*, vol. 44, no. 18, pp. 4781–4788, Jul. 2009.

[11] J. F. Moulder, W. F. Stickle, P. E. Sobol, and K. D. Bomben, *Handbook of X-ray Photoelectron Spectroscopy*. ULVAC-PHI, Inc; Physical Electronics USA, Inc, 1992.

[12] Y.-S. Ko and Y.-U. Kwon, "Electrochemical deposition of platinum on fluorine-doped tin oxide: The nucleation mechanisms," *Electrochim. Acta*, vol. 55, no. 24, pp. 7276–7281, Oct. 2010.

[13] O. Paschos, *High Aspect Ratio, Nanostructured, Platinum Based Electrodes for Proton Exchange Membrane Fuel Cells: Design, Development and Ionic Conduction of the Proposed Structures*. State University of New York at Albany: ProQuest, 2008, pp. 85–86.

[14] K. Miettunen, "Performance and Stability of Dye Solar Cells on Stainless Steel," Helsinki University of Technology, 2009.

[15] N. Papageorgiou, "An Iodine/Triiodide Reduction Electrocatalyst for Aqueous and Organic Media," *J. Electrochem. Soc.*, vol. 144, no. 3, p. 876, 1997.

[16] B. Zhang, D. Wang, Y. Hou, S. Yang, X. H. Yang, J. H. Zhong, J. Liu, H. F. Wang, P. Hu, H. J. Zhao, and H. G. Yang, "Facet-dependent catalytic activity of platinum nanocrystals for triiodide reduction in dye-sensitized solar cells.," *Sci. Rep.*, vol. 3, p. 1836, May 2013.

[17] S. Mukherjee, B. Ramalingam, L. Griggs, S. Hamm, G. a Baker, P. Fraundorf, S. Sengupta, and S. Gangopadhyay, "Ultrafine sputter-deposited Pt nanoparticles for triiodide reduction in dye-sensitized solar cells: impact of nanoparticle size, crystallinity and surface coverage on catalytic activity.," *Nanotechnology*, vol. 23, no. 48, p. 485405, Dec. 2012.

[18] R. Narayanan and M. a. El-Sayed, "Shape-Dependent Catalytic Activity of Platinum Nanoparticles in Colloidal Solution," *Nano Lett.*, vol. 4, no. 7, pp. 1343–1348, Jul. 2004.

[19] N. Papageorgiou, S. Haruyama, K. Fujimoto, H. Konno, B. R. Pearson, M. Nagayama, N. Kagaku, T. Technology, and R. S. Alwitt, "An Iodine / Triiodide Reduction Electrocatalyst for Aqueous and Organic Media," *J. Electrochem. Soc.*, vol. 144, no. 3, pp. 876–884, 1997.

5 *Corrosion of metallic substrates in liquid based DSC electrolyte*

5.1 Introduction

In liquid based DSCs, the electrolyte is of critical importance, which is clearly shown by the vast quantity of literature on the makeup and interactions of the many viable electrolytes with other cell components. The previous chapters focused on the particular interaction at the counter electrode, the reduction of the triiodide species to iodide *via* the accelerating medium of a catalyst. This important reaction addresses loss mechanisms or "overpotentials" in the cell and seeks to improve the fill factor through the reduction of the cell internal resistance at the counter electrode (R_{ce}). As the interaction at this electrode/electrolyte interface is crucial, it was thought that an investigation into the working electrode/electrolyte interface would also provide significant insights. Typically, DSC devices use stable FTO coated glass substrates, these are fairly fragile and inflexible, so will not be compatible with a roll to roll process. Comparatively, metal substrates are lower in cost, robust and flexible, in addition to having inherently higher electrical conductivity than FTO-glass [1]. Unfortunately, the seminal study by Toivola *et al.* found that the typically used iodide/triiodide DSC electrolyte is known to be corrosive to certain industrial sheet metals such as aluminium and zinc coated carbon steels [1], [2]. Previous experience has shown that only titanium and stainless steel, thus far, are resistant to corrosion and are currently undergoing study for use as flexible DSCs substrates [3]–[6].

The initial aim of this chapter is to prove the viability of a time-lapse photographic monitoring and image analysis technique for use in monitoring corrosion through a colour change that occurs as the triiodide species is reduced on interaction with a vulnerable metal surface. This method will be compared through comparison with a diffuse-reflectance UV-Visible light spectrophotometry technique (DR-UV/Vis) where a cell containing an electrolyte layer is fitted to the reflectance aperture and the absorption measure through time-lapse scanning. This has already been established as a viable monitoring method for dye uptake in DSC cells [7]. The time-lapse photography and image analysis method reported in this study has the ability to passively monitor a large number of corrosion cells simultaneously, unlike the DR-UV-Vis technique that actively analyses only one sample per scan. These observation and characterisation methods monitor the reduction of triiodide ions on interaction with the metal substrate over a period of 1000 hours. Equation 5.1 shows a typical reaction that will occur between a metal substrate and

the triiodide species, [Where *"M" denotes the metal, I_3^- is triiodide, M^{x+} indicates metal ion with oxidation number "x", and I^- is the iodide ions.]*:

$$M + \left(\frac{x}{2}\right) I_3^- \rightarrow M^{x+} + \left(\frac{3x}{2}\right) I^- \qquad (5.1)$$

On interaction, there is a visible loss of colour from the dark brown/yellow of triiodide to clear, which is the characteristic appearance of only iodide ions remaining in thin layer cells. The reduction of triiodide is known to decrease the number of charge carriers in the electrolyte, which will lead to a degradation in cell performance [8][9]. Both these methods are *in situ* and non-destructive thus removing the need for additional sample preparation.

Following the successful comparison of a DR-VIS observation and analysis technique with the image analysis method, the image analysis method is then used to assess the performance of several possible corrosion inhibiting chemicals. These are comprised of several nitrogen-containing heterocyclics compounds, hereafter termed NHC's, that are currently in use as performance enhancers in DSC devices [10].

It was initially thought that when under illumination, the DSC devices would provide a potential between both electrodes that should prohibit corrosion. However, a recent study by Miettunen *et al.* has cast doubt on this theory [2]. Despite this factor, a key period that cells are thought to require protection is in darkness or periods of low activity, where the operating potential is removed, lifting any impressed current anti corrosion protection. This study uses corrosion cells without the inclusion of a TiO_2 semiconductor in order to assess if any degradation will occur in these periods of low or zero potential. Furthermore, when the TiO_2 electrode is present it will cover most of the metal substrate meaning that only a small area is vulnerable to damaging interaction by triiodide.

5.2 Experimental

There are three main sections to this chapter: The first addresses the UV-VIS and image analysis techniques in order to compare their output. The second observes the inhibition possibilities of nitrogen-containing heterocyclic compounds in liquid electrolyte and the third details the application of image analysis to large scale observation of test cells and suggests conclusions drawn from the data. The metal substrates studied in this work, along with their purity and compositions are shown in Table 5.1.

Table 5.1: Metals substrates and their purity and composition

Metals	Purity
Nickel	99.98% Ni
Aluminium	99.999% Al
	99.9% Al
Inconel 625	61% Ni, 22%Cr, 9%Mo, 5%Fe
Iron	99.5% Fe
Titanium	99.6% Ti
Molybdenum	99.9% Mo
Stainless steel 316	18%Cr, 10%Ni, 3%Mo
Stainless steel 304	18%Cr, 10%Ni
Zinc	99.9% Zn
Tungsten	99.95% W
Chromium	99.95%Ch

In this study, two main types of observation cell were constructed: The single window observation cell used for DR/UV-Vis analysis and the multi-cell type used for the time-lapse image analysis studies, Figure 5.1.

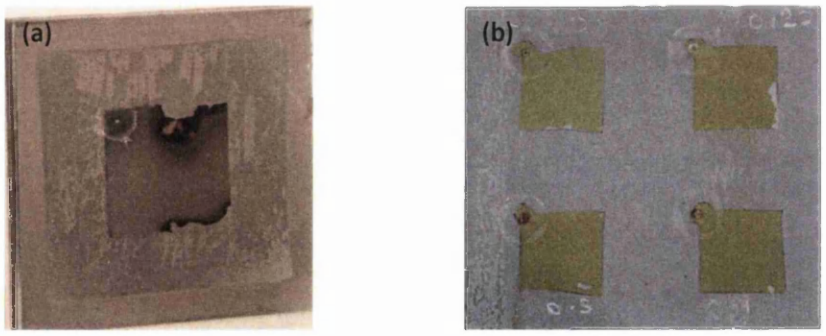

Figure 5.1: (a) UV-VIS observation cell (b) Time-lapse imaging cell

A simple three component DSC electrolyte, as described in Chapter 2, was used for all monitoring cells, with the addition of the additives 4-*tert*-butylpyridine (4-TBP), 1-

methylbenzimidazole (1-MBI) and 1, 3, 5-triazine (135T) for the corrosion inhibition study. The electrolyte formulation was further limited to simple chemical compounds, lithium Iodide (LiI) and iodine (I_2); in place of room temperature ionic liquids such 1-methyl-3-propylimidazolium iodide (PMII) in order to remove the complex interactions in more performance orientated DSC liquid electrolytes. Other commonly used performance enhancing compounds such as guanidinium thiocyanate were also avoided for the same reason.

5.3 *In situ* corrosion analysis

The initial study compares two monitoring and characterisation methods and assesses any degradation that occurs in the interaction of a basic three component iodine-based DSC electrolyte with a variety of metallic substrates. The techniques presented in this study provide a complimentary dataset to assess the accuracy of each. The metals tested have been previously listed in Table 5.1, with emphasis on iron based and other inexpensive bulk substrates, due to their common use as industrial construction materials.

5.3.1 DR/UV-Vis absorbance measurement

Initially, the DR/UV-VIS method was trialled using a simple iron substrate, time-lapse scans of a fresh corrosion cell were recorded, as shown in Figure 5.2a. This clearly shows that the absorbance of the cell decreases with time using the reduction in the initial peak value of 410nm, indicating a loss of triiodide as it is reduced by interaction with the metal substrate through Equation 5.2:

$$Fe + I_3^- \rightarrow Fe^{2+} + 3I^- \qquad (5.2)$$

This figure also illustrates the time dependant behaviour of the absorption spectra as the electrolyte interacts with the metal substrate. In comparison, the titanium substrate in Figure 5.2b shows little change over time; mainly due to a strongly bonded and quickly repaired oxide layer that forms on the substrate surface despite the attempted surface activation measures.

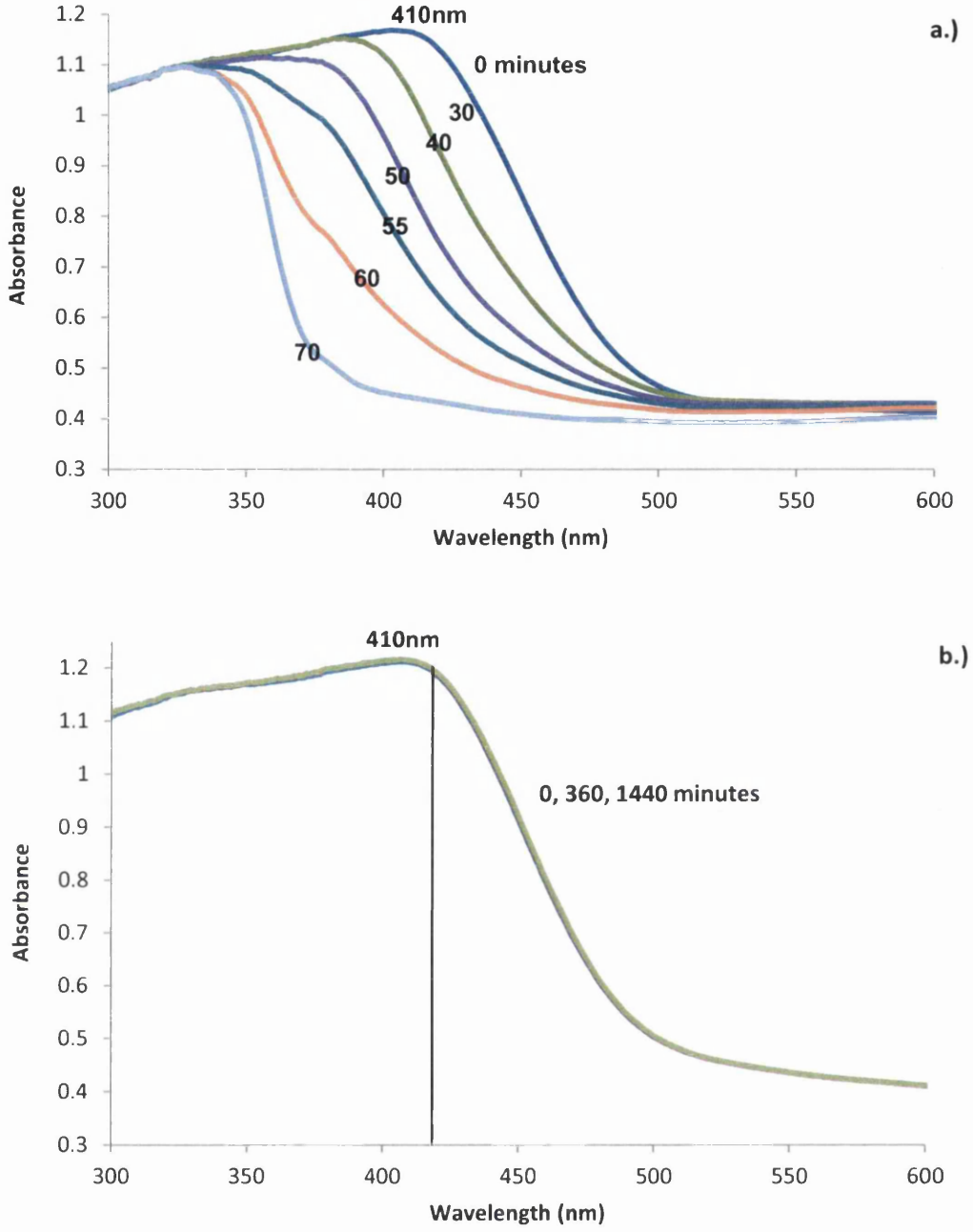

Figure 5.2: DR UV/Vis Absorbance spectra for I_3^- and for metal corrosion rate, using the reflectance setting for encapslated corrosion cells for substrates (a) Iron and (b) Titanium

The drawback to the DR UV/Vis method is that only a single sample can be run at any time, an analysis bottleneck that will increase the risk of low quality devices on a production line. Due to the long testing periods of up to 1000 hours required for a comprehensive study, this method is not viable for rapid large scale industrial analysis. Thus, an alternative was investigated using a similar time-lapse imaging technique as used previously for dye uptake analysis, where it was used to monitor the variation in average red/blue/green colour

change over a set time period [7]. The UV-VIS data can be compared with the average RGB analysis in order to assess the viability of the latter technique for the characterisation of cell degradation, Figure 5.3a.

5.3.2 RGB image analysis method

This method uses image analysis for the mass monitoring of corrosion cells with a $1cm^2$. Photographic observation and image analysis was used to isolate the variation in Red/Blue/Green (RGB) colours over time. As explained previously, observation cells were constructed and placed within a consistently lit environment and imaged every 5 minutes throughout the experimental study. The colour change is analysed by using the RGB data extracted from the images using the Sigma Scan Pro software. The data on average RGB in addition to the specific red, blue and green colour changes, was taken from the Sigma Scan Pro software package and plotted versus time, as seen in Figure 5.3. Here it was seen that there is a definate correlation between the change in measured DR-UV/VIS absorbance and the average RGB value measured through timelapse image analysis. The degradation was seen to occurs rapidly within a 2 hour period for both methods. The decrease in I_3^- is immediantly visible at the experiment start, ending in the complete disappearance of the I_3^- colour from the observation cell. The slight decrepency between the degredation times for each methods was believed to be the result of small differences in electrolyte volumes between cells. This is due to the difficulty in controlling the thickness of the 25µm Surlyn gasket spacer when using a compression and melting process to seal the cell. A larger volume of electrolyte will take a longer time to show the degradation of triiodide colour. Since the study by Toivola *et al* utilised much larger volumes of electrolyte than the estimated $0.015cm^3$ volumes used in this study and as a result this is thought to be the reason for the longer degredation time of 2 months reported in their study [1].

The RGB analysis method has a significant advantage over DR-UV/VIS characterisation as the progression of the corrosion caused electrolyte colour change is visible over the range acquired images – rather than concealed within the UV-VIS equipment while the reaction occurs. Furthermore, multiple samples can be analysed simultaneously, decreasing the time needed for a comprehensive study.

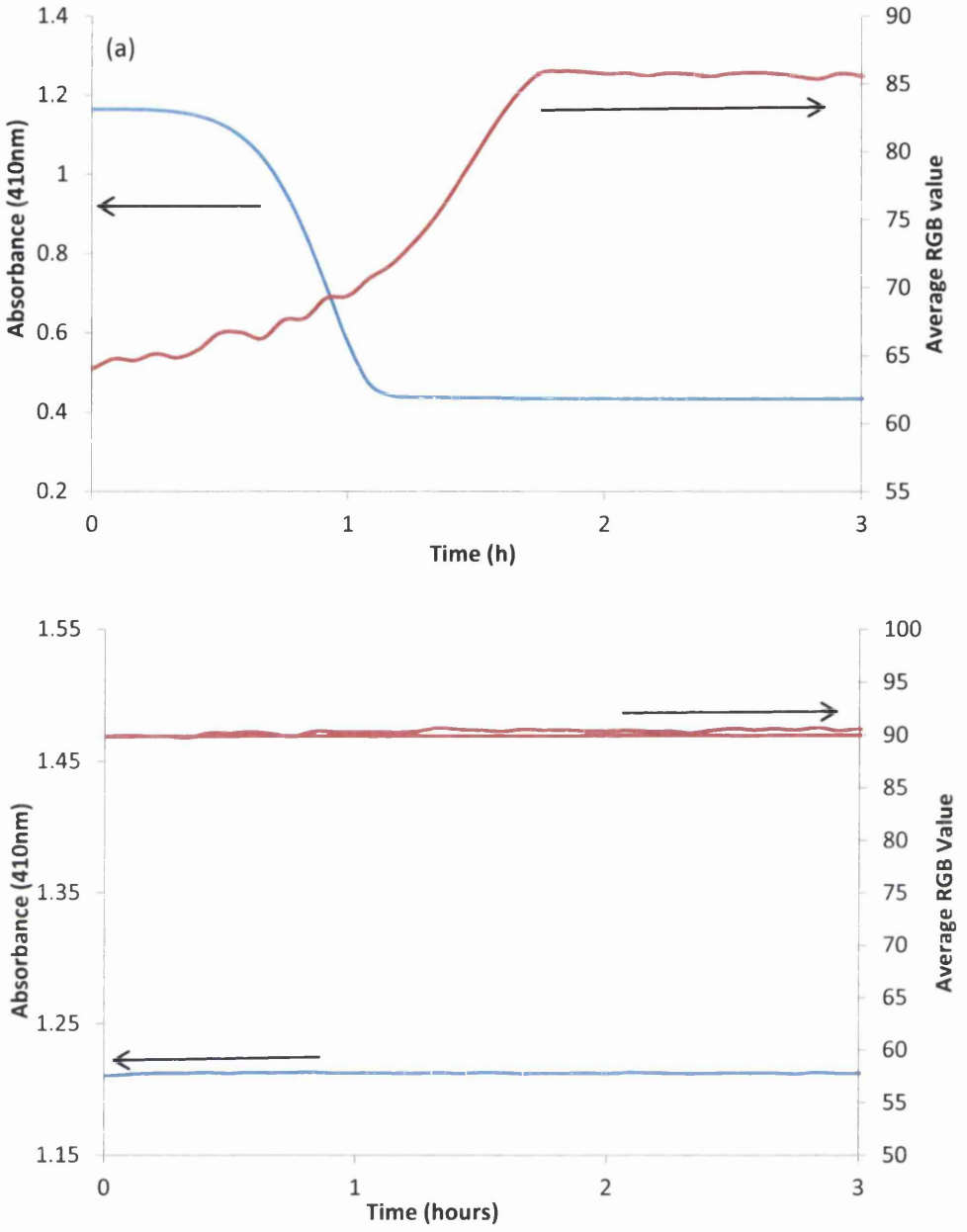

Figure 5.3: Change of I_3^- amount shown by decrease in absorbance or average colour intensity (RGB) over time using DR UV/Vis or time-lapse photography. (a) Iron (b) Titanium

The data presented in Figure 5.3 proves the viability of electrolyte colour change as an indicator of DSC device stability. In addition, the *in situ* monitoring of multiple samples results in a large quantity of data collected simultaneously, using a low cost camera set up rather than an expensive spectrophotometer, so multiple units may be purchased and used in place of one spectrometer. Furthermore, the photographic monitoring and image analysis process has the potential for quality control applications on a DSC production line. This wealth of data does have its drawbacks in that the Sigma Scan Pro software used for

the RBG analysis can only analyse a certain number of selected sites and the process has a large need for computing power.

Iron and titanium, the initial metals studied, are of major importance as they are used in both pure and alloy form as major industrial construction materials with potential for use in BIPV. The results strongly suggest that carbon steel and other iron based metals will be extremely susceptible to degradation in iodine based DSC electrolytes, which is in contradiction of previous studies of the stability of carbon steels metals in DSC electrolyte [1]. The study here showed that corrosion, evidenced by electrolyte decolourisation, is visible within two hours of electrolyte injection into the corrosion cell using iron substrate.

The visible change in electrolyte colour from yellow to colourless on the prepared iron substrate indicated a reduction in the triiodide concentration over the initial two hours of the testing period. In comparing the two analysis methods, the small variation in the data was attributed to the small differences in electrolyte volumes in each type of cell. This caused by variable compression under heating of the 25μm Surlyn polymer gaskets used for joining and sealing. The 25μm thickness was used to ensure the cell was sensitive to small changes in electrolyte composition. The difference in electrolyte volume should also be taken into account when comparing the results of this study, chiefly because the majority of these use bulk volumes of electrolyte in excess of what is used for thin layer DSC devices. Our volumes of electrolyte will be $0.0025m^2$ for 25μm Surlyn and $0.0050m^2$ volume of electrolyte for cells using 50μm thick Surlyn. Furthermore, there will be variation from differences in composition or surface finish that will affect the results obtained, though these were expected and minimised through careful sample selection and preparation of the metal surfaces. Finally, there will be slight variation in output of the light source needed for the photographic monitoring method which will cause minor fluctuations in the RGB values.

5.3.3 Metal corrosion study

This section of work uses photographic monitoring, coupled with image analysis to study a selection of industrial metals considered as substrates for DSC working electrode substrates. Table 5.2 summarises the performance of these metals when in contact with the three component iodide/triiodide electrolyte.

Table 5.2: Corrosion performance of metal substrates from RGB analysis (up to 1000hrs), "-" indicates no change over the study duration

Metal Type	Time to complete I_3^- removal (h)
Titanium	-
Iron 99.5%	2
Stainless steel (316L and 304)	-
Zinc 99.9%	0.03
Aluminium 99.0%	-
Aluminium 99.0 % surface activation	30
Aluminium 99.999% surface activation	~ 200
Nickel 99.98%	~ 65
Inconel (625)	-
Tungsten 99.95%	-
Molybdenum 99.9%	-
Chromium 99.95%	-

Many of the potential candidate materials for use as DSC substrates or as possible protective metallic coatings for iron based substrates were found to be vulnerable in the electrolyte. Aside from the pure iron substrate, the most vulnerable metals were found to be zinc and surface activated aluminium metal sheet of 99.0% purity. Ironically, these metals are typically used as protective coatings or cladding for iron-based structural applications. Zinc reacts rapidly with triiodide, as per Equation 5.3, giving a visible loss of colour from triiodide yellow to iodide clear. As a result the common galvanising method of corrosion and environmental protection will not be available for use in DSC cells containing the triiodide species.

$$Zn + I_3^- \rightarrow Zn^{2+} + 3I^- \qquad (5.3)$$

Briefly, in an encapsulation cell using zinc metal substrate, the electrolyte loses colour rapidly, with complete colour loss occurring within two minutes (0.03 hours) of electrolyte injection. This indicated the complete reduction of triiodide to iodide and therefore a loss

of electrolyte viability through a large reduction in charge carriers. This result complements that of Toivola *et al.* regarding the immersion of zinc in a large quantity of DSC electrolyte, where they reported degradation times for zinc coated carbon steel varying from 1 hour to 1 day [1]. The difference in timescales for the onset and completion of the corrosion action was considered to be due to the variation in electrolyte volumes. Thin layer cells will be more sensitive due to less triiodide ions per substrate surface area, so therefore giving an increased rate of reaction as the triiodide interacts with the zinc substrate.

More complex behaviour was observed when differently prepared aluminium substrate was exposed to the electrolyte. In none surface-activated 99.0%Al substrate, a negligible loss of triiodide was seen, indicating less aggressive interactions between the electrolyte and the substrate. However, on surface activation, both the 99.0%Al and highly pure 99.999%Al gave an increased degradation rate leading to the complete disappearance of triiodide. However, the timescale did vary with the purity of the metal substrate.

The non-activated sample surface consists of an unbroken alumina (Al_2O_3) layer that is known to be an effective barrier to interaction by aggressive species, protecting the metal from further oxidation by the triiodide species. The surface activation of Al through abrasion and polishing with Al_2O_3 powder removes the protective alumina layer and produces an active layer of aluminium metal. This was found to behave differently from the metal oxide covered substrate of as-received aluminium foil [11]. Equation 5.4 details the reaction between Al metal and triiodide, which leads to corrosion shown through the total loss of triiodide:

$$Al + I_3^- \rightarrow Al^{3+} + 3I^- \qquad (5.4)$$

The difference between the behaviour of surface treated and non-treated Al 99.0% substrate is illustrated clearly through the average RGB value taken from image analysis. On activation of the 99.0% Al metal surface, a colour change occurs over *ca.* 5 hours shifting the average RGB value from 160 to 190 indicating the removal of the yellow triiodide colour, Figure 5.4. The surface layer of Al_2O_3 is known to be *ca.* 5nm if air formed at ambient temperature and gives sufficient coverage to act as an efficient uniform corrosion barrier [12], inhibiting the interaction of the very reactive Al substrate with triiodide ions.

However, if the samples are subject to a surface treatment, the rate of degradation is then dependent on the purity, with the reduction of triiodide occurring 7x faster for low purity aluminium (99.0% Al) than for the higher purity 99.999% Al, see Table 5.2. The evidence

suggests that this increase was due to the greater density of impurities inherent in the 99.0%Al metal substrate, increasing the quantity of active sites where triiodide can be easily reduced. In pure aluminium, there are less impurities and defects, so the rate of degradation will be slower.

If aluminium is eventually used as a DSC substrate care must be taken to ensure the coverage and quality of the protective alumina layer before the device is constructed and that this continues throughout the manufacturing process, however this layer is also electrically insulating, so there must be a compromise between substrate protection and electrical conductivity that may require further corrosion prevention methods to be explored. This will potentially add time and cost, especially when using pre-rolled coiled sheet metal, which could cause damage to the surface layer.

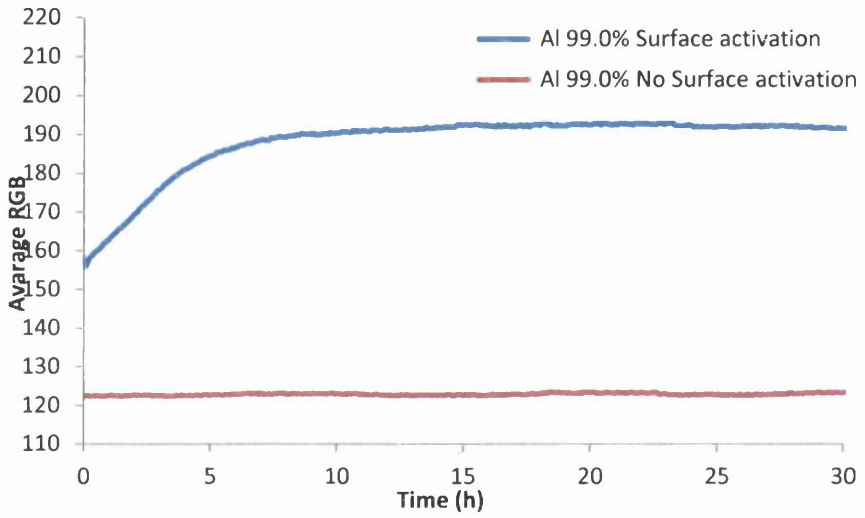

Figure 5.4: Difference in corrosion behaviour of surface activated and non-surface activated Al 99.0% substrate

Next, metals such as nickel, chromium and nickel-chromium alloys (Inconel 625) along with molybdenum, tungsten and stainless steel are analysed due to their industrial potential. The nickel samples showed complete degradation to colourless in *ca.* 65 hours, a direct contradiction to the previous study by Ma *et al.*, that reported the stability of nickel in I_3^-/I^- electrolyte [13]. Comparison of other reports has revealed a clear difference in behaviour when using bulk or thin layer electrolyte quantities [1]. As previously mentioned, the quantity of triiodide per metal surface area increases in thin layer cells and therefore will be much more sensitive to changes in internal conditions and variations in the electrolyte. A further study on large scale DSC devices by Okada *et al.* indicated that sputter deposited nickel grids were resistant to corrosion to greater than 1600hrs [14]. Since our study

showed that bulk nickel interacts with the triiodide causing colour loss and so cell failure within 65 hours, it is thus suggested that the high purity structure of the sputtered materials increases its corrosion resistance. Nickel-Chrome based (Ni-Cr) alloys, such as the Inconel 625 used in this study, exhibited good performance under exposure to the electrolyte, remaining stable for over 1000 hours. This remains comparable with previous literature demonstrating the manufacture of DSCs using Ni-Cr alloys as the substrate [2], [15]. Molybdenum, Tungsten, Chromium and Stainless Steel are already well known for their resistance to several forms of corrosion in aggressive operating environments, such as those found in turbines and power stations [16]. Their resistance is known to be due to the formation of the strong oxide layers such as WO_3, Cr_2O_3 in the case of Tungsten and Chromium. Molybdenum has a corrosion resistance similar to Tungsten. However, this was reported to come from the inherent un-reactivity of the material rather than the formation of a strongly bonded oxide layer. The work presented in this section excitingly confirms the stability of Molybdenum, Tungsten and Chromium in DSC iodide/triiodide electrolyte for up to 1000 hours, a study that has not previously been undertaken.

Negligible change was seen in the average RGB for Stainless Steel, which compares well to DR-UV/VIS analysis and previous reports for stainless steel DSC devices [2], [4], [17]–[21]. A caveat to the resistance of these materials was reported by Miettunen *et al.*, showing that the Stainless Steel used in their study exhibited corrosion in the form of surface pits and EDX analysis indicated the presence of a corrosion residue comprising of iodine and stainless steel [4], [22].

One of the most important insights that came from this first study was the need to test substrates in a simulated cell environment, rather than with bulk quantities of electrolyte, *á la* Toivola *et al* [1]. Using thin layers and small volume study better reflects the actual state of the DSC cell operating environment. In addition, the high ratio of metal surface area to electrolyte species means that the cell is very sensitive to changes in internal conditions. This should lead to a clearly visible interaction between components, in this case exhibited by the yellow to clear colour change. The next study moves to using 50µm Surlyn gasket rather than the 25µm used up to this point, in order to better match the architecture of the proposed sheet DSCs that will use 50µm Surlyn to ensure clearance between electrodes when the cell is flexed. To ensure comparability between studies, 50µm Surlyn iron substrate cells were compared with a cell using 25µm Surlyn, Figure 5.5. The small difference exhibited here can be related to the previously mentioned variation between the DR-UV/VIS and RGB comparison observation cells, confirming that the difference in

degradation time can be related to the change in electrolyte volume. Once the difference in behaviour was compared, the RGB analysis method could then be transferred between the different cell thicknesses uses in this study.

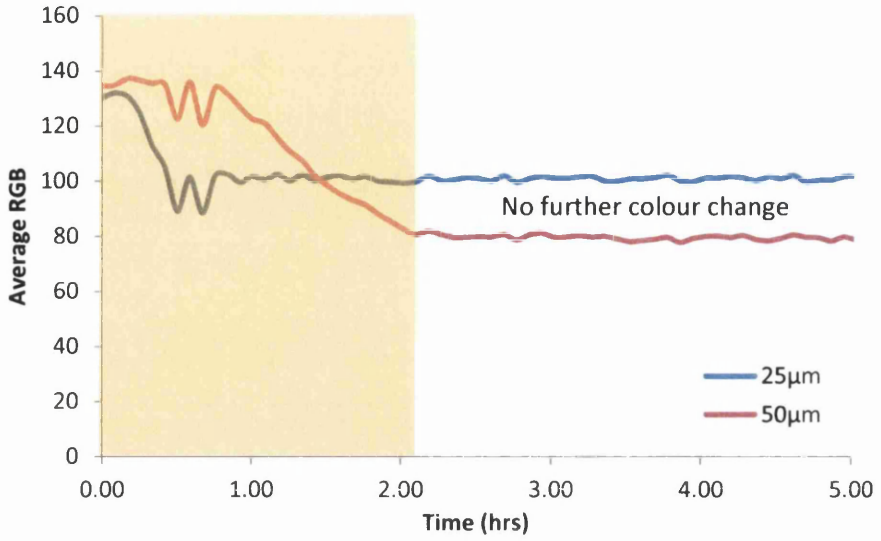

Figure 5.5: Comparison between RGB data for 25µm and 50 µm Surlyn corrosion cells on iron substrate adjusted for background average RGB data. Yellow area denotes yellow to colourless colour transition zone

A major point of comparison between the electrolyte used in this study and that of those used in the literature is the varying degrees of electrolyte complexity. Common literature electrolytes include compounds such as 4-*tert.*-butylpyridine (4-TBP), guanidine thiocyanate or 1-methyl-3-propylimidazolium iodide (PMII) an ionic liquid as one of the primary chemical constituents. To establish if increasing the electrolyte complexity could change cell corrosion processes, 4-TBP was initially added to a test cell in order to determine the effects, if any, of this addition. The 4-TBP compound was used for trial due to its common inclusion as a performance enhancer in literature since the inception of the DSC device in the early 1990s [23]. It was discovered that the addition of 4-TBP was able to give a measure of corrosion protection for certain metal substrates, a result that is tested further in Section 5.4.

5.4 Electrolyte additions for corrosion inhibition

Typically, DSC electrolytes usually consist of several other components to improve performance, such as guanidine thiocyanate [24], [25] and compounds such as PMII in place of iodine and for use in non-solvent containing electrolytes [26]. Other additives used are compounds known as nitrogen-containing heterocyclics (NHC's), the most commonly known is 4-*tert*.-butylpyridine (4-TBP). These are used as performance enhancers and act through adsorption onto uncovered TiO_2 sites and thus inhibit the back electron transfer [27]. Further to this, these compounds shift the conduction band to a more negative value, enhancing cell V_{oc} through the widening of the gap between the electrolyte redox potential (V_{red}) and the TiO_2 flatband potential (V_{fb}) [28], [29].

In order to study whether the addition of further chemical components to the electrolyte had an effect on the degradation behaviour of metal substrates, a corrosion cell containing electrolyte with 0.5M 4-TBP additive was compared against a simple three component DSC electrolyte (LiI, I_2 and 3-MPN as the solvent), the results obtained are presented as average RGB *vs.* time in Figure 5.6.

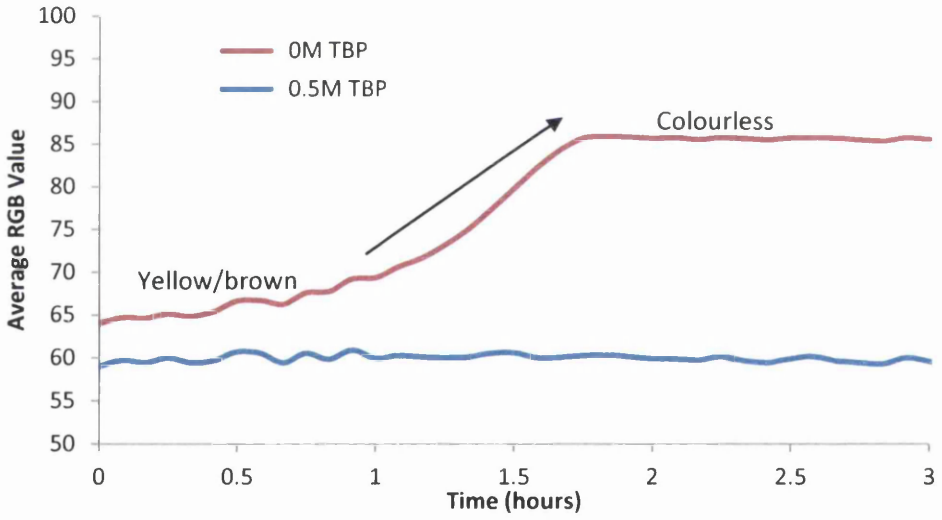

Figure 5.6: Change in average RGB value with time on iron substrate, the electrolyte used was 0.1M LiI, 0.05M I_2 in 3-MPN on iron substrate, with as test quantity of 0.5M 4-tBP added to a cell

It should be noted that the 0.5M concentration of 4-TBP is typical in DSC literature, hence the choice of concentration as an example additive in this particular case. The change in corrosion behaviour was quite revealing. The addition of 0.5M TBP to the electrolyte visibly inhibited cell degradation, preventing the reduction of the triiodide through interaction

with the metal substrate over the measured time period. This result could also offer an explanation of the different behaviour of substrates in previous corrosion studies [1], [13].

The report by Kanta *et al.*, supports our findings by stating that the presence of 4-TBP was instrumental in preventing the degradation of the stainless steel 304 working electrode in their electrochemical study [30].

The pyridine based additive 4-*tert*-butylpyridine (4-TBP) is not the only nitrogen containing heterocyclic compound (NHC) used to increase DSC performance. Several key studies produced by Kusama *et al.* have detailed many different types and structures of additive compounds such as NHC and compared their effect on DSC performance [31]–[35]. Currently, NHC's are used simply to boost performance through the inhibition of recombination and through other synergistic electrochemical effects on DSC components. Heterocyclic compounds such as 4-TBP and other pyridines are previously known as excellent industrial corrosion inhibitors and as a result it is expected that our selected compounds will perform a similar function in DSC cells as for industrial applications. In a DSC device, there is a further requirement to retain the performance enhancing ability of these chemicals and also allow them to navigate the mesoporous network of the TiO_2 in order to reach the metal substrate. An analysis of previous studies has led to three different simple structures being chosen for further study; an alkyl pyridine, a benzimidazole and a simple triazine. This are exhibited in Figure 5.7 in the form of 4-*tert*-butylpyridine (4-TBP), 1-methylbenzimidazole (1-MBI) and 1, 3, 5-triazine (135T). It was thought that the difference in carbon skeleton and the number of nitrogen atoms would vary the corrosion inhibition behaviour of these small compounds to allow the inhibition effect to be further tailored.

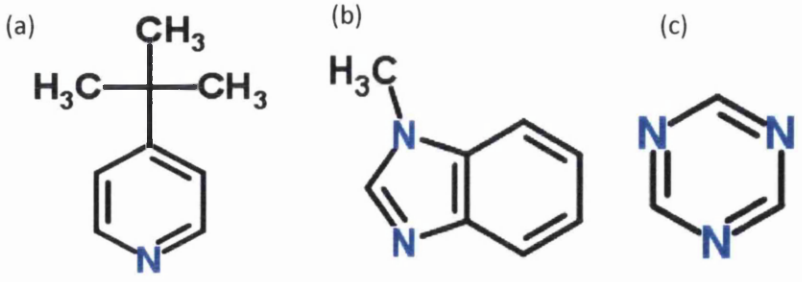

Figure 5.7: Structure of NHC compounds used in this study. (a) 4-TBP (b) 1-MBI (c) 1,3,5-T

This next section investigates the effect of varying the concentrations of these three NHC compounds to assess the impact on their corrosion inhibition ability on the industrial sheet metals previously listed in Table 5.1.

5.4.1 Industrial Metal Corrosion Inhibition

This next section utilises the, now characterised, RGB analysis method on a wider range of industrial metal substrates. Figure 5.8 to Figure 5.18 summarise the stability of metallic substrate corrosion cells containing three different additives, 4-TBP, 1-MBI and 135-T in the electrolyte. By monitoring the colour change over 1000 hours, the interaction between the triiodide and the metal substrate can be observed and the effect of the differing types and concentration of NHC inhibitor can be characterised as a function of time. On each substrate, a control cell was maintained containing no additives to better compare between the effects of each compound on different substrates. The other concentrations chosen were 0.25M, 0.5M and 1M to assess the optimum quantity for inhibition, while ensuring no chemical wastage.

Figure 5.8 details the inhibition effect of a variety of 4-TBP concentrations in the electrolyte formulation over the metal substrates observed. As expected, the titanium and stainless steel substrates were completely resistant to corrosion, showing no degradation of the cell throughout the experiment regardless of 4-TBP inclusion. Both metals have strongly bonded oxide layers that passivate the metal surface and reduce the exposure of the metal to the aggressive triiodide species. The addition of varying concentrations of NHC will only serve to enhance degradation resistance in case of surface damage.

The stainless steel and titanium substrates were both reported in literature and found in this study to be corrosion resistant, with the control cells showing no discolouration or corrosion products. However, the nickel and iron substrates exhibited much different behaviour. As shown in Figure 5.6 and Table 5.2, the iron substrates degraded quickly when in the control cell where no additives were included. However, the addition of 4-TBP prolongs the lifetime of the yellow triiodide colour, suggesting an increasing corrosion inhibition effect.

In the nickel control cell, the triiodide colour lasted only 22 hours, giving way to a red colouration, thought to be a nickel (II) iodide compound. The addition of 0.25M 4-TBP increases the longevity of the triiodide to 35 hours, after which the electrolyte discolours to brown/yellow. The electrolyte lifetime is raised further to 110 hours when the concentration of 4-TBP is doubled to 0.5M, thus indicating a threshold concentration that will halt the triiodide degradation. At the maximum tested concentration of 1M, the nickel cell remains stable up to the full 1000 hours observed. In the iron cell, a concentration of 0.25M 4-TBP increases the lifetime to 137 hours, but maximum protection can be achieved

if the concentration is raised to 0.5M and 1M, where the cell remained stable over and above the 1000 hours duration of this study.

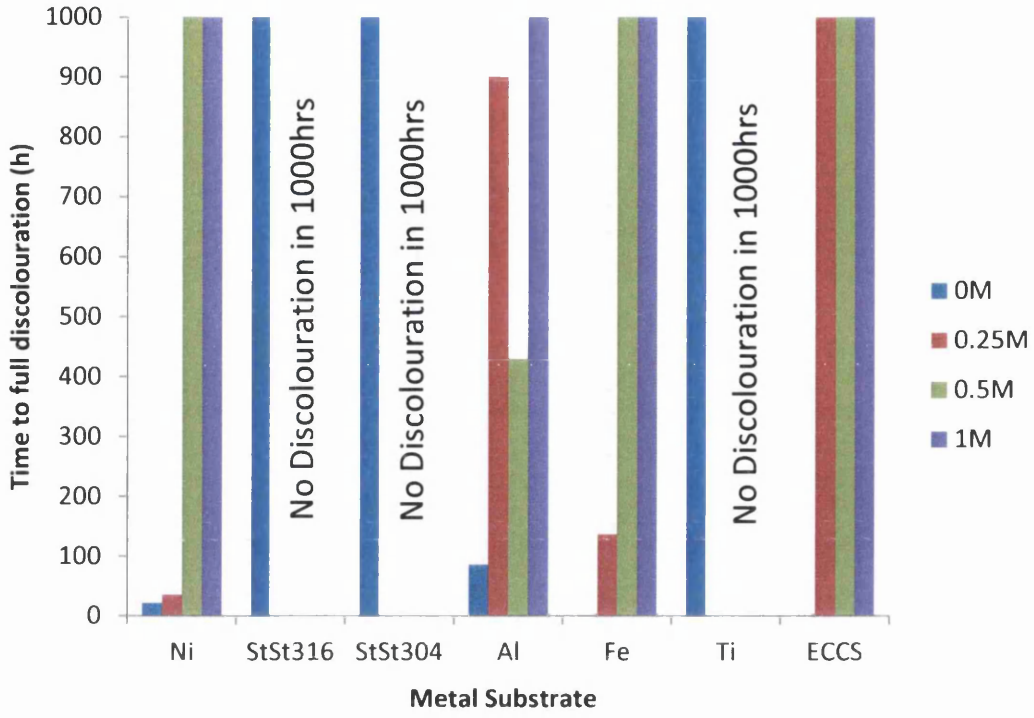

Figure 5.8: Time to complete cell degradation in iodide/triiodide electrolyte containing quantities of 4-TBP. Sections that reach 1000hrs indicate no discolouration throughout the duration of this experiment, and are used if there is varying times on one substrate

As reported in the first section of this study, certain grades of aluminium react strongly to the action of triiodide. The removal of the Al_2O_3 layer through abrasion and the activation of the Al surface facilitate the corrosion of the normally resistant Al substrate. The control cell containing no 4-TBP degrades fully in 88 hours due to the rapid and unhindered reduction of triiodide at the very reactive metal surface. In comparison, the cell containing 1M 4-TBP retains the triiodide colour, at an RGB value of *ca.* 140, throughout the 1000 hours observation time.

However, it is the 0.25M and 0.5M concentrations that given unexpected results. The 0.25M concentration shows a much greater inhibition effect than 0.5M, with full degradation occurring at near 1000 hours, though as Figure 5.9 shows, the initiation of degradation starts at *ca.* 50 hours and continues at a constant rate. The 0.5M concentration shows degradation to be complete in 500 hours. The degradation in this case starts rapidly, as shown by the steep gradient, compared to the shallow slope of the 0.25M cell. The decreasing rate is suggested to be due to the increased effect of the 4-TBP

on the reduced quantity of triiodide. Unfortunately, the inhibition effect is still not enough and the cell once more degrades to clear. The unexpected degradation pattern was suspected to be due to partial oxidation or a variation in activation of the Al surface, where the preparation step did not fully activate the surface around the 0.25M cell. Despite the maximum concentration of 1M showing high resistance to degradation throughout the study, there is evidence of an increase in RGB at 900 hours. This leads to the conclusion that the Al substrate remains vulnerable to attack, though at a much reduced rate. It should be noted that the less pure 99.0%Al was used rather than the ultra-pure 99.99%Al, as it is a more feasible substrate for use in mass processing, mainly due to its reduced cost, and greater availability. This reduced purity will result in more sites vulnerable to attack by the triiodide species and contribute to the corrosion susceptibility of the substrate.

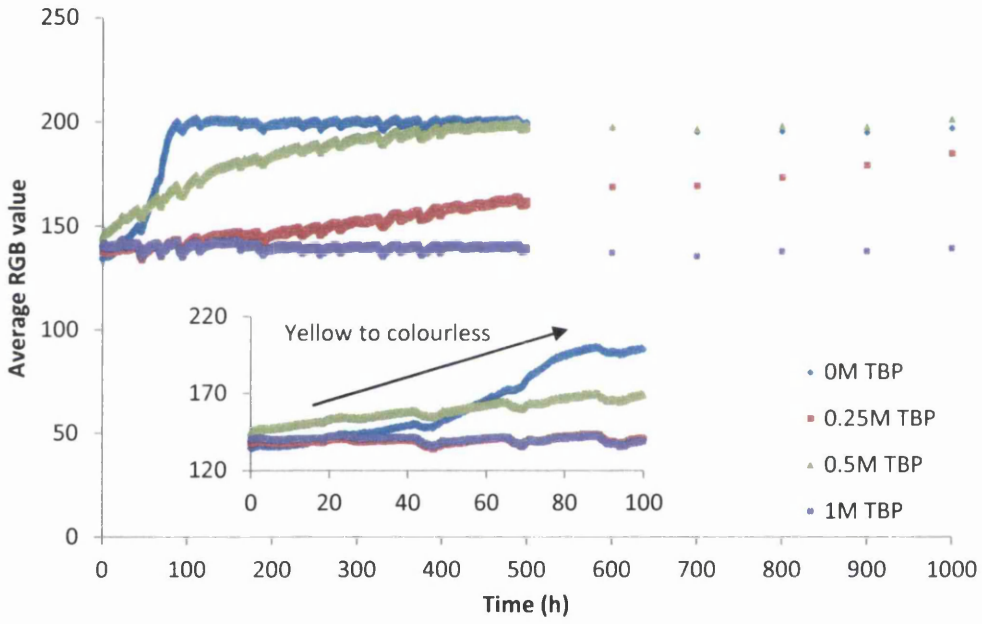

Figure 5.9: Variation in 99.0%Al cell stability with electrolyte containing different 4-TBP quantities. Inset graph showing the first 100 hours observation

An additional metal considered as a viable DSC substrate was electrolytically chromium coated steel (ECCS), Figure 5.10. This simply consists of a low carbon steel sheet that has been electrolytically coated with chromium and chromium oxide, the outer coating is hydrated chromium oxide and the inner layer consists of chromium metal [36]. The study indicated that the chromium/chromium oxide coating by itself was not enough to resist the aggressive triiodide-substrate interaction, with the ECCS control cell showing complete colour loss after 1.92 hours. This was unexpected due to the high ability of Chromium to resist attack previously found for chromium metal, Table 5.2. The fluctuations in the

average RGB on this figure are due to changes in the light intensity from the light sources used, and appear due to the time lapse nature of the study.

Following this finding, the vulnerability of ECCS was suggested to be due to defects in the electrolytic chromium coating that will allow the triiodide to access the vulnerable low carbon steel substrate. If this substrate is also subjected to similar surface preparation methods as Al, this will strip the protective layer from the metal and simply leave low carbon steel, which is known from literature to be very susceptible to attack and resulting in rapid degradation of the triiodide colour [1].

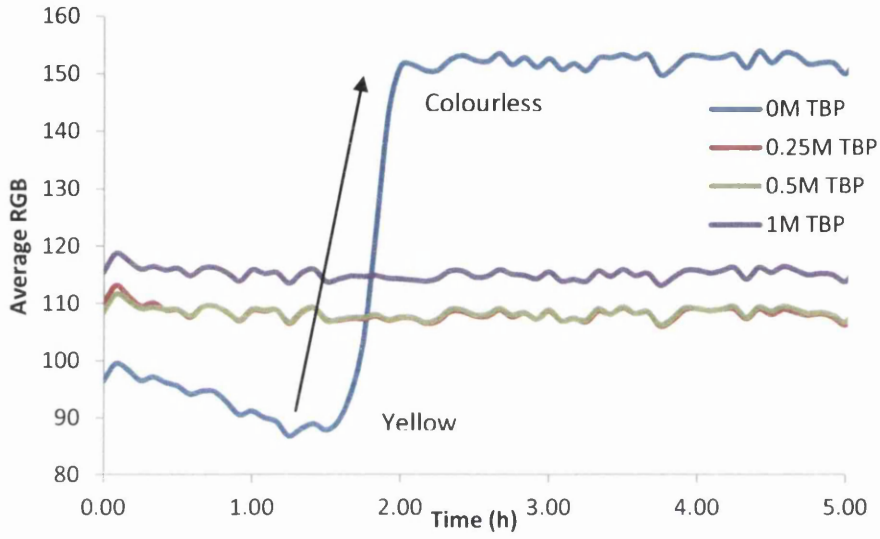

Figure 5.10: Initial 150 hours graph showing the average RGB vs. time for an ECCS substrate corrosion cell

However, once the 4-TBP was added in concentrations as low as 0.25M, the stability of the substrate increased dramatically, showing no colour degradation in the 1000 hours observation time. This was believed to be due to the blocking action of 4-TBP on exposed active sites where the chromium coating was damaged or not continuous. A physical block will stop triiodide from interacting with the carbon steel substrate base of ECCS and ensure that degradation of the triiodide colour does not occur.

5.5 1-methylbenzimidazole (1-MBI)

The 4-TBP compound is not the only additive used in the pursuit of higher DSC performance, 1-methylbenzimidazole (1-MBI) has also been used as a performance enhancer for the improvement of dye solar cell open circuit voltage (V_{oc}) through the suppression of the dark current and the movement of the flat band potential (V_{fb}) [37], [38]. Figure 5.11 summarises the effect this additive has on the longevity of the corrosion cells

on the selection of metal substrates used in this study. As previously reported in literature and reinforced through this study, titanium and stainless steel of 316L and 304 grades prove resistant to aggressive attack by the triiodide species in the control cell, which was expected as they are specifically tailored to be resistant to corrosion in aggressive environments, such as acidic conditions.

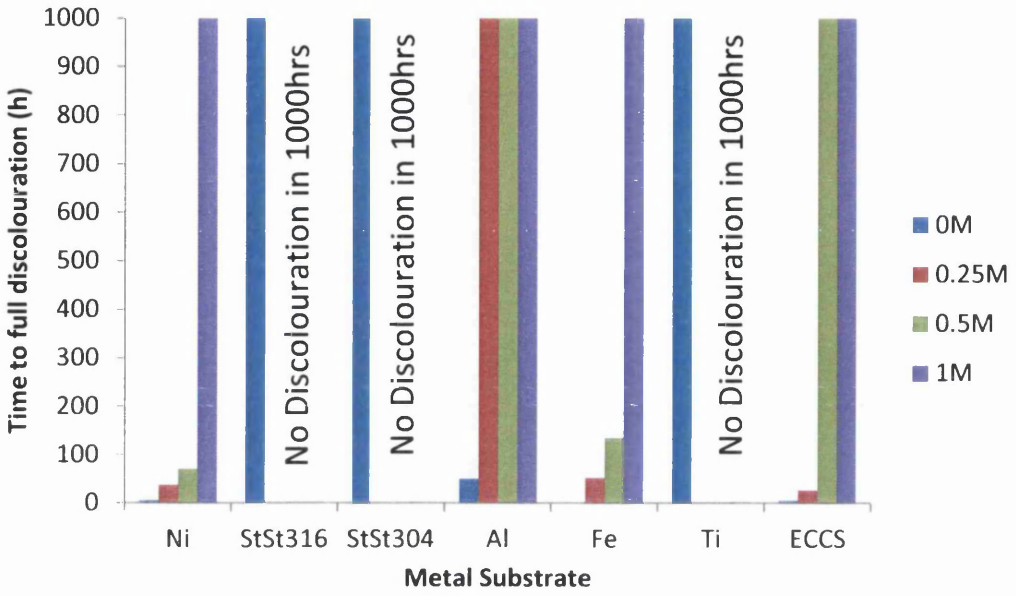

Figure 5.11: Stability of corrosion cells containing 1-MBI in the electrolyte at varying concentrations

The nickel substrate in contact with electrolyte containing 1-MBI behaves in a similar manner to that in the previous section on 4-TBP. The control cell quickly changes colour, transitioning from a value of *ca.* 120 for the yellow triiodide, to red at *ca.* 40, Figure 5.12. It should also be stressed that this is very different from the expected and conventional yellow to colourless reaction seen for the other metal observation cells.

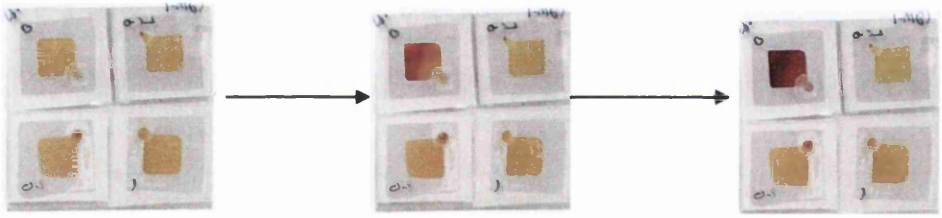

Figure 5.12: Progression of cell degradation for Ni substrate with electrolyte containing 1-MBI. Time progression is: 0hrs, 2.5hrs, 5hrs. Clockwise from top left, the concentrations are 0M, 0.25M, 0.5M and 1M in each cell.

The 0.25M concentration degrades over *ca.* 30 hours which matches the 4-TBP result. However, a yellow tint was observed to remain in the cell, indicating that there may be some remaining triiodide. It is possible this simply represents the white/cream colour of

the 3-MPN solvent containing corrosion products. The 0.5M 1-MBI containing cell degrades completely too colourless in 68 hours, again showing the conventional yellow-colourless transformation rather than the yellow-red transition of the nickel control cell. The 1M concentration shows the complete cessation of cell degradation for the 1000 hours observation time used in this study. The slight negative shift in the average RGB for 1M over time, Figure 5.13, is thought to be an indicator of electrolyte – NHC complex formation due to the large concentration of NHC molecules in the cell.

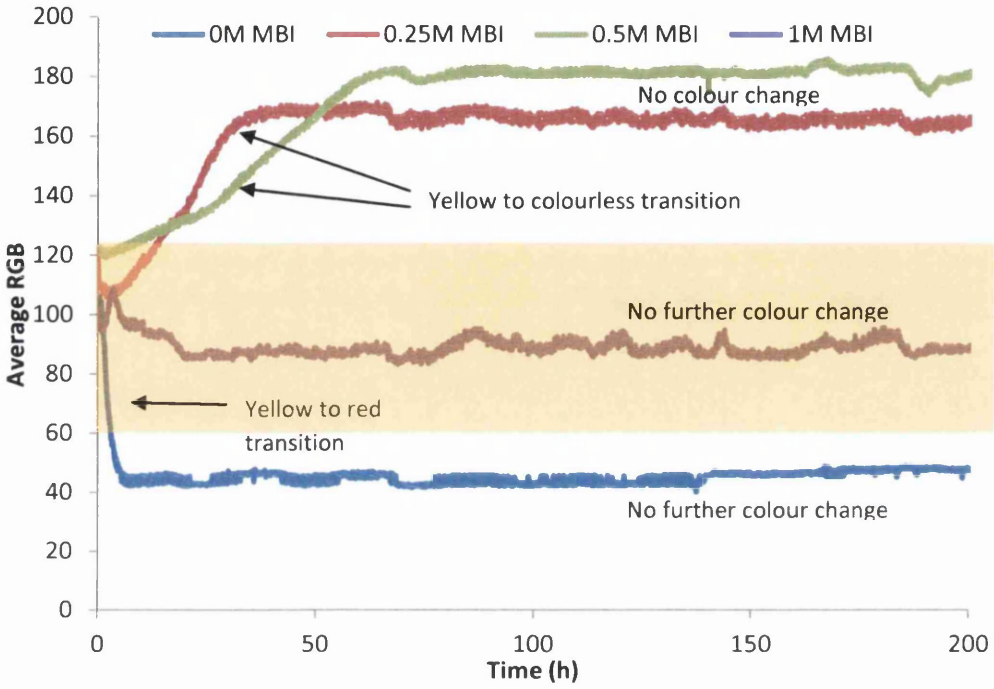

Figure 5.13: Degradation of Nickel substrate over time in electrolyte containing 1-MBI, shown by change in RGB value; Yellow shading indicates area of initial triiodide colour presence

The RGB value at the experiment start remains the range 100-120, the variety due to small differences in the metal surface and small variations in electrolyte volume between cells. As the experiment progresses, the disparity in values widen as degradation occurs. If it is indeed the triiodide attacking the Ni substrate then the inhibitor will prohibit the movement of the species toward the metal surface; it is also known that some NHC molecules are able to form a complex with triiodide, therefore it was thought something similar could be occurring here. The unusual red transformation of the 0M control cell is believed to be due to the formation of nickel(II) iodide, which is believed to occur through bonding with iodide in the electrolyte rather than the triiodide. This is a possible explanation, though it has not yet been explored fully.

Nonetheless, the end result is that the 0M, 0.25M and 0.5M are discoloured, indicating the degradation of the cell. The 0M cell also shows a green residue near the electrolyte injection hole after 200 hours, an indication of nickel oxide formation following cell degradation, Figure 5.14.

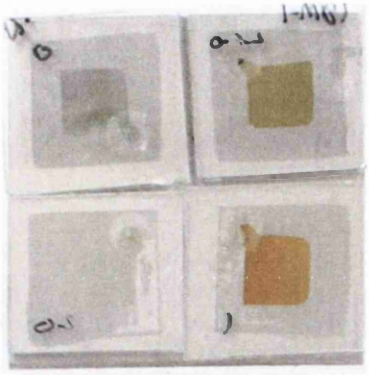

Figure 5.14: Nickel substrate observation cell after 200 hours; Clockwise from top left cell: 0M, 0.25M, 0.5M, 1M

The next substrate analysed was iron, which shows an almost exponential improvement in corrosion resistance as the 1-MBI additive concentration is increased. The 0.25M concentration remains stable for *ca.* 20 hours, before slowly degrading to colourless at 52 hours to match the final RGB value of the 0M control cell at 170. The 0.5M 1-MBI concentration typically used in DSC electrolytes slows cell degradation up to *ca.* 150 hours, after which it fails fully. This is in contrast to the effect of 0.5M 4-TBP on iron which extends the lifetime up to 1000 hours. The cell containing 1M concentration remains at an RGB value of 120 throughout the experimental time period, indicating no degradation has occurred. The iron substrate seems to exhibit the clearest response to the addition of the NHC compounds, where the increase additive concentration ensures full coverage of the metal substrate from the triiodide. It is believed that this inhibition mechanism functions in parallel to the complexation of the 1-MBI and triiodide species in a manner similar to 4-TBP [38]. However, a recent study by Hansen *et al.* clearly stated that no interaction was observed when 4-TBP and triiodide were mixed [39], this report has serious implications for the work here, as it negates one of the possible routes for the inhibition of cell degradation that was thought to exist.

As previously reported, the behaviour of the aluminium substrate depends on metal purity and surface finish. Compared with the previous inhibitor, 4-TBP, all concentrations of 1MBI showed increased stability. An issue that should be addressed is the discrepancy between control cells containing no additives on each Al substrate. This was due to the varying

metal surface that is present following preparation and cell construction, as the Al surface will oxidise quickly when exposed to air and later heat during cell sealing. As a result the control cell will have variable surface layer protection due to different levels of surface oxide coverage at the time of electrolyte injection. In this case, the control cell degrades in 45 hours, a much shorter period than seen for the 4-TBP control cell containing the iodide and triiodide species but no additives. The response from the three concentrations of 1MBI is remarkably similar, with the yellow triiodide colour fading to colourless in a similar timeframe of 176 hours. All these cells leave a purple/brown residue in place in the cell which, though currently unanalysed, is thought to be aluminium iodide. What is interesting about the 0.25M response is that by the half way test period of 500 hours, the yellow colour has returned, leaving only a few of the supposed aluminium iodide purple deposits. The 0.5M and 1M concentration cells however, remain clear with deposits within the cell, Figure 5.15.

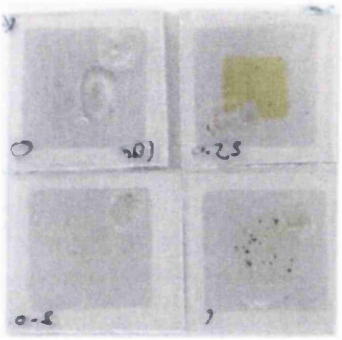

Figure 5.15: Aluminium substrate after 500 hours in contact with electrolyte and 1-MBI. Left to right and from top and bottom, the cells contain 0M, 0.25M, 0.5M and 1M of 1-MBI. Electrolyte contains LiI, I_2 in 3-MPN

In order to characterise how much protection the aluminium oxide layer will give the metal substrate in these observation cells, several identical observation cells were processed, only without the application of the surface activation method used previously in this study. Figure 5.16 illustrates that not even the control cell degraded after 1000 hours if the oxide layer remained in place, which contrasts strongly with the result shown in Figure 5.15 where all cells have degraded to colourless, with the exception of 0.25M. The exception in Figure 5.16 was the 0.5M concentration cell, which exhibited a loss in colour after 500 hours, and the formation of small purple/brown precipitates similar to those found in the 0.25M cell, Figure 5.15. It is thought these precipitates form where there is damage to the aluminium oxide layer that was not visible during the initial substrate preparation, allowing the reaction of the electrolyte species with the vulnerable aluminium metal.

So the question was thus, "Why use inhibitors in the first place?" The presence of the NHC is designed to be twofold in full DSCs, as performance enhancers first, and then as a corrosion inhibitor when required. Thus, passivated aluminium with an unbroken alumina layer is protected from the aggressiveness of the triiodide species. As a comparison of Figure 5.16 and Figure 5.17 show, surface activated aluminium is too reactive for even 1M of 4-TBP or 1-MBI to successfully inhibit for 1000 hours. With Figure 5.17 showing degradation of the colour of the triiodide and the substrate surface exposed to the electrolyte within the cell.

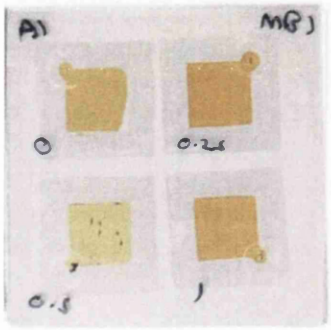

Figure 5.16: Aluminium substrate without surface treatment, in contact with electrolyte containing 1-MBI after 500 hours; Left-right and top to bottom, the 1MBI concentrations are 0M, 0.25M, 0.5M and 1M

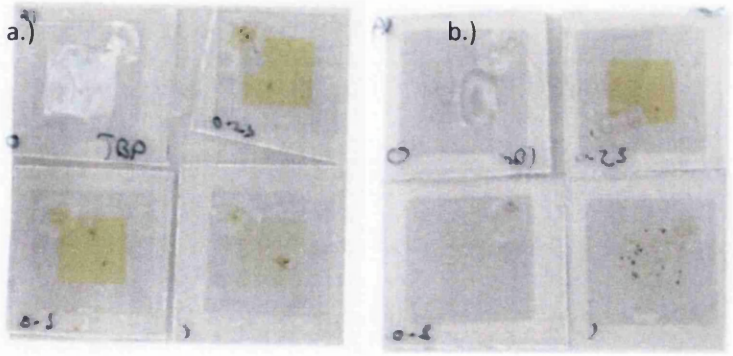

Figure 5.17: Surface activated Al in contact with electrolyte containing (a) 4-TBP and (b) 1-MBI after 500 hours; Left-right and top to bottom, the 1MBI concentrations are 0M, 0.25M, 0.5M and 1M for both cells

The 0.25M concentration of 1-MBI only increases the triiodide lifetime to 27 hours, before complete colour loss occurs. As the concentration is increased to 0.5M and above, the lifetime was seen to match the equivalent 4-TBP concentrations, showing no discolouration for the full 1000 hour observation time.

5.6 1, 3, 5-triazine (135T)

The final additive studied in this work is 1,3,5-triazine (135T or *s*-triazine), this is the least understood of the compounds selected for this study and despite the advantages to performance reported by Kusama *et al.,* 135T has not been widely used for DSC devices at this time [10]. Its performance as a corrosion inhibitor for industrial metals is summarised in Figure 5.18.

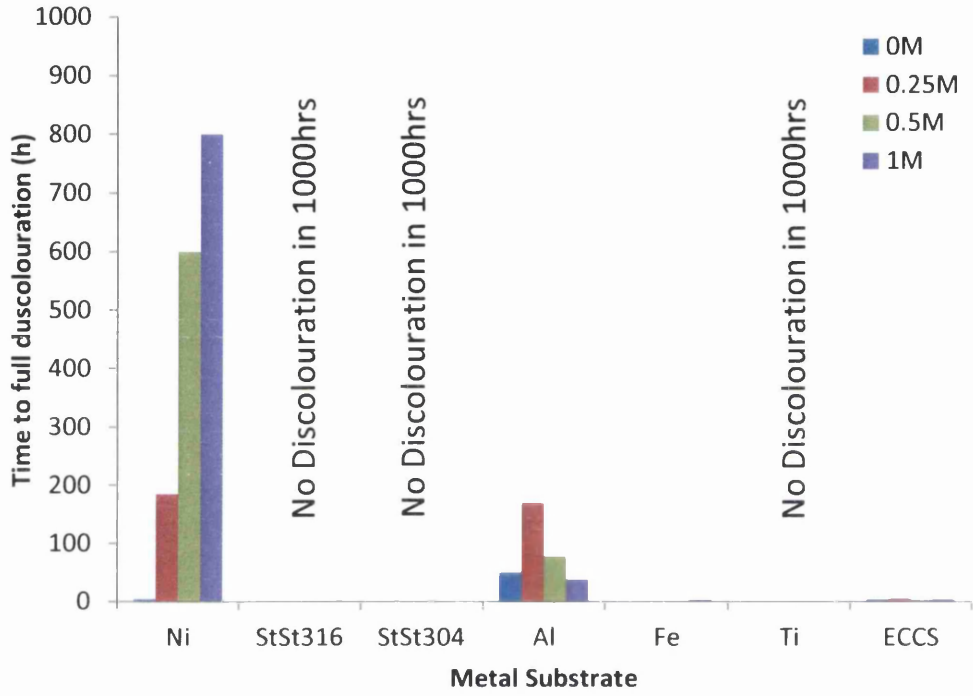

Figure 5.18: Stability of corrosion cells containing 1,3,5T in the electrolyte at varying concentrations

When using 135T, the nickel substrate showed increased longevity at 0.25M concentration compared with 1-MBI or 4-TBP. However, even when the concentration is increased to 0.5M or 1M, the maximum lifetime of the triiodide colour is 600 and 800 hours respectively. Surface activated 99.0%Al, the other vulnerable metal tested, shows a variable results set that did not conform to the expected relationship of increasing corrosion inhibition with concentration. The degradation of both the control and 1M additive containing cells occurs within 5 hours, an unexpected result for the 1M concentration in particular. The 0.25M and 0.5M concentrations show a complete loss of colour at 170 and 78 hours respectively. Since the result for aluminium did not fit the predicted trend, further notice was taken of the sample condition at several points throughout the study, as there may be an issue with the surface uniformity. These images taken throughout the experiment show areas of complete discolouration, surrounded by the yellow presence of triiodide, as illustrated in Figure 5.19.

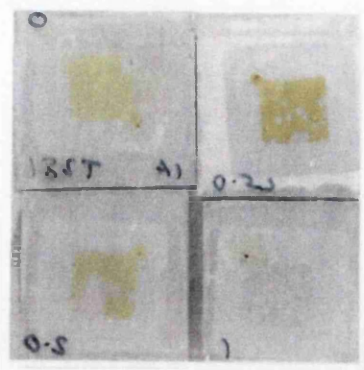

Figure 5.19: Observational analysis of Al metal samples with 135T additive present in the electrolyte. ; Left-right and top to bottom, the 135T concentrations are 0M, 0.25M, 0.5M and 1M

Once the condition of the samples was ascertained through visual inspection, the RGB changes became easier to understand, Figure 5.20. The slow change in average RGB colour is due to the inconsistent nature of the degradation over the $1cm^2$ cell area. All the observed cells lost much of the triiodide yellow in the initial 5 hours of interaction, with RGB values from 140-170 representing the pale yellow colour that remained after the majority of the triiodide reacted with the substrate.

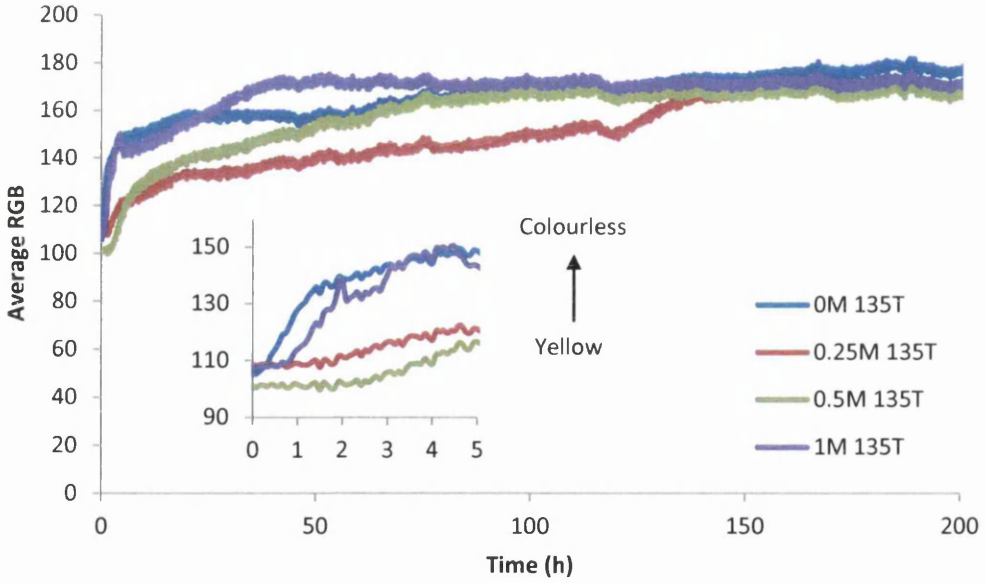

Figure 5.20: Average RGB vs. time for Al substrate exposed to triiodide/iodide electrolyte containing different concentrations of 135T (0-200hours); Inset showing the first 5 hours of degredation

After 200 hours this remnant continues to fade until by 1000 hours the cells are clear, Figure 5. The remaining slight cream colouration is from the solvent and the slight remnants of iodine or iodide compounds in solution.

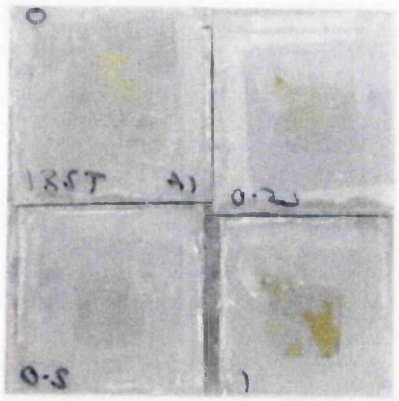

Figure 5.21: 99.0%Al substrate in contact with electrolyte containing 1,3,5T after 1000 hours; Left-right and top to bottom, the concentration of 135T is 0M, 0.25M, 0.5M, 1M

Similarly, 135T shows little effect on the degradation of the iron and ECCS substrate cells. On the iron cells, a rapid colour change was observed in the cells containing 0M additive and 0.25M 135T, where the triiodide colour degraded to clear in less than one hour. In the 0.5M and 1M cells, this time was extended to 1-3 hours respectively. The ECCS substrate resisted a little better, no doubt due to residual electro-chrome coating, giving an overall lifetime of 5 hours.

5.7 Inhibition mechanisms - theoretical analysis

It is possible to theorise what inhibition mechanisms are occurring over time in the observation cells using the data collected, supported by current literature on the subject of nitrogen containing heterocyclics and electrolyte interactions. The mechanism of NHC inhibition on metals substrates has been the source of study in several previous reports, with different forms of inhibition seen as the NHC compound concentration and structure was varied [40][41][42][43], [44][45]. Several mechanisms of inhibitor action have thus been suggested:

1. Steric hindrance or diffusion limiting action
2. Nitrogen lone pairs to metal substrate reactive site bonding
3. Bonding *via* the pyridine ring π-electrons to the metal substrate surface
4. Bonding *via* electrostatic attraction to the metal surface
5. Formation of a complex ion between NHC and electrolyte components (Li^+ or the I^- and I_3^- species)

Our choice of additive compound was primarily decided by their performance enhancing abilities and their small molecular size reported in the studies by Kusama *et al* as it was not

known what factors would benefit both DSC performance and perform a degradation inhibiting action.[10]. The main structural differences between the compounds are the presence of an alkyl group or a variation in the number of nitrogen heteroatoms contained within the compounds. In addition, these compounds all contain an extremely versatile pyridine ring structure, consisting of π electrons that are contributed from the *p*-orbitals of the carbon ring and to varying extent, the nitrogen atoms. These are able to form areas of high electron density above and below the plane of the NHC compound, Figure 5.22, and allow the electrostatic attraction between the negatively charged ring and a positive metal surface.

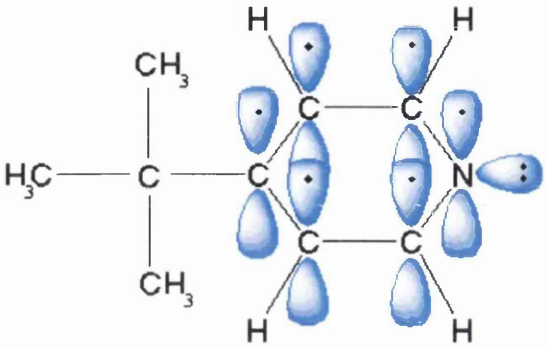

Figure 5.22: Electronic structure of 4-TBP

Figure 5.23 shows skeleton diagrams for the three NHC compounds used in this study, note the attached methyl and butyl groups and their positions on the 4-tBP and 1MBI molecules. There are several electron lone pairs from specific nitrogen heteroatoms in the chemical structure, these can also be seen in Figure 5.23 and indicate areas of high electrophilic activity, i.e. high electron donating ability, though this will depend on the makeup of the NHC compound. This will be covered later in this section.

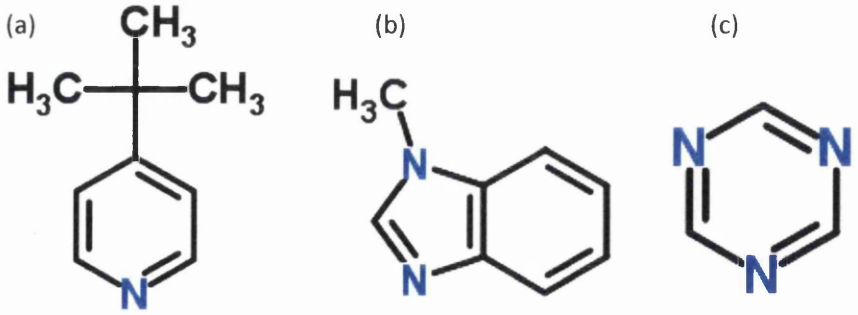

Figure 5.23: Structure of (a) 4-TBP, (b) 1-MBI and (c) 135T

Previous reports have noted that certain metals only allow adsorption of NHC's in certain orientations, leading to different inhibition effects. Lashkari *et al.* reported that the

orientation of the transition metal orbitals leads to different favourable (low energy) orientations of the NHC compounds [45]. This report focused on the pyridine molecule, which was shown to bond in either vertical or parallel orientation to the iron substrate used in the study. This preference for orientation is due to the plethora of vacant *d*-orbital orientations in iron. In contrast, pyridine was only able to bond vertically to an Al substrate as only the P_z orbital here is free, thus resulting in a minimum energy orientation when bonded vertically. A further complicating factor which decides the compound orientation is the inclusion of functional groups into the NHC structure. These groups, such as the *tert*-butyl or methyl groups seen in the 1-MBI additive affect the lone pair donating ability of the nitrogen heteroatom located within the pyridine ring structure repelling away from the N atom, allowing it to be donated more easily. The compounds have several methods of adsorbing to the metal surface due to the existence of both "Pi" and lone pair electrons, which will also decide the orientation.

The first inhibition method considered is the bonding *via* chemisorption of the NHC compound to sites of Lewis acidity, such as vacant *d*-orbitals in the transition metal atoms. This is achieved by using the sp^2 lone pair on the nitrogen heteroatom. The electron transfer will create a chemisorptive bond between the NHC and the metal surface, iron in the case of the literature examples given by Maksoud *et al* and Lashkari *et al.* [42], [45]. It is proposed that in the case of 4-TBP, the compound bonds in a vertical orientation due to the presence of the *tert*-butyl group opposite the nitrogen heteroatom. According to the widely accepted theory presented by Nyholm and Gillespie, otherwise known as "valence shell electron pair repulsion theory" (VSEPR), these groups change the electron density of the NHC, increasing the electro-negativity of the nitrogen atom so increasing its ability to donate its lone pair electrons [46]. In accordance with VSEPR, the lone pair electrons move further from the atom centre allowing for more probable bonding with the metal surface [47]. Furthermore, this could create preferential conditions for the 4-TBP to adsorb vertically, where the molecule extends out into the electrolyte solution. The presence of the NHC's will perform a physical blocking action at the interface of the triiodide with the metal substrate, desirably prolonging cell lifetime.

The vertical orientation should provide an interface layer extending from the surface into the Helmholtz layer and restricting diffusion of the triiodide, an effect known as steric hindrance. Since triiodide reduction is a comparatively slow process compared with the outer-sphere electron transfer of other electrolyte species such as cobalt complexes, the triiodide must fully adsorb to the metal surface for electron transfer to occur. Depending

on the metal or electrolyte solvent involved, an alternative bond maybe formed using the π-electrons in the ring structures, which is thought to bond using electrostatic attraction between the positively charged metal and the compound due to the negative charge of the dissociated π-electrons. This was considered to be the most likely mechanism for the 1MBI and 135T compounds.

The condition of the metal surface also has a key relationship with inhibitor performance. In metals, defects such as steps, dislocations or dangling bonds are considered to be active sites and vulnerable to attack from the triiodide species [41]. In the corrosion inhibition study, all the metals had their surfaces abraded and cleaned. This treatment is designed to remove any oxide layer, dirt or surface impurities, but has the disadvantage of increasing the surface roughness, enabling a greater area vulnerable to triiodide attack. The result of this can be seen in Figure 5.4, which compares the degradation of cells fabricated using either activated or non-activated Al substrate. The activated substrate reacts much quicker as the protective oxide has been removed and the surface area has increased with the roughness.

Strong chemisorption will physically block these reactive sites on the metal surface from attack. Restricting the interaction between the metal and triiodide should slow or completely inhibit cell degradation. Therefore a bond would be required where the molecules are held close to the substrate, or at an orientation that provides high coverage in order to improve the inhibition effect. If a passivation layer is already in place on the metal surface, *á la* titanium and aluminium, then little aggressive interaction will occur. If this layer has defects or only partial coverage it will allow the ingress of triiodide and thus aid in surface attack and possible de-lamination of this oxide layer through corrosion of the underlying metal. Furthermore, constant interaction with triiodide could cause potential weakening of the surface layer and lead to gradual cell degradation.

An important factor in the efficiency of the inhibitor is the concentration used within the electrolyte and as expected, higher concentrations generally have a larger inhibition effect. However, there are certain discrepancies, such as for Al and 1-MBI or 4-TBP, Figure 5.8 & Figure 5.11, where lower concentrations have given greater than expected inhibition effects. The initial conclusion was to suspect the uniformity of the surface preparation method, as there could be a partial alumina layer of varying thickness present that will affect the progression of the degradation reaction. Despite this possibility, this effect has been documented in previous literature where corrosion inhibitors were used in metals

immersed or exposed to an acidic environment [42]. These reports indicated that at lower concentrations, the inhibitor molecules congregated mainly on the grain boundaries or metal defects, rather than the centre of the grain itself. It is at these boundaries or defects that the corrosion reaction is more likely to progress at a higher rate. The concentration of the inhibitors at these locations will provide a higher than expected inhibition effect and so increase the longevity of the triiodide species. As the concentration is increased the coverage of the surface by the inhibitor increases up to full coverage and therefore complete inhibition, as can be seen for most of the 1M NHC concentrations tested in this study. It was also suggested that at high concentrations, the double layer at the metal-electrolyte interface will be saturated and therefore inhibit the movement of the triiodide toward the substrate.

The 1,3,5-triazine (135T) additive, also known as s-triazine, has no alkyl or other functional group attached to effect the electron density. However, as shown in the literature, the s-triazine molecule has several methods of bonding to other species, which has made it an invaluable building block in supramolecular chemistry [48]. S-triazine molecules are able to form coordinate bonds with metals, bond to nitrogen or oxygen (impurities in this study) *via* lone-pair π or σ interactions, stack to other s-triazine molecules by π-σ stacking or combine with anions or cations *via* π or σ interactions, thus there are many possible routes for inhibition when using this molecule. However, in this study it gave poor inhibition performance. The lack of inhibition effect for ECCS, iron and surface activated aluminium indicates that the these substrates require a more active form of inhibition due to their increased reactivity once the oxide layer is removed. Since *s*-triazine does not have an alkyl group attached as in 4-tBP or 1MBI, its electronic structure will be less electronegative and will not easily donate the nitrogen lone pair electrons to facilitate bonding to the substrate.

A different pathway to inhibition was suggested in literature, involving the formation of dissociated charge transfer complexes under steady state conditions. This was achieved through the interaction of pyridine and pyridine derivatives according to the Equation 5.5 below, in a polar solvent such as 3-MPN, or ACN [49]–[51]:

$$2(Pyr^{*}I_2) \leftrightarrow Pyr_2I^{+} + I_3^{-} \qquad (5.5)$$

While this route will not reduce the amount of triiodide in the electrolyte, the presence of a large positively charged molecule, i.e. Pyr_2I^{+} adjacent to the substrate is thought to be able to restrict the diffusion of triiodide and could slow or reduce the interaction of the triiodide and the metal substrate.

Boschloo *et al.* reported that a large enough concentration of 4-TBP has a significant effect on the iodine electrochemistry in DSC electrolyte when 3MPN is used as the solvent [52]. They concluded that for a high enough concentration of 4-TBP, the amount of iodine not in a complex with 4-TBP is low, thus reducing the free iodine and the concentration of triiodide in solution, a similar possibility exists for the 1-MBI additive. It is thought therefore that this reaction plays an integral part in the inhibition of electrolyte degradation a recent study by Hansen *et al* concluded that there was no other interaction between 4-tBP and I_3^- in a DSC electrolyte. This also indicates that the structure of NHC compounds is critical, as shown by the comparison between the active triiodide/pyridine reaction and the lack of reaction between triiodide/4-tBP.

A study by Fischer *et al.* and Kusama *et al.* analysed the formation of a compound between 1-MBI and triiodide, which again proved to lower the concentration of the latter, affecting the progression of the degradation activity [53], [54]. The decrease in triiodide causes a change in the concentration of species adjacent to the substrate. The remainder of un-complexed 4-TBP or 1-MBI can thus act to block the interaction of the now lower concentration of triiodide with the metal substrate.

The inclusion of NHC's as DSC performance enhancers in sufficient quantities to reduce or completely inhibit corrosion is thus the final goal of this study. The performance of 4-tBP, 1MBI have shown that this is possible, though further optimisation will be required to synchronise both to produce the most efficient and stable dye sensitised solar cell. In addition, the study has shown that the difference in NHC structure plays a critical part in deciding the inhibition factor, exhibited by large difference between the effects of 4TPB and 135T. So clearly, it is not the amount of nitrogen heteroatoms that are included in the compounds, but the overall chemical structure that is important.

5.8 Current use of metal substrates in DSCs

Metal foils are a popular choice as a replacement substrate for FTO-glass due to their higher durability and conductivity. Unfortunately, metal substrate DSC development has remained behind traditional FTO-glass cells in performance and in addition some of the most attractive substrates such as steels increase cell degradation through depletion of the triiodide charge carriers through corrosion processes.

One of the first major studies in this area was undertaken by Ma *et al.* This assessed several substrates including stainless steel 304, which is one of the most commonly used and low cost stainless steels. Nickel, aluminium and copper were also assessed [13]. The

metals were used for the counter electrode rather than the photoelectrode substrate, a placement designed to increase cell performance, as the light intensity will not be reduced through the requirement of travel through the electrolyte solution as would occur in metal photoelectrode substrate devices. The device efficiencies varied from 1.95% to 5.24%, depending on the platinisation method, with sputtered platinum giving the highest efficiency cells. This paper concluded by showing that stainless steel and nickel had good stabilities in the DSC environment and that the excellent electrical conductivity of the metal substrate improved device performance through the reduction of internal resistance. This will benefit large area devices especially.

Improving upon the previously mentioned study, Kang *et al* showed that the use of stainless steel substrate was able to produce stable high performing devices, with an average efficiency of 4.2%. The high temperature tolerance of the flexible steel substrate is a key point for this paper, as it allows the processing of TiO_2 through high temperature sintering, resulting in a stable high performance photoelectrode, rather than the previous use as the counter electrode substrate. As mentioned previously, the reduction in light intensity due to absorption by the electrolyte will decrease the device J_{sc} and thus efficiency when compared with front illuminated cells. However, due to the reflective metal substrate, this loss can be mitigated through reflection of light from the substrate back to the photoelectrode. Three types of stainless steel were used in this study: Stainless 461, ITO coated stainless steel and SiO_x coated stainless steel. Unfortunately, no stability study was run, leaving the longevity of these cells in doubt [17].

Fast becoming one of the most popular substrates for flexible cells, titanium foil was investigated by Ito *et al.*, as the DSC photoelectrode substrate [5]. Titanium is known for its high resistance to both corrosion and temperature, excellent for use in the aggressive triiodide/iodide solution and also able to withstand the high temperatures required for the processing of efficiency DSC devices. The DSCs performed with an efficiency of 7.2%, which is double that of the stainless steel devices assessed by Kang *et al.,* however the stability of these devices was reduced due to the use of volatile acetonitrile as the electrolyte solvent, which has a tendency to evaporate from the cell, and the reduced performance of the Pt coated polymeric counter electrode due its low charge transfer efficiency.

A key study for the assessment of metallic substrates for DSCs was undertaken by Miettunen *et al.* They produced a study on the stability of DSCs with metal substrate photoelectrodes. The metals included common stainless steels 316, 316L, 304, 321, in

addition to several highly resistant metals such as the nickel alloy Inconel 600 and titanium. The compositions of the stainless steels were described to differ mainly through additive elements such as Mo and Ti [2]. The DSCs produced, including the glass substrate control cell were illuminated through the counter electrode, producing a reduction in performance. An additional effect of reverse illumination is that the electrons generated in the photoelectrode will have a longer path length to the collecting substrate than for forward illuminated cells. This length from generation to collection could cause recombination losses and a further decrease in performance. Like the previous studies, the FTO-glass based cells produced the highest J_{sc} and efficiency at 11.3mA/cm^2 and 4.6% respectively for forwards illuminated cells and 8.7mA/cm^2 and 3.5% respectively for reverse illuminated cells. Cells using titanium foil reached comparable values of 7.9mA/cm^2 and 3.4%, using 0.13mm thick foil and 7.0mA/cm^2 and 3.0% for 0.03mm foil. This difference was reported to be caused by a difference in the thickness of the TiO_2 layer through experimental issues.

Despite the high performance reported for the Stainless 304 substrate cells, the Miettunen paper also shows that all stainless steel substrate cells assessed showed degradation through interaction with the electrolyte [2]. This outcome is the reverse of that seen by the study in this thesis chapter. One possibility for the difference between these works is that Miettunen *et al.* studied active DSC devices containing different electrochemical processes to our simple corrosion cells. The addition of other processes could provide an added driving force for corrosion. Thus it is recommended that further in-depth studies be completed if possible to prove the long term viability of stainless steel substrates.

An interesting cause of performance losses in DSCs using metallic substrates was current leakage. This can be mitigated through the use of a compact TiO_2 blocking layer that will reduce the recombination of triiodide with electrons collected at the metal electrode substrate. The Ti foil substrates used throughout the literature have a naturally occurring blocking layer of TiO_2, which will minimises current leakage and contributes to the high performance of the Ti substrate cells over the stainless steel devices. Lee *et al.* also studied cells manufactured with a compact TiO_2 layer beneath the dyed-TiO_2 photo electrode [55]. Care was taken here as the typical $TiCl_4$ process is acidic and leads to substrate corrosion. Instead, another route was used using $Ti(OH)_4$ to form a TiO_2 sol. Unfortunately, this process takes 8-10 hours using the method described in literature and therefore would not be viable for roll to roll produced DSCs. The metal substrate cell produced an efficiency of 2.58% without the compact TiO_2 layer and 4.51% with a compact TiO_2 layer.

Electrochemical studies undertaken by Kanta *et al.* worked to further assess the effect of the electrolyte solution on stainless steel 304L counter electrode substrates [56]. EIS was used to monitor the decrease in impedance from the initial passivated state. After 24hrs, the EIS showed an inductive loop, a characteristic of corrosion and for stainless steel this takes the form of pitting, corrosion mechanism seen previously by Miettunen *et al.* The electrolyte was thought to be attacking the substrate through the breakdown of the passive surface layer and thus activating the steel surface. Following the first 24hrs, the impedance was seen to increase due to the presence of surface corrosion products, which were thought to re-passivate the surface. However the reduction in triiodide charge carriers would have already occurred, leading to an irreversible performance loss. Due to the ability of EIS to give a fundamental insight into corrosion processes, it is recommended this be included as further work in the study of corrosion inhibition in DSC devices.

One of the key issues addressed by Kanta *et al.* was the presence of oxygen and water molecules in the electrolyte solution [56]. The presence of water and oxygen are known accelerants for metal corrosion and as a result, their presence is thought to be detrimental to metal substrate cells. These were removed in this study through dehydration and deoxygenating processes in order to minimise their effect on the substrate and cell performance. Dehydration was shown to make little difference to the cell quality and lifetime. However, the deoxygenating treatment had much more interesting effects. The removal of oxygen from the electrolyte inhibits the reduction of dissolved oxygen at the metal surface, thus slowing the corrosion process [56]. Unfortunately, it is very difficult to completely deoxygenate the electrolyte solution - especially if the cells were to be manufactured by a mass production process.

Watson *et al.* assessed the viability of DSC constructed onto aluminium coated steel and steel pre-sputtered with titanium [57]. The efficiency recorded was 2.9%, compared to a full titanium substrate cell at 3.2% and is still low compared with 7.2% recorded by Ito *et al* [5]. The reduction in efficiency was due to lower fill factor, caused by damage of the sputtered titanium layer. The future work suggested in this paper on the use of zinc-aluminium alloy coated steels for DSCs, has been shown by this thesis to be less viable as in an iodide/triiodide environment. Aluminium was seen to be vulnerable to degradation, Figure 5.4. In addition, the work of Miettunen *et al.* also indicated that zinc also exhibits corrosion in iodide/triiodide electrolytes, therefore an investigation into other anti-corrosion additives and coating are thus suggested instead [2].

Miettunen *et al.* published a paper concentrating on metal substrate counter electrodes rather than photoelectrodes [15]. This paper assessed the same metals as the previous 2010 study: Stainless steel 304, 321, 316, 316L, Inconel 600 and Titanium. Previous research has already shown stainless steel 304 to be more susceptible to corrosion than other stainless compositions when used in full DSC cells [2], [56]. Since this thesis has reported that both Stainless Steel 304 and 316 appear to have good lifetimes in simple iodide/triiodide corrosion cells, it is thought that the active DSC processes influence and increase the rate of the degradation processes.

As a counter electrode substrates, the results for these metals was variable. The method of Pt application to the substrate was critical in determining their stability. The high temperature thermal platinisation process caused serious degradation of DSC performance over the testing period of 6 weeks in the 304, 321 and Inconel cells. These metals were shown to have degraded substantially before the initial measurement was taken. Inconel, normally a highly corrosion resistant material was thought to be vulnerable due to its high nickel content and as shown in this thesis nickel substrate is easily attacked by triiodide, remaining stable for only 65 hours compared with the 2000 hour lifetime of stainless steels 304 and 316, Figure 5.8, Figure 5.10, Figure 5.11 and Figure 5.18. Interestingly, Miettunen *et al.* reported that a thin sputter coating of Pt provided a modicum of corrosion protection for the stainless steels, though due to pin holes and imperfections in the sputtered layer, the Inconel metal cells still degraded rapidly [15].

Methods of physically coating vulnerable metal substrates for corrosion protection were investigated by Ouyang & Tai, this study used titanium nitride (TiN) as an anticorrosion coating for stainless steel 301 [58]. TiN of varying thicknesses was applied through a sputtering process. Their results show an improvement in the corrosion resistance of Stainless Steel 301 in contact with a triiodide/iodide electrolyte. The single TiN layer and the bi-layer TiN/Ti are both able to protect the steel substrate. However, the single layer also increased the sheet resistance of the substrate and reduced performance. Once a Ti interlayer was added, this compensated for the reduction on using TiN. The DSC results showed an increase of over 200% from an efficiency of 1.64% for naked stainless 301 to an average of 4.09% for steel coated with TiN. The suggestions for the improvement in performance were the increased surface roughness of the TiN promoting increased contact area of TiO_2 and as a result a larger area of dye molecules. This seems to be indicated in the J_{sc} increase from *ca.* 4.5mA/cm^2 for steel to an average of 9.95mA/cm^2. This type of physical corrosion inhibitor was further assessed through the work of Vyas *et al.* who

studied the use of a combined TiN/Polyimide coating as both a conductive layer and an anticorrosion substrate for DSC devices [59], [60]. At the time of writing, this coating was in the process of being investigated in full DSC devices.

Titanium was also assessed as a sputtered coating by Meng *et al,* on stainless steel 304 sheets in order to increase the stability of the steel substrate [61]. A thin Ti-layer was used instead of bulk metal in order to reduce costs. The DSC device efficiencies for titanium coated steel are comparable to those of the FTO glass based control cells at 2.26% and 3.15 efficiency respectively. The highest efficiency was produced when the sputtered Ti was applied at 700°C. The different temperatures of sputter deposition were seen to reduce the R_{ct} of the photoelectrode from 261.3Ω when sputtered at room temperature to 45.0Ω when applied at 700°C. This reduction was said to be the source of the improvement in efficiency for the Ti-coated steel DSCs, as R_{ct} of the counter electrode was unaffected, as was V_{oc}, FF and R_s. The high temperature sputtering reduces defects in the sputtered Ti layer and improves the connection between the Ti layer and the TiO_2 semiconductor, which will increase the charge collection efficiency and as a result raise the J_{sc} of the device and thus cell efficiency.

The current state of the art of metal substrate solar cells appears to be focused on physical protection of the counter electrode through barrier coatings of resistant metals, rather than the use of potentially less expensive, though possibly more complex use of additive in the electrolyte as utilised in this thesis. Coating processes and more resistant metals add materials or process expenses to an already high cost process. It is thus beneficial for a means of corrosion protection to be found that will support the usage of low cost mass produced stainless steel.

This thesis has sought to develop a method of this through the addition of nitrogen containing heterocyclics (NHC) to the electrolyte. These previous works have shown that metal substrate cells with high performance are possible, but are currently handicapped from reaching a comparison with FTO glass device due to stability issues. The findings in this chapter show that for corrosion cells, degradation is effectively halted for 2000hrs in stainless steel 304 and 316L, in addition to aiding the stability of aluminium sheet metal. Therefore it is hoped that this will result in high performance and good stability of metal substrate DSC, through the combined anticorrosion and performance enhancing effects of the NHC compounds.

5.9 Conclusions

In the first section of this chapter it was confirmed that the RGB image analysis method was a viable *in situ* method of observing and characterising the corrosion of metal substrates in iodide/triiodide electrolyte, which correlated well with an existing DR-UV-VIS characterisation method. The most vulnerable industrial metal substrates were found to be Fe (99.5%); Ni (99.5%) and surface activated Al (99.0%). Stainless steel 304 and 316L along with titanium have proven to be resistant to cell degradation and the inclusion of a chemical corrosion inhibitor such as 4-tBP or 1MBI at 1M concentration will increase this native resistance and add a performance enhancing effect to DSC devices. Since these compounds are already known as DSC performance enhancers, their inclusion should not destabilise the cells. Further work should be done on assessing other viable substrates.

The second section of this chapter analysed the effectiveness of three nitrogen containing heterocyclics, 4-tBP, 1MBI and 135T that have already been reported as DSC performance enhancers. It was found that the differences in concentration and molecular structure had large effects on the performance of the compound on a variety of metal substrates.

In commonly used DSC electrolyte formulations, concentrations of 0.5M are typically used for 4-TBP and 1-MBI additives. The results obtained in this chapter show that this concentration slows but does not fully inhibit cell degradation. The higher 1M concentration of 4-TBP and 1-MBI fully inhibits the vulnerable Al, Ni and Fe substrates observed in this study. In comparison, the 135T compound gave poor performance for vulnerable metals, which was suggested to be due to the balanced and poorly electronegative structure, which will not easily donate electrons to form bonds. It was then proposed that the NHC inhibition effect will occur through a combination of mechanisms, ranked in the following order of effect:

- **Reactive site blocking** through adsorption on to the metal surface
- Causing **steric hindrance** of the triiodide molecules
- Potential **formation of an NHC to I_3^- or I^- complex** (steric hindrance and reduction of aggressive species)

While only three additives have undergone testing here – the choice of compounds of varying structure has meant that predictions on the inhibition efficiency can be made for the vast variety of NHC compounds available, with particular emphasis on those indicated as excellent performance enhancers from the studies of Kusama *et al.* [29], [34], [35], [54], [62], [63].

5.10 References

[1] M. Toivola, F. Ahlskog, and P. Lund, "Industrial sheet metals for nanocrystalline dye-sensitized solar cell structures," *Sol. Energy Mater. Sol. Cells*, vol. 90, no. 17, pp. 2881–2893, Nov. 2006.

[2] K. Miettunen, X. Ruan, T. Saukkonen, J. Halme, M. Toivola, H. Guangsheng, and P. Lund, "Stability of Dye Solar Cells with Photoelectrode on Metal Substrates," *J. Electrochem. Soc.*, vol. 157, no. 6, p. B814, 2010.

[3] X. Fang, T. Ma, M. Akiyama, G. Guan, S. Tsunematsu, and E. Abe, "Flexible counter electrodes based on metal sheet and polymer film for dye-sensitized solar cells," *Thin Solid Films*, vol. 472, no. 1–2, pp. 242–245, Jan. 2005.

[4] K. Miettunen, J. Halme, M. Toivola, and P. Lund, "Initial Performance of Dye Solar Cells on Stainless Steel Substrates," *J. Phys. Chem. C*, vol. 112, no. 10, pp. 4011–4017, Mar. 2008.

[5] S. Ito, N.-L. C. Ha, G. Rothenberger, P. Liska, P. Comte, S. M. Zakeeruddin, P. Péchy, M. K. Nazeeruddin, and M. Grätzel, "High-efficiency (7.2%) flexible dye-sensitized solar cells with Ti-metal substrate for nanocrystalline-TiO2 photoanode.," *Chem. Commun. (Camb).*, no. 38, pp. 4004–6, Oct. 2006.

[6] "G24 Innovations," 2013. [Online]. Available: http://www.g24i.com/. [Accessed: 12-Jul-2013].

[7] T. Watson, P. Holliman, and D. Worsley, "Rapid, continuous in situ monitoring of dye sensitisation in dye-sensitized solar cells," *J. Mater. Chem.*, vol. 21, no. 12, p. 4321, 2011.

[8] A. Hagfeldtt and M. Gratzel, "Light-Induced Redox Reactions in Nanocrystilline Systems," *Chem. Rev.*, vol. 95, no. 1, pp. 49–68, 1995.

[9] S. Y. Huang, G. Schlichthorl, A. J. Nozik, M. Grätzel, and A. J. Frank, "Charge Recombination in Dye-Sensitized Nanocrystalline TiO2 Solar Cells," *J. Phys. Chem. B*, vol. 5647, no. 96, pp. 2576–2582, 1997.

[10] H. Kusama, M. Kurashige, and H. Arakawa, "Influence of nitrogen-containing heterocyclic additives in I− I3−redox electrolytic solution on the performance of Ru-dye-sensitized nanocrystalline TiO2 solar cells," *J. Photochem. Photobiol. A Chem.*, vol. 169, pp. 169–176, 2005.

[11] C. Vargel, "Chapter B.1 The Corrosion of Aluminium," in *Corrosion of Aluminium*, Illustrate., Elsevier, 2004, p. 81.

[12] J. E. Hatch, *Aluminium: Properties and Physical Metallurgy*. American Society for Metals International, 1984, p. 242.

[13] T. Ma, X. Fang, M. Akiyama, K. Inoue, H. Noma, and E. Abe, "Properties of several types of novel counter electrodes for dye-sensitized solar cells," *J. Electroanal. Chem.*, vol. 574, no. 1, pp. 77–83, Dec. 2004.

[14] K. Okada, H. Matsui, T. Kawashima, T. Ezure, and N. Tanabe, "100mm x 100mm Large-Sized Dye Sensitized Solar Cells," *J. Photochem. Photobiol. A Chem.*, vol. 164, no. 1–3, pp. 193–198, Jun. 2004.

[15] K. Miettunen, I. Asghar, X. Ruan, J. Halme, T. Saukkonen, and P. Lund, "Stabilization of metal counter electrodes for dye solar cells," *J. Electroanal. Chem.*, vol. 653, no. 1–2, pp. 93–99, Apr. 2011.

[16] J. Olsson and B. Wallen, "Experience with a high molybdenum stainless steel in saline environments," *Desalination*, vol. 44, no. 1–3, pp. 241–254, May 1983.

[17] M. Kang, N. Park, K. Ryu, S. Chang, and K. Kim, "A 4.2% efficient flexible dye-sensitized TiO2 solar cells using stainless steel substrate," *Sol. Energy Mater. Sol. Cells*, vol. 90, no. 5, pp. 574–581, Mar. 2006.

[18] Y. Jun, J. Kim, M. G. K. Ã, and M. Kang, "A study of stainless steel-based dye-sensitized solar cells and modules," *Sol. Energy Mater. Sol. Cells*, vol. 91, no. 9, pp. 779–784, 2007.

[19] J. H. Park, Y. Jun, H.-G. Yun, S.-Y. Lee, and M. G. Kang, "Fabrication of an Efficient Dye-Sensitized Solar Cell with Stainless Steel Substrate," *J. Electrochem. Soc.*, vol. 155, no. 7, p. F145, 2008.

[20] M. T. Ã, J. Halme, K. Miettunen, K. Aitola, and P. D. Lund, "Nanostructured dye solar cells on flexible substrates — Review," *Int. J. Energy Res.*, no. September, pp. 1145–1160, 2009.

[21] M. I. Asghar, K. Miettunen, S. Mastroianni, J. Halme, H. Vahlman, and P. Lund, "In situ image processing method to investigate performance and stability of dye solar cells," *Sol. Energy*, vol. 86, no. 1, pp. 331–338, Jan. 2012.

[22] K. Miettunen, "Performance and Stability of Dye Solar Cells on Stainless Steel," Helsinki University of Technology, 2009.

[23] B. O'Regan and M. Gratzel, "A low-cost, high-efficiency solar cell based on dye-sensitized colloidal TiO2 films," *Nature*, vol. 353, no. 6346, pp. 737–740, Oct. 1991.

[24] L. Peter, "Characterization and Modeling of Dye-Sensitized Solar Cells," *ECS Trans.*, vol. 6, pp. 555–565, 2007.

[25] Z. Yu, M. Gorlov, G. Boschloo, and L. Kloo, "Synergistic Effect of N - Methylbenzimidazole and Guanidinium Thiocyanate on the Performance of Dye-Sensitized Solar Cells Based on Ionic Liquid Electrolytes," *J. Phys. Chem. C*, vol. 114, no. 50, pp. 22330–22337, Dec. 2010.

[26] P. Wang, S. M. Zakeeruddin, J. Moser, and M. Gra, "A New Ionic Liquid Electrolyte Enhances the Conversion Efficiency of Dye-Sensitized Solar Cells," pp. 13280–13285, 2003.

[27] M. K. Nazeeruddin, A. Kay, R. Humphry-Baker, E. Muller, P. Liska, N. Vlachopoulos, and M. Grätzel, "Conversion of Light to Electricity by cis-X2Bis(2,2'-bipyridyl-4,4'-dicarboxylate)ruthenium(11) Charge-Transfer Sensitizers (X = Cl-, Br-, I-, CN-, and SCN-) on Nanocrystalline Ti02 Electrodes," *J. Am. Chem. Soc.*, no. 4, pp. 7863–7863, 1993.

[28] N. Kopidakis, N. R. Neale, J. van de Lagemaat, and A. J. Frank, "First Demonstration of Surface Passivation in Dye-sensitized TiO2 Solar Cells by an Additive in the Electrolyte," in *2004 DOE Solar energy technologies program review meeting*, 2004.

[29] H. Kusama, H. Orita, and H. Sugihara, "TiO2 band shift by nitrogen-containing heterocycles in dye-sensitized solar cells: a periodic density functional theory study.," *Langmuir*, vol. 24, no. 8, pp. 4411–9, Apr. 2008.

[30] A.-F. Kanta and A. Decroly, "Stainless steel electrode characterizations by electrochemical impedance spectroscopy for dye-sensitized solar cells," *Electrochim. Acta*, vol. 56, no. 27, pp. 10276–10282, Nov. 2011.

[31] H. Kusama, Y. Konishi, H. Sugihara, and H. Arakawa, "Influence of alkylpyridine additives in electrolyte solution on the performance of dye-sensitized solar cell," *Sol. Energy Mater. Sol. Cells*, vol. 80, no. 2, pp. 167–179, Oct. 2003.

[32] H. Kusama and H. Arakawa, "Influence of quinoline derivatives in I−/I3− redox electrolyte solution on the performance of Ru(II)-dye-sensitized nanocrystalline TiO2 solar cell," *J. Photochem. Photobiol. A Chem.*, vol. 165, no. 1–3, pp. 157–163, Jul. 2004.

[33] H. Kusama, H. Sugihara, and K. Sayama, "Nitrogen-Containing Heterocycles' Interaction with Ru Dye in Dye-Sensitized Solar Cells," *J. Phys. Chem. C*, vol. 113, no. 48, pp. 20764–20771, Dec. 2009.

[34] H. Kusama and H. Sugihara, "Theoretical studies of 1:1 charge-transfer complexes between nitrogen-containing heterocycles and I2 molecules, and implications on the performance of dye-sensitized solar cell," *J. Photochem. Photobiol. A Chem.*, vol. 181, no. 2–3, pp. 268–273, Jul. 2006.

[35] H. Kusama and H. Arakawa, "Influence of pyrimidine additives in electrolytic solution on dye-sensitized solar cell performance," *J. Photochem. Photobiol. A Chem.*, vol. 160, no. 3, pp. 171–179, Aug. 2003.

[36] T. M. Watson, "Corrosion Mechanisms and Inhibition on Organic Coated Packaging Steel," University of Wales, Swansea.

[37] G. Boschloo, H. Lindström, E. Magnusson, A. Holmberg, and A. Hagfeldt, "Optimization of dye-sensitized solar cells prepared by compression method," *J. Photochem. Photobiol. A Chem.*, vol. 148, no. 1–3, pp. 11–15, May 2002.

[38] C. Zhang, J. Dai, Z. Huo, X. Pan, L. Hu, F. Kong, Y. Huang, Y. Sui, X. Fang, K. Wang, and S. Dai, "Influence of 1-methylbenzimidazole interactions with Li+ and TiO2 on the performance of dye-sensitized solar cells," *Electrochim. Acta*, vol. 53, no. 17, pp. 5503–5508, Jul. 2008.

[39] P. E. Hansen, P. T. Nguyen, J. Krake, J. Spanget-larsen, and T. Lund, "Dye-sensitized solar cells and complexes between pyridines and iodines. A NMR, IR and DFT study.," *Spectrochim. Acta. A. Mol. Biomol. Spectrosc.*, vol. 98, pp. 247–251, Dec. 2012.

[40] S. L. Granese, "Study of the Inhibitory Action of Nitrogen-Containing Compounds ' s," pp. 322–327, 1987.

[41] K. F. Khaled, "The inhibition of benzimidazole derivatives on corrosion of iron in 1 M HCl solutions," *Electrochim. Acta*, vol. 48, no. 17, pp. 2493–2503, Jul. 2003.

[42] S. A. Abd El-Maksoud and A. S. Fouda, "Some pyridine derivatives as corrosion inhibitors for carbon steel in acidic medium," *Mater. Chem. Phys.*, vol. 93, no. 1, pp. 84–90, Sep. 2005.

[43] X. Wang, H. Yang, and F. Wang, "An investigation of benzimidazole derivative as corrosion inhibitor for mild steel in different concentration HCl solutions," *Corros. Sci.*, vol. 53, no. 1, pp. 113–121, Jan. 2011.

[44] A. Popova, M. Christov, S. Raicheva, and E. Sokolova, "Adsorption and inhibitive properties of benzimidazole derivatives in acid mild steel corrosion," *Corros. Sci.*, vol. 46, no. 6, pp. 1333–1350, Jun. 2004.

[45] M. Lashkari and M. . R. Arshadi, "DFT studies of pyridine corrosion inhibitors in electrical double layer: solvent, substrate, and electric field effects," *Chem. Phys.*, vol. 299, no. 1, pp. 131–137, Mar. 2004.

[46] R. J. Gillespie and R. S. Nyholm, "Inorganic stereochemistry," *Q. Rev. Chem. Soc.*, vol. 11, no. 4, pp. 339–380, 1957.

[47] D. Landolt, *Corrosion and Surface Chemistry of Metals*. CRC Press, 2010, pp. 549–551.

[48] T. J. Mooibroek and P. Gamez, "The s-triazine ring, a remarkable unit to generate supramolecular interactions," *Inorganica Chim. Acta*, vol. 360, no. 1, pp. 381–404, Jan. 2007.

[49] T. Tassaing and M. Besnard, "Ionization Reaction in Iodine / Pyridine Solutions : What Can We Learn from Conductivity Measurements , Far-Infrared Spectroscopy , and Raman Scattering ?," *J. Phys. Chem. A*, vol. 101, pp. 2803–2808, 1997.

[50] Z. Kebede and S.-E. S.-E. Lindquist, "Donor–acceptor interaction between non-aqueous solvents and I2 to generate I−3, and its implication in dye sensitized solar cells," *Sol. Energy Mater. Sol. Cells*, vol. 57, no. 3, pp. 259–275, Mar. 1999.

[51] C. Reid and R. S. Mulliken, "Molecular Compounds and Their Spectra. IV. The Pyridine-Iodine System," *J. Am. Chem. Soc.*, vol. 76, no. 15, pp. 3869–3874, 1954.

[52] G. Boschloo, L. Häggman, and A. Hagfeldt, "Quantification of the effect of 4-tert-butylpyridine addition to I-/I3- redox electrolytes in dye-sensitized nanostructured TiO2 solar cells.," *J. Phys. Chem. B*, vol. 110, no. 26, pp. 13144–50, Jul. 2006.

[53] A. Fischer, H. Pettersson, A. Hagfeldt, G. Boschloo, L. Kloo, and M. Gorlov, "Crystal formation involving 1-methylbenzimidazole in iodide/triiodide electrolytes for dye-sensitized solar cells," *Sol. Energy Mater. Sol. Cells*, vol. 91, no. 12, pp. 1062–1065, Jul. 2007.

[54] H. Kusama, H. Arakawa, and H. Sugihara, "Density functional study of imidazole–iodine interaction and its implication in dye-sensitized solar cell," *J. Photochem. Photobiol. A Chem.*, vol. 171, no. 2, pp. 197–204, Apr. 2005.

[55] C.-L. Lee, W.-H. Lee, W.-T. Li, C.-H. Yang, and P.-C. Kao, "StSt/TiO2 compact layer/TiO2 triple-layered conducting substrates for large active area dye-sensitized solar cells," *Mater. Res. Bull.*, vol. 48, no. 7, pp. 2625–2629, Jul. 2013.

[56] A.-F. Kanta and A. Decroly, "An investigation of the electrolytic solution effects on stainless steel electrode for dye-sensitized solar cells," *Mater. Chem. Phys.*, vol. 130, no. 3, pp. 843–846, Nov. 2011.

[57] T. M. Watson, G. J. Reynolds, and D. a Worsley, "Painted steel mounted dye sensitised solar cells: titanium metallisation using magnetron sputtering," *Ironmak. Steelmak.*, vol. 38, no. 3, pp. 168–172, Apr. 2011.

[58] F.-Y. Ouyang and W.-L. Tai, "Enhanced corrosion resistance of TiN-coated stainless steels for the application in flexible dye-sensitized solar cells," *Appl. Surf. Sci.*, vol. 276, pp. 563–570, Jul. 2013.

[59] N. Vyas, D. A. Wragg, C. Charbonneau, M. Carnie, and T. M. Watson, "Low Cost TCO Less Counter Electrodes for Dye-Sensitized Solar Cell Application," *ECS Trans.* , vol. 53 , no. 24 , pp. 39–46, Oct. 2013.

[60] N. Vyas, C. Charbonneau, M. Carnie, D. A. Worsley, and T. M. Watson, "An Inorganic/Organic Hybrid Coating for Low Cost Metal Mounted Dye-Sensitized Solar Cells," *ECS Trans.* , vol. 53 , no. 24 , pp. 29–37, Oct. 2013.

[61] L. Meng, M. Wu, Y. Wang, W. Guo, C. Ma, T. Ma, and R. Silva, "Effect of the compact Ti layer on the efficiency of dye-sensitized solar cells assembled using stainless steel sheets," *Appl. Surf. Sci.*, vol. 275, pp. 222–226, Jun. 2013.

[62] H. Kusama and H. Arakawa, "Influence of alkylaminopyridine additives in electrolytes on dye-sensitized solar cell performance," *Sol. Energy Mater. Sol. Cells*, vol. 81, no. 1, pp. 87–99, Jan. 2004.

[63] H. Kusama, H. Sugihara, and K. Sayama, "Nitrogen-Containing Heterocycles' Interaction with Ru Dye in Dye-Sensitized Solar Cells," *J. Phys. Chem. C*, vol. 113, no. 48, pp. 20764–20771, Dec. 2009.

6 *Corrosion behaviour of cobalt electrolytes*

6.1 Introduction

As Chapter 5 has shown, the triiodide/iodide based electrolyte reacts aggressively with certain industrial metals. Following this study, alternative electrolytes such as a cobalt (II/III) redox couple have been assessed as possible alternative liquid electrolytes in DSC devices as they are known to be less aggressive and give higher performance when optimised. As previously mentioned in Chapter 1, cobalt (II/III) complexes undergo an outer sphere, one electron transfer, and usually have a redox potential that will give a higher V_{oc} than the 0.75V typical for the iodide/triiodide DSCs when matched with a suitable dye [1]. This usual iodide/triiodide redox couple operates through an inner-sphere electron transfer process, which proceeds at a slower rate to the cobalt complex electron transfer. It has been stated in the literature that a cobalt based redox couple is not corrosive to some metal substrates [2], [3]. However, no dedicated corrosion monitoring study has so far been published. This chapter seeks to monitor the interaction of cobalt with several metal substrates over a set time period, using the same *in situ* corrosion monitoring method that was developed for the triiodide corrosion analysis in Chapter 5.

6.2 Experimental

The electrolyte solutions and corrosion monitoring cells were prepared as detailed in Chapter 2. The cobalt complex selected for this study was the commercially available -(2,2'-bipyridine)cobalt(II) di(hexafluorophosphate) or cobalt(bpy)$_3$ PF_6 based complex (Dyenamo AB, Sweden) [4]. Briefly, 0.2M of Co^{2+} complex and 0.02M Co^{3+} or 0.2M of Co^{3+} were dissolved in 3-methoxypropionitrile (3-MPN). A further compound, 0.1M $LiClO_4$, was also added to the DSC electrolyte as a source of lithium ions to improve performance. Further to this, additions of 0.25M and 0.5M 4-*tert.*butylpyridine (4-TBP) were also added to two of the formulations in order to assess the corrosion inhibition effect of 4-TBP when used with a cobalt complex electrolyte. DSC devices on FTO-glass, using this electrolyte were successfully constructed and tested, showing that the electrolyte formulation was viable for use. Figure 6.1 demonstrates the comparison between a successful cobalt cell and a traditional DSC containing iodide/triiodide electrolyte.

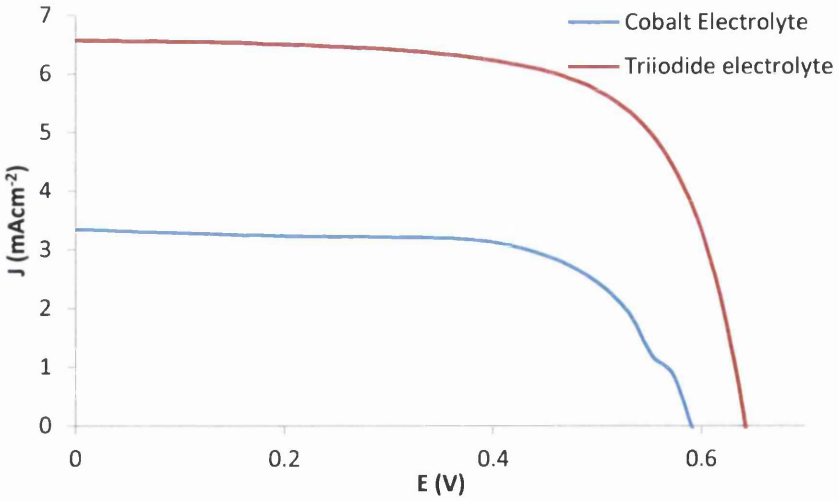

Figure 6.1: I-V curve illustrating the successful performance of cobalt electrolyte using 0.2M Co^{2+}/ 0.02 Co^{3+} in a DSC device compared with a standard triiodide/iodide electrolyte device

In the current non-optimised configuration, an operational DSC device was still able to be constructed, though the J_{sc} and V_{oc} values are much less than for the comparison triiodide based device. The discrepancy between cells was the result of unfamiliarity with the cobalt electrolyte in a DSC format and the non-optimised components of the solar cell with regards to the cobalt complex. The substrates tested in this study are listed here. Only the most relevant structural or vulnerable substrates were tested in this study:

- Iron
- Iron covered with TiO_2 blocking layer
- Stainless Steel 304
- Titanium
- Nickel
- Copper

Iron is the common base to many industrial substrates, and as a result provides an ideal starting point for this analysis. An iron substrate was also covered with a TiO_2 blocking layer, to understand whether this could provide some corrosion protection - a TiO_2 layer is critical in a cobalt complex cell, as it acts as a blocking layer to prevent the recombination of electrons with the Co^{3+} species, this happens rapidly due to the outer sphere electron process [5]. Stainless steel 304 is a common type of stainless steel, used in many applications from structural to tableware, thus it will be important to assess this material's stability in this electrolyte formulation, compared to with the iodide/triiodide electrolyte. Titanium was included as a control metal, as it is known for the high corrosion resistance imparted by a strongly bonded oxide layer that forms rapidly in air. Nickel was studied as it

remains one of the most common alloying elements, and further a possible replacement for silver contacts in dye solar cells. Finally, copper was included as it is a commonly used connector used in DSC cells. This substrate was not previously tested in Chapter 5, as it is already proven to be extremely vulnerable in triiodide electrolyte, even in literature reports containing 4-TBP as an additive. The only additive used in this study was 4-TBP, as this is the only performance enhancing compound reported for cobalt electrolyte DSCs in the current literature. Further electrochemical studies are necessary before other NHC can be utilised, due to the current lack of data for cobalt electrolytes containing performance enhancing additives, compared with iodide/triiodide DSC devices. The goal was to assess if the cobalt electrolyte required a corrosion inhibitor and also if 4-TBP could fulfil the requirement.

6.3 Assessment of cobalt complex electrolyte

Before analysis of the metal corrosion could progress, the UV-VIS spectra of both the Co^{3+} and Co^{2+} species was assessed, see Figure 6.2. The Co^{2+} complex was seen to absorb strongly in the 400-520nm range, resulting in a green/yellow tint. The Co^{3+} absorbance is much reduced in the same region, resulting a much weaker coloration of the solution. The large absorbance from 200nm to 325nm indicates absorbance in the UV region, typically from the 3-MPN solvent.

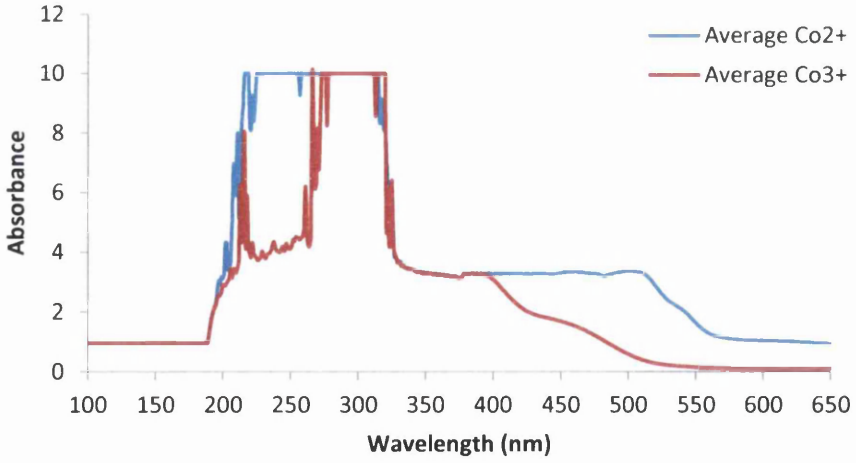

Figure 6.2: UV-VIS spectra of a 0.2M Co^{2+} solution and a 0.02M Co^{3+} solution. The solvent for each is 3-MPN

In literature, the initial synthesis study by Sapp *et al.* reports that the $Co(bpy)_3(PF_6)_x$ complex exhibits similar spectra to other cobalt complexes, where the Co(II) complex gives a weak absorption around the 440-450nm range, resulting in an electrolyte with a green tint, compared to the yellow coloured triiodide that has a strong absorption at 360nm to 500nm [2]. Crucially, it was reported that the absorbance of the Co(III) species was minimal

in comparison, which is the reverse of the triiodide/iodide species. Further to this, the point was made that any partial oxidation of the Co(II) complexes would reduce the overall absorbance of the electrolyte solution, rendering it more colourless. These features indicate that the RGB image analysis method may not be as viable as for the traditional triiodide DSCs. Sapp *et al.* also investigated the effect of adding pyridine molecules such as 4-*tert*-butylpyridine (4-TBP) to the electrolyte. Their results show a similar increase in the V_{oc} to the effect in the triiodide/iodide electrolyte system. However, in certain cases the J_{sc} of cobalt electrolyte system DSCs also increases slightly. The V_{oc} effect was due to the shifting of the Fermi level and the reduction of dark current at vacant TiO_2 sites. Since the effect reported matched that of the iodine based electrolyte used in Chapter 5, it was thought that there would be no detrimental effect on future DSC performance through the addition of the compound as a possible corrosion inhibitor in this Chapter.

6.4 Assessment of metal substrates

Table 6.1 summarises the metals used in this study, in addition the cell components and resulting lifetimes observed.

Table 6.1: Lifetime and purity of metal substrates against Co^{3+} and 4-tBP concentration used in this study "-" denotes no degradation over the observed experimental period

Metal	Purity	Co^{3+} (M)	4-tBP (M)	Lifetime (hrs)
Iron	99.5%Fe	0.02	N/A	2
"		0.2	N/A	0.5
Iron + $TiCl_4$ blocking layer	99.5%Fe	0.02	N/A	23
"		0.2	N/A	22
"		0.02	0.25	~24
"		0.02	0.5	25
Stainless Steel 304	18%Cr, 10%Ni	0.02	N/A	-
"		0.2	N/A	-
Ti	99.6%Ti	0.02	N/A	-
"		0.2	N/A	-
Ni	99.98%Ni	0.02	N/A	-
"		0.2	N/A	-
Al	99.95%Al	0.02	N/A	-
"		0.2	N/A	-
Cu	99.9%Cu	0.02	N/A	100
"		0.2	N/A	-
"		0.02	0.25	-
"		0.02	0.5	-

It should be noted that 4-TBP additions are only used for further study on the most vulnerable substrates and not throughout this chapter due to the need to focus mainly on the interaction of the cobalt complex with the substrate, rather than with chemical additions.

6.4.1 Iron

The preliminary study observed an iron substrate prepared using the surface preparation method detailed in Chapter 2. Two different concentrations 0.02M and 0.2M were used to determine if the concentration of the Co^{3+} ion affected the corrosion behaviour of this electrolyte. Initially, the cells degrade rapidly, giving a colour change from light yellow/green to blood red, Figure 6.3. The yellow/red transition was found to be already underway in the high concentration cell in the first five minutes of the study. It was interesting that the reaction started in the corners of the cell, thought to be where the cell is thinnest following the pressure sealing. This would lower the volume at the corner point and promote faster degradation. The yellow to red colour change matches that found by Miettunen *et al.* in cells containing a $[Co(bipy)_3]/[Co(bipy)_2]$ redox couple [3]. Interestingly, this is the same colour change that was found for nickel substrates exposed to a triiodide/iodide electrolyte containing no additives.

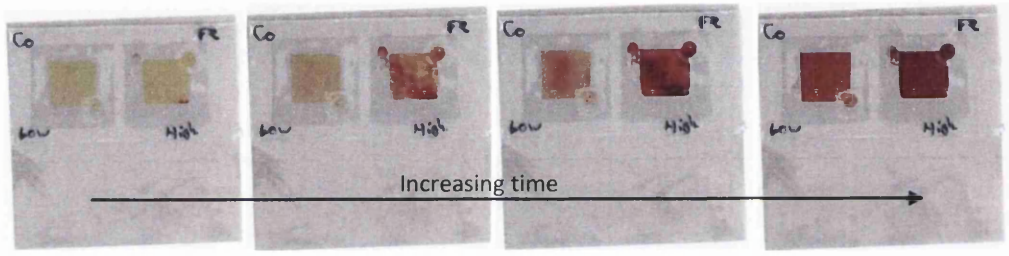

Figure 6.3: Degradation of Iron substrate in a cell containing cobalt electrolyte. Left cell contains the low 0.02M Co^{3+} concentration; the right cell contains the 0.2M high Co^{3+} concentration

The reaction was confirmed to be chiefly between the iron substrate and the Co^{3+} complex through isolation experiments using Co^{3+} or Co^{2+} in 3-MPN, Figure 6.4. The cell containing Co^{3+} changes to a defined red colour, while the Co^{2+} cell remains mostly yellow/green, but begins to show a red colouration.

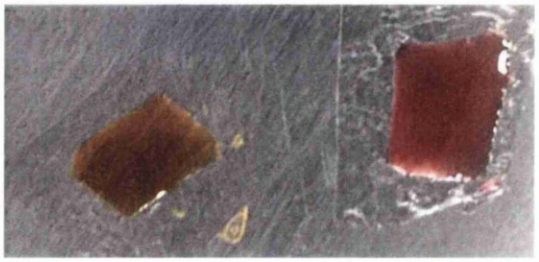

Figure 6.4: Isolation test showing the effects of either Co^{2+} or Co^{3+} species on the Fe substrate

Figure 6.5 indicates that this shift from yellow to red with Co^{3+} occurs fully within 2 hours regardless of the concentrations of Co^{3+}, though the end value of low concentration 0.02M cell did not reach the same point as the higher concentration 0.2M. As mentioned

previously, this was theorised to be due to differences in the cell volume and material surface finish. The onset of the colourless region was also seen to be variable, with the higher concentration fully transitioning to colourless at 1 hour compared to the 2.5 hours for the 0.02M concentration. The faster transition was thought to be due to the higher concentration of Co^{3+} ions in the electrolyte solution.

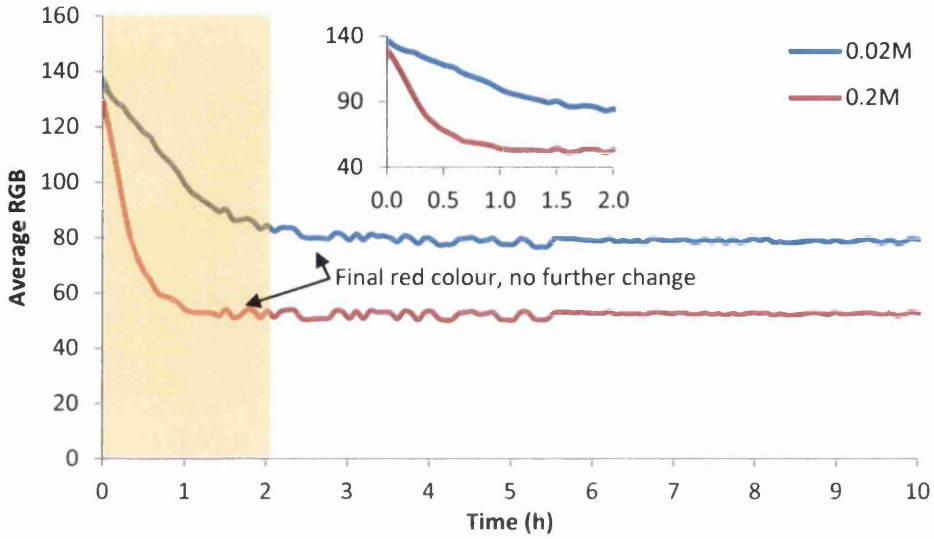

Figure 6.5: Average RGB value vs. time for Iron substrate corrosion cells containing cobalt electrolyte. Yellow shaded area denotes green/yellow to red transition. Inset figure shows first 2 hours of degradation.

The multifaceted nature of the cobalt complex ion means that several different interactions will be possible between it and the iron substrate. The cobalt metal ion, the bipyridyl ligands and the PF_4 counter ion are all possible candidates. Without further testing using the complex components, it was suggested that the red colouration represents the substitution of the Co iron in the complex by a Fe ion, which will cause degradation in the performance of the electrolyte.

Due to the unexpected susceptibility of the Fe substrate to attack when in contact with the cobalt electrolyte, a further study was undertaken where a blocking layer was applied to the vulnerable iron substrate through immersion and heating in $TiCl_4$ solution. A blocking layer is a necessary component in cobalt electrolyte DSC with metal substrate, due to the inherent fast electron transfer exhibited by outer-sphere electron transfer complexes to highly conductive substrates [5]. When a TiO_2 blocking layer is applied though $TiCl_4$ treatment, the cell remained stable for 20 hours, Figure 6.6. This is in contrast to the sub-1 hour life time of the of the electrolyte exposed to bare iron, Figure 6.5, the blocking layer appears to have been partially successful in protecting the substrate as a physical barrier to

cobalt species movement, though it is thought that the simultaneous degradation of both high and low Co^{3+} concentrations at *ca.*20 hours is the result of the treatment rendering the iron substrate more vulnerable through the heating and chemical exposure during the $TiCl_4$ process. This seems to be supported by the similar degradation of the cells which included 4-TBP and a low 0.02M Co^{3+} concentration.

As a result of the success of 4-tert.butylpyridine (4-TBP) as a corrosion inhibitor in triiodide/iodide based DSCs, the compound was assessed further for vulnerable metallic substrates exposed to a cobalt electrolyte. However, the resulting study found that the 4-TBP only has a small effect on the degradation. This was believed to be indicated by the difference in final transition, Figure 6.6 inset, where the final change is slowed in the 0.25M and 0.5M 4-TBP cells, compared to the control cell. As reported in the paper by Koh *et al.* the 4-TBP species increases the viscosity of the electrolyte and will slow down diffusion of the Co^{3+} species [6]. In addition it was also thought to bond to the substrate or TiO_2 and inhibit movement toward the electrode, which previous literature has proven [7].

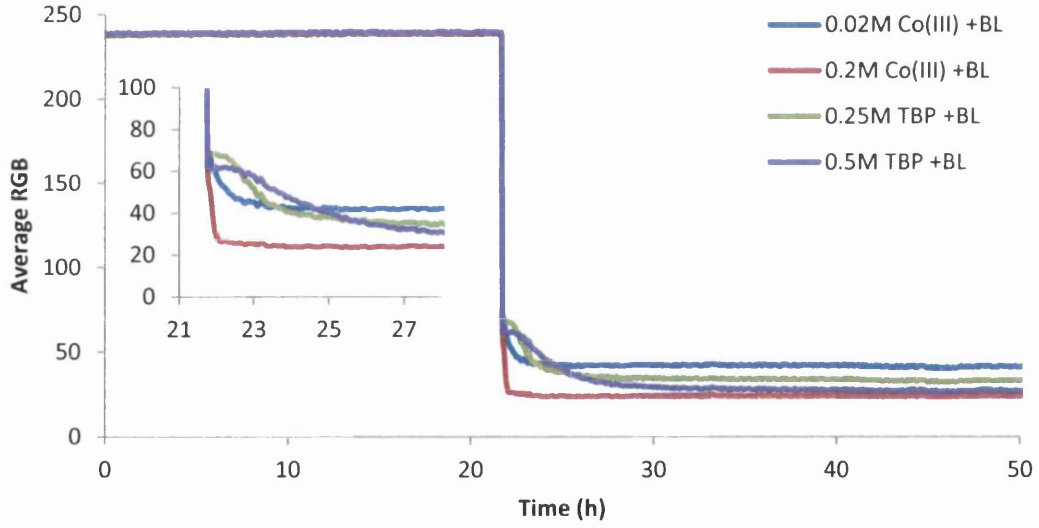

Figure 6.6: Average RGB value vs. time for iron substrate coating with a $TiCl_4$ blocking layer (BL) and exposed to 0.02M Co^{3+} cobalt complex electrolyte and 4-TBP. Inset figure shows the 21-28hours section where the colour transition occurs

One key observation in the reaction between the cobalt electrolyte and the substrate, is that there is a colour change to red rather than colourless, shown by the drop in average RGB from 240 to 25-30 mentioned previously in Figure 6.6. This is also evidenced in Figure 6.7 showing the change in colour from 0hrs to 500hrs.

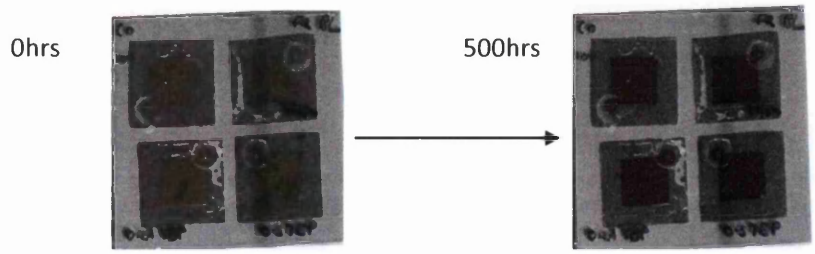

Figure 6.7: Titania blocking layer coated nickel substrate in exposed to cobalt based electrolyte. Clockwise from top left: 0.02M Co^{3+}, 0.2M Co^{3+}, 0.02M Co^{2+} + 0.25M 4-tBP, 0.02M Co^{3+} + 0.5M 4-tBP.

This is theorised to be due to the substitution of the Co complex ion by Fe, the resulting iron complex would then be red in colour. However, without further testing of the electrolyte, this has yet to be fully confirmed.

6.4.2 Titanium & Stainless Steel 304

Titanium has already proven to be resistant to the iodide/triiodide electrolyte, which is a much more aggressive electrolyte than this cobalt complex. The cobalt electrolyte containing low and high concentrations of Co^{3+} species was studied to make certain this resistance is carried over to a metal complex electrolyte species with different chemistry. As expected, no noticeable change in RGB value was observed when studying the cobalt electrolyte and titanium substrate interaction, Figure 6.8. The green/black residue external to the observation cells at 100hrs is not metal corrosion, but dried cobalt complex, which stresses the importance of ensuring cell integrity when manufacturing full DSCs.

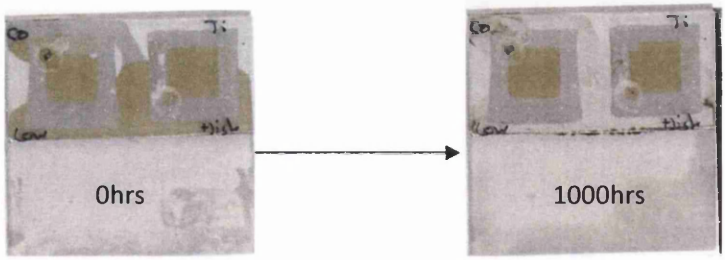

Figure 6.8: Titanium substrate in contact with cobalt electrolyte. Left cell contains 0.02M Co^{3+}; right cell contains 0.2M Co^{3+}

Stainless steel 304, hereafter written as StSt304, was studied in order to verify the data of previous literature, and its common use in the construction industry. Figure 6.9 shows the lack of colour change in the electrolyte over 1000 hours testing time, a similar response to that of 304 in contact with triiodide in Chapter 5.

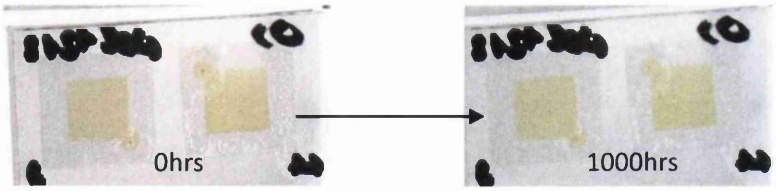

Figure 6.9: Stainless steel 304 in contact with cobalt electrolyte. Left cell contains 0.02M Co^{3+}, right cell contains 0.2M Co^{3+}

The results of this test were supported by a previous study from Miettunen *et al.*, who reported up to 500 hour stability for this metal [3].

6.4.3 Aluminium & Nickel

The activated aluminium samples showed negligible colour change after 1000 hours contact with the cobalt electrolyte at both high and low Co^{3+} concentrations, though there is a larger disparity in their average RGB than expected due to concentration differences, Figure 6.10. It was though that this was caused by the light colour and high reflectivity of the substrate compared with the previous observed metals. The low concentration is much closer to the base cream-yellow colour of the 3-MPN solvent, hence its high relative RGB. The long lifetime seen for activated Al metal is an excellent result compared to the 88hr lifetime for the aluminium substrate cell containing no inhibitors, Figure 6.10.

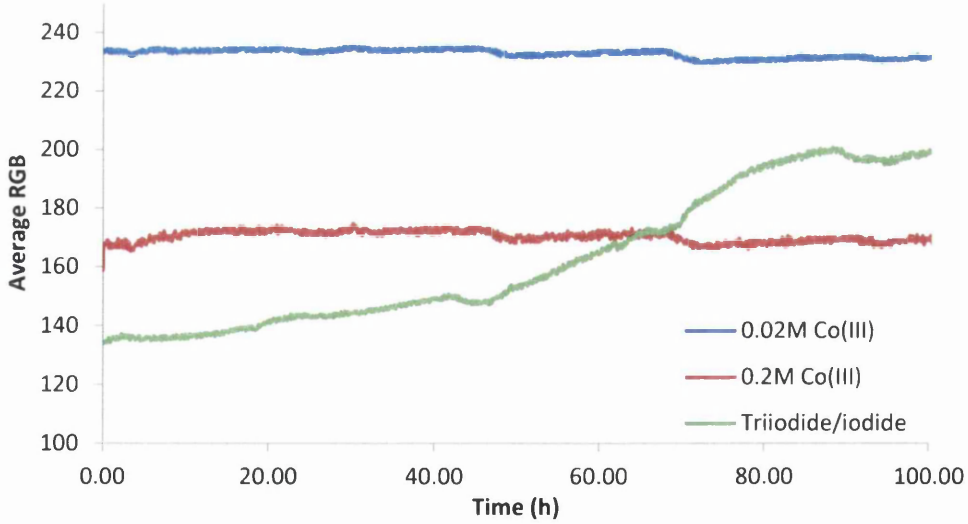

Figure 6.10: Comparison of Al substrate exposed to triiodide electrolyte and cobalt electrolyte at either 0.02M Co^{3+} or 0.2M Co^{3+}

This behaviour matches well with previous literature on the subject, reporting the lack of visible corrosion or cell instability [3].

The nickel cells also improve vastly upon the performance of the equivalent substrate in contact with triiodide/iodide electrolyte, Figure 6.11. This shows no degradation in comparison to full loss of colour in 60hrs for an uninhibited triiodide test cell. An interesting result was that the Ni/cobalt cells did not exhibit the same yellow to red initial colour change that was shown by the Ni/triiodide cells, Figure 6.11. The final RGB value of the triiodide cell matches that of the un-reacted cobalt containing cells, indicating that the cobalt cells RGB is very close to that of the 3-MPN solvent on this substrate, therefore care was taken to check the RGB analysis method, so that it was able to compensate for the reduction in RGB value *versus* that of the background chemicals.

Despite previous evidence that different concentrations of Co^{3+} provoke different RGB values, the difference between 0.02M and 0.2M Co^{3+} is remarkably small. It was thought that the variation is dependent on the background reflectivity and colour of the substrate, especially since the cobalt electrolyte is clearly much paler in colour to the triiodide electrolyte.

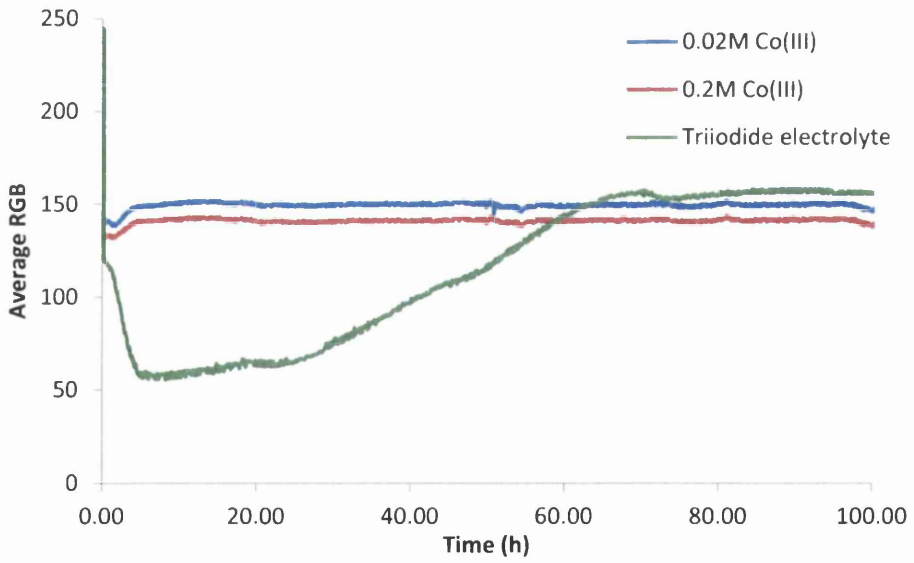

Figure 6.11: Comparison of Ni substrate exposed to triiodide electrolyte and cobalt electrolyte at either 0.02M Co^{3+} or 0.2M Co^{3+} concentration

However, these samples are still potentially vulnerable with some reports stating that microscopic analysis has observed small quantities of metal debris elsewhere in the test devices following cell aging.

6.4.4 Copper

Just as important as the bulk metallic substrates, the corrosion behaviour of conductive layers is of critical importance. One of the major issues with iodide/triiodide cells was the use of the robust but poorly conductive FTO or ITO layers, as superior conductors such as copper and silver were susceptible to corrosion by the triiodide species [8]. Since the cobalt based electrolyte has been reported to be less aggressive towards metal substrates, this following study observe how conductive materials will perform in a thin layer cell arrangement. Copper tape has been used as a current collector and external connection point in dye sensitised solar cells, it is an excellent connection material that would increase the performance of the DSC if the tape or a printed copper ink was able to survive in the cell environment as an internal current collector to replace the FTO or ITO layer. Unfortunately, even using the less aggressive cobalt electrolyte, the copper was still found to be vulnerable to attack, Figure 6.12. The cells initially show some instability in RGB value, which from experimental analysis is deemed to be from interference within the observation environment and the effects of the lighting system, as the copper is an extremely reflective substrate.

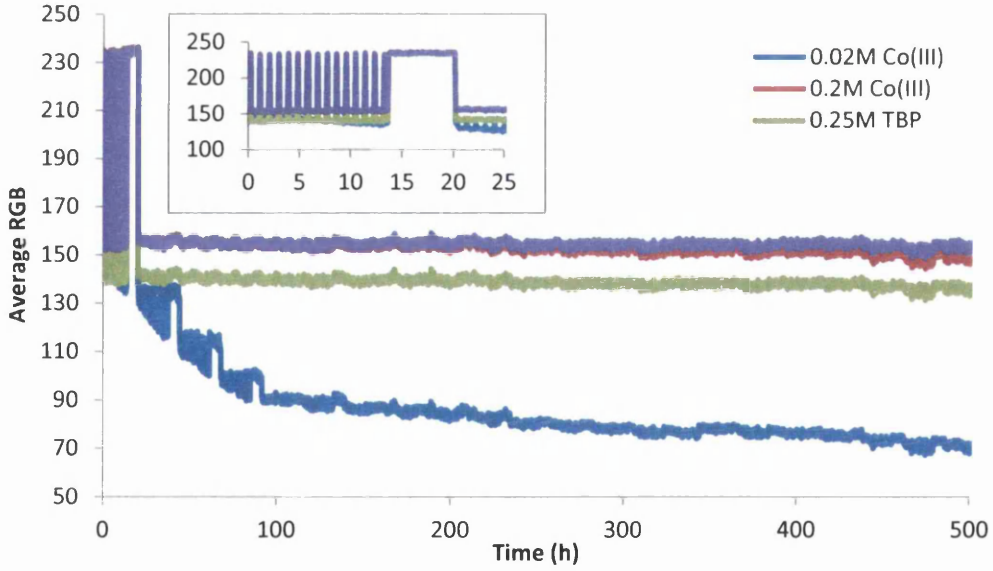

Figure 6.12: Average RGB vs. time for copper substrate with varying concentrations of Co^{3+} complex and TBP

Despite this observation, the instabilities were seen to settle at *ca.* 20 hours. The instability, shown by the inset in Figure 6.12 has been deliberately left in to these results as it shows the possible variability of this image analysis technique. Given enough images and a baseline RGB for each component, this can be identified, interpreted and still return viable observation data for DSC quality management.

The initial degradation of the 0.02M cell in the period 0-100 hours is visible through a colour change from pale yellow to blood red, Figure 6.13. The average RGB value was seen to reduce from 150 reducing to 90, with the colour change showing similarity to the study with triiodide and nickel substrate in Chapter 5.

Figure 6.13: Copper substrate after exposure to cobalt electrolyte. Clockwise from top left: 0.02M Co^{3+}, 0.2M Co^{3+}, 0.02M Co^{3+} + 0.25M 4-tBP, 0.02M Co^{3+} + 0.5M 4-tBP

The low and high concentration Co^{3+} vary by *ca.* 60 relative RGB units, with the low 0.02M concentration falling to 90 and indicating further reductions after 500 hours. The majority of the Co^{3+} loss takes place in the first 100 hours of observation, though from 100 hours on the rate of colour loss decreases, suggesting the loss of the majority of Co^{3+} ions. In contrast, the high 0.2M Co^{3+} concentration remains at *ca.* 150 relative RGB for the full 500 hours observed, though it can be seen that there is a slow reduction in the RGB value over time. Interestingly, the higher concentration of 0.2M Co^{3+} appears to decrease the rate of colour loss, suggesting that either the lower concentration renders the cell more sensitive, or that the higher concentration has other inhibiting mechanisms in play.

The addition of 0.25M or 0.5M 4-TBP to the 0.2M Co^{3+} cells also reduces degradation to match that of the 0.2M Co^{3+} cell. As previously suggested, the large concentration of the complex ion, Co^{3+}, is thought to self-restrict the diffusion of molecules toward the metal surface. This then slows the interaction/degradation reaction and therefore the colour loss in the cell. Similar to in the triiodide cells in Chapter 5, the lower concentration of Co^{3+} made this experiment more sensitive to the degradation interactions within each test cell, whereby the coloured Co^{3+} compound reduces to Co^{2+}. Thus degradation will occur over a much longer time period than used in this study. It is still thought that the potential produced by a DSC device will inhibit corrosion while the device is active, so the longer degradation time and less aggressive behaviour of the cobalt electrolyte would allow the investigation of copper current collectors to replace the FTO or ITO in use currently. However, the study by Miettunen *et al.* puts doubt on this assumption, through reporting the degradation of cells, despite being under illumination and operating conditions [9].

6.5 Comparison of electrolyte degradation using image analysis

In Chapters 5 & 6 we have sought to prove the viability of a mass sample observation and analysis process that could potentially be transferred to a pilot or full size production line as a quality management method. In the process we have also shown that certain substrates behave differently in thin layer cells compared to reported studies. In brief this section compares several of the key metal substrates analysed, in order to quantify the difference in cell stability, Table 6.2.

Table 6.2: Comparison of electrolyte colour life times for metal in contact with cobalt based or triiodide based electrolyte. "-" indicates no colour visible change

Metal	Lifetime (h)	
	Cobalt	**Iodide/triiodide**
Bare Fe	0.33	1.5
Inhibited Fe	20	-
Ti	-	-
StSt304	-	-
Surface Activated 99.0%Al	-	88
Ni	-	9
Copper	160	<1

Surprisingly, the iron substrate in contact with cobalt electrolyte exhibits a colour change before the equivalent triiodide containing cell. However, the red colouration to the cells indicated that the reaction was somewhat different than what was expected. As mentioned previously, it was believed that the Co and Fe atoms were substituted, forming a red coloured iron complex molecule. In addition, the cobalt electrolyte, with NHC inhibitors included, lasted only 20 hours when compared to the equivalent 4-tBP containing triiodide cell. Since the metal used was of the same batch and subjected to the same treatment, it was concluded that the cobalt complexes outer sphere electron transfer ability was able to negate the inhibition action of the NHC compound, which was successful in inhibiting the I_3^- chemisorption with the metal substrates in Chapter 5.

The Nickel substrate in contact with triiodide electrolyte also exhibits a yellow to red transition, believed to be evidence of the formation of a nickel iodide compound. This resulted in a short cell lifetime of 9hrs in comparison to the stable cobalt cells on Ni substrate observed throughout this study. A similar difference was found for surface activated 99.0%Al, where the cobalt cell appeared unchanged under RGB analysis, whereas the triiodide colour was removed from the observation cells containing no additives in

88hrs. An interesting comparison result is for copper metal. Lasting for 100 hours in cobalt electrolyte, compared to less than one for triiodide. It was believed that copper did not have as strong an affinity for the Co-complex molecule as it does when attacked by triiodide. Because of this, an appropriate inhibiting compound similar to NHC's may aid in the protection of copper substrate, to the extent that is could be used as an internal current collector in DSC devices.

These results have shown that the corrosion performance of this cobalt complex electrolyte is equally as variable as the triiodide containing electrolyte. A conclusion made for the different reaction of Ni and Al was that differing sizes of the Co^{3+} and I_3^- species allow the latter to move closer to the substrate and attack more active sites. The larger cobalt species is thought to self-restrict movement through the electrolyte, so that is does not approach that closely to the substrate surface.

6.6 Metal substrate DSCs using cobalt electrolytes

There have been several papers to date that have used metal sheets as DSC substrates to test their usability in full DSC containing cobalt complex electrolytes. Miettunen *et al.* published a paper concentrating on metal substrate counter electrodes [3]. The metals used were comparable to the previous work on DSCs in 2010 with metal photoelectrodes containing triiodide/iodide electrolytes. This paper focuses heavily on stainless steels such as 304, 321, 316, 316L, as these are the most attractive substrates for metal DSCs due to their low cost, durability and abundance in the form of large quantities of rolled sheets. This work also assessed the highly resistant metals Inconel 600, titanium and aluminium. Nickel and Zinc were also assessed, although these metals are commonly used as anti-corrosion coatings rather than sheet metal. Finally copper was also assessed, a high efficiency electrically conductive material that is extremely vulnerable to corrosion in the more usually used triiodide/iodide electrolyte. Initial reports from Miettunen *et al* agreed with the findings exhibited in this thesis, in that the copper metal is still vulnerable to corrosion in the cobalt electrolyte. Corrosion products were found on the copper electrode, identified by the study as pitting corrosion. Unfortunately, this will still prevent this metal being used as high efficiency charge collectors in DSC cells.

An interesting comparison is that Aluminium corrosion products were found in the study cells. However in the work presented in this thesis, the aluminium sheet sample showed no visible deterioration in the simple metal observation cells. It is possible that the active electrochemical nature of the DSC cells used in the Miettunen study could prove

detrimental to the Al substrate, therefore further work on the stability of metal substrates in complete DSCs with cobalt electrolytes is recommended. Of particular interest was the comparison of stainless steel 304 in a complete DSC cell with that of this thesis. The active cell showed no corrosion marks or products when stainless 304 was used as a counter electrode. The performance of these cells varied with the applied catalyst, the highest reached with chemically applied Pt at 1.9%, with a J_{sc} of 6.4mA/cm^2 and V_{oc} of 0.69V. This compared strongly with cobalt electrolyte cells on FTO glass substrates with 2.8% efficiency and with thermal Pt, but still unfortunately low compared with iodine based FTO glass cells which reached 4.1% efficiency, 8.1mA/cm^2 and 0.781V for V_{oc}.

6.7 Conclusions

Due to the recent interest in cobalt electrolyte based DSCs, there is a need for further exploration and experimentation in the study of the interaction with metal substrates. This would assess whether novel architectures using metallic substrates will still be vulnerable and be to be used long term in DSC devices. Using the RGB analysis method developed in Chapter 5, this study showed that the non-corrosive aspect of a cobalt complex electrolyte is strongly dependent on the metal substrate. Contrasting with the iodide/triiodide electrolyte study, the observed nickel and aluminium substrates show high resistance to degradation while in contact with the cobalt complex electrolyte. As expected, titanium and stainless steel 304 continue to be resistant to degradation and have high potential for DSC devices, though the high cost of titanium does detract from its performance. The susceptibility of the iron substrate to degradation by both low and high concentrations of cobalt electrolyte was unexpected and led the conclusion that there was an unforeseen interaction between the complex and the iron that was not susceptible to the inhibition methods studied here. Further assessment of the chemical reaction and other inhibition routes is recommended if DSCs are to be build using iron or low carbon substrates.

A further conclusion gained from this study is that nitrogen containing heterocyclics, such as the commonly used concentrations of 4-TBP compound have a negligible effect on the progress of the degradation reaction. It is thought that the size of the complex and the fast outer sphere electron transfer mechanism of the Co^{3+} complex ion avoid the 4-TBP barrier. Finally, it is clear that the corrosion aspects of this complex require further study, especially for DSC devices on sheet metal substrates. It is recommended that the progress be monitored electrochemically in future work to assess the reactions occurring within the observation cells.

6.8 References

[1] J.-H. Yum, E. Baranoff, F. Kessler, T. Moehl, S. Ahmad, T. Bessho, A. Marchioro, E. Ghadiri, J.-E. Moser, C. Yi, M. K. Nazeeruddin, and M. Grätzel, "A cobalt complex redox shuttle for dye-sensitized solar cells with high open-circuit potentials.," *Nat. Commun.*, vol. 3, p. 631, Jan. 2012.

[2] S. A. Sapp, C. M. Elliott, C. Contado, S. Caramori, and C. A. Bignozzi, "Substituted polypyridine complexes of cobalt(II/III) as efficient electron-transfer mediators in dye-sensitized solar cells.," *J. Am. Chem. Soc.*, vol. 124, no. 37, pp. 11215–22, Sep. 2002.

[3] K. Miettunen, T. Saukkonen, X. Li, C. Law, Y. K. Sheng, J. Halme, a. Tiihonen, P. R. F. Barnes, T. Ghaddar, I. Asghar, P. Lund, and B. C. O'Regan, "Do Counter Electrodes on Metal Substrates Work with Cobalt Complex Based Electrolyte in Dye Sensitized Solar Cells?," *J. Electrochem. Soc.*, vol. 160, no. 2, pp. H132–H137, Dec. 2012.

[4] S. M. Feldt, E. A. Gibson, E. Gabrielsson, L. Sun, G. Boschloo, and A. Hagfeldt, "Design of organic dyes and cobalt polypyridine redox mediators for high-efficiency dye-sensitized solar cells.," *J. Am. Chem. Soc.*, vol. 132, no. 46, pp. 16714–24, Nov. 2010.

[5] P. J. Cameron, L. M. Peter, S. M. Zakeeruddin, and M. Grätzel, "Electrochemical studies of the Co(III)/Co(II)(dbbip)2 redox couple as a mediator for dye-sensitized nanocrystalline solar cells," *Coord. Chem. Rev.*, vol. 248, no. 13–14, pp. 1447–1453, Jul. 2004.

[6] T. M. Koh, K. Nonomura, N. Mathews, A. Hagfeldt, M. Grätzel, S. G. Mhaisalkar, and A. C. Grimsdale, "Influence of 4- tert -Butylpyridine in DSCs with Co II/III Redox Mediator," *J. Phys. Chem. C*, p. 130722085010008, Jul. 2013.

[7] M. K. Nazeeruddin, A. Kay, R. Humphry-Baker, E. Muller, P. Liska, N. Vlachopoulos, and M. Grätzel, "Conversion of Light to Electricity by cis-X2Bis(2,2'-bipyridyl-4,4'-dicarboxylate)ruthenium(11) Charge-Transfer Sensitizers (X = Cl-, Br-, I-, CN-, and SCN-) on Nanocrystalline Ti02 Electrodes," *J. Am. Chem. Soc.*, no. 4, pp. 7863–7863, 1993.

[8] T. Ma, X. Fang, M. Akiyama, K. Inoue, H. Noma, and E. Abe, "Properties of several types of novel counter electrodes for dye-sensitized solar cells," *J. Electroanal. Chem.*, vol. 574, no. 1, pp. 77–83, Dec. 2004.

[9] K. Miettunen, X. Ruan, T. Saukkonen, J. Halme, M. Toivola, H. Guangsheng, and P. Lund, "Stability of Dye Solar Cells with Photoelectrode on Metal Substrates," *J. Electrochem. Soc.*, vol. 157, no. 6, p. B814, 2010.

7 *Conclusions and further research*

The initial studies of platinum electrodeposition concluded that the methods previously trialled in literature were not easily reproducible or adaptable to faster processing at sub-30 seconds deposition time. Furthermore, electrodeposition resulted in the deposition of larger platinum quantities than seen in the more commonly used chemical and thermal platinisation methods, an extremely undesirable result considering the current high cost of platinum. The basic electrodeposited catalysts gave poor catalytic performance, the highest value for J_{lim} being 0.051A/cm^2 for constant potential deposition, versus 0.067A/cm^2 for the chemical method, despite SEM imagery showing the presence of much more material seen than when chemical platinisation was utilised. A particular point of note is the difference in platinum deposit size, from 5-50nm in the case of the chemically platinised FTO-glass to 500nm to 2µm in the case of electrodeposited. Despite the published evidence of high performing devices using electrodeposited platinum counter electrodes, the technique is more complex and variable than the usual thermal or chemical platinisation. As a result of the variable and low performing nature of these initial methods, Chapter 4 explores other variations on the electrochemical deposition of catalytic material.

Research on catalyst development reported a technique known as Single Layer Redox Replacement (SLRR), utilising a low cost, easily deposited template material to aid in the initial formation of the desired catalyst microstructure. Chapter 4 details the successful development of this technique using FTO-glass as the substrate. The formation of small nanometre Pb clusters, characterised through SEM and XPS, allowed finer control of the deposit morphology leading to the galvanic replacement of Pb by Pt and the formation of small nanometre deposits of catalytic platinum on the FTO surface. Pulse potential deposition was deemed the most efficient method of controlling the electrodeposition, the short potential pulse resulting in small nanometre diameter Pb deposits and the potential off time resulted in the galvanic replacement of Pb by Pt. Due to the short pulses and the electroless nature of the replacement, this process also seemed to be the most efficient, power wise, for use in large scale production. After electrochemical analysis to determine the optimum potential setup, these counter electrodes were used in DSC devices, where efficiencies ranged from 3% to 3.5% compared with 3.53% using chemical CEs. The fill factor of these devices ranged from 55.48% at 1 cycle to a respectable 63.34% at 20 cycles, leading to a good comparison with the DSCs using chemically produced CEs at 68.80%.

Further optimisation was thus thought to result in a stable catalyst to rival thermal or chemically platinisation.

Since the eventual aim of industry is to use ITO-Polymer, future research suggested is the trial and optimisation of this technique on the conducting polymer material. Furthermore, as lead is a toxic material, other metals should be investigated for use as the template. In particular, Sn has the correct potential difference to Pt to be able to be galvanically replaced. In addition, there is greater industrial expertise in the field of tin plating.

The second part of this thesis studied the relationship between the electrolyte and bulk metal substrates that are available for use in flexible metal DSC devices. This follows the thesis theme of electrolyte interactions with the various materials or substrates used in DSC architecture. Chapter 5 successfully presents a quantative method of the mass *in situ* monitoring and characterisation of samples, utilised for metal substrates exposed to a simple two component iodide/triiodide electrolyte. In a passive environment, damage to the metal substrate can easily be replaced or repaired, but in a DSC environment this is not possible so increasing substrate lifetime or resistance was deemed necessary. In addition to this, the degradation reaction in the cell depletes the number of charge carriers available in solution and thus decreases DSC performance, so it is vital for industry to have a rapid means of device assessment for quality control and bulk sample analysis.

The initial study in Chapter 5 compared time-lapse image RGB analysis with DR-UV-VIS absorbance measurements which are more commonly used. This successful comparison showed negligible difference between the methods, indeed it was concluded that the RGB method was superior as more samples can be processed simultaneously and there is always a sample visible, rather than hidden in the equipment.

This analysis further concluded that iron was intensely vulnerable to attack, showing cell failure in 2 hours. This also cast doubt on the use of low cost carbon steel as a DSC substrate. Zinc was also shown to have a major vulnerability to attack, leading to the galvanisation method of corrosion protection of steels being unusable in DSC devices. Low purity aluminium (99.0%) was only shown to react when surface activation occurred to remove the protective oxide layer on the surface and the nickel substrate showed cell failure at 65 hours and above. Despite this evident vulnerability, the metals are only exposed to corrosion when the DSC device is not operating, i.e. at night. Therefore, the 30 and 65 hour degradation times for Al and Ni respectively may allow their usage in constantly operating devices. High cost materials such as titanium, tungsten, molybdenum

and chromium were shown to be resistant, as did two grades of stainless steel 316L and 304, which are formulated for high corrosion resistance, particularly in aggressive environments, such as acids. The alloy known as Inconel 625 was also found to be highly resistant to attack from the triiodide species.

Since a typical DSC electrolyte consists of more components than the iodide and triiodide, the additive 4-tBP was included in the initial testing to ascertain the reaction of a more complex electrolyte. The unexpected conclusion of this research was that the small nitrogen containing heterocyclic compound (NHC) functioned as a corrosion inhibitor, noticeably retarding the degradation of an iron substrate corrosion cell. Since large molecule NHC's have been extensively proven as corrosion inhibitors in industrial environments, the dual use of small NHC's as performance enhancers and corrosion inhibitors will have a positive impact on DSC construction. This research found that concentrations of 0.5M to 1M were sufficient to seriously retard, or fully inhibit the degradation reactions on the Al and Ni substrates. Iron was inhibited for up to 400 hours when high 4-tBP and 1-MBI concentrations were included, though unfortunately little effect was seen when the 135T compound used, thought to be due to the lack of functional groups on the triazine ring compared to 1-MBI and 4-tBP. It was concluded that the choice of functional group in the structure of small NHC's is a critical factor in determining the impact of the inhibitor compound. The known methods of corrosion inhibition using organic compounds were studied and the most likely method, steric hindrance, was concluded to be the most viable method of inhibition observed in these samples.

This chapter also theoretically explored the bonding mechanism used by the NHC's using the nitrogen lone pairs to bond to the metal surface. This will position the NHC compounds close to the metal and prohibit the interaction between the triiodide and the metal substrate. Future research should investigate the bonding mechanism between NHC's and the metal substrates in a full DSC environment.

Chapter 6 utilised the RGB analysis method presented in Chapter 5 for the study of the behaviour of a cobalt bipyridyl complex electrolyte in contact with metal substrate. This research concluded that iron substrate was vulnerable in cobalt electrolyte. This was evidenced despite changing the Co^{3+} concentration and applying a TiO_2 blocking layer to the metal surface, or including 4-TBP in the electrolyte. The majority of the industrial metals tested proved resistant to cobalt electrolyte degradation, result that is supported by available literature. Unfortunately, copper was shown to be as vulnerable to the cobalt

electrolyte as the triiodide/iodide electrolyte. In order to further quantify these results, it is recommended that other cobalt complexes undergo a similar monitoring procedure. This will show if the design of the complex is able to aid in corrosion inhibition. Further to this, it was thought that other alternative electrolytes, both solid state and liquid state electrolytes should be subjected to study through the RGB image analysis method due to its rapid and easily comparable nature.